

Some studies for trace elemental characterization of technological and environmental samples using TXRF

by

KAUSHIK SANYAL
CHEM 01201404016

Bhabha Atomic Research Centre, Mumbai

A thesis submitted to the
Board of Studies in Chemical Sciences

In partial fulfillment of requirements
for the Degree of

DOCTOR OF PHILOSOPHY

of

HOMI BHABHA NATIONAL INSTITUTE, Mumbai 400094, India

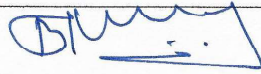
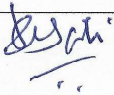


July, 2018

Homi Bhabha National Institute

Recommendations of the Viva Voce Committee

As members of the Viva Voce Committee, we certify that we have read the dissertation prepared by **Mr. KAUSHIK SANYAL** entitled “**Some studies for trace elemental characterization of technological and environmental samples using TXRF**” and recommend that it may be accepted as fulfilling the thesis requirement for the award of Degree of **Doctor of Philosophy**.

Chairman – Prof. S. Kannan		Date: 5.10.18
Guide / Convener – Prof. N. L. Misra		Date: 5/10/18
Examiner – Prof. Devinder Mehta		Date: 5/10/18
Member 1- Dr. M. K. Tiwari		Date: 05.10.18
Member 2- Dr. A. K. Pandey		Date: 5.10.2018
Member 3- Dr. S. K. Sali		Date: 5/10/18

Final approval and acceptance of this thesis is contingent upon the candidate's submission of the final copies of the thesis to HBNI.

I/We hereby certify that I/we have read this thesis prepared under my/our direction and recommend that it may be accepted as fulfilling the thesis requirement.

Date: 5/10/18
Place: Mumbai


(Signature)
Guide

STATEMENT BY AUTHOR

This dissertation has been submitted in partial fulfillment of requirements for an advanced degree at Homi Bhabha National Institute (HBNI) and is deposited in the Library to be made available to borrowers under rules of the HBNI.

Brief quotations from this dissertation are allowable without special permission, provided that accurate acknowledgement of source is made. Requests for permission for extended quotation from or reproduction of this manuscript in whole or in part may be granted by the Competent Authority of HBNI when in his or her judgment the proposed use of the material is in the interests of scholarship. In all other instances, however, permission must be obtained from the author.

Kaushik Sanyal,
05.10.2018
Kaushik Sanyal

DECLARATION

I, hereby declare that the investigation presented in the thesis has been carried out by me. The work is original and has not been submitted earlier as a whole or in part for a degree / diploma at this or any other Institution / University.

Kaushik Sanyal, 05.10.2018
Kaushik Sanyal

List of Publications arising from the thesis

Journal

Published

1. “Results from a new low-Z High-Z TXRF Spectrometer”, **Kaushik Sanyal**, Buddhadev Kanrar, Sangita Dhara, N.L. Misra, Peter Wobrauschek, Christina Strelis, *Advances in X-ray analysis*, 2016, **59**, 125-143.
2. “A comparative study on the total reflection X-ray fluorescence determination of low Z elements using X-ray tube and synchrotron radiation as excitation sources”, **Kaushik Sanyal**, Buddhadev Kanrar, N. L. Misra, M. Czyzycki, A. Migliori, A.G. Karydas , *X-Ray Spectrom.* 2017, **46**, 164–170.
3. “Direct determination of fluorine in high-purity water samples using vacuum sample chamber total reflection X-ray fluorescence spectrometry”, **Kaushik Sanyal**, N. L. Misra, *J. Anal. At. Spectrom.* 2018, **33**, 876-882.
4. “Improved approach for the determination of low-Z elements in uranium samples using a vacuum chamber TXRF spectrometer”, **Kaushik Sanyal**, Sangita Dhara, N.L. Misra, *X-ray Spectrometry*, 2017, **46**, 442–447.
5. “Direct multi elemental trace determinations in plutonium samples by Total reflection X-Ray Fluorescence spectrometry using very small sample amount” **Kaushik Sanyal**, Sangita Dhara, N. L. Misra, *Anal. Chem.*, 2018, **90** (18), 11070–11077.
6. “Direct Determination of Oxidation States of Uranium in Mixed-Valent Uranium Oxides Using Total Reflection X-ray Fluorescence X-ray Absorption Near-Edge Spectroscopy”, **Kaushik Sanyal**, Ajay Khookha, Gangadhar Das, M.K. Tiwari, N.L. Misra, *Analytical Chemistry*, 2017, **89**, 871-876.

7. "Trace element determinations in uranium by Total reflection X-Ray Fluorescence spectrometry using a newly developed polymer resin for major matrix separation", **Kaushik Sanyal**, Sankarrao Chappa, Nimai Pathak, Ashok Pandey, N. L. Misra, *Spectrochimica Acta Part B*, 2018, **150**, 18-25.

Conferences

1. "Determination of low Z elements in uranium with better analytical results using vacuum sample chamber of a low Z – high Z TXRF Spectrometer", **Kaushik Sanyal**, Sangita Dhara and N. L. Misra, Paper presented in **EXRS-2016 (European Conference on X-Ray Spectrometry)** - 2016 conference, June 19-24, 2016, at Gothenburg, Sweden
2. "Trace element determinations in uranium by TXRF using newly developed BisMEP-AMPS based polymer resin for major matrix separation" **Kaushik Sanyal**, Sankara Rao Chappa, A.K. Pandey, N.L. Misra; presentation at the **TXRF 2017 Conference**, held in Brescia, Italy, 19-22 September 2017
3. "TXRF Speciation of arsenic using membrane based preconcentration methodology" **Kaushik Sanyal**, Sankara Rao Chappa, A.K. Pandey, N.L. Misra; presented at the **TXRF 2017 Conference**, held in Brescia, Italy, 19-22 September 2017

Kaushik Sanyal
05.10.2018
Kaushik Sanyal

ACKNOWLEDGEMENTS

I would like to express my deep gratitude to my Ph.D. supervisor **Dr. N. L. Misra** for his guidance, encouragement and advice he has provided to me throughout my Ph. D. carrier. I have been extremely lucky to have such a guide caring so much about my work. I really get motivated from his dedication and love for science.

I would like to thank **Dr. S. Kannan**, Chairman of my Ph.D. Doctoral committee for his keen interest in my work. I would also like to thank my Ph.D. Doctoral committee members **Dr. M.K. Tiwari, Dr. A. K. Pandey, Dr. S. K. Sali** for providing me valuable comments and suggestions during my Ph. D. In addition, I am thankful to **Dr. A.K. Pandey** and **Dr. M.K. Tiwari** and their lab members for their guidance and immense support during various experiments. I am thankful to **Dr. B. S. Tomar**, former chairman of my Ph. D. Doctoral committee, for his keen interest, encouragements and constructive suggestions.

I am very much thankful to my colleagues **Dr. Sangita Dhara** and **Mr. Buddhadev Kanrar** for their constructive advice and help throughout my Ph.D. carrier. They have been always there to help me in any matter regarding my Ph.D. I am also thankful to my friend as well as colleagues **Dr. Nimai Pathak** and **Mr. Abhijit Saha** for their help. I am thankful to my other colleagues **Dr. Balgovind Vats, Dr. Ruma Gupta, Mr. Ashok Yadav, Mr. Sankar Chappa, Dr. Naveen Kumar N** and **Mr. S. Sanjay Kumar** for their help and supports during the course of my Ph.D. work.

I would also like to acknowledge the **International Atomic Energy Agency (IAEA)** for the support in form of opportunity to work at **Elettra Sincrotrone, Trieste, Italy** under the

ongoing CRP in my Division. I would like to acknowledge the XRF beamline staff also for facilitating the delivery of optimum operational conditions for the synchrotron experiment and **Dr. Andreas Karydas, Dr Janos Osan, Prof. Peter Wobrauschek and Prof. Christina Strelt** for providing critical comments during manuscript writing.

My acknowledgement would be incomplete without my family members. I am deeply grateful to my **parents**. They raised me with great care and love. They have sacrificed many things in their life for my education. I am very much thankful to my **maternal uncles (Mama)** for their immense help and supports during my childhood days. I would not be able to reach in this milestone without their love, care and support. I sincerely acknowledge the love and support given to me by my **parent- in-laws**. I have no words to thank my wife **Mrs. Tanaya Sanyal** for her immense support, encouragement, patience and care during my Ph. D. work. I am very much blessed to have her in my life.

During the course of my work, I received help from many, whose name I could not mention. I thank all of them.

Kaushik Sanyal
5. 10. 18
Kaushik Sanyal

CONTENTS

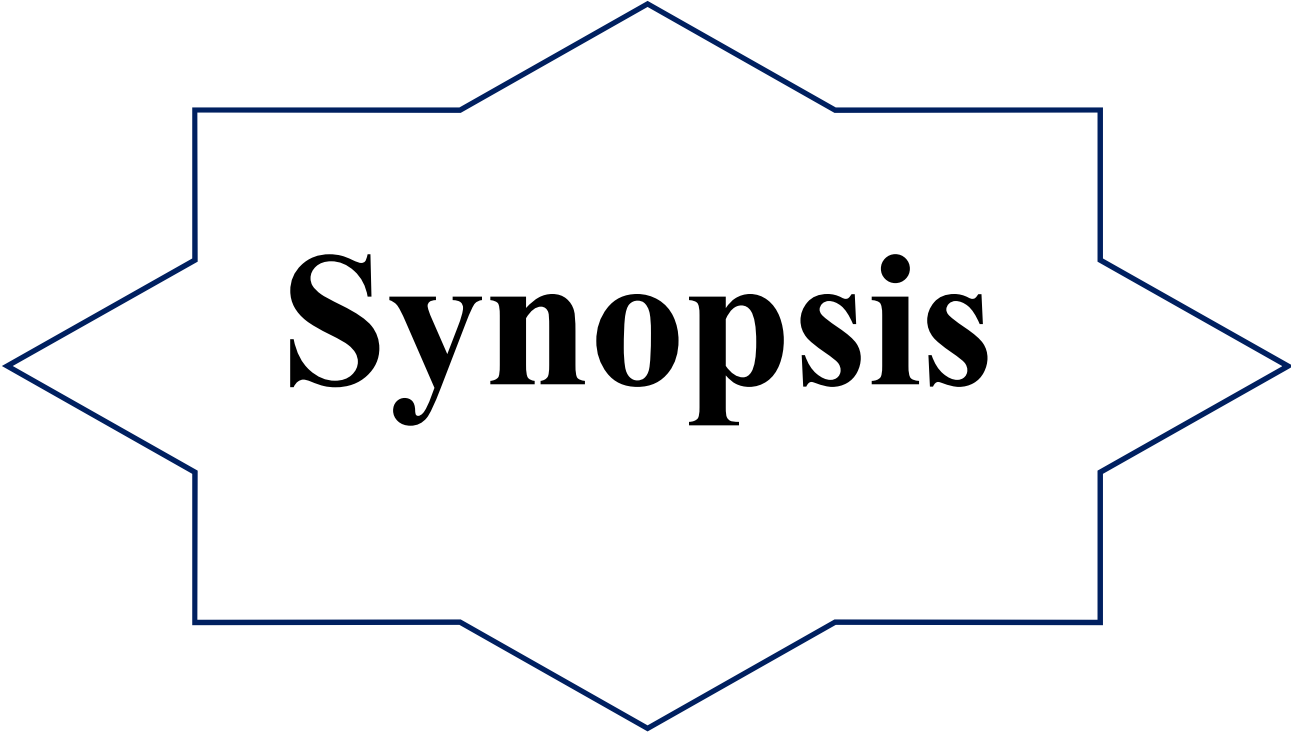
	Page No
SYNOPSIS	i
LIST OF FIGURES	xv
LIST OF TABLES	xxii
Chapter 1	
Introduction	1
1.1. General introduction	2
1.1.1. Technology for improvement of human life	2
1.1.2. Technologically important materials	2
1.1.2.1. Technologically important materials in nuclear industry	3
1.1.2.1.1. Nuclear fuel	3
1.1.2.1.2. Other technologically important nuclear materials	6
1.2. Relation between technology and environment	8
1.2.1. Environmental aspects of nuclear technology	11
1.3. Importance of trace elemental characterization in nuclear and environmental samples	12
1.3.1. Trace elemental characterization in nuclear fuel samples	12
1.3.1.1. Effects of trace constituents	13
1.3.1.2. Characterization of oxidation behaviors in nuclear fuel	16
1.3.2. Trace elemental characterization in environmental samples	16
1.4. Techniques used for trace elemental characterization and their limitations	18
1.4.1. Comparison of TXRF with all other trace element analytical techniques	21
1.5. Application of TXRF for the analysis of technologically important and environmental samples	23
1.6. Improved sample preparation methodology for chemical characterization of trace elements using TXRF	24
1.7. Scope of the thesis	25

Chapter 2	Theory and instrumentation	27
	2.1. Introduction	28
	2.2. Interaction of X-rays with matter	30
	2.2.1. Photoelectric absorption	31
	2.2.2. Scattering	32
	2.3. X-ray Fluorescence (XRF)	33
	2.4. Production of X-rays	34
	2.4.1. X-ray tubes	34
	2.4.2. Radioisotope sources	36
	2.4.3. Synchrotron based X-ray sources	37
	2.5. Total reflection X-Ray Fluorescence (TXRF) spectrometry	41
	2.5.1. Basics of TXRF	42
	2.5.2. Sample supports for TXRF measurements	46
	2.5.3. Monochromator for TXRF measurements	49
	2.5.4. Detection system in TXRF analysis	50
	2.5.5. Instrumental parameters for TXRF analysis	53
	2.5.6. Alignment for TXRF condition	54
	2.5.7. Instrumental calibration and analysis by TXRF	54
	2.6. TXRF-XANES technique	59
	2.6.1. X-ray absorption	59
	2.6.2. Absorption edges	61
	2.6.3. XAS measurements in fluorescence mode	61
	2.6.4. TXRF-XANES measurement procedure	62
	2.7. TXRF facilities used in this work	63
	2.7.1. Lab source based TXRF instrument	63
	2.7.1.1. ITAL STRUCTURE TX-2000	63
	2.7.1.2. Low Z High Z TXRF spectrometer	64
	2.7.2. Synchrotron based TXRF	66
	2.7.2.1. XRF beamline at Elettra Synchrotron Trieste, Italy	66
	2.7.2.2. Micro-focus beam line (BL-16), Indus-2, RRCAT, Indore, India	69
	2.8. Data analysis software used	71
	2.9. Other instruments used	71

Chapter 3	Trace elemental determination of low Z elements by TXRF	73
	3.1. Introduction	74
	3.2. A comparative study on the TXRF determination of low Z elements using X-ray tube and synchrotron radiation	80
	3.2.1. Experimental	80
	3.2.1.1. Sample preparation	80
	3.2.1.2. Instrumentation	81
	3.2.2. Results and discussions	81
	3.2.2.1. Studies on inhomogeneous distribution of elements	81
	3.2.2.2. Detection limits	83
	3.2.2.3. TXRF quantification	88
	3.3. Determination of low Z elements in uranium samples by TXRF	90
	3.3.1. Experimental	90
	3.3.1.1. Reagents	90
	3.3.1.2. Instrumentation	91
	3.3.1.3. Sample preparation	91
	3.3.2. Results and discussions	93
	3.4. Direct determination of fluorine in water samples by TXRF	99
	3.4.1. Experimental	99
	3.4.1.1. Sample preparation	99
	3.4.1.2. Instrumentation	100
	3.4.2. Results and discussions	100
	3.4.3. Analysis without using an internal standard	106
	3.5. Conclusions	112
Chapter 4	Trace elemental determination in plutonium Samples by TXRF	115
	4.1. Introduction	116
	4.2. Experimental	119
	4.2.1. Reagents	119
	4.2.2. Instrumentation	120
	4.2.3. Sample preparation	120
	4.3. Results and Discussions	124
	4.4. Analysis of real Pu based samples	129
	4.5. Conclusions	131

Chapter 5	Trace elemental determination in uranium samples by TXRF after major matrix separation by solid phase extraction	132
	5.1. Introduction	133
	5.2. Experimental	134
	5.2.1. Reagents	135
	5.2.2. Preparation of polymer gel	136
	5.2.3. Instrumentation	137
	5.2.4. Uranium extraction efficiency	138
	5.2.5. Molarity studies	139
	5.2.6. Sorption isotherm	139
	5.2.7. Kinetic study	139
	5.2.8. Regeneration of polymer resin	139
	5.3. Results and Discussions	140
	5.3.1. Characterization of polymer resin	140
	5.3.2. Uranium absorption studies	147
	5.4. Application of the resin for trace elemental determination in uranium	153
	5.5. Conclusions	158
Chapter 6	Elemental speciation by TXRF	159
	6.1. Introduction	160
	6.2. Speciation of mixed valent uranium oxides by TXRF-XANES	169
	6.2.1. Preparation of standards and compounds	169
	6.2.2. TXRF-XANES specimen preparation and measurements	169
	6.2.3. Results and Discussions	170
	6.3. Speciation of arsenic at ultra trace levels by TXRF using pre-concentration and separation	176
	6.3.1. Experimental	176
	6.3.1.1. Chemicals and instrument	176
	6.3.1.2. Immobilization of NMDG on quartz surface	177
	6.3.1.3. Loading Au-Np's as internal standard	179
	6.3.1.4. Speciation studies	181
	6.3.1.4.1. Determination of As (V) concentrations	181
	6.3.1.4.2. Determination of total As concentration	182
	6.3.1.4.3. Speciation of real water samples	183

	6.3.2. Results and Discussions	183
	6.3.2.1. Effect of pH of water samples	184
	6.3.2.2. Effect of sample volume	185
	6.3.2.3. Determination of pre-concentration factors	186
	6.3.2.4. Calibration and validation of the method	187
	6.3.2.5. Speciation of real water samples	189
	6.4. Conclusions	190
Chapter 7	Summary and future scopes	192
References		200



Synopsis

Technologically important materials have very significant contribution in advancement of technology for betterment of human life. There are many types of technologically important materials being used in industries e.g. semiconductor, nuclear, medical, electronic etc. The composition of such materials is specified in terms of major as well as trace elements for their specific use. Any deviation from the specified composition would lead to the malfunctioning of these materials and may lead to their inefficient and unsafe usage. Due to this reason, it is very important that chemical composition as well as level of trace impurities in such materials should be maintained to satisfy the specifications laid down. Moreover, different elements can remain as different species in these materials due to which not only the concentration of the elements, but the species and oxidation states, in form of which the elements are present, also affects the properties of these materials.

In addition, due to various human activities for the technological advancements as well as some natural activities, the environment gets polluted with many toxic trace contaminants. These trace contaminants in environmental samples have to be quantified and their oxidation states are required to be determined to assess and control the adverse effect of these contaminants on the human life. For such elemental characterization, a simple, fast and multielement analytical technique is required.

Nuclear energy is one of the important technological advancements for betterment of human life. It is one of the prominent and clean sources for the generation of electricity in the long run. India has an ambitious indigenous nuclear power programme and aims to supply 25% of its electricity requirements from nuclear power by the year 2050. There are many technologically important materials involved in the nuclear industry which include nuclear fuel, coolant, moderator, cladding materials etc. Uranium, thorium and plutonium are important

elements in nuclear energy generation program. Uranium (^{235}U and ^{233}U) and plutonium (^{239}Pu) are used as nuclear fuels in the nuclear reactors for electricity generation whereas ^{232}Th and ^{238}U are used as fertile fuel elements to produce fissile elements ^{233}U and ^{239}Pu respectively [i-iii]. Different types of trace elements get incorporated in such fuel during their production/fabrication operations e.g. extraction from ores, grinding, pelletization etc [iv]. These impurities can be low atomic number (Z) elements like F, Cl, Ca, Mg, Al as well as medium and high Z elements like Fe, Co, Ni, Mo, Sm, Gd, Cd, Pb etc [v]. Presence of these impurities in excess of the specified amount can cause different adverse effects and damages to fuel, cladding as well as structural materials. Due to these reasons it is extremely important to determine the concentrations of these trace impurities in such materials and ensure that they are well within the specified limits. For such chemical quality control, several well established techniques e.g. Atomic Absorption Spectrometry (AAS), Atomic Emission Spectrometry (AES), Inductively Coupled Plasma - Mass Spectrometry (ICP-MS), Ion Chromatography (IC) etc. are used routinely. Total Reflection X-ray Fluorescence (TXRF) is a variant of Energy Dispersive X-ray Fluorescence (EDXRF) and has proved a very efficient trace elemental analytical technique having analytical detection limits comparable with well established trace element analytical techniques. TXRF has an edge over other conventional trace element determination techniques as it requires very small amount of sample, can determine metals and non metals alike and is non consumptive/non destructive. TXRF has been used in many environmental as well as nuclear sample characterization studies [vi-vii]. As very small amount of sample is needed in TXRF for the characterization of the materials, this technique is very much suitable for the analysis of radioactive, forensic as well as precious samples [iv, viii]. In addition, TXRF has an added advantage that it can be used for the speciation studies also for different elements with very small amount of analyte (in ng level).

Different mixed valent uranium oxides are used as fuel in nuclear reactors. Knowledge about the oxidation states of uranium in these oxides and other compounds of uranium is very important to understand the properties of these compounds essential to use them for different applications e.g. fuel production, spent fuel reprocessing, magnetic and electrical properties etc [ix]. In addition to the trace elemental determination and speciation for the quality control of uranium, its determination as well as speciation is also important in environmental samples e.g. water, air, soil etc. Since the presence of uranium shall be at trace levels in the environmental samples and it is imperative to take very small amount of the precious fuel and other structural materials due to their radioactive nature for their elemental characterization, TXRF may be a very good technique for such characterization due to its features mentioned above. However, there are not much studies reported for such applications of TXRF i.e. trace determinations and speciation of nuclear fuel and other structural materials. In view of the above points, it was decided to explore the applications of TXRF for trace elemental determination of low, medium and high Z elements as well elemental speciation of uranium based materials in nuclear fuel and water samples which are technological and environmental materials respectively. For all these studies, TXRF in ambient and air atmosphere, with lab based and Synchrotron Radiation (SR) based sources were used. SR based TXRF-XANES (X-ray Absorption Near Edge Spectroscopy): an advanced X-ray spectrometric technique was used for elemental speciation. The main advantage of TXRF is requirement of very small amount of sample due to which it shall be well suited for Pu based materials as these are highly radiotoxic. Studies were made to implement TXRF for trace determinations in Pu based samples without putting the instrument inside a glove box. For the trace elements determinations in nuclear fuel samples it is very important to separate the major matrix e.g. U, Pu etc. from the sample matrix. During the separation process it is also desirable

that the amount of analytical waste generated should be minimum as possible. TXRF in combination with improved sample preparation methods can be useful for the trace elemental determinations in nuclear fuel. For low Z elements more rigorous separation is needed to avoid the interference of U M lines escape peaks with Al K lines as well as to avoid absorption of low Z X-ray lines in U and Pu matrix of high Z.

Environmental samples include water samples, air particulates, soil etc. Fluorine and arsenic contamination in drinking water is a major environmental concern for human health. Intake of excess amount of fluorine or arsenic may cause severe health hazards. In addition, to quantification, speciation of arsenic is very important because the toxicity of this elements highly dependent on the oxidation states [x]. Advanced TXRF techniques with improved sample preparation approach can be applied for the analysis as well as speciation studies of these environmental samples.

Keeping these points in mind, advanced features of TXRF along with better sample preparation methodologies have been used in this thesis for trace determinations and speciation studies of nuclear fuel and water samples as a specific example of technological and environmental samples respectively. However, similar approach after suitable modifications can be used for similar characterization of other technological and environmental samples. The thesis is divided into seven chapters given bellow.

Chapter 1: Introduction

This chapter gives a brief introduction about the technologically important materials as well as different types of environmental samples. It also describes about the Indian nuclear power programme and the role of various kind of technologically important materials used in nuclear technology. The importances of trace elemental determinations as well as speciation

studies in different types of nuclear fuel materials are discussed. There are stringent limits of trace impurities which can be tolerated in different kinds of nuclear fuels. This limit is different for different elements and the presence of these impurities beyond the specified limits can cause severe damage to the fuels as well as cladding materials. This chapter will discuss briefly about such effects of various trace impurities on the performance of nuclear materials. There will be a brief description about how the technological development is related with environment and the effect of these technological developments, including nuclear technology, to the environment. This chapter will also give a brief introduction about various techniques which are used for chemical characterization of nuclear and environmental samples. The features of TXRF which make it a suitable candidate technique for elemental characterization of nuclear and environmental samples are also discussed here.

Chapter 2: Theory and instrumentation

In this chapter the theory, principle and instrumentation involved in TXRF spectrometry including TXRF-XANES are described in brief. TXRF technique is very much comparable with the well established trace elemental analysis technique like AAS (Atomic Absorption Spectroscopy), AES (Atomic Emission Spectrometry), ICP-MS (Inductively Coupled Plasma Mass Spectroscopy) etc with respect to detection limit with some added advantages. In TXRF, the X-rays fall on the quartz sample support having thin layer of sample at an angle below critical angle. In this situation the X-rays get totally reflected from the sample support, and both the incident as well as totally reflected X-rays will excite the sample. There are limitations of TXRF for the determination of low Z elements. Vacuum chamber TXRF having ultra thin window detector with low energy excitation source can be a better option for the determination of low Z elements. The details of the instruments used in the present thesis e.g. 1. Ital Structure

TXRF spectrometer: TX-2000, 2. Low Z –High Z TXRF spectrometer is given in this chapter. In some studies, synchrotron based TXRF technique has been used for trace determinations as well as speciation. Two different SR based beamlines were utilized. Details of these two beamlines: 1. XRF beamline of Elettra, synchrotron light source; Trieste, Italy, 2. Micro focus beamline; BL-16 of Indus 2, synchrotron light source, RRCAT, Indore for TXRF, EDXRF and XANES studies shall also be given in this chapter.

Chapter 3: Trace elemental determinations of low Z elements by TXRF

The determination of low Z elements with $Z < 15$ is important in several technological and environmental areas. The maximum amount of low Z elements e.g. F, Na, Mg etc which can be tolerated in environmental samples, so that they do not have any adverse effect on human health, is specific. The presence of low Z elements in nuclear reactor fuels beyond specified limits is detrimental for reactor safety and efficient power production. The detection and the quantification of such elements using different techniques has always been a challenging task. A fast analytical method for the determination of low atomic number elements with minimum sample amount and at trace levels is desirable for trace elemental determination in nuclear materials as well as environmental samples. In this chapter we have used vacuum chamber TXRF as well as synchrotron based TXRF for the analysis of low Z elements in nuclear fuel and water samples.

The TXRF analytical capabilities as well as the detection limits for various low Z elements were compared for lab and synchrotron based excitation sources. It was observed that there is significant improvement in the TXRF detection limits obtained with synchrotron XRF beamline, Elettra, Trieste, Italy for elements having atomic number $Z \leq 13$ (Al); especially for F (down to 0.19 ng), an improvement almost by a factor of twenty seven (27) with respect to the

laboratory set-up (Cr K α excitation, vacuum sample chamber and thin polymer window detector), The results obtained have clearly indicated that in the case of the laboratory TXRF spectrometer further improvement in the DLs can be achieved by means of lower energy X-ray tube based sources (instead of the Cr K α tube based radiation). The present study using line scan also indicated that the non-uniformity of the samples on TXRF sample supports is a major issue while determining them by TXRF.

The capability of the low Z – high Z TXRF spectrometer in our laboratory was tested in terms of detection limits, RSD (Relative Standard Deviation 1 σ) of the determinations and deviation of the TXRF determined values from the expected concentration of elements in the samples made by mixing single element standards. These studies conclude that the present TXRF spectrometer is capable of analyzing low, medium and high Z elements from C to U using the two excitation sources: Cr and Rh K α . The detection limits achieved for C, F, Ti, Y and U were found to be 58 ng, 5.2 ng, 29 pg, 50 pg and 202 pg respectively, indicating that these values are comparable with those obtained with high power TXRF spectrometer used for such purpose. The average deviation of the analytical results from the expected values was 10% and the RSD (1 σ) observed was within 5%.

The low Z – high Z vacuum chamber TXRF spectrometer was successfully used for the analysis of low Z trace impurities in real uranium oxide samples after complete separation of uranium from the sample matrix solution. Complete separation of uranium using eight 30% TBP (Tri n-Butyl Phosphate) based extraction and removal of any dissolved TBP in aqueous phase with the help of n-dodecane is helpful in betterment of TXRF analysis results. Such improved separation approach reduces the background counts and avoids interference of U M escape peaks with Al K α . The TXRF determined results were found to have an average precision of 8 % (1 σ ,

n=3) and the average deviation of the TXRF determined values from the certified concentrations of low Z elements was 7.3 %.

A methodology was developed for the determination of F; a low Z element of high importance value in environmental samples, using the low Z - high Z vacuum chamber TXRF spectrometer. We have developed a simple direct approach for the determination of fluorine in drinking water samples by TXRF without using any internal standard. Two sets of sample carriers: quartz and Si wafer were used. Fluorine could be determined directly at trace concentration levels of as low as 100 ng/mL, in low matrix water samples using Si wafer supports deposited specimens. The TXRF detection limits for F was found to be 1873 pg with Si wafer support specimens and was better by three times than the detection limit obtained using quartz supports. The RSD values of F determination by TXRF using Si wafer supports were found to be 5.1% (1σ , n=3) and the results deviated from the expected values by 4.1% on average. The methodology could be extended for trace determination of F in RO (Reverse Osmosis) water samples. The quartz sample supports can be used for trace determinations for the samples with F concentrations $> 5 \mu\text{g/mL}$.

Chapter 4: Trace elemental determinations in plutonium samples by TXRF

The main advantage of TXRF for toxic, precious and radioactive materials is the requirement of very small amount of samples due to which this technique seems to be very much useful for the analysis of radioactive samples like plutonium as the involved radiation dose to the operator and the radioactive waste generation will be very small. The methodologies developed earlier for trace element determinations in uranium were extended to Pu based samples after proper modifications resulting in a TXRF method for the trace elemental determinations in Pu samples for the first time. The Pu matrix was selectively removed from the solution using TBP

based solvent extraction. All these process were carried out in a fume hood with sample vials doubly sealed in PVC. Aliquots of 5 μL of aqueous phases were deposited on quartz TXRF supports in triplicate. After ensuring that there is no loose contamination on the quartz surface, the TXRF spectra of the specimens were measured without touching the deposited spot. It was observed that almost 99.9% of the Pu could be separated during above matrix separation. The trace elements in Pu were determined using the TXRF spectra obtained and predetermined sensitivity values. The average deviation of the TXRF determined values with expected values was better than 10% with an RSD value of 10% (1σ) which are satisfactory. All these procedures are discussed in detail in this chapter.

Chapter 5: Trace element determinations in uranium samples by TXRF after major matrix separation by solid phase extraction

Solid Phase Extraction (SPE) technique has emerged to be a very good technique for the matrix separation over liquid-liquid based extraction due to the features like simplicity, less laborious, fast, producing less amount of waste, not forming emulsions and the extractant used can be regenerated and reused. It can be helpful for the trace elemental determinations in uranium and plutonium based samples after their separation. Using this approach, an environment friendly TXRF method has been developed for the determination of trace elements in uranium oxide samples, using a newly developed polymer resin, which can selectively remove uranium from the sample matrix at 4M HNO_3 medium. The polymer resin gel was prepared by 1:1 combination of monomers – [(methacryloyloxy) ethyl] phosphate (MEP) and 2-acrylamido-2-methyl propane sulfonic acid (AMPS). Photoluminescence (PL), Fourier-Transform Infra Red (FTIR), Field Emission Scanning Electron Microscopy (FE-SEM) were used to characterize the polymer resin gels. The synthesis as well as the characterization of resin gels is discussed in

detail in this chapter. Experimental results show that this newly developed polymer resin gel can extract uranium just by dipping it in uranium solutions and has a loading capacity of 600 μg of U/mg of resin. The higher loading capacity is well suited for complete separation of uranium from the sample matrix. As the resin gel after the experiment can be regenerated and used for fresh experiments, the organic waste generation will minimum. Requirement of very small amount of sample in TXRF and generation of very small organic waste combined with ease of separation by just dipping the gel in solution make this methodology very useful for the handling and analysis of plutonium based radioactive samples. This methodology has been tested for the analysis of real uranium samples using a Certified Reference Material (CRM-IV) for uranium oxide. The average deviation of TXRF determined values with certified values and RSD obtained for the analysis of CRM (IV) are 9.2% and 7.6% (1σ) respectively (excluding Fe). The method can be extended in similar manner for plutonium based samples.

Chapter 6: Elemental speciation by TXRF

This chapter describes two studies on speciation:

1. Non-destructive speciation methodology for U in mixed valent uranium oxides using TXRF-XANES.
2. Speciation of arsenic in water samples using a newly developed novel\ absorbent grafting on the surface of quartz sample supports.

SR based TXRF-XANES may be a very suitable and reliable technique for the speciation studies of mixed valent uranium oxides compared to X-ray photo electron spectroscopy (XPS). We have done the speciation studies of two mixed valent uranium oxides; e.g. U_3O_8 and U_3O_7 using XANES measurements in TXRF geometry. The main advantage of doing XANES measurement in TXRF geometry is requirement of very small amount of sample (ng level)

compared with normal XANES (mg level). A very small amount of sample is taken on a quartz support and rubbed with the help of a small pipette tip to spread it in a small area of about 2 mm diameter. The support is then dabbed on a clean tissue paper so that any loose particle not sticking on the support comes out. The sticking sample amount on the support is sufficient for TXRF measurements. This type of sample preparation is very useful for the speciation studies of radioactive, precious, forensic and environmental samples where analyte amount available and desirable is very small. The details of the TXRF-XANES measurements on uranium oxides are discussed in this chapter. The study concluded that U_3O_8 contains uranium in U (V) and U (VI) states with relative amounts of 70 and 30 % respectively. These values are in agreement with the theoretical values of 66 and 34% respectively. These results are in agreement with the earlier literature reported XANES data using UM edge measurements. Similarly for U_3O_7 , uranium was found to be in mixed valent states of U (IV) and U (VI) (70% and 30 % respectively).

TXRF can also be applied for the speciation of environmental samples like water, air particulates, soils etc. We have developed a TXRF based simple method for the speciation of arsenic in water samples using N-Methyl-D-Glucamine (NMDG) a novel absorbent grafting on the surface of quartz sample supports. The details of the grafting of membrane on the quartz sample supports are discussed in detail in this chapter. Gold nano particles, loaded on the NMDG membrane, was used as an internal standard. This membrane grafted quartz sample support was simply dipped into the As (V) solution. This membrane is very much selective to the arsenate species [As (V)] and the interaction is mainly electrostatic. It was observed that at pH 6-7 this membrane has the highest As (V) uptake capacity. A calibration curve was obtained using different concentrations of As (V) species ranging from 1-50 ng/mL and respective As $K\alpha$ /Au $L\alpha$ intensity ratio in their TXRF spectra. A linear curve was obtained with very good correlation

coefficient. The As detection limit obtained using this methodology is lower compared to the earlier reported TXRF based technique. The total arsenic concentration can be determined by oxidizing As (III) into As (V) by adding a few drops of 30 % H₂O₂; which is a strong oxidizer. The As (III) concentration can be derived by subtracting the As (V) concentration from the total arsenic concentration. This methodology has been applied for the speciation of arsenic in some real water samples like tap water; ground water etc and the results obtained are very satisfactory.

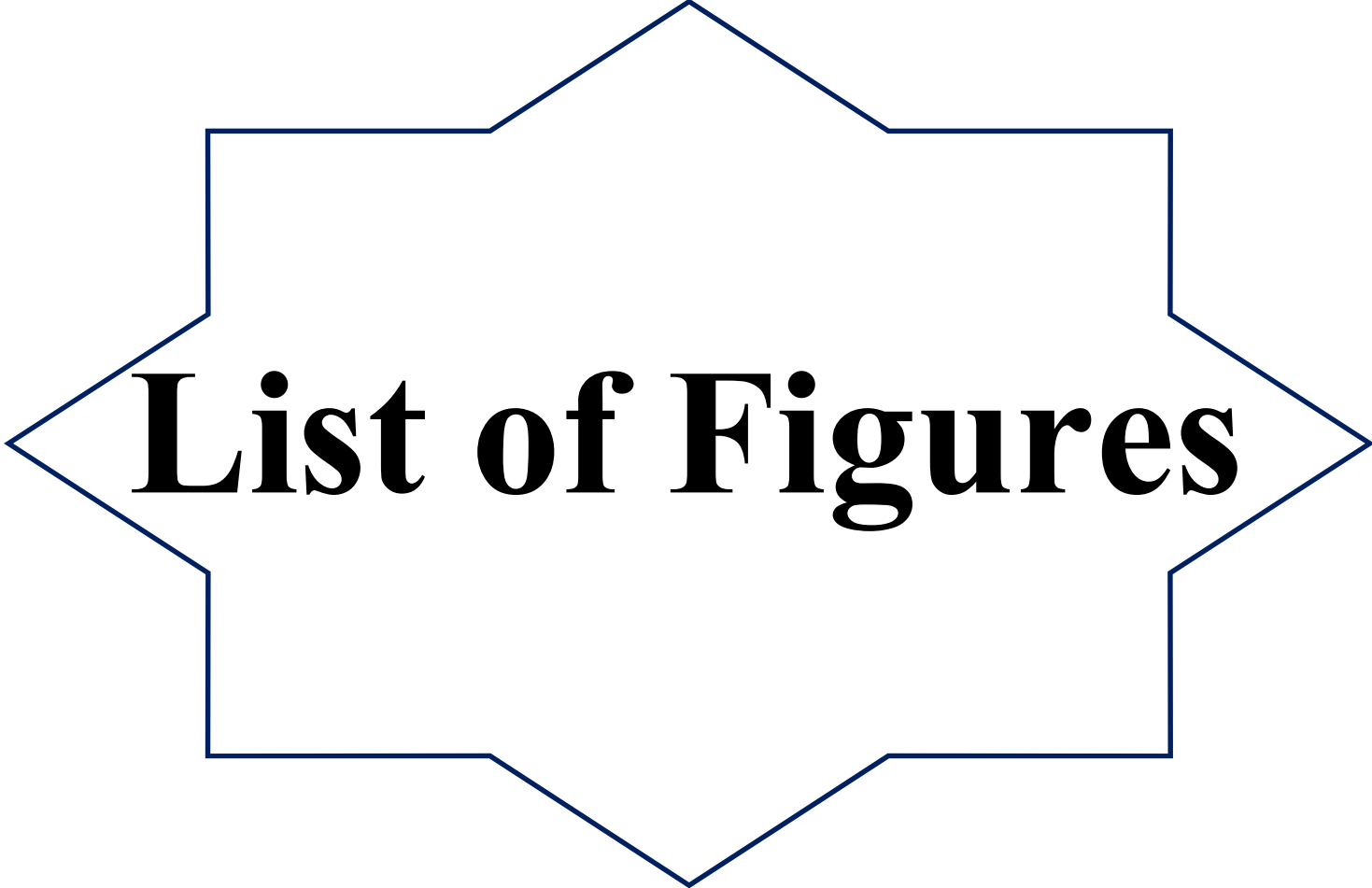
Chapter 7: Summary and future scopes

Overall this thesis gives emphasis on the advanced features of TXRF in combinations with improved sample preparation approach for the analysis as well as speciation of technologically important and environmental samples with specific example of uranium/plutonium and waster samples respectively. The thesis emphasizes the important role which TXRF can play for the speciation studies of nuclear and environmental samples. This thesis also enlightens the fact that as TXRF requires very small amount of sample and can be utilized very well for the analysis of very precious, radioactive, biological and forensic materials where more amount of sample for the analysis purpose is not available. A brief summary of important work carried out in the thesis are given in this chapter.

References:

- i) P. C. Burns, R. C. Ewing, A. Navrotsky, *Science*, 2012, **335**, 1184-1188.
- ii) A. Radkowsky, A. Galperin, *Nucl. Technol.* 1998, **124**, 215-222.
- iii) C. Ganguly, P.V. Hegde, *J. sol-gel. Sci. Techn.* 1997, **9**, 285-294
- iv) N.L. Misra, K.D. Singh Mudher, V.C. Adya, B. Rajeswari, V. Venugopal, *Spectrochim Acta B.* 2005, **60**, 834-840.

- v) V. Venugopal, *IANCAS Bulletin*, 2005, **4**, 205-212
- vi) N.L. Misra, K.D. Singh Mudher, *Prog. Cryst. Growth. Ch.* 2002, **45**, 65-74.
- vii) R. Klockenkämper, *Total reflection X-ray fluorescence analysis, Chemical Analysis*, 1996, **140**, John Wiley and Sons, New York
- viii) F. Saverio Romolo, P. Margot, *Forensic Sci. Int.* 2001, **119**, 195
- ix) K. O. Kvashnina, S. M. Butorin, P. Martin, P. Glatzel, *Phys Rev Lett.* 2013, **111**, 253002
- x) R. Gupta, J. S. Gamare, A. K. Pandey, D. Tyagi, J. V. Kamat, *Anal. Chem.* 2016, **88**, 2459–2465



List of Figures

Chapter 1

1. Figure 1.1. MOX fuel pellets
2. Figure 1.2. Different components of nuclear reactors
3. Figure 1.3. Different steps involved during fuel fabrication

Chapter 2

1. Figure 2.1. Different phenomenon occur while interaction of X-rays with matter
2. Figure 2.2. Photo electric absorption process
3. Figure 2.3. Compton scattering and Rayleigh scattering
4. Figure 2.4. Schematic cross section of an X-ray tube
5. Figure 2.5. A typical tube spectrum using Rh as target material
6. Figure 2.6. Schematic planar view of a synchrotron based light source
7. Figure 2.7. Spectral distribution of synchrotron radiation
8. Figure 2.8. Comparison of average brightness of SR source of different generations with typical X-ray tube based X-ray source
9. Figure 2.9. Arrangement of XRF measurement using synchrotron based radiation source
10. Figure 2.10. EDXRF and TXRF geometry
11. Figure 2.11. X-rays falling from medium 1 to medium 2 can be refracted away from the boundary (A) or it can be refracted towards the boundary (B) according to Snell's law
12. Figure 2.12. Penetration of X-rays depending on the grazing angle for 17.5 keV radiation in silicon
13. Figure 2.13. Picture of a clean quartz sample support (A) and a quartz sample support having 5 μ L of liquid sample deposited on the centre of it (B).
14. Figure 2.14. TXRF spectra of a clean quartz sample support using Rh tube as an excitation source (live time: 300 seconds)
15. Figure 2.15. Working principle of a Si (Li) detector system
16. Figure 2.16. Working principle of SDD detector
17. Figure 2.17. TXRF spectra of a multi elemental standard solution having elemental concentration of 10 μ g/mL; using Rh K α as an excitation source
18. Figure 2.18. Plot of the RS vs. atomic number for medium Z elements (K to Y), using K α analytical lines, B: Plot of the sensitivity values vs. atomic number for High Z elements (Cd to U), using L α analytical lines

19. Figure 2.19. Preparation of TXRF sample specimen for the analysis of an unknown solution
20. Figure 2.20. Plot of detection limit with atomic number using $K\alpha$ as analytical line and Rh $K\alpha$ as excitation source for elements K to Y
21. Figure 2.21. A typical X-ray absorption spectrum
22. Figure 2.22. Different excitation states give different absorption edges
23. Figure 2.23. Different regions of an XAS spectrum including XANES and EXAFS
24. Figure 2.24. XAS measurements using absorption and fluorescence mode
25. Figure 2.25. Picture of ITAL STRUCTURE TX-2000
26. Figure 2.26. Picture of a Low Z – High Z TXRF spectrometer having Cr and Rh targeted X-ray tube
27. Figure 2.27. Diagram of the UHV chamber along with load lock chamber and 7 axis sample manipulator inside the UHV chamber
28. Figure 2.28. The arrangement of sample inside the main experimental chamber
29. Figure 2.29. Totally reflected beam (top) and direct beam (bottom) shown by the CCD camera indicating that TXRF conditions are satisfied during the sample measurements

Chapter 3

1. Figure 3.1. A comparison of three overlapped TXRF spectra of 20 $\mu\text{g/ml}$ MES solution deposited in triplicate on different quartz sample supports and measured by using the Cr $K\alpha$ as excitation source, in vacuum atmosphere for a live time of 1000s
2. Figure 3.2. The distribution of X-ray line intensities of different elements along X-axis obtained by scanning the SR beam across the sample residue (by dividing the sample residue into different slices) with beam energy 5.41 keV at the XRF beamline. The counting time per slice was 20 s, and the counts recorded for different elements were normalized with respect to their respective value at the slice #20
3. Figure 3.3. Comparison of TXRF elemental detection limits (expressed in absolute analyte mass) by using different excitation sources
4. Figure 3.4. Representative TXRF spectra (1000 s measuring time) of a MES solution containing elements with 10 $\mu\text{g/ml}$ concentration (except the Mg and Sc with 5 $\mu\text{g/ml}$ concentration) measured by using a 5.41 keV synchrotron radiation excitation (equivalent to Cr $K\alpha$ energy) and the tube-based Cr $K\alpha$ excitation

5. Figure 3.5. The experimental (dots) and fitted TXRF spectra (continuous line) of 10 μ g/mL, MES solution obtained using (a) 5.41 keV SR, (b) 3.8keVSR and (c) Cr K α tube based excitation
6. Figure 3.6. Comparison of the quantitative results obtained for the multi-elemental standard with 10 μ g/ml (A) and 30 μ g/ml elemental concentrations (except Sc with 5 μ g/ml concentration) by using the low Z–high Z TXRF spectrometer providing the Cr K α excitation and two SR beams with 5.41 and 3.8 keV exciting energies, respectively, versus the expected concentrations
7. Figure 3.7. Flow chart of the sample preparation steps for the processing of uranium oxide samples for trace low-Z elements determination by TXRF
8. Figure 3.8. Plot of relative sensitivity values (Cr K α as excitation source and Ti as an internal standard) against atomic number
9. Figure 3.9. A comparison of TXRF spectra of a processed uranium oxide (CRM-IV) after five and eight extraction with TBP and subsequent three equilibrations with n-dodacane.
10. Figure 3.10. AXIL fitted TXRF spectra of uranium oxide CRMs after selective removal of uranium
11. Figure 3.11. Comparison of TXRF spectra of solutions containing 10 μ g/mL of fluoride prepared in Milli-Q water at pH 6.5 and in 0.1 M HNO₃ medium
12. Figure 3.12. TXRF specimen prepared with 5 μ L volume of fluoride sample on Si-wafer and quartz sample supports.
13. Figure 3.13. Comparison of repeatability of F K α intensity in TXRF spectra of different specimens prepared by depositing 5 μ L aliquots of 10 μ g/mL fluoride solution on Si-wafer and quartz supports
14. Figure 3.14. AXIL-fitted TXRF spectra of fluoride solution (5 μ g/mL) deposited on (A) quartz and (B) Si-wafer supports.
15. Figure 3.15. Comparison of TXRF spectra of fluoride solutions (2.5–25 μ g/mL) obtained using quartz and Si-wafer supports
16. Figure 3.16. Comparison of calibration plots for direct TXRF determination of F using specimens deposited on Si-wafer and quartz supports
17. Figure 3.17. Calibration plot for TXRF determination of F in samples with F concentration in the range of 100-600 ng/mL. The solutions were deposited on Si wafer supports

18. Figure 3.18. Comparison of TXRF spectra of tap water and RO water from same source

Chapter 4

1. Figure 4.1. Separation of plutonium from the sample matrix for the trace elemental analysis in it using TXRF
2. Figure 4.2. Comparison of the TXRF spectra for MES solution having elemental concentration of 10 μ g/mL before and after equilibration with 30% TBP in n-dodacane
3. Figure 4.3. TXRF spectra of the aqueous phase of the blank solutions for trace element determinations in Pu after separation of plutonium using TBP
4. Figure 4.4. AXIL fitted TXRF spectra of the solution obtained after the separation of plutonium from the sample matrix having multi elemental standard of elemental concentrations 5 (A) and 20 (B) μ g/mL respectively with Se internal standard having concentration of 10 μ g/mL in each of these solutions
5. Figure 4.5. TXRF spectra of real Pu based sample

Chapter 5

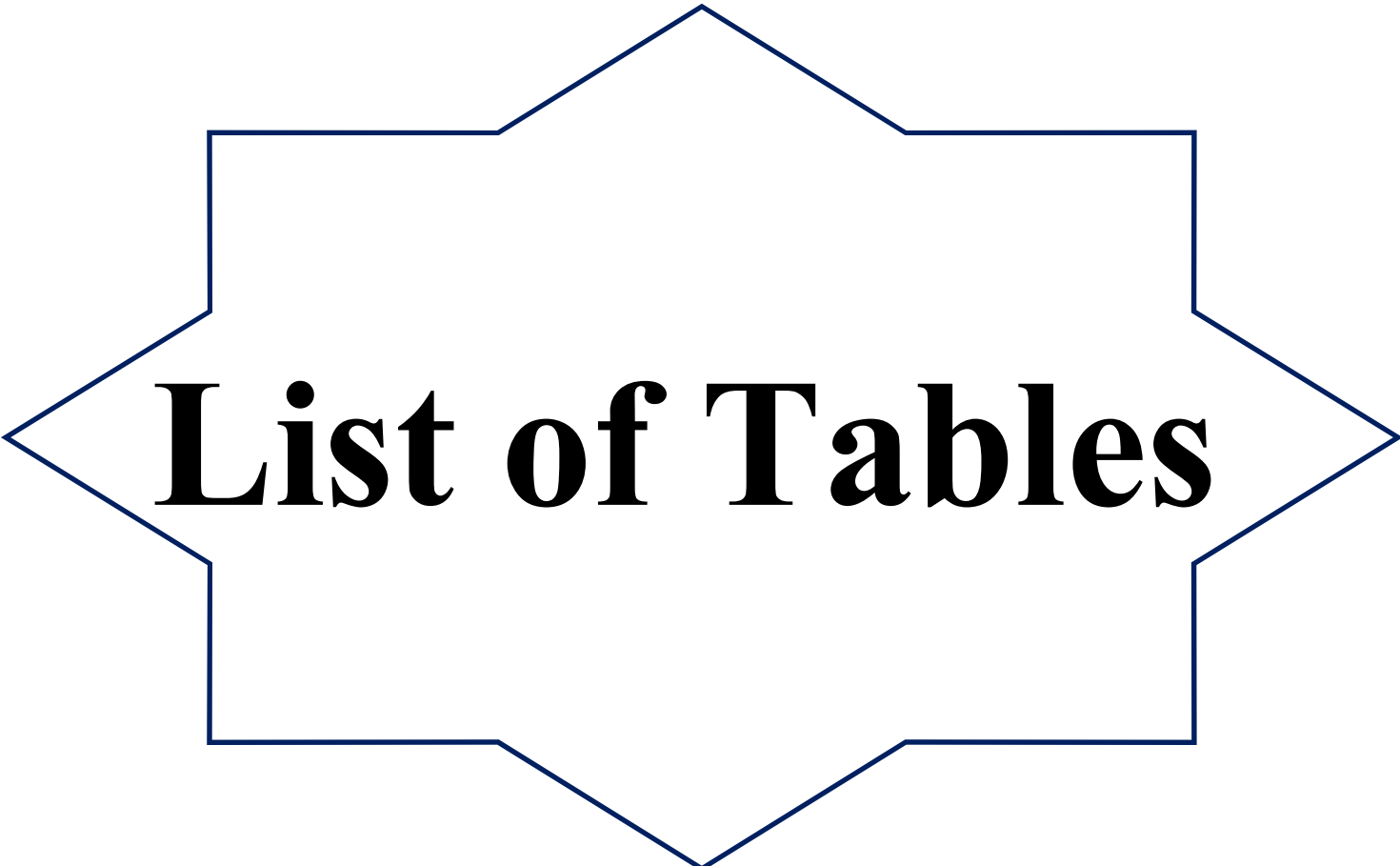
1. Figure 5.1. Schematic of the preparation of Bis-MEP based polymer resin gel (RESIN 1) (a) and three possibilities of 1:1 combination of Bis-MEP and AMPS based polymer resin gel (RESIN 2 (b))
2. Figure 5.2. Emission spectra of uranium loaded Resins: Resin 1 and -2 at an excitation wavelength of 230 nm
3. Figure 5.3. TRES spectra of uranium loaded resin 1 and 2, at an excitation wavelength of 230 nm
4. Figure 5.4. Decay curves for uranium loaded resin 1 and 2 at $\lambda_{\text{ex}} = 230$ nm and $\lambda_{\text{em}} = 546$ nm
5. Figure 5.5. Schematic of coordination of UO_2^{2+} moieties in 4M HNO_3 medium with the two types of polymer resins
6. Figure 5.6. FTIR spectra of resin 2 before and after loading of uranium
7. Figure 5.7. FE-SEM images of resin 2 (a) and EDS image of the uranium loaded resin 2 (b)
8. Figure 5.8. Photograph of resin 2 before (a) and after absorption of uranium (b)
9. Figure 5.9. Plot of uranium extraction efficiency of resin 2 as a function of molarity of HNO_3 medium

10. Figure 5.10. Variation of elemental concentration in MES solutions of 10 $\mu\text{g/mL}$ concentration prepared in different HNO_3 molarities after overnight equilibration of 50 mg of polymer resin 2
11. Figure 5.11. TXRF spectra of solutions in 4M HNO_3 having lanthanides before and after equilibration of resin 2 with the solution
12. Figure 5.12. Adsorption isotherm of U (VI) ions on resin 2, having weight of 150 mg in 4M HNO_3 medium for overnight contact
13. Figure 5.13. Recovery of uranium from its 4M HNO_3 solutions on first (A) and second (B) contact with resin 2 as a function of time
14. Figure 5.14. Pseudo second order kinetic model used to fit the sorption profile of the polymer resin gel for the absorption of uranium in 4M HNO_3 medium
15. Figure 5.15. TXRF spectra of the multi elemental standard solution having concentration of 5 $\mu\text{g/mL}$ before and after separation of the uranium matrix by resin 2
16. Figure 5.16. Schematic diagram of the separation of uranium from real uranium oxide (CRM-IV) sample matrix using polymer resin 2.
17. Figure 5.17. TXRF spectrum of processed CRM-IV solution after separation of uranium from the solution matrix using polymer resin 2

Chapter 6

1. Figure 6.1. TXRF spectrum of U_3O_8 specimen during TXRF XANES measurements
2. Figure 6.2. TXRF-XANES spectra of U_3O_8 along with standard compounds
3. Figure 6.3. First derivative of the TXRF-XANES spectra of different uranium oxides showing shift in the edge position
4. Figure 6.4. Linear combination fitting of TXRF-XANES spectra of U_3O_8 using two different oxidation state combinations: U (V) + U (VI) and U (IV) +U (VI)
5. Figure 6.5. Linear combination fitting of TXRF-XANES spectra of U_3O_7 using two different oxidation state combinations: U (IV) +U (V) and U (IV) +U (VI)
6. Figure 6.6. Schematic representation of immobilization of NMDG on quartz sample supports
7. Figure 6.7. Quartz sample supports after immobilization of NMDG
8. Figure 6.8. Schematic representation of immobilization of Au NPs on the membrane attached with quartz sample supports

9. Figure 6.9. Absorption spectra of the Au-loaded NMDG membrane showing the surface Plasmon resonance around 500-600 nm due to the formation of Au-Nps
10. Figure 6.10. TXRF spectra of the quartz sample support loaded with Au NPs
11. Figure 6.11. Pre-concentration procedure for As (V) species using NMDG membrane immobilized on the quartz sample support
12. Figure 6.12. Arsenic absorption efficiency of the membrane as a function of pH of the aqueous medium
13. Figure 6.13. Effect of sample volume on arsenic absorption by NMDG membrane immobilized on quartz sample supports
14. Figure 6.14. : TXRF spectra of a As solution having concentration of 50 ng/mL before and after pre-concentration using SPE based methodology
15. Figure 6.15. Calibration curve obtained using the SPE based pre-concentration method in combination with TXRF across the As (V) concentration range of 1- 50 ng/mL
16. Figure 6.16. AXIL fitted TXRF spectra of a water sample containing 50 ng/mL of arsenic along with fixed amount of Au as internal standard



List of Tables

Chapter 1

1. Table 1.1. Specification limits of different trace impurities in typical thermal and fast reactors fuels.
2. Table 1.2. Permissible limits of different elements in drinking water prescribed by different authorities.
3. Table 1.3. Comparison of TXRF technique with all other well established trace elemental analytical techniques.

Chapter 2

1. Table 2.1. Different radio-isotopic X-ray sources
2. Table 2.2. Comparison of different sample supports for TXRF analysis

Chapter 3

1. Table 3.1. Comparison of detection limits obtained using different excitation sources and energies
2. Table 3.2. Results of TXRF determination of low Z elements in different CRM Standards (all values in $\mu\text{g/g}$)
3. Table 3.3. Detection limits for fluorine obtained using vacuum chamber TXRF ($\text{Cr K}\alpha$ excitation) with samples deposited on quartz and Si-wafer as sample supports
4. Table 3.4. Comparison of TXRF determination results of fluorine in water samples having F concentration in the range of 1.5-20 $\mu\text{g/mL}$ using quartz and Si wafer sample supports
5. Table 3.5. Results of TXRF determination of fluorine in solution samples having F concentration in the range of 100-600 ng/mL using Si wafer Supports
6. Table 3.6. Results of TXRF determination of fluorine in RO water samples spiked with fluorine at different concentration levels in the range of 2-16 $\mu\text{g/mL}$ using Si wafer supports

Chapter 4

1. Table 4.1. Details description of plutonium based sample as well as blank preparation before the separation with TBP
2. Table 4.2. Comparison TXRF determined and expected elemental concentrations in a multi-element standard solution after equilibration with 30% TBP in n-dodacane and analyzed by TXRF.

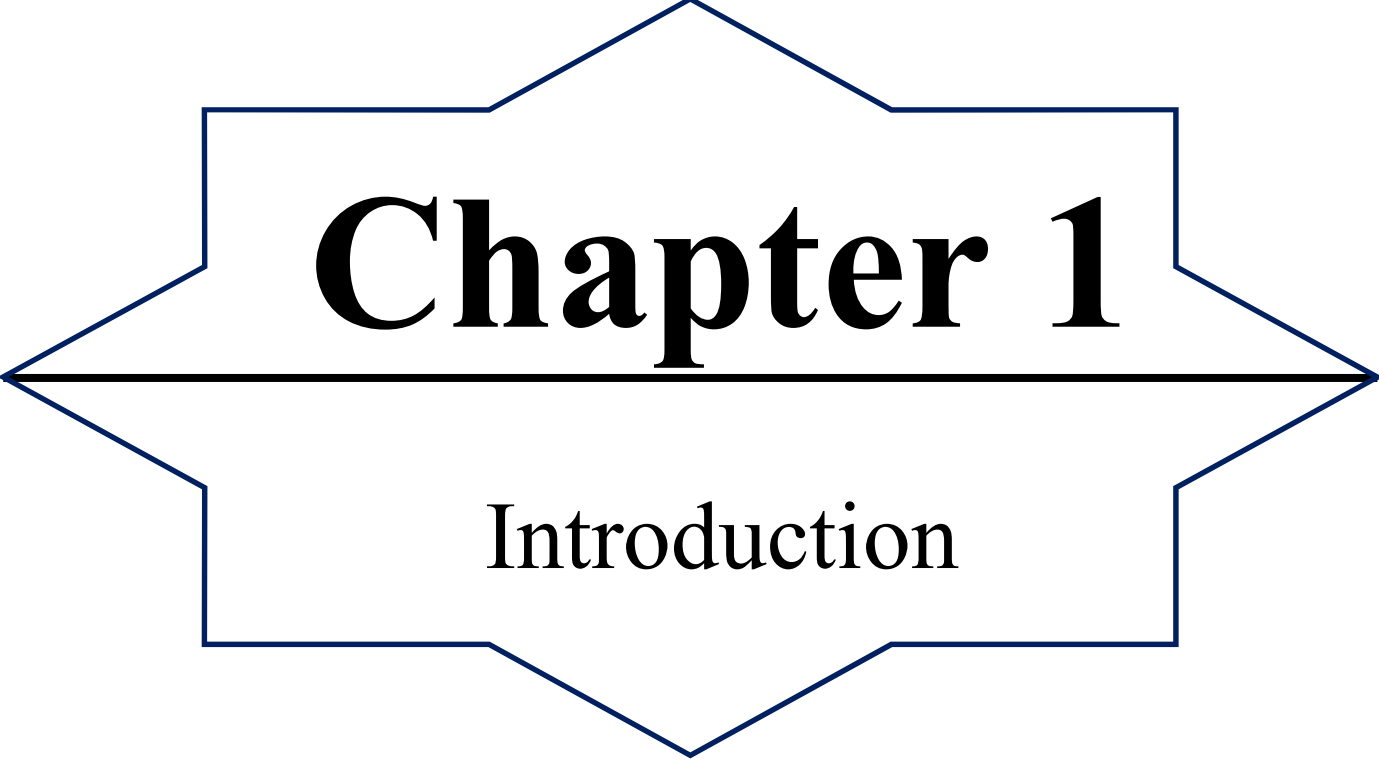
3. Table 4.3. Percentage of Pu separated in all the Pu based samples using 30% TBP in n-dodacane and net amount of Pu deposited on TXRF sample supports
4. Table 4.4. TXRF determined elemental concentrations of three Pu based samples after separation of almost all the Pu (>99.9%) from the sample matrix
5. Table 4.5. Result for the trace elemental analysis in a real Pu based sample by TXRF

Chapter 5

1. Table 5.1. Lifetime values obtained by fitting the decay curve of uranium loaded Resin 1 and Resin 2
2. Table 5.2. The intensity ratio of lanthanide elements $L\alpha$ lines and Ga $K\alpha$ before and after equilibration of the 4M HNO_3 solution of lanthanides with Resin 2
3. Table 5.3. Comparison of expected and TXRF determined elemental concentrations in a multi-element standard solution containing uranium as major matrix after separation of uranium by TBP
4. Table 5.4. Comparison of TXRF determined elemental concentrations and certified elemental concentrations for the trace elements present in CRM-IV.

Chapter 6

1. Table 6.1. The edge energy values of different oxide compounds of uranium as obtained from the maxima of the second derivative of their TXRF-XANES spectra
2. Table 6.2. The relative amounts of U (V) & U (VI) or U (IV) & U (VI) present in U_3O_8 from the linear combination fit of the TXRF-XANES spectra of U_3O_8
3. Table 6.3. The relative amounts of U (IV) & U (VI) or U (IV) & U (V) present in U_3O_7 from the linear combination fit of the TXRF-XANES spectra of U_3O_7
4. Table 6.4. Comparison of detection limit of arsenic before and after pre-concentration by using the SPE methodology in combination with TXRF
5. Table 6.5. Determination of the total arsenic content in a simulated samples containing As (III) and As (V) (sample volume 50 mL, n = 3)
6. Table 6.6. Speciation of As (III), As (V) in natural water samples (mean \pm standard deviation, n =3, and sample volume 50 mL)



Chapter 1

Introduction

1.1.General introduction

1.1.1. Technology for improvement of human life

Human life cannot be imagined today without use of technology. It is a vast field of knowledge dealing with developments in areas of industrial, arts, engineering, applied science, and pure science etc. It is very much correlated with our life, society, and the environment. Technology has affected the growth of the human civilization in several ways and helped to raise the standard of our day to day life. In recent years technology has grown at very fast rate and many people from different fields are working to improve it. If we look around; we can find ourselves surrounded with various types of technological developments and their applications in various industries like electronic, agricultural, power production, medical, aeronautics, environmental etc. Nuclear industry is one of the important power production industries. With the growth of technological advancements, there is a need for production of energy all over the world. There are many types of conventional sources of energy like thermal, hydro-electrical, solar etc. The need of energy is growing day by day, whereas reserve of coal, a major source of energy is depleting continuously. In such situation nuclear power can be a very important alternative source of energy for the developing nations like India. At present India have total 22 nuclear reactors in operation for the production of electricity. About 3% of the total electricity generated in India, comes from nuclear power. India has a plan to increase this value to 50% by the year 2050 [1]. Due to above reasons the nuclear technology is going to play a very important role for the growth of the country.

1.1.2. Technologically important materials

Technologically important materials are those materials which play an important role in technology and thereby in the development of human life standards because of their significant

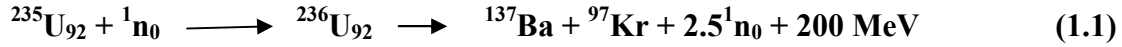
contributions in progress of different areas of science and technology. There are many scientific areas e.g. electronics, medicine, aeronautics, space-science, civil-engineering etc where high purity materials are very necessary. In electronic industry high purity binary group III-V materials (GaAs, InAs, InP etc.), ternary III-V materials (GaAs/P, InAs/P), binary II-VI compounds (ZnS, CdS, CdSe etc.), and binary Si-Ge alloys were used [2]. There are many technologically important materials which can be used as superconductors. They are very complex in structure as well as composition; so they have to be made very carefully [3]. Similarly magnetic materials have a significant role in electric power and telecommunication industries [4]. Oil, petroleum are very important materials and their quality is very much dependent upon their composition. For scientific research, high purity materials are very important. Similarly in nuclear industry also there are several materials which have technological importance and shall be discussed in details in subsequent part of the thesis [5-7].

1.1.2.1. Technologically important materials in nuclear industry

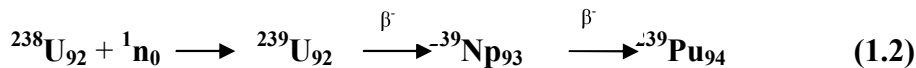
1.1.2.1.1. Nuclear fuel: the most important technological materials in nuclear industry

Nuclear fuel is the source of electricity in a nuclear reactor and it is fabricated in different chemical forms depending on reactor type [8]. It is the most important component of nuclear reactor. The reactor fuels can be used in the reactors until they reach their operating limit. So during the reactors operating condition, their performance as well as efficiency is very much dependent upon the fuel quality [9]. Different actinides like uranium, plutonium and thorium are mainly used as nuclear fuel. These actinides have many isotopes and all isotopes are not fissile. Natural uranium has mainly three isotopes, e.g. ^{238}U (99.275%), ^{235}U (0.72 %) and ^{234}U (0.0054%) [10]. Among these three isotopes only ^{235}U are fissile in nature. These isotopes undergo fission reaction with the thermal neutrons. During such fission reaction, huge amounts

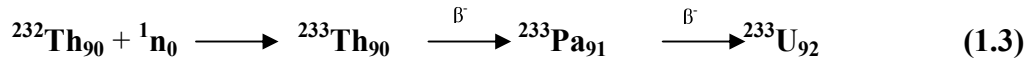
of energy as well as additional number of neutrons are produced. The neutrons produced carry out further fission reaction and this fission propagated. A typical fission reaction can be represented as follows:



Uranium nucleus breaks into different nuclei after fission. The elements Ba, Kr etc shown here are one of the several possible fission products and 2.5 neutrons are approximate value of average number of neutrons produced in a fission reaction. There can be several other fission products that can be generated during fission reactions. The numbers of neutrons produced get multiplied in the number during the fission process and in a nuclear reactors this production of neutrons are kept under control. During fission of each nucleus, a huge amount of energy is released and this energy is utilized for power production. Both natural uranium and enriched uranium can be used as fuel depending upon the type of reactors. Another actinide which is used as fuel in reactor is plutonium (Pu). Plutonium is not a natural element but is produced in the reactors. Plutonium also can have several isotopes like ${}^{239}\text{Pu}$, ${}^{240}\text{Pu}$, ${}^{241}\text{Pu}$, ${}^{242}\text{Pu}$ etc. ${}^{239}\text{Pu}$ is a fissile isotope that is the second most used nuclear fuel in nuclear reactors after ${}^{235}\text{U}$, and it is produced from ${}^{238}\text{U}$ by neutron capture followed by two beta decays as shown bellow.



Thorium (Th) is also used in nuclear fuel but as a fertile element. The most stable isotope of Th is ${}^{232}\text{Th}$; which is a fertile one. ${}^{232}\text{Th}$ when bombarded by slow neutrons, undergo neutron capture to become ${}^{233}\text{Th}$, which undergoes two consecutive beta decays and produces first ${}^{233}\text{Pa}$ and then the fissile ${}^{233}\text{U}$ which has a higher probability (92.0%) of fission upon neutron capture than that of ${}^{235}\text{U}$ (85.5%) or ${}^{239}\text{Pu}$ (73.5%) [11, 12]. The reaction is shown below:



India has vast reserves of thorium due to which thorium occupies a very important place in the Indian nuclear power programme. It is very important to utilize the domestic uranium and thorium reserves of the country in an optimized manner for providing a long term energy security. The third stage of Indian nuclear power program will be based on ${}^{232}\text{Th} - {}^{233}\text{U}$ fuel cycle [13]. Different forms of U, Th and Pu have been used as fuel in nuclear reactors. Enriched UO_2 is used as fuel in PWR (Pressurized Water Reactors), BWR (Boiling Water Reactor). Natural uranium oxide is used in PHWR (Pressurized Heavy Water Reactor). Mixed uranium-plutonium mono-carbide (MC) with a controlled amount of mixed sesqui-carbide (M_2C_3) is used as fuel in FBTR (Fast Breeder Test Reactor). MOX (Mixed Oxide) fuel like (U, Pu) O_2 can be used in PFBR (Prototype Fast Breeder Reactor) [14-17]. Metallic uranium has higher fissile element density and it is considered to be an ideal fuel material in terms of power production. But metallic uranium and its alloy fuels are generally used in small research reactors as their melting points are low.

Generally the fuels in reactors are used as pellets with a height, and diameter of about 1 centimeter. The height of fuel pellets is greater than the diameter. Figure 1.1 shows the picture of some typical MOX fuel pellets. These pellets are stacked inside a metallic cladding tube [9].

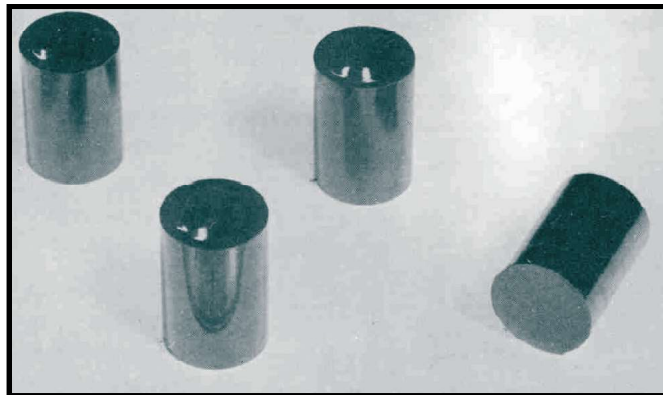


Figure 1.1: MOX fuel pellets [ref-9]

1.1.2.1.2. Other technologically important materials used in nuclear reactors

Apart from nuclear fuel there are many other technologically important materials also which are used in nuclear reactors e.g. cladding materials, coolants, moderators, reflectors, control rod, structural materials etc. The cladding is an important component of nuclear reactor. The pellets are enclosed in a metallic cladding tube which contains fission products during fission reaction, ensures mechanical support for the pellets, and allows the exchange of heat generated by the nuclear fission reaction to the coolant fluid. There are many parameters for the selection of cladding materials for the reactor e.g. neutron absorption cross section, maximum service temperature, creep resistance, mechanical strength, toughness, neutron radiation resistance, thermal expansion, thermal conductivity and chemical compatibility with fissile products and coolant, moderator and fuel materials [18]. Different types of cladding materials depending upon the type of reactors are used. The aluminum and its alloy have been used as cladding materials in different research reactors. Al is a corrosion resistant metal with a relatively low neutron absorption cross section. Zirconium also has good corrosion and radiation resistance property with very low neutron absorption cross section. It is used in form of its alloys called zircalloy as cladding materials in most of the nuclear reactors. Several types of zircalloy are reported depending upon the composition of the alloying elements. Zircalloy-2 is used in boiling water reactors (BWR), while for PHWR; zircalloy-4 is used. Zr-Nb alloys are used as pressure tubes of PHWRs. Nb present in Zr-Nb alloy increases the mechanical strength of the cladding [19-21]. In FBTRs and PFBRs using fast neutrons for fission reactions, stainless steel is used as cladding materials. Moderator and coolant are also very important components of nuclear reactors. The neutrons emitted from the fission reaction are of very high kinetic energy (2 MeV) and these neutrons must be slowed down to the thermal energy level (0.025 keV) for an efficient

fission reaction. Thermal neutrons have larger effective neutron absorption cross section than fast neutrons to induce further fission and to maintain a sustainable chain reaction. For this reason fast neutrons has to be slowed down to cause the fission, especially where natural uranium is used as nuclear fuel. The materials that are used to slowdown the energy of the fast neutrons are called moderators. Moderators are also technologically important materials. A good moderator should have high value of neutron scattering cross section and low neutron absorption cross section. Generally H_2O and D_2O are used as moderators. Water has higher neutron absorption cross section than heavy water and that's why reactor which uses H_2O as moderator has to use enriched UO_2 to compensate the neutron loss [22]. Coolant is another important material for nuclear reactor. It is used to transfer the heat generated during nuclear fission from clad to the steam generator. Different types of coolants are used in different types of reactor according to their operating conditions. FBTR uses liquid Na as coolant. In PHWRs, D_2O is used both as coolant as well as moderator. BWR uses light water as both coolant and moderator. The coolants should have good thermal conductivity, low neutron absorption cross section and it should be chemically compatible with fuel, clad and other structural materials.

In addition to above main technologically important materials, there are other technologically important materials used in the nuclear reactors e.g. reflectors, control rods etc. Reflector is used to minimize the loss of neutrons through leakage. These materials reflect back the neutrons and these neutrons will propagate the fission process. Pure water, heavy water, beryllium, graphite etc are used as reflecting materials. Control rod is a very crucial material to control the fission process. These control rods are made of those elements which have high neutron absorption cross section. Elements like boron, cadmium, samarium, gadollium etc or

their alloys are used as control rod materials. Figure 1.2 shows the different component of nuclear reactors which are technologically very important materials [23, 24].

One of the important parameter considered for the use of above technologically important materials in nuclear industry is purity of the above materials in terms of presence of trace elements in them.

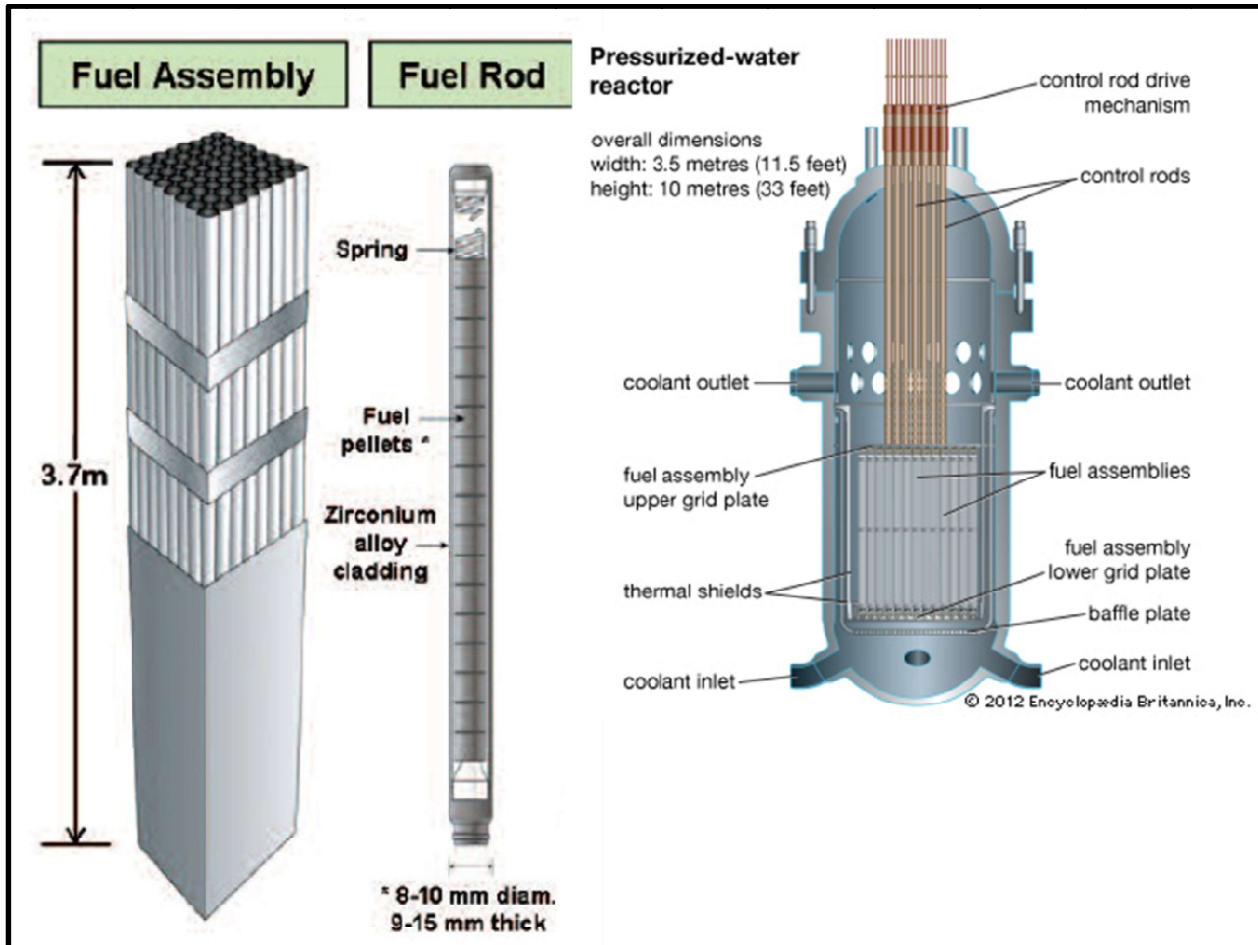


Figure 1.2: Different components of nuclear reactors: [ref-23, 24]

1.2. Relation between technology and environment

Technological advancement made human life very much comfortable. Technology helped to accelerate the production of many goods which are very much necessary for the growth of trade and commerce, created globalization of the industries and exchange of knowledge.

However there are some negative impacts of this technological advancement on natural environment. The air, soil and water get certain degrees of pollution, get degraded and contaminated as the human progresses in technology.

There are some technologies which deal with the burning of fossil fuels and thereby create huge pollution. The power plants which run on coal are a major contributor to air pollution as well as contamination of our lakes and river systems and natural water bodies. Highly toxic metals such as mercury, lead etc are released from these plants which harm different creatures residing in the lakes or oceans. The fertilizers, used in our field contaminate the soil due to the presence of harmful chemicals containing elements like arsenic, cadmium, lead and uranium etc. Presences of these elements pose risks to the health of grazing animal, human population by contaminating food and soil. There are some industries in India; which manufacture harmful insecticide and discharge the industrial effluents in the soil because of which ground water has been found to be contaminated with arsenic [25, 26]. Semiconductors are very essential technological material in present age which has changed the human life rapidly due to its various types of applications in computers, televisions, and electronic devices. These industries use toxic metals of the IIIA, IVA, and VA families, including gallium (Ga), indium (In), and arsenic (As). These elements are very toxic and can cause carcinogenesis in animals and humans if consumed. Symptoms of acute poisoning like gastrointestinal problem, vomiting, unconsciousness, and sometimes death usually occurs within 30 min of intake of GaAs and InAs. Arsenic has been classified by International Agency for Research in Cancer (IARC) as a Group I carcinogen [27]. World Health Organization (WHO) and Environment Protection Agency (EPA) strictly recommended that the concentration of arsenic in drinking water should remain in the range of 5-10 ng/mL [28, 29].

Fluorine is another very harmful element for the environment. Fluoride contamination of the environment occurs through natural presence of it in the earth's crust and industrial activities, especially semiconductor, glass, steel, ceramic and fertilizers industries. Fluorine compounds are technologically and industrially important and are extensively used in semiconductors, fertilizers, aluminum industries, and nuclear applications [30]. Toxic wastes containing fluorine/fluoride are generated in all industries using fluorine or its compounds as a raw material. Although different industries use very rigorous treatments before discharging the effluent, still some amount of fluorine is being released to the environment. Some amount of fluorine is required in tooth paste for treatment of dental cavities, but its presence more than that can cause detrimental effects to human health. In excess of 1.5 to 2.0 mg/L fluoride in drinking water is known to cause permanent gray or black mottling of teeth enamel and the long-term intake of 3 to 10 mg/L may result in abnormal bone growth in both humans and animals. The WHO limit of fluorine in drinking water is 1.5 mg/L [31].

Chromium is another element which has widespread industrial applications; hence, large quantities of chromium are discharged into the environment. There are many industries which causes chromium contamination in water like mining, leather tanning, dyeing, etc. Many chemical factories also use chromium [32]. Cr (VI) has very high solubility in water and it can spread easily to all natural water bodies. Due to this reason it is designated as class-A carcinogenic species. Thus we can see that trace elements concentration monitoring is very much essential for the clean environment, food materials, drinking water and thereby a better human health.

1.2.1. Environmental aspect of nuclear technology

It is very important to monitor the different environmental aspects of energy production plants. Nuclear energy is considered to be a clean energy which does not emit fly ash or produce green house gases to the environment as compared to the fossil fuel based power plants, but the radioactivity from the products of the nuclear fission can cause some damage to the environment if it is spread to environment due to any nuclear accidents [33]. The spent nuclear fuel contains different carcinogenic radionuclide isotopes such as Sr^{90} , I^{131} and Cs^{137} , and also includes very long-lived trans-uranic elements like Am^{241} and different isotopes of plutonium. So it is very important to dispose these wastes in some special facilities or in repositories which should be located very deep underground in suitable geologic as well as chemical formations. Radioactive effluents released from nuclear power plants have to be monitored and controlled to reduce exposure of the public [34]. These radionuclide can migrate into the environment. The spent nuclear fuel contain significant amount of fission products as well as actinides. It is very important to know their amounts to have an idea about the outcomes of release of these elements at any time during the transportation from one place to another. The nuclear waste management is also very important from environmental perspective. India has closed fuel cycle programme where most of the spent fuel is reprocessed, but some amount of nuclear waste is deeply buried in repositories. Uranium di-oxide is the main component of nuclear fuel in most of the nuclear reactor and it is considered to be the safest chemical form for disposal purposes because of the low solubility of U (IV) over a wide range of environmental conditions. In contact with air, UO_2 quickly undergoes to surface oxidation even at room temperature. To avoid the risk related to the release of radionuclides to the environment during the disposal of nuclear waste, U_3O_8 is often recycled to spent nuclear oxide fuel [35, 36]. The environmental impacts associated with

uranium mining can be classified into impact on land and water (through soil and waste water arising from mine drainage and/or from water used in drilling) and occupational health hazards. It should be noted that the environmental impacts and occupational hazards associated with coal mining (to operate a 1000 MWe plant), is more significant than those associated with uranium mining (to operate a plant with the same capacity).

1.3. Importance of trace elemental characterization in nuclear and environmental samples

1.3.1. Trace elemental characterization in nuclear fuel samples

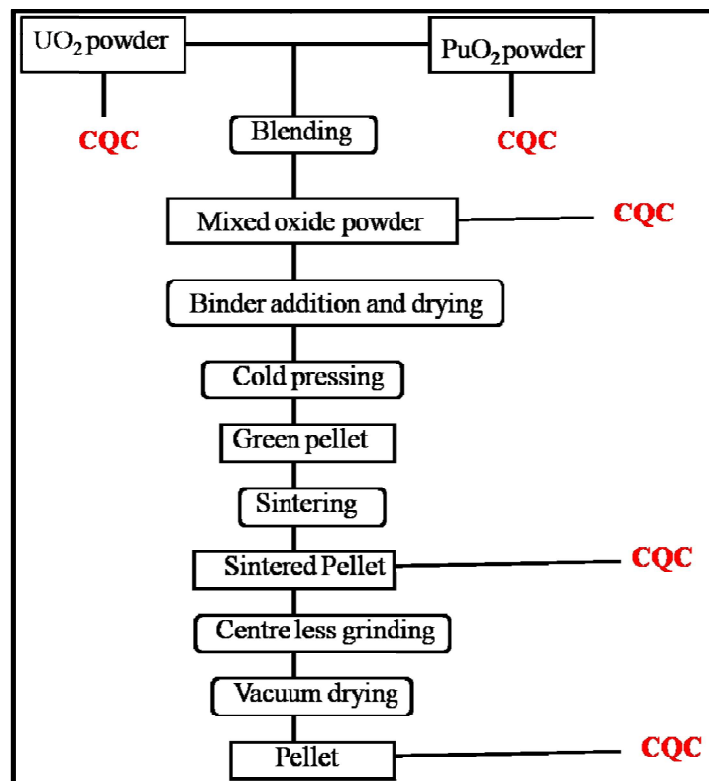


Figure 1.3: Different steps involved during fuel fabrication by Powder Metallurgical Compaction route, CQC: Chemical quality control

As stated before, trace element determinations as well as chemical characterization are very important steps for the quality control of fuel which is the heart of the reactor. Starting from mining, till, the fuel material goes through a series of wet chemical processes which include dissolution (in nitric acid), purification by solvent extraction and precipitation. Finally the

fabrication of fuel also involves many steps like enrichment, grinding, pelletization etc. During these fuel fabrication procedures the fuel can get contaminated with various types of trace impurities. These impurities may behave in different manners during fuel irradiation and may cause different types of adverse effect on safety and efficient operation of the reactor. For the efficient operation of a reactor; each fuel batch has to be subjected to comprehensive chemical quality control for trace constituents, and its stoichiometry. A flow chart for preparation of mixed oxide fuel using Powder Metallurgical Compaction route is given in Figure 1.3.

1.3.1.1. Effects of trace constituents

An efficient nuclear fission occurs only with fissile isotopes like ^{233}U , ^{235}U , and ^{239}Pu . During nuclear fission many fission products are formed inside the reactor fuel, making the fuel very heterogeneous in nature. Before putting the nuclear fuel in a reactor, it has to be as pure as possible. But practically some impurities always come during the fabrication of the fuel as described in Figure 1.3. So there is a stringent limit of these impurities, which can be tolerated for safe and efficient operation of the reactor. As different impurities behave in different manners during fuel irradiation, different specification limits are prescribed for the different fuels for the safe operation of the reactors. Neutrons are the primary particles causing nuclear fission, so neutron economy is of utmost importance. They should not be absorbed by any other impurity elements present in the reactor system and thus causing the loss of neutrons and reducing the fission rate. Elements like B, Eu, Gd, and Cd have very high cross section for neutron absorption. So it is utmost important to control their amount while fabricating the fuel pellets [37]. Some halogens like fluorine and chlorine are very corrosive and it is very important to keep these elements concentration in the fuel and other components within the specified limits. Even at very low concentrations, they can lead to de-passivation of the oxide film on the surface of the

clad, thereby leading to corrosion of the cladding material. In presence of moist environment in nuclear reactor the corrosive effect become more prominent as they will form their corresponding acids on reacting with the moisture [38]. Carbon can react with oxygen and will form gaseous carbon monoxide, which facilitates transfer of carbon from fuel to clad and cause carburization of it [37]. Sintering of the fuel pellets are carried out in inert hydrogen atmosphere. If sulphur is present in the fuel above specific limits, it can form H_2S during sintering and the pressure of it can break the pellets onto pieces [39]. Hydrogen content in nuclear fuel is also a very important parameter that has to be controlled. It can lead to damages (“sunbursts”) of the zircaloy cladding tube. This point is of main importance in the case of the nuclear fuel cladding tubes of the pressurized water reactors (PWR), which are the first confinement barrier, preventing the release of radioactive materials in the water of the primary circuit [40]. Low Z impurities like nitrogen should also be present below some specific limit because it can produce ^{14}C by neutron reaction $^{14}N (n, p) ^{14}C$ and affects the reprocessing process for the spent fuels [41]. Nuclear fuel during reactor operating condition is a very complex system. During nuclear fission, very high temperature is reached and many trace impurities present in the nuclear fuel at this elevated temperature and in presence of liberated oxygen can cause detrimental effect on the performance of the fuel. As an example Zn is a low melting metal and if this impurity present in nuclear fuel beyond some specific amount, it can cause liquid metal embrittlement. On the other hand refractory elements such as tungsten, molybdenum and tantalum may cause “creep resistance” and resulting damage of clad [42-43]. Low Z elements like sodium, magnesium and aluminium, if present in the nuclear fuel in amounts higher than the specified levels, can reduce the fissile material density and form appreciable amounts of uranates of these elements with uranium in lower and higher oxidation states in reactor operating and transient conditions,

respectively. These uranates being comparatively low density may cause expansion of fuel volume and pressurizing the clad leading to rupture of it. Hence quantifying these elements is very necessary. Presence of iron and nickel in high concentration leads to problem in sintering of the fuel, which is required to increase the fuel density for higher power production. Table 1.1 shows the specifications of different trace impurities in typical thermal and fast reactor fuels.

From Table 1.1 we can see that the trace impurities can be low, medium or high Z elements. Presence of each of these elements beyond the specified values can cause detrimental effect during the reactor operating condition.

Table 1.1: Specification limits of different trace impurities in typical thermal and fast reactors fuels.

Trace impurity	Thermal reactors (ppmw)			Fast Reactors (ppmw)		
	UO ₂	PuO ₂	(U,Pu)O ₂	UO ₂	PuO ₂	(U, Pu)O ₂
B	0.3	2	1	0.3	2	2
C	200	200	200	200		
N		100	100		100	100
F	10	25	10	10	25	
Na			400			100
Mg	50	200	200	10	200	50
Al	25	250	400	25	250	500
S	3	250	300	30	250	800
Cl		25	15			
Ca	50	500	250	50	500	100
V			400			100
Cr	25	200	400	15	200	300
Mn	10	100	400	10	100	200
Fe	100	500	400	100	500	1000
Co		25	75		25	200
Ni	20	200	400	20	200	500
Cu	20	50	400	10	50	100
Zn		200	400		200	100
Zr						100
Mo	4	200	400	2	200	200
Ag	1	10	25	1	10	20
Cd	0.2	6	1	0.2	6	1
Gd	0.1		1	0.1	1	
Dy		1				
W					200	200
Pb		200	400		200	200
²⁴¹ Am		2500			2500	

1.3.1.2. Characterization of oxidation behavior in nuclear fuel

Uranium dioxide (UO_2) is the main component of nuclear fuel in most of the power reactors. For many years scientist have done a lots of studies regarding the stepwise oxidation of UO_2 in air to form U_3O_7 and U_3O_8 due to its relevance of dry storage and disposal of used nuclear fuel as well as UO_2 powder storage. There are many important aspects of oxidation process of uranium oxides that are not yet fully understood. The oxidation of UO_2 is a two steps reaction: $\text{UO}_2 \longrightarrow \text{U}_3\text{O}_7/\text{U}_4\text{O}_9 \longrightarrow \text{U}_3\text{O}_8$

Uranium dioxide has fluorite type structure. The intermediate oxides like U_4O_9 and U_3O_7 result due to placement of oxygen atoms in the unoccupied interstitial sites of fluorite type UO_2 lattice structure accompanying with displacement of neighboring uranium sites. On the other hand U_3O_8 has totally different types of crystal structure. U_3O_8 has 38% more volume than UO_2 . So this volume expansion can potentially damage the first confinement barrier (also known as fuel cladding) in the case of direct storage of fuel elements. The phase of U_3O_8 occurs as an end product not only with UO_2 as a starting material but also when other nuclear fuel sources like U di-carbides and U hydrides are used. The conversion of UO_2 to U_3O_8 involves a complex conversion of uranium oxidation states. So a complete knowledge of the kinetics and mechanism of U_3O_8 formation is needed to determine the upper limit temperature of the air storage of used nuclear fuel [44-45]. In addition, the definite knowledge of oxidation state of uranium in uranium oxide fuel is very much essential.

1.3.2. Trace elemental characterization in environmental samples

It was discussed previously how the technological development added the byproduct like different harmful carcinogenic elements into the environment. So it is also necessary to characterize those trace elements to monitor and control their concentrations in the environment.

Water is one of the essential ingredients of environment. We get water from several sources like rivers, lakes, glaciers etc. In spite of such abundance, there is a shortage of drinking water all over the world. Water contamination can occur due to, chemicals, heavy metals, pesticides, water disinfectants etc. These are the byproducts of industrial as well as agricultural activities. The regular deposition of these carcinogenic byproducts into natural water has become a threat to human health in several regions of world. There are some organization like World Health Organization (WHO), Indian Standard Institution (ISI), Central Pollution Control Board (CPCB) and Indian Council of Medical Research (ICMR), which are regulating the concentrations of different chemicals in water and they have given a permissible limit of different elements in drinking water which is given in Table 1.2. The concentrations of those elements should not go beyond these limits [46].

Table 1.2: Permissible limits of different elements in drinking water prescribed by different authorities

Elements	USEPA (mg/mL)	WHO (mg/mL)	ISI (mg/mL)	ICMR (mg/mL)	CPCB (mg/mL)
Fe	-	0.1	0.3	1.0	1.0
Cl ⁻	250	200	250	1000	1000
NO ₃ ⁻	-	-	45	100	100
SO ₄ ²⁻	-	-	150	400	400
Ca	-	75	75	200	200
Mg	-	50	30	-	100
Cu	1.3	1.0	0.05	1.5	1.5
F ⁻	4.0	1.5	0.6-1.2	1.5	1.5
Hg	0.002	0.001	0.001	0.001	No relaxation
Cd	0.005	0.005	0.01	0.01	No relaxation
Se	0.05	0.01	-	-	No relaxation
As	0.05	0.05	0.05	0.05	No relaxation
Pb	-	0.05	0.10	0.05	No relaxation
Zn	-	5.0	5.0	0.10	15.0
Cr	0.1	-	0.05	-	No relaxation

Arsenic is one of the very toxic elements and arsenic contamination in ground water is a worldwide problem, especially in countries like India, Bangladesh, and China. Contamination of

arsenic in drinking water causes several diseases like skin diseases, cancer, blood circulation disorder etc. Fluorine is an element which is essential for us up to certain amount but in large concentrations in drinking water, it becomes harmful. Fluoride concentrations above 1.5 ppm in drinking water cause dental fluorosis and much higher concentration causes skeletal fluorosis.

The surface water may contaminate with chlorides due to rocks containing chlorides, pesticides, chemical waste from industries, and water treatment plants. Chlorides have very high corrosive property. In presence of high concentration of chloride in water; fish and other aquatic animals cannot survive. Elements like Pb, Hg, and Cd are extremely poisonous for human health and they should not be present in drinking water. So it is utmost important to determine the concentrations of these elements at very trace level.

In addition to determination of concentrations, it is very necessary to determine the oxidation states of the elements in environmental samples also. It is well known that extent of toxicity is dependent upon the oxidation states or the chemical forms of different elements. For example arsenic has both organic and inorganic form, but inorganic arsenic species are more toxic than the organic one. Inorganic arsenic also has two types of oxidation states i.e. As^{+3} and As^{+5} ; among them As^{+3} is much more toxic than As^{+5} . Similarly chromium also has two stable oxidation states e.g. Cr^{+3} and Cr^{+6} . Now Cr^{+3} is necessary for proper functioning of living organism; on the other hand Cr^{+6} is very much carcinogenic and toxic due to its capability of oxidizing other species including DNA.

1.4. Techniques used for the trace elemental characterization and their limitations

There are many techniques available now days for the trace and ultra-trace characterization of different technologically important and environmental samples. During these

characterizations many elements with different atomic numbers have to be determined at trace and ultra trace level in different type of matrices. Due to this reason; the method required should have multi-elemental analytical capability, very good detection ability and at the same time it should be economical.

Atomic absorption spectroscopy (AAS) is one of the routinely used methods of elemental determinations. However, it is single element technique requiring different lamps for different elements. The electro thermal AAS (ET-AAS) is another method which has capability to determine elements at ultra trace level, but this technique is also single elemental technique. The calibration procedure using standard addition method is also very laborious. Inductively coupled plasma optical emission spectroscopy (ICP-OES) is another popular method for trace elemental determination. It is a multi-elemental analytical technique; but requires a few mL sample volume. Several laser spectroscopy based techniques are also used now days for the trace elemental characterization, based on absorption, fluorescence or ionization of a cloud of atomic vapor by using strong laser. Although the detection limits obtained by such techniques are very low (fg level); but they are very costly and yet to be fully developed. There are some other highly developed and well established powerful techniques for the trace elemental analysis e.g. instrumental neutron activation analysis (INAA) and inductively coupled plasma mass spectrometry (ICP-MS). INAA is a nondestructive method in principle and direct analysis of solid samples can be done without any sample preparation. But this technique requires a nuclear reactor and it is not suited for solutions as it is forbidden to irradiate solutions as safety precaution. ICP-MS on the other hand is a destructive technique where the sample has to be fully dissolved. The matrix also has to be removed before analyzing the samples by ICP-MS and concentrated solutions have to be diluted before analyzing by ICP-MS. Both ICP-MS and INAA

need large sample amount. There are also limitations of analyzing some elements in these techniques. ICP-MS cannot determine elements like N, O which are introduced by the air in the plasma. For elements like F, P, S the ionization by using plasma is very difficult. The main advantage of ICP-MS is its capability to distinguish and analyze different isotopes of elements which are not possible by many analytical methods. Very high degree of reliability can be achieved by this method but the calibration procedure is very laborious. Moreover severe spectral interferences and memory effect are the problems of this technique. Neither matrix effect nor memory effect is present in INAA; but this technique is time consuming as large time is needed for the irradiation of the sample. Moreover this technique is very costly as it requires high neutron flux which is available only in reactors.

An ideal technique for the characterization of nuclear materials especially nuclear fuel should have the following qualities:

1. Multi-elemental analytical capability
2. Very simple and fast
3. Should be non-destructive/consumptive
4. Very less amount of sample should be sufficient for the characterization
5. Should cover almost all the elements in the periodic table
6. It should be economical

Total reflection X-ray fluorescence (TXRF) spectrometry is a variant of XRF and has emerged out to be a very promising technique to fulfill all of these requirements, due to which it has attracted the attention of analytical scientists all over the world in recent years [47].

1.4.1. Comparison of TXRF with other trace element analytical techniques

Table 1.3 compares TXRF spectrometry with other well established trace elemental analytical techniques like ICP-MS, ICP-AES, INAA and Electro analytical techniques in terms of the of sample characteristics, detection limits, quantification procedure, cost etc. From this comparison it can be said that TXRF is very much suitable for the characterization of nuclear as well as environmental samples. The detection limits obtained by using this technique are comparable with other well established analytical techniques. It also has multi-elemental analytical capabilities. It can determine elements from C-Pu in the periodic table including metals and non metals. So the elemental range of this technique is larger than any other technique. The running cost of this technique is also very low. The matrix effect associated with this technique is negligible so one need not to use matrix matched calibration standards. One single element standard can be used to determine all the elements in different type of samples using predetermined sensitivity values. This reduces the tedious calibration procedure compared to the other techniques like ICP-MS, AAS, and AES etc. The sensitivity values for the elements whose standards are not available can be determined by interpolation. The main advantage of this technique is the requirement of very small amount of sample (ng level); which is very advantageous for the analysis of radioactive, biological, forensic as well as precious samples where one cannot use more amount of samples for the analysis purpose [48, 49]. Moreover while analyzing technologically important nuclear samples having elements like uranium, thorium or plutonium etc. which are highly radio-toxic it is always desirable that the sample amount needed for the analysis should be minimum, so that the radioactive dose to the analyst as well as the radioactive waste generation will be very low and complicated procedure of radioactive waste management can be avoided.

Table 1.3: Comparison of TXRF technique with all other well established trace elemental analytical techniques

Analytical features	ICP-MS	TXRF	INAA	ICP-AES	ET-AES	Electro-analytical
Samples						
Volume or mass	2-5 mL	2-10 μ L	10-100 mg	2-5 mL	5 μ L	2-5 mL
Preparation of samples	Digestion or suspension	Digestion or suspension	None	Digestion or suspension	Digestion or suspension	Digestion or suspension
Dissolution portion	<1%	<0.4%	any	<0.4%	-	-
Dilution of acids	1:100	Not needed	none	-	-	-
Consumption	Yes	No	No	Yes	Yes	No
Detection						
Detection limits	Excellent	Very good	Very good	Moderate	Very good	Very good
Elemental limitations	H, C, N, O, F, P, S	Z < 6	Z < 9; Tl, Pb, Bi	Non-metals	Refractory elements	-
Spectral interference	Several	Few	Few	Moderate	None	None
Isotope detection	Yes	No	No	No	No	No
Quantification						
Calibration	Many standards	Only one standard	Pure element foil	Many standards	Standard for each elements	-
Matrix effects	Severe	None	None	Moderate	Moderate	Moderate
Memory effects	Yes	No	No	Yes	No	-
Measuring time	<180 seconds	~5-15 minutes	20 min-30 days	~300 seconds	~ 300 seconds	~ 1000 seconds
Expenditure						
Capital cost	Medium	Medium	Very high	High	Low	Low
Running cost	High	Low	High	High	Low	Low

TXRF has another advantage over other techniques due to its ability to do speciation in trace level in combinations with XANES (X-ray absorption near edge spectroscopy). So for environmental samples or radioactive samples where only small amount of sample is available; one can still do both quantification as well as speciation studies using TXRF in combination with XANES. The main limitation of TXRF is the impossibility of totally non-destructive analysis,

limitations for volatile liquids and high matrix content samples and restriction to flat, smooth and highly polished surface.

1.5. Application of TXRF for the analysis of technologically important and environmental samples

Due to the simplicity, multi-element capability and detection power, TXRF is highly suitable for the analysis of technologically important materials which have very high industrial applications. This method is very much helpful for quality control of ultra pure materials needed for electronics, cosmetics and pharmaceutical industries. High purity grade acids, bases and solvents including high purity water samples can be analyzed down to ppb level. Polished wafers are very important materials for semiconductor devices. Since they are optically flat and polished they are ideally suited for the characterization by TXRF. Most of these studies are on Si-wafers [50-52]. The thin layer structure which is single or double layer has made off pure metals, metal alloy, metal oxides or nitrides have several technological applications. X-ray reflectivity (XRR) together with grazing incidence X-ray fluorescence (GIXRF) measurements can be used as a sensitive probe to evaluate depth-resolved micro structural parameters of a buried layer inside those multilayer structures [53]. Nano-particles are also very important materials having several applications in medicine, pharmacy, material science etc. Chemical characterization of these very fine fractions of nano-particles on surfaces can be deduced from experiments using the grazing incidence X-ray Standing Waves (XSW) by means of Total Reflection X-ray Fluorescence (TXRF) [54]. As discussed earlier that nuclear materials especially nuclear fuel is a highly important technologically important material and there are some studies reported to characterize it by TXRF, a more detail study shall be beneficial for characterization of nuclear fuel for trace elements present in them.

There are many avenues to beneficially exploit TXRF in the field of environmental studies for the pollution control as well as protecting human life. This technique is very much suitable for ultra trace determination in high purity water samples such as rain water, drinking water etc. TXRF is also very efficient for the analysis of airborne particulate matter. This air sample can be collected on flat polished surface of quartz support and then can be directly analyzed. In addition it can do elemental speciation with ultra trace elemental concentration level as stated earlier.

1.6. Improved sample preparation methodology for the chemical characterization of trace elements using TXRF

Sample preparation is one of the very important steps in analytical sciences. TXRF technique in combination with better sample preparation methodology can be applied very successfully for the trace elemental characterization of nuclear fuel as well as environmental samples. In presence of high Z matrix uranium, plutonium or thorium; it is mandatory to separate this matrix before trace analysis. The use of improved separation methodology in combination with TXRF will make the procedure very simple and will generate less organic waste. Making the main matrix separation methodology very simple will be much helpful for the trace elemental analysis in highly radioactive samples. Not only the separation, but the improved sample deposition methodology will also be helpful for the characterization of environmental as well as nuclear material. Development of solid phase extraction methodology in combination with TXRF technique can be very helpful for matrix separation as well as pre-concentration and speciation studies of different environmental samples and has been studied in this work.

1.7. Scope of the thesis

In view of the preceding discussions, it is now clear that TXRF has many advantageous features for nuclear and environmental samples for trace elemental determinations as well as speciation studies. As very small amount of sample is needed in TXRF for the characterization of the materials and it has capability to probe trace and ultra trace elements, this technique is very much suited for the analysis of radioactive nuclear materials and environmental samples for the elements present at trace level for their determination as well as speciation. The speciation studies can be done using XANES measurements in TXRF mode. Different mixed valent uranium oxides are used as fuel in nuclear reactors. Knowledge about the oxidation states of uranium in these oxides and other compounds of uranium is very important to understand the properties of these compounds essential to use them for different applications e.g. fuel production, spent fuel reprocessing, magnetic and electrical properties etc. with requirement of a very small amount of sample. TXRF can play an important role in such studies for elemental and oxidation state determinations with minimum amount of sample required and minimum sample preparation. However, there are not much studies reported for such applications of TXRF i.e. trace determinations and elemental speciation of nuclear fuel and other structural materials. Due to above reasons, it was decided to explore the applications of TXRF for trace elemental determination of low, medium and high Z elements with improved sample preparation and introduction methodologies in nuclear technologically important materials. Studies were also made for trace elemental speciation in uranium based samples in a non destructive manner. In view of the possible applications of such studies for environmental samples, the features of TXRF were applied for elemental speciation and determinations in environmental samples. The scope of thesis may be categorized as:

1. Studies on improved approach for TXRF trace elemental determination of low, medium and high Z elements in nuclear materials using better instrumentation and sample introduction methodologies.
2. Extension of the above studies to the real plutonium based samples.
3. Uranium speciation in nuclear fuel samples using TXRF –XANES in non destructive manner.
4. TXRF based elemental speciation and trace elemental determinations using improved sample preparation, pre-concentration and introduction methodologies for societal benefit applications.

Chapter 2

Theory and instrumentation

2.1. Introduction

The important analytical characterization parameters of different technological and environmental samples are:

- a. Determination of elemental composition in terms of trace and major elements
- b. Speciation studies

Several instrumental techniques are used for above purpose. X-rays are very important probe for the characterization of different types of materials. X-rays are electromagnetic radiations having wavelengths in the range of 0.01 to 10 nm, corresponding to energy in the region of approximately 100 eV to 100 keV. Since the days of discovery by German physicist Wilhelm Conrad Roentgen on 8th November 1895; X-rays are playing an important role in almost all areas of science like medical, material science, industry, Physics, Chemistry etc [55]. X-rays have properties like polarization, diffraction, reflection, refraction etc similar to the visible light. It can also ionize the gases.

X-rays can be produced mainly by two types of phenomenon. When electrons or any charged particles interact with some target material; they lose their energy in steps due to de-acceleration while passing through the columbic field of the nucleus of the target material. This types of phenomenon produces X-rays having energies in continuous range (zero to some maximum value which is the maximum energy of electron/charged particles), and are called '*Bremsstrahlung*' or '*continuous X-rays*'. On the other hand, when the energy of these electrons is so high to knock out one of inner cell electron of the target atom which becomes unstable and the atom starts emitting X-rays of specific energies, characteristic to the atom. These X-rays are called "Characteristic X-rays".

The emission of characteristic X-rays is the basis of X-ray spectrometry. There are many X-ray spectrometric techniques available for the characterization of technologically important and environmental materials. Most of these techniques are based on the scattering, absorption and emission properties of X-rays [56]. These techniques are XRF (X-ray fluorescence), XRD (X-ray diffraction), XAS (X-ray absorption spectroscopy), XPS (X-ray photoelectron spectroscopy) etc. Different types of information can be obtained using these techniques. For example XRF based techniques will give the information about the elemental composition in a material. Whereas XRD will give information about the crystal structure, different phases present in it as well as the average bond length in a crystal structure. X-ray Absorption Spectrometry (XAS) is another group of advanced X-ray spectrometric techniques giving the information about the oxidation states of the elements present and local structure like co-ordination number, bond length, local defects etc. XPS technique is very widely used for the determination of oxidation states, electronic states density of states and elemental composition. It is to be remembered that each technique has its own advantages and limitations. No technique is self sufficient for the full characterization of any material. Each of these techniques complements each other to obtain maximum information about any material [57-59].

XRF is one of the X-ray spectrometric methods having very high importance in the analysis of technologically important as well as environmental samples due to its simple instrumentation, non-destructive nature and multi-elemental analytical capability. Different industries routinely use this technique for bulk elemental analysis. One of the limitations of XRF is its poor detection limits compared to other well established analytical techniques like ICP-MS, AES, DC-ARC etc. TXRF (Total reflection X-ray spectroscopy) is another variant of XRF which is emerging as a very promising technique for the trace and ultra trace determination in different technologically

important and environmental samples; with an added advantage of requirement of very small amount of sample [60, 61]. TXRF combined with XAS can give simultaneously elemental concentration as well as oxidation states of the elements at very low concentrations. These features of TXRF are very useful in the study of technologically important and environmental samples. This combined technique is called TXRF-XANES (TXRF-X-ray absorption near edge spectroscopy). There are very few reports on this technique for the characterization of different types of samples [62, 63].

2.2. Interaction of X-rays with matter

When a beam of X-ray photon having wave length λ and intensity I_0 falls on a sample; having uniform thickness of d cm and density ρ g/cc, different types of phenomenon can occur. The final intensity of the transmitted X-ray photon can be expressed by the equation:

$$I = I_0 e^{-\mu\rho d} \quad (2.1)$$

Here μ is the mass absorption co-efficient of the absorber at some particular wavelength (λ). There is a loss of intensity of X-rays while passing through the absorber. A number of phenomenon e.g. photo-electric absorption, Rayleigh scattering and Compton scattering are responsible for that as shown in Figure 2.1 [64].

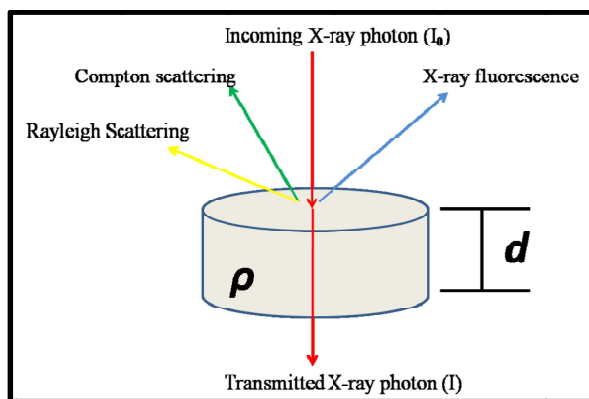


Figure 2.1: Different phenomenon occurring by e interaction of X-rays with matter

2.2.1. Photo electric absorption

In photoelectric absorption process photon of a particular sufficient energy is completely absorbed by the atom and an inner shell electron is ejected from it. An inner shell vacancy is created and the atom comes in an excited state. In order to stabilize the atom, electrons from outer shell fill up the vacancy thus formed and the atom immediately returns to the ground state by either emitting another electron which is called Auger electron or a characteristic X-ray photon. The latter process is called X-ray fluorescence. The ratio of the number of emitted characteristic X-rays photons to the total number of inner-shell vacancies created in a particular atomic shell is called the fluorescence yield of that shell (ω_K). For light elements ($Z < 20$), predominantly Auger electrons are produced during the relaxation upon K shell ionization ($\omega_K < 0.2$) while the medium to heavy elements are preferentially relaxing in a radiative manner ($0.2 < \omega_K < 1.0$). Photo electric absorption occurs only when the energy of X-ray photon is equal or greater than the binding energy of the electrons. For lower Z elements, Auger Effect is more prominent than XRF. The phenomenon of photo electric absorption is shown in Figure 2.2 [56].

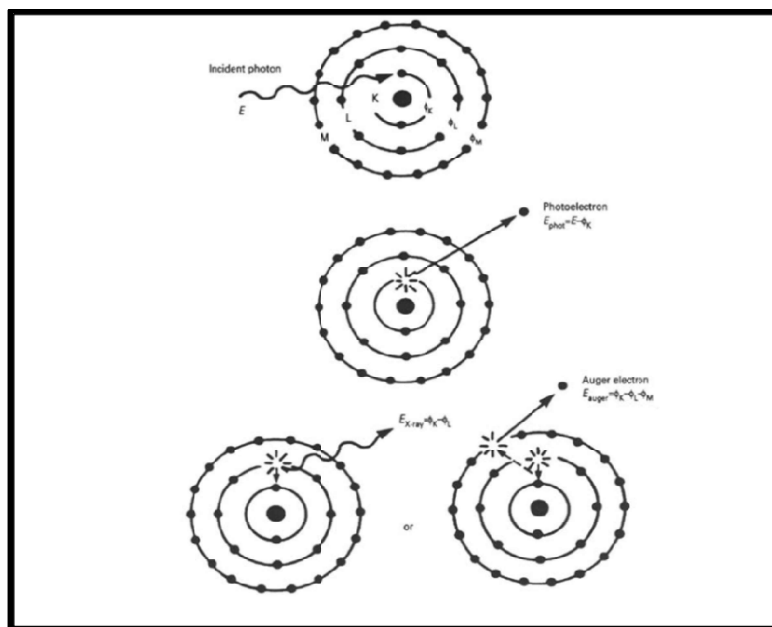


Figure 2.2: Photo electric absorption process

2.2.2. Scattering

A part of the incoming X-rays is scattered by the sample. Two types of scattering phenomenon can occur; 1) Compton scattering and 2) Rayleigh scattering. In Compton scattering the X-ray photon loses a part of its energy which is taken by the electrons and the energy of X-rays is reduced by this amount. This type of scattering occurs when X-rays interact with a loosely bound electron.

Another type of scattering is called Rayleigh scattering or elastic scattering, where X-ray photon interacts with strongly bound electron. After the collision of the X-ray photon with that electron, the electron stays in its shell but starts oscillating at the frequency of the incident X-ray radiation. Due to this reason the oscillating electron would emit electromagnetic radiation at the same frequency as the incoming radiation. This gives an impression that the incident X-ray is reflecting from the atom. Low Z elements have more no of loosely bound electrons, so they give more Compton scattering and high Z elements having more number of strongly bound electrons. These two types of scattering phenomenon are shown in Figure 2.3 [56, 64].

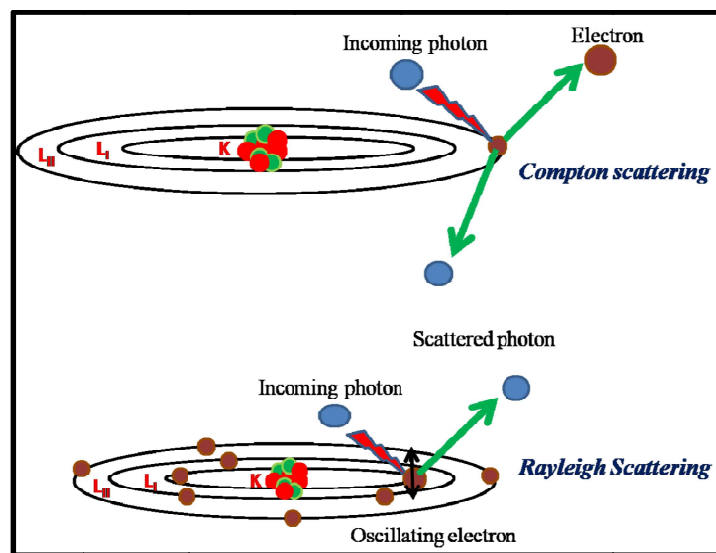


Figure 2.3: Compton scattering and Rayleigh scattering

2.3. X-ray Fluorescence (XRF)

XRF (X-ray fluorescence) is a powerful analytical tool for spectro-chemical determination of almost all the elements ($Z > 5$) present in a sample. The sample is irradiated with X-rays of sufficient energy to knock out the inner shell electrons and an electron vacancy is created. This vacancy creation makes atom unstable and subsequently the atom gets stable by filling this vacancy from outer shell electrons. Since an electron from higher energy shell comes to lower energy shell in this process, the energy difference of the electron in the two shells involved in transition is emitted in form of electromagnetic radiation. These energy levels differ for different elements hence the X-ray radiation emitted from different elements differ and are specific to that atom. Due to this reason these X-ray radiations are called characteristics X-rays of the elements. The wavelength of the characteristic X-rays and atomic number of the elements are related to each other, which is expressed by Moseley's law:

$$1/\lambda = k (z - \sigma)^2 \quad (2.2)$$

Here, λ is wavelength of characteristic radiation; z is atomic number of element, k and σ are constant which depend upon the spectral series. There is a relation between wavelength and energy of X-rays which can be expressed by the equation

$$\lambda \text{ (nm)} = 1.24/E \text{ (keV)} \quad (2.3)$$

X-ray analysis is mostly done in the range of 1-50 keV. The energy of X-rays emitted in XRF is characteristic of the elements whereas the intensities of the emitted X-rays depend upon the concentrations of the corresponding element. So both qualitative as well as quantitative information can be obtained using this technique. XRF analysis can be done up to approximately 100 μm below the surface layer of the sample. Different types of samples like solid, liquid, slurry material powder etc can be analyzed by this technique. The samples can be analyzed

nondestructively, which is very important advantage of this technique. Except low Z elements, all the elements having atomic number more than 11 can be analyzed by this technique in ambient atmosphere. For low Z elements special instrumental arrangement is required [65, 66]. This technique is sensitive up to ppm level and matrix matched calibration standards are required to obtain precise and accurate results. Due to the above features, this technique is very much helpful in different specific materials based industries for quality control, environmental monitoring, medical, geological and forensic laboratories [67-72]. There are two modes of XRF; EDXRF (Energy dispersive X-ray fluorescence) and WDXRF (Wave length dispersive X-ray fluorescence). From the name of these two methods we can understand that the basic difference between these two systems is their detection systems. In EDXRF, energy of X-ray is directly measured by the detector with the help of multi channel analyzer. In WDXRF, the X-rays emitted from the sample are dispersed by a dispersion crystal and wavelength/energy of each emitted X-rays is detected by the detector sequentially.

2.4. Production of X-rays

The sample excitation source in XRF is X-rays. There are many types of sources of X-rays, which can be used for X-ray spectrometric techniques which are used depending on the type of requirement. The three major sources of X-ray production used in XRF are X-ray tubes, radioisotopes and synchrotron radiation (SR) [73, 74]. X-ray tubes are the most common source of sample excitation used in laboratories .

2.4.1. X-ray tubes

X-ray tube is a vacuum sealed tube which converts electrical input power into X-rays. W. D. Coolidge in year 1913 proposed the basic design of the modern X-ray tubes [75].

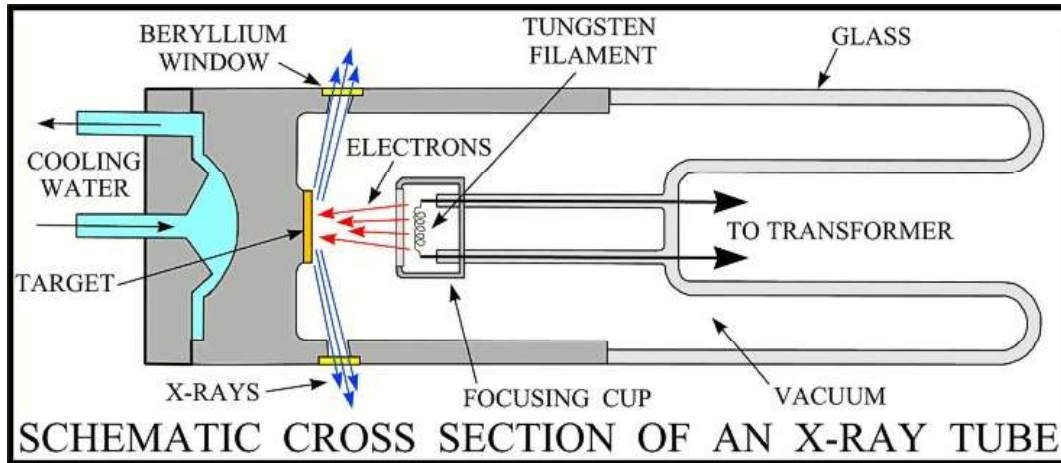


Figure 2.4: Schematic cross section of an X-ray tube.

Figure 2.4 shows the schematic cross section of an X-ray tube. There is a spiral filament in the X-ray tube which acts as cathode material. The X-ray tube also has a copper block which acts as anode. Both anode and cathode are sealed in an evacuated glass metal cylinder. The cathode is operated at high negative potential, while the anode is earthen. There is a coating of the actual anode material on copper block. The different anode materials used are Cr, Mo, W, and Rh etc; depending upon the requirement. When a current is passed through the filament, it is heated and emits electrons from it. These electrons are accelerated towards the target material by applying a huge potential between them. So the anode is bombarded with the electrons having very high kinetic energy. When the high energy electrons are stopped by the anode, they lose their energy either in steps or in one time. The lost energy is emitted as X-rays. However only 0.1% of the energy of the electrons is converted into X-rays and rest of the energy is dissipated as heat. So the target material gets heated very quickly and can melt down if left as such. To prevent this, a constant supply of cold water is required to cool down the anode. Now a day's low power X-ray tubes are used which use air cooling or Peltier cooling, instead of water cooling [76, 43].

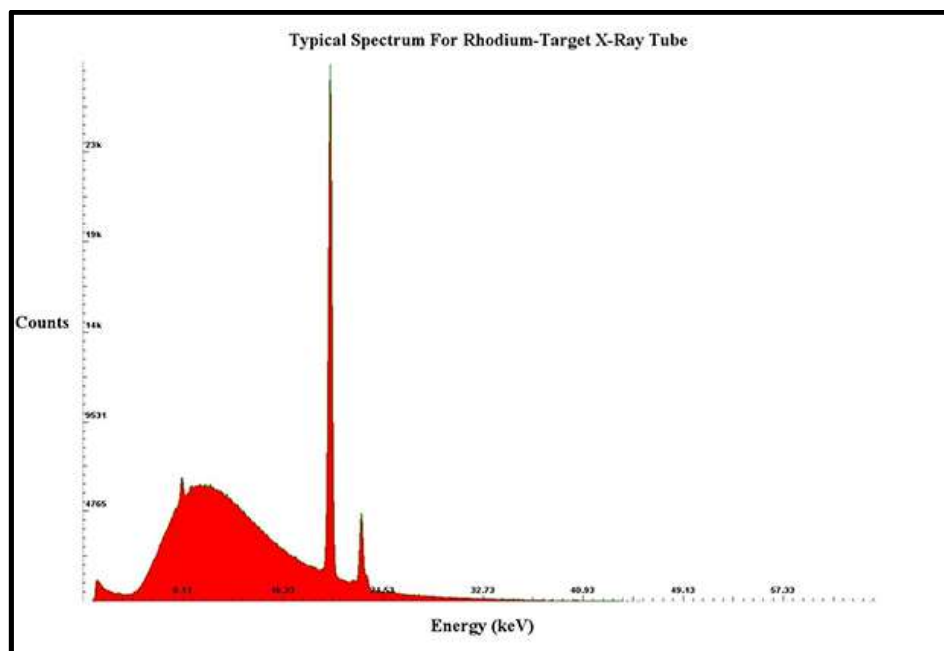


Figure 2.5: A typical tube spectrum using Rh as target material

Figure 2.5 shows a typical tube spectrum of Rh target X-ray tube [77]. The characteristic lines of the Rh target material i.e. Rh $K\alpha$ and Rh $K\beta$ are superimposed on Bremsstrahlung. In order to achieve better detection limits for different elements; Rh target is used in combination with filters or secondary targets. Depending upon the requirements different types of X-ray tubes are available. For example for the analysis of both low Z and high Z elements; dual target X-ray tube consisting of two separate targets are used. To obtain very high brilliance/intensity; rotating anode X-ray tube is used [66, 78].

2.4.2. Radioisotope sources

These types of sources are generally used in portable EDXRF spectrometer. There are mainly three types of mechanisms which are responsible for emission of X-rays by the radionucleolus. Radioisotopes which decay by γ emission may undergo internal conversion where the γ photon is absorbed by the atom and the energy is utilized to eject an inner cell electron. This

will create vacancies and electronic rearrangement takes place resulting in emission of characteristic X-rays. The other two ways to emit X-rays are β emission and orbital electron capture (EC). There are some advantages as well as disadvantages of using radio-isotopic X-rays sources. The advantages are; they are compact in size which is very useful for onsite measurements, they are very simple, in expensive [79]. The limitations of these types of X-ray sources are; 1) The output of these types of X-ray sources are very low compared to other types of X-ray sources, 2) The output decreases constantly with time depending upon the half-life of the radio-isotopic source. The energy and intensity of the X-rays obtained from a particular X-ray tube can be varied by varying the applied voltage and current. Thus X-ray tube based sources are much more flexible and versatile, but it is bit more expensive and complex in nature. Table 2.1 shows few radio isotopic sources [43].

Table 2.1: Different radio-isotopic X-ray sources

Radioisotope Source	Decay process	Half-life	Type of radiation emitted	Energy of X-rays emitted (KeV)
$^{129}_{53}\text{I}$	β^-	60 days	Xe $K\alpha$	29.8
$^{55}_{26}\text{Fe}$	EC	2.7 years	Mn $K\alpha$	5.9
$^{57}_{27}\text{Co}$	EC	270 days	Fe $K\alpha$	6.4
$^{210}_{82}\text{Pb}$	β^-	22 years	Bi $L\alpha$	10.8

2.4.3. Synchrotron based X-ray sources

Synchrotron Radiation (SR) based X-ray sources are most popular and advanced X-ray source being used now a day for advanced XRF and other X-ray related measurements. When electrons or any other charged particles are forced to move on a circular orbit at relativistic speed, they emit an electromagnetic radiation which is known as synchrotron light. There are

several synchrotron light sources in the world. These light sources consist of storage ring; which contain circular evacuated pipes. The electrons are forced to follow a circular path by strong bending magnets placed along the circumference of the ring. Before entering into the storage ring; the electrons are accelerated by a linear accelerator or 'linac' until their energy reaches to several MeV level and then they are made to enter in a booster ring that will boost the energy of the electrons from several MeV to GeV (Giga electron volt) level. After reaching this energy the electrons are finally transferred to the main circular ring. A schematic diagram of the SR source system is shown in Figure 2.6.

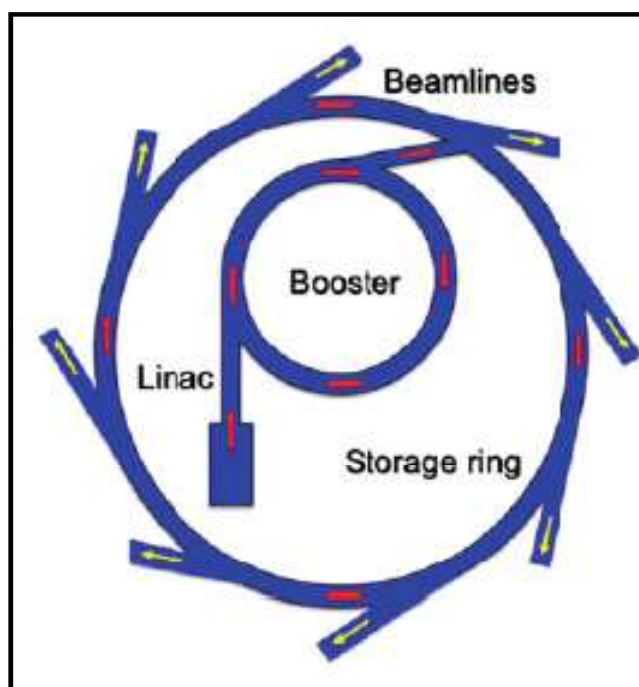


Figure 2.6: Schematic planar view of a synchrotron based light source

This synchrotron energy sources have very broad energy spectral distribution from infrared to hard X-ray region as shown in Figure 2.7. A suitable monochromator is needed to obtain X-rays of desirable energy to do XRF measurements. Generally double crystal monochromator (DCM) is used in such XRF beam-lines [80].

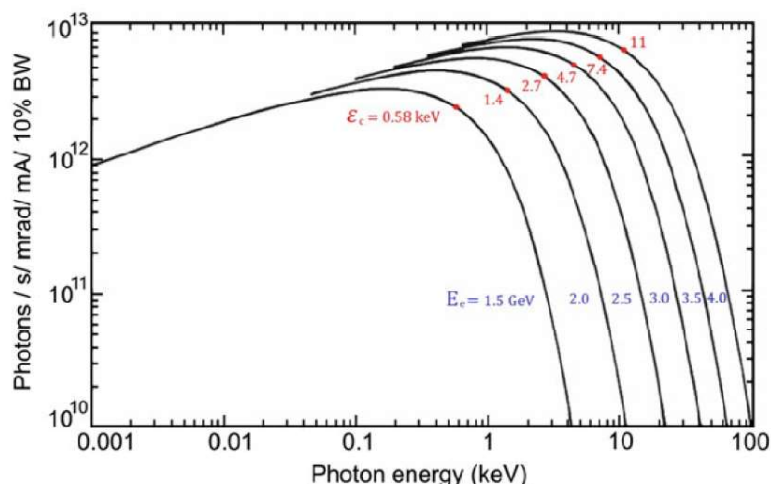


Figure 2.7: Spectral distribution of synchrotron radiation

There are many advantages of using synchrotron based excitation source for XRF measurements;

- a. Due to the very high spectral brightness of synchrotron based light source; the intensity of primary X-rays is many times of magnitude compared to that of conventional X-ray tubes. The brightness of synchrotron based light source in different generations SR sources (including free electron laser source [FELs]) is compared with that of a typical X-ray tube based X-ray source in Figure 2.8 [80].
- b. Since synchrotron based radiation covers a broad energy range of the X-ray spectrum, these are very much suitable for energy tuning. As discussed earlier a DCM is used to choose optimum excitation energy for any particular element. The ability to tune the energy is also very useful to do XAS measurements, which will give information about the speciation, local structure, bond length etc.
- c. During XRF measurements using lab based sources, one problem observed frequently is the scattering phenomenon, which increases the background as well as the detection limit. Synchrotron based radiation is 100% linearly polarized at the plane of the ring. To make use of this effect; the XRF experimental set up should be like as shown in Figure 2.9. In this figure the detector is placed in horizontal plane with its axis normal to the

synchrotron beam. With this type of arrangement; the scattered background will be reduced very much and we can reach to the lowest detection limit up to femto-gram level [81].

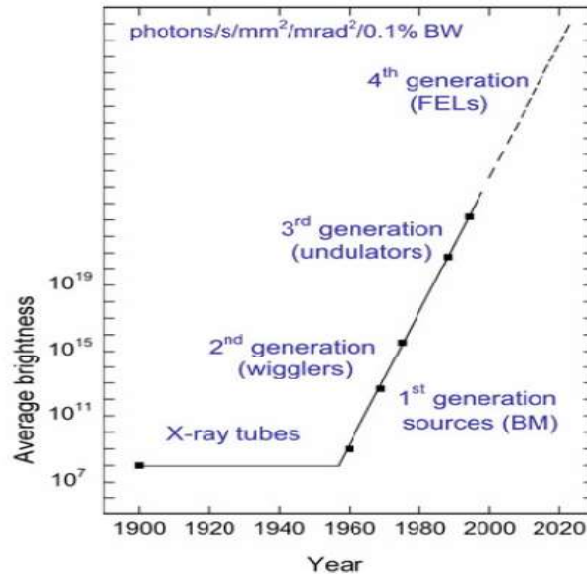


Figure 2.8: Comparison of average brightness of SR source of different generations with typical X-ray tube based X-ray source.

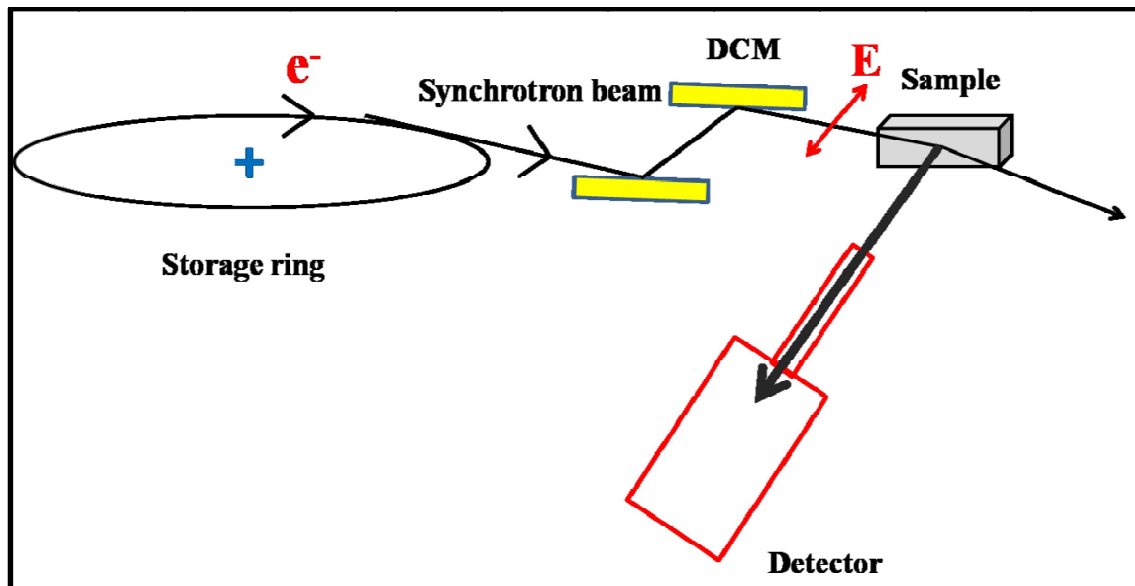


Figure 2.9: Arrangement of XRF measurement using synchrotron based radiation source

The only disadvantage of SR X-ray sources is its installation as well as maintenance cost which is huge compared to other conventional X-ray source.

2.5. Total reflection X-ray fluorescence (TXRF) spectrometry

The phenomenon of X-ray reflection was discovered by Compton in the year of 1923 [82]. He observed that the reflectivity of a flat polished surface increases many times when X-rays falling on it below some critical angle. In 1971, two Japanese scientists Yoneda and Horiuchi proposed that the use of total reflection of the X-ray beam on optically flat sample support can reduce the background drastically and also showed its application for XRF with much improved detection limits [83]. This variant of EDXRF is now known as Total Reflection X-Ray fluorescence (TXRF) Spectrometry.

The basic difference between EDXRF and TXRF is their geometry, which is shown in Figure 2.10. In EDXRF the X-rays falling on the sample at an angle of about 45° ; whereas in case of TXRF, the X-rays falling on the sample at very low angle of less than 0.1° and totally reflected from the surface of the sample. Because of this geometry in EDXRF; the X-rays penetrate deep into the sample and produce lots of scattered background. Due to this reason EDXRF has poor detection limit. In TXRF, due to the following reasons the detection limit is much lower compared to EDXRF;

- a. The primary beam falling on the sample at an angle less than the critical angle in the range of $< 1^\circ$ and getting totally reflected from the sample supports. So the incident X-rays do not penetrate into the sample supports. Due to this reason the scattered background is drastically reduced in this geometry and it leads to significant improvement in detection limit.

- b. Both the primary beam as well as totally reflected beam exciting the sample and thus increasing the intensity of fluorescent X-rays compared that in EDXRF

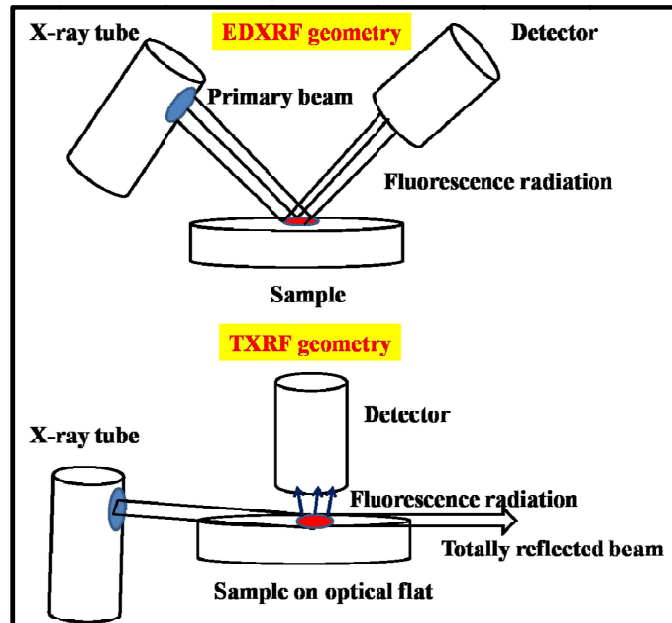


Figure 2.10: EDXRF and TXRF geometry

- c. The emitted fluorescence intensity from the sample is detected by the detector mounted at an angle of 90° with respect to the sample support. Hence the geometry in case of TXRF is $0-90^\circ$. Now due to this geometry; the detector can be placed very close to the sample, so the solid angle of detection becomes very high which gives maximum counts.

2.5.1. Basics of TXRF

To understand the basics of TXRF it is very much important to know the following:

- Concept of critical angle
- Penetration depth
- Reflectivity

X-rays passing through a homogeneous medium; behave like light beam which follows a straight line path. But if the beam touches the boundary surface between two mediums, it will be deflected from its path. Some part of the X-rays will be reflected back to the first medium and some part will refract into the second medium. This is shown in Figure 2.11 where X-rays passing from medium 1 to medium 2; and according to this figure the following rules are valid;

- The incident, reflected and the refracted beam are situated in a plane perpendicular to the boundary plane.
- The glancing angle of both incident beam and reflected beam are equal, i.e. $\alpha_1 = \alpha_1^*$
- The glancing angle of incident beam and refracted beam will follow Snell's law,

$$n_1 \cos \alpha_1 = n_2 \cos \alpha_2 \quad (2.4)$$

Here n_1 and n_2 are refractive index of medium 1 and 2 as shown in the figure.

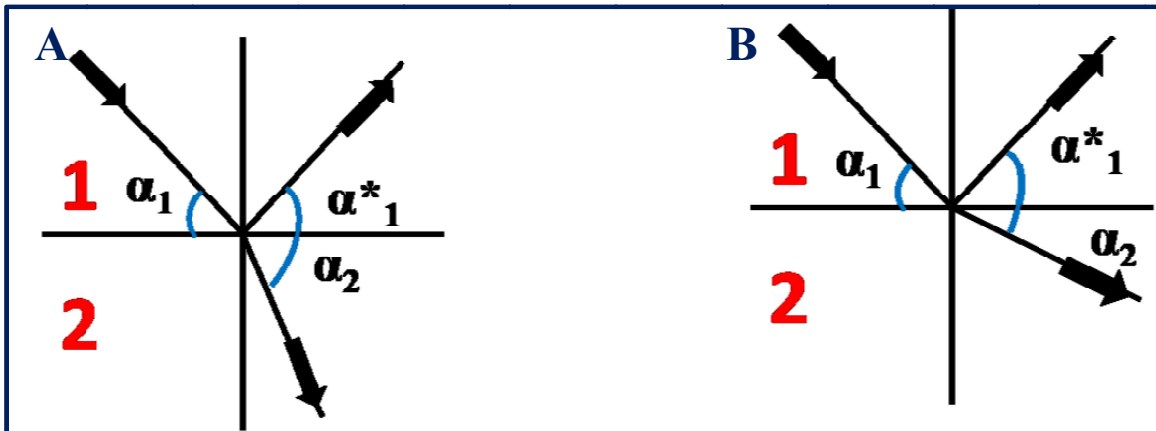


Figure 2.11: X-rays falling from medium 1 to medium 2 can be refracted away from the boundary (A) or it can be refracted towards the boundary (B) according to Snell's law

Now there can be two types of cases possible when X-rays travel from one medium to another medium. If the first medium is optically rarer than the second medium ($n_1 < n_2$); then X-rays will be refracted off the boundary ($\alpha_2 > \alpha_1$) between the two mediums. While for the vice

versa case ($n_1 > n_2$); X-rays will be refracted towards the boundary ($\alpha_2 < \alpha_1$). These two situations are shown in Figure 2.11. In TXRF flat polished quartz is used as a sample supports on which a few microlitre of the liquid sample is deposited as a thin film. So X-rays are falling from air medium to quartz medium. For X-rays any medium is optically less dense than vacuum or air. When X-rays fall on quartz sample support it will be refracted towards the boundary as shown in Figure 2.11 B. Now if α_2 becomes zero; the refracted beam will go tangentially to the boundary surface. If we recall the Snell's equation 2.4 and assume refractive index of air (n_1) is equal to one; the equation will be modified to:

$$\cos \alpha_{\text{crit}} = n_2 \quad (2.5)$$

So there is a minimum critical angle $\alpha_1 = \alpha_{\text{crit}}$ possible where the refracted X-ray beam just touches the boundary of these two medium. Further if α_1 is lower than this critical angle; the X-rays will no further enter into the second medium and instead of that it will be totally reflected from the boundary of the two surfaces. This phenomenon is called total external reflection, which is the basic point of TXRF spectrometry. The critical angle (α_{crit}) can be expressed by the following equation:

$$\alpha_{\text{crit}} \approx \frac{1.65}{E} \sqrt{\frac{Z\rho}{A}} \quad (2.6)$$

Here E is energy given in keV, ρ is the density of the second medium in g/cm^3 , Z and A are the atomic number and atomic mass of the medium material, respectively. This approximation is valid for photon energies above the absorption edges of the medium.

Another important parameter is the reflectivity of the medium; which is defined as the ratio of the intensity of reflected beam and the incident beam. In TXRF it is always desirable that the X-rays should be almost 100% reflected from the surface of the sample support; so that the scattering background would be minimum possible. Now as described earlier, when X-rays fall

on the sample support at an angle $> \alpha_{\text{crit}}$; reflectivity is very less at that situation (less than 0.1%). However when X-rays fall on the support at an angle below critical angle; its reflectivity suddenly increases many more times and become almost 100%. Materials like Plexiglas, glassy carbon, quartz, silicon wafer can be used as sample support for carrying out TXRF measurements, as the reflectivity of X-rays are very high using these types of sample supports.

Penetration depth is other important parameters that should be emphasized while discussing about the TXRF geometry. It is defined by that depth of a homogeneous medium a beam can penetrate while its intensity is reduced to $1/e$; or 37% of its initial value. For satisfying TXRF geometry the penetration depth should be as low as possible (few nm); so that the scattering background become minimum. Figure 2.12 shows the penetration depth of X-rays having a fixed energy, as a function of its glancing angle on a silicon support. It is observed that the penetration depth at angles greater than the critical angle is of the order of a few micrometers but below critical angle; the penetration depth is drastically reduced and becomes constant to few nm ranges. The very less penetration at incident angles below critical angle makes this technique inherently sensitive for depth profiling and surface analysis also [43].

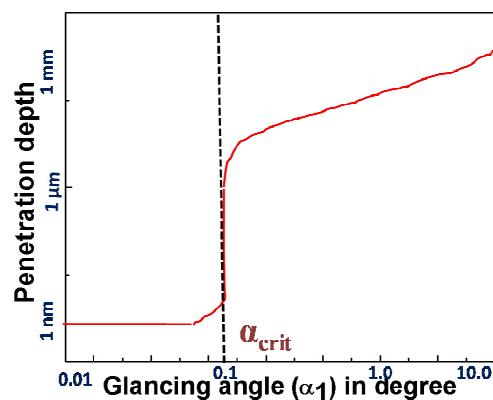


Figure 2.12: Variation of penetration of X-rays with the glancing angle for 17.5 keV X-ray radiation in silicon

2.5.2. Sample supports for TXRF measurements

Sample supports are also a very important part of TXRF analysis. As mentioned that for TXRF analysis samples are deposited on sample supports as thin film specimens. To satisfy the TXRF conditions the support should be perfectly flat polished and should have very less surface roughness. The average roughness of the surface should be of the order of few nm and the average flatness should be typically $\lambda/20$ ($\lambda=589$ nm; the mean visible light wavelength). There are many reports in the literature where different sample supports have been assessed for TXRF measurements [84-87]. There are some general requirements of a TXRF sample supports;

- It should be highly reflecting and optically flat as described above
- The support should be made of chemically inert material
- It should be free from any trace contaminations
- The fluorescence peak from the sample support should not interfere with any peak present in the sample
- It should be easy to clean and reuse
- The support should not be very costly

Table 2.2 compares important characteristics like reflectivity, critical angle, smoothness, purity, surface quality etc of different sample supports used for TXRF measurements using Mo K α excitation source [88]. By comparing all the features of different supports; it can be concluded that quartz can be used very efficiently as a TXRF sample support for TXRF analysis. Plexiglas can also be used for TXRF analysis. It is very cheap in price, but these types of supports cannot be reused. So each time new sample support have to be used for TXRF measurements; and will produce lots of waste, which is not desirable for the regular analysis of highly radioactive or radiotoxic samples. So although quartz sample supports are bit costly but as

it can be easily cleaned and reused; these are ideal candidate for carrying out TXRF measurements. Generally TXRF supports are circular having a diameter of 30 mm and thickness of 3 mm. It can be easily cleaned with 1 M suprapure HNO_3 and milli-Q water. These quartz materials are available in highly pure state and they have a very high reflectivity of X-rays below its critical angle around 0.1° . Figure 2.13 shows a picture of a clean quartz sample support and another quartz support having liquid sample of $5\mu\text{L}$ of volume deposited at the centre of it. Figure 2.14 shows TXRF spectrum of a clean quartz sample support using Rh $\text{K}\alpha$ excitation source. It can be seen that using quartz sample support; only Si $\text{K}\alpha$ and Ar $\text{K}\alpha$ peaks are visible. Here Ar $\text{K}\alpha$ is coming from the air, which can be avoided by carrying out the measurements in vacuum atmosphere and Si $\text{K}\alpha$ peak is coming from the sample supports; and no impurities are present in the sample support.

Table 2.2: Comparison of different sample supports for TXRF analysis

Features	Quartz	Plexiglas	Glassy carbon	Boron nitride
Reflectivity (R)	0.994	0.998	0.998	0.999
Critical angle (α_{crit})	0.10	0.08	0.08	0.10
Purity	Very good	Zn impurity	Fe, Cu, Zn impurity	Zn impurity
Surface quality	Very good	Good	Satisfactory	Good
Fluorescence peak	Si	None	None	None
Cleaning	Easy	Impossible	Difficult	Easy
Cost (\$)	30	0.1	30	60

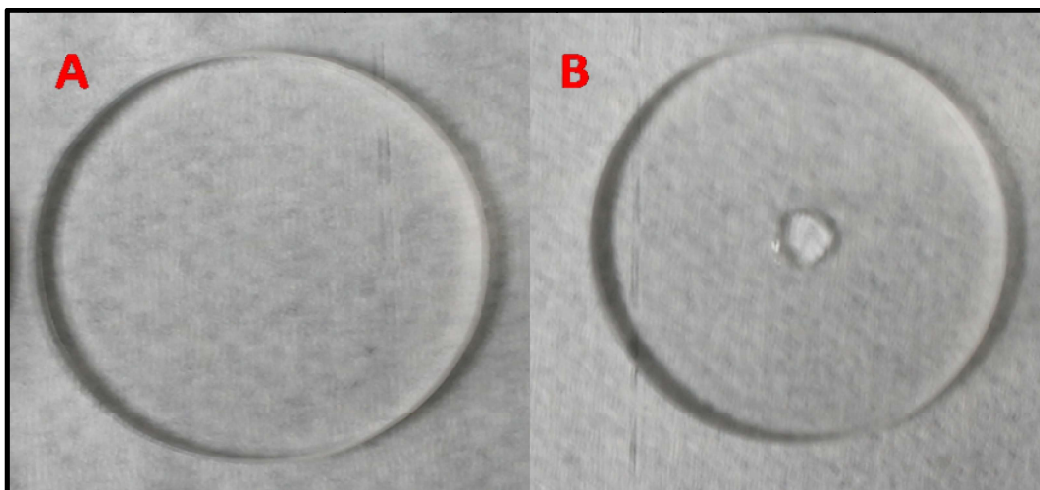


Figure 2.13: Picture of a clean quartz sample support (A) and a quartz sample support having 5 μ L of liquid sample deposited on the centre of it (B)

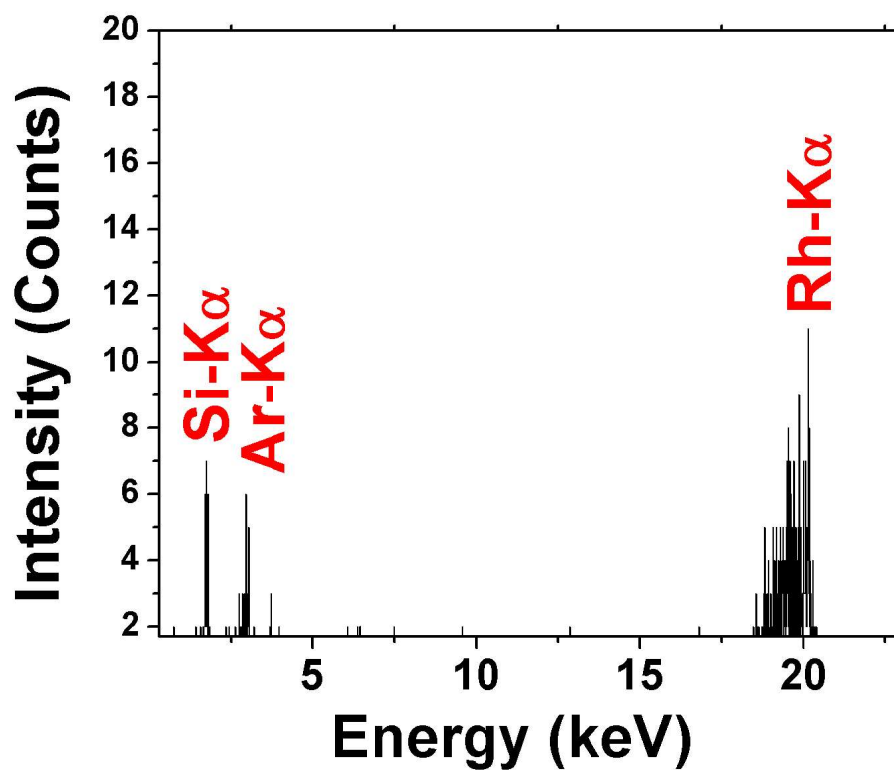


Figure 2.14: TXRF spectra of a clean quartz sample support obtained using Rh K α as an excitation source (live time: 300 seconds)

2.5.3. Monochromator for TXRF measurements

In order to obtain better detection limits as well as analytical parameters during TXRF analysis, the X-ray beam has to be monochromatic in nature. Mostly two types of monochromators are used in TXRF: one is natural crystal and another is multilayer. In both types of monochromators, concept of Bragg's reflection is used to diffract a definite energy band selected at a particular angle of reflection. This angle should be set in accordance to the Bragg's Law ($2d\sin\theta = n\lambda$). When polychromatic X-rays are falling on these reflectors at a particular angle (θ); X-rays of a particular wavelength (λ) or energy (E) only will be reflected from it. For chosen photon energy E in keV the angle can be calculated by the following equation:

$$\alpha = \arcsin (0.620/Ed) \quad (2.7)$$

Here d is the inter-planer spacing's (in nm) of the reflector being used.

The use of single crystals for monochromatization of the excitation radiation in TXRF results in relatively low efficiency. Due to the strict arrangement of the crystalline structure, only small part of the selected X-ray anode characteristic radiation line (e.g. $K\alpha$ with energies $E_0 \pm \Delta E$) fulfils the condition of Bragg diffraction. In practice, the intensity of the diffracted beam is of about 5 % of the intensity of characteristic radiation in the primary beam. That's why single crystal based monochromator should be used in such cases where the tenability of energy is required and the flux available is very high, like synchrotron based X-ray source [89].

Multilayered structured devices are developed by of arranging consecutive layers of a light element and heavier elements on a flat polished reflector, thus creating a periodic ($2D$ pseudo-crystalline, with a total thickness of several hundreds of nm) structure ensuring a larger effective reflectivity (~ 30 to 70 %). While adjusting the tilt angle of these devices respective to the incident beam it is possible to observe the occurrence of both total reflection (on the

substrate) and Bragg diffraction (on the multilayered structure) effects. These types of multi-layer monochromators are used in combination with lab based X-ray tube where very high loss of X-ray flux during monochromatization process is not desirable. Single crystal based reflectors will give highly monochromatic X-ray beam where one can resolve even $K \alpha_1$ and $K \alpha_2$ of a lines, whereas multi-layer monochromator have slightly poor monochromaticity but high reflectivity.

Monochromatic excitation reduces the background to obtain better detection limits. However, Kunimura and Kawai in their recent work showed that polychromatic excitation in TXRF measurements gives better detection limits compared to those obtained with monochromatic X-ray excitation [90].

The development of TXRF analysis can be broadly divided in six phases: Possibility of use of TXRF for very small amount of elemental detection proposed by Yoneda and Horiuchi, use of TXRF for trace element determination by German and Austrian Groups, use of TXRF for Silicon wafer analysis, environmental analysis by TXRF, development of TXRF spectrometer by Austrian Groups for soft X-rays and possibility of picogram elemental detection by TXRF spectrometry using polychromatic excitation source proposed by Kunimura and Kawai [90,91].

2.5.4. Detection system in TXRF analysis

A detector is very important part of the instrumentation of TXRF. The X-ray fluorescence radiation emitted from the sample after their excitation is collected in the detector. Energy dispersive semiconductor detector is generally used for TXRF, which will collect the X-rays and determine the intensity in terms of counts as well as their energies. These detectors consist of pure silicon or germanium crystal of several millimeter thickness and should have very high purity. Si crystals cannot be prepared with such high purity and a small amount of impurity like

boron is present in it at ppb (parts per billion) level. This modifies Si crystal into a p type semiconductor material with decreased resistivity. To suppress this conductivity, another impurity i.e. lithium is diffused into the crystal at elevated temperature which drifts under the influence of an electric field. Here Li acts as a donor to suppress the effect of boron acceptor. This arrangement generates two thin layers of p type and n type at the two ends and a huge intrinsic region in the middle of it. Such crystal based detector is called lithium drifted silicon detector or Si (Li).

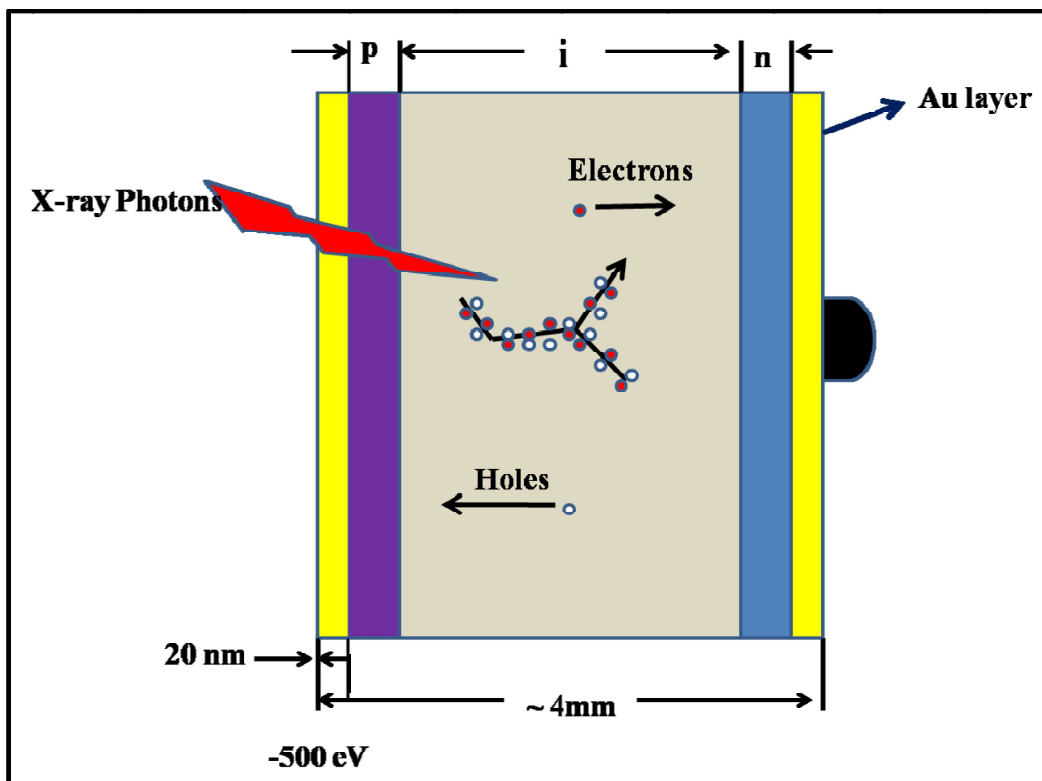


Figure 2.15: Working principle of a Si (Li) detector system

The working principle of the detector system is depicted in Figure 2.15. A reverse bias (p type layer $-Ve$ and n type layer grounded) is applied and the total configuration is called p-i-n diode with a reverse bias as it is shown in this figure. These types of detectors are kept under liquid N_2 temperature (77 K) to reduce thermal leakage current and prevent the reverse diffusion

of Li ions. Now in this condition an incident X-ray photon interacts with the crystal and ionizes the crystal atom and creates photoelectron and Auger electrons. These electrons lose their energies in several steps and raise outer shell electrons from valence band to conduction band. So electron holes are created in the valence band. A total track of electron-hole pair is produced until the incident photon energy is totally used up. As an electric potential is applied between the two electrodes, electron-hole pairs are separated, electrons will be drifted towards positive electrode and holes will be drifted towards the $-Ve$ electrode. So a charge pulse will be produced whose magnitude will be proportional to the energy of the photon.

Silicon drift detector (SDD) is another advanced form of semiconductor detector which is now days used in TXRF measurements. This type of detector consists of fully depleted silicon crystal having a very high resistivity.

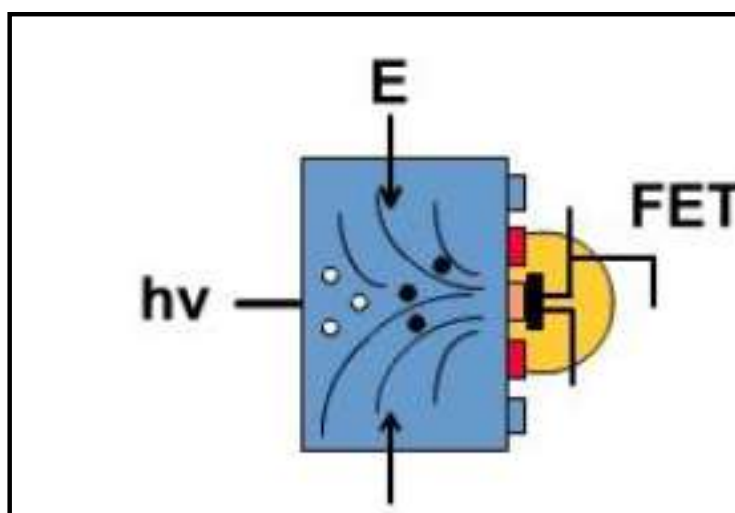


Figure 2.16: Working principle of SDD detector

The working principle of a SDD detector is shown in Figure 2.16. Here electrons are produced after the interaction of X-ray photons with the crystal and an electric field with a strong component parallel to the surface drives them towards a small sized collecting anode. Due to the

small size of the anode, the capacitance value of it is extremely small; which is a unique property of this type of detector. This feature results higher energy resolution at shorter shaping time compared to conventional Si (Li) detector. So SDD type of detectors are highly recommended where the X-ray photon flux is very high, like in synchrotron based radiation sources. Another advantage of using SDD detector is due to advanced technology used for manufacturing SDD; the leakage current is very low, and it can be operated with moderate Peltier based cooling technique. So by using these types of detector systems we can avoid the expensive and inconvenient liquid nitrogen cooling process.

2.5.5. Instrumental parameters for TXRF analysis

There are several parameters in TXRF, which can influence the analytical capability of the instrument for different elements like X-ray tube source, tube voltage, tube current, multi-layer, tube position, measurement time etc. TXRF is a multi-elemental analytical technique. Thus during the analysis of these samples it is very important to use an optimized condition, so all the elements will give reasonable counts. The first condition for the TXRF analysis of any sample is choosing the excitation source. The energy of the excitation source must be greater than the absorption edge of the elemental line that we are going to analyze by it, but it should not be too high. It is to be remembered that the excitation of an element will be maximum when the energy is just above the absorption edge of that elemental X-ray line. For the analysis of elements having atomic number $Z > 13$, Mo, Rh target based X-ray tubes can be used. But for analysis of low Z elements like C, F, Mg etc it is better to use excitation energy of Cr $K\alpha$, W $L\alpha$, Al $K\alpha$, Sc $K\alpha$ etc for the efficient excitation of these elements. The angle of the X-ray tube and multilayer position is also very important factor to maintain the TXRF condition during the analysis procedure. They have to be maintained in such a way that the incident X-ray beam should fall on

the sample support at an angle which is 70% of the critical angle. Instruments equipped with dual target tubes like Cr, Rh can analyze both low Z and high Z elements. The tube current should be maintained at an optimum value so that the dead time during the measurement should not exceed 30%. The optimum tube voltage is determined by the choice of excitation source during TXRF measurement. Generally tube voltage is kept twice the absorption edge of the element present in the target material. So for Mo target (Mo $K_{\text{abs}} = 19.97$ keV) tube voltage of 40 keV and for Rh target (Rh $K_{\text{abs}} = 23.20$ keV) 50 keV is applied.

2.5.6. Alignment for TXRF condition

Before the analysis, it is very important to obtain the perfect TXRF condition. For proper alignment of the instrument, at first it has to be ensured that the beam coming from the X-ray tube should be horizontal. A typical beam coming from an X-ray tube has a width of 10 mm and a height of 1 mm. The beam is allowed to fall on a multilayer monochromator in such a way that it cuts the beam into half and this can be achieved by moving the tube very carefully in vertical direction. The multilayer should be adjusted at such an angle that it would diffract monochromatic beam Mo $K\alpha$ / Rh $K\alpha$ /W $L\alpha$ /W $L\beta$ etc. So if a fluorescent screen is kept in the path of the beam we can see direct beam and diffracted beam above it in TXRF conditions. Now by rotating the tube shield; the diffracted beam is made to fall on the quartz sample supports at an angle which is 70% of the critical angle. This condition is considered optimum for TXRF measurement [91].

2.5.7. Instrumental calibration and analysis by TXRF

Before doing the elemental analysis by TXRF; it is very important to carry out instrumental calibration, which includes preparation of calibration solution, determination of relative sensitivities (RS) of elemental X-ray lines of different elements with respect to some

internal standard (IS), determination of detection limit for different elements etc. Now during determination of RS, an internal standard is required with respect to which the sensitivity values are determined. The internal standard should not be present in the sample that has to be analyzed by TXRF. For the analysis of medium and high Z elements generally Ga, Y or Co are used as an IS. For the analysis of low Z elements (C-Ti) generally elements like Mg, Sc etc are used. This calibration is different for K, L or M lines as analytical line. Generally for the analysis of low and medium Z elements (C to Mo) K lines and for high Z elements (Tc-Pu) L lines are used as analytical line. During the calibration process the excitation energy, as well as current and voltages has to be fixed. Figure 2.17 shows the TXRF spectra of a multi elemental solution having elemental concentration of 10 µg/mL using Rh K α excitation source. For calibration during TXRF studies, the multi-elemental standard solution were prepared by mixing MERCK ICP single element standard solutions of K, Sc, Cr, Co, Se, Ga and Y. Ga was used as an internal standard and RS of each elemental K α lines were calculated with respect to it. For quantitative analysis, the net intensities of the principal peak (N_x), obtained after correction of the spectral background and the overlapping neighboring peaks, is determined after recording the spectra. There is a linear relationship exists between the intensity of the main elemental peak area and its concentration (C_x) in the sample which is expressed by the following equation [81]:

$$N_x = S_x * C_x \quad (2.8)$$

Here S_x is called the absolute sensitivity of the element. The plot of this equation always gives straight line in case of TXRF geometry and it is known as calibration plot. This observation is very rare in case of EDXRF due to the high matrix effect. So for EDXRF; to obtain calibration plot for each sample we need different matrix matched calibration standards. But in case of TXRF; as we are taking a very small amount of sample as a thin film on the centre

of a sample support and the X-rays do not penetrate into the sample, the matrix effect is almost negligible. Now to determine the relative sensitivity with respect to Ga; absolute sensitivity of that element has to be divided with the absolute sensitivity of Ga $K\alpha$; $(RS)_x = S_x/S_{Ga}$. This relative sensitivity value is fixed for every element; irrespective of the matrix; if same excitation condition is used in TXRF geometry. So once we knew the RS of an element, we can use this RS to determine the concentration of the element in any types of samples by TXRF, using same excitation conditions.

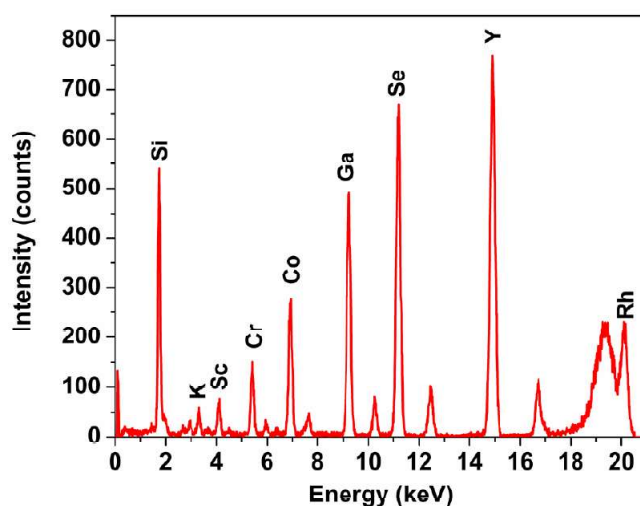


Figure 2.17: TXRF spectra of a multi elemental standard solution having elemental concentration of 10 $\mu\text{g/mL}$ obtained using Rh $K\alpha$ as an excitation source.

The relative sensitivities of different elemental X-ray lines were plotted against the respective atomic numbers of these elements and were found to increase with the atomic number. This plot could be fitted with a polynomial equation of order of 3 or 2. Figure 2.18 shows the Plot of the RS vs. atomic number for medium Z elements (K to Y) for $K\alpha$ analytical lines and high Z elements (Cd to U) for $L\alpha$ analytical lines. We can see in both the plots; the RS is increasing with atomic number and they are fitted with polynomial equation of order 3. The

nature of the calibration plots indicate that TXRF conditions are well satisfied and instrument is well calibrated. The RS of those elements whose standard are not available can be obtained by simply interpolating the curve using the polynomial equation. This is great advantage of TXRF determinations.

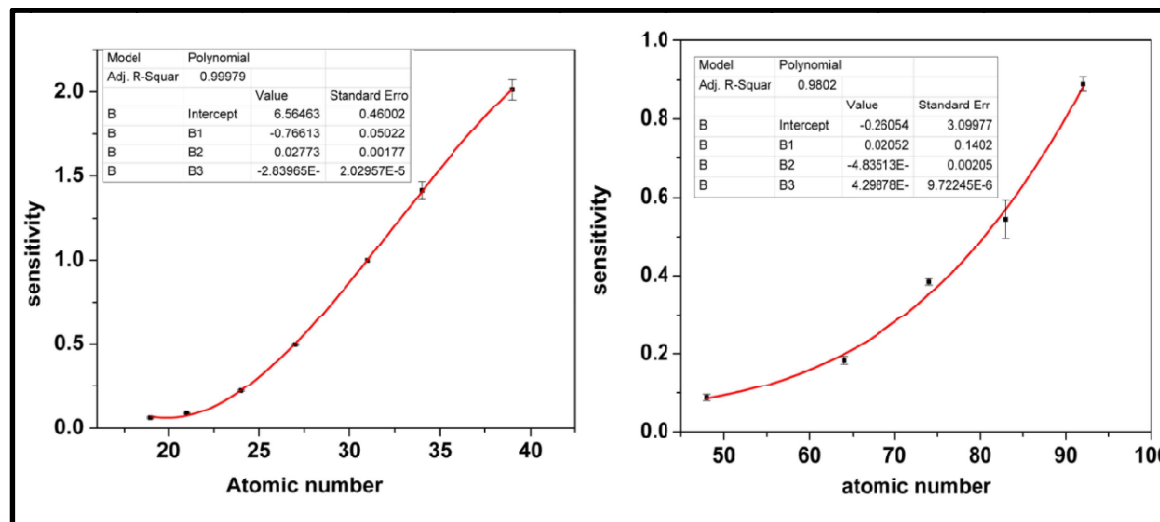


Figure 2.18: Plot of the RS vs. atomic number for medium Z elements (K to Y), using $K\alpha$ analytical lines, B: Plot of the sensitivity values vs. atomic number for High Z elements (Cd to U), using $L\alpha$ analytical lines

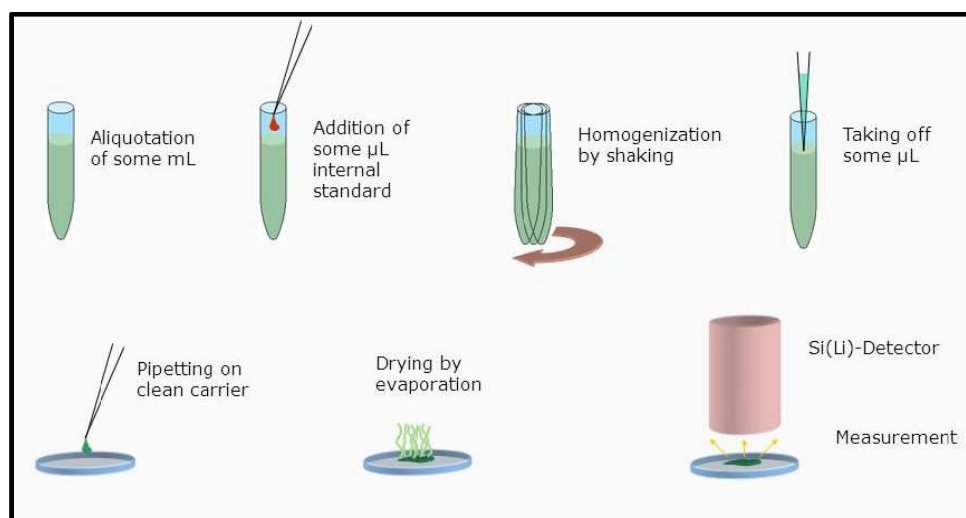


Figure 2.19: Preparation of TXRF sample specimen for the analysis of an unknown solution

For TXRF analysis of any solution; a known volume of this solution is taken in a small centrifuge vial (1.5 mL) along with the known volume of one IS of a fixed concentration and the solutions are mixed well to make a homogeneous solution. An aliquot of 2-10 μL of the resultant solution is deposited on the centre of a quartz sample support as a small droplet and finally dried on a hot plate or under an IR lamp. The whole sample preparation process is depicted in Figure 2.19.

After that, the TXRF spectrum of the sample specimen is measured in similar way. The concentration of an element (C_x) in the sample is determined by using the following equation:

$$C_x = \frac{N_x}{N_{IS}RS_x} * C_{IS} \quad (2.9)$$

Where C_x is the concentration of the x^{th} element present in the sample, N_x and N_{IS} are the net intensities of (x) and (IS) internal standard, RS_x is the relative sensitivity value of (x) with respect to (IS) and C_{IS} is the concentration of (IS).

As discussed earlier that another important parameter for TXRF analysis is the detection limits (DLs) of different element of interest. TXRF is especially valuable technique for its high detection power. DL is that amount of analyte that gives net line intensity equal to three times the square root of the background intensity for a specified counting time [56]. The absolute detection limit of any element can be expressed by the following equation:

$$DL = \frac{3 * \sqrt{I_B}}{I_P} * m_i \quad (2.10)$$

Here I_B is the area under the background in TXRF spectra, I_P is the area of the peak of interest and m_i is the mass of the analyte. Figure 2.20 shows plot of detection limit of different elements (K to Y) v.s. atomic number for a counting time of 1000s, using Rh $K\alpha$ as an excitation source, applying tube voltage and tube current of 50 keV, 700 μA respectively. It is observed

that with increasing atomic number DLs of elements are decreasing and the absolute detection limit of elements like Se, Y are in the order of pictogram (DL of Se: 71, Y:50 pg). For the determination of detection limits a very dilute solution should be used for TXRF measurements.

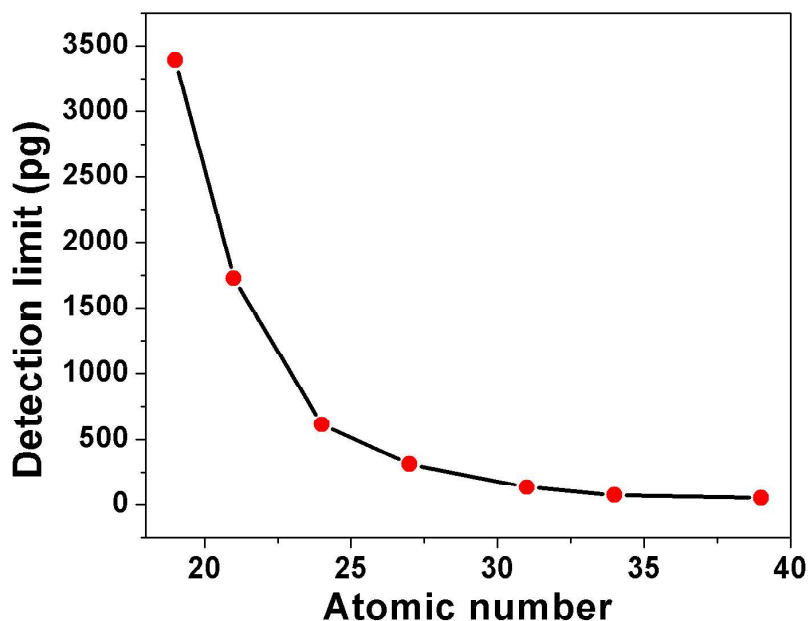


Figure 2.20: Plot of detection limit with atomic number using $K\alpha$ as analytical line and $Rh K\alpha$ as excitation source for elements K to Y

2.6. TXRF-XANES technique

TXRF technique can be combined with another technique called XANES (X-ray absorption near edge spectroscopy) to obtain the information about the oxidation state of different elements. To understand about XANES it is important to know about XAS (X-ray absorption spectroscopy).

2.6.1. X-ray absorption

X-rays have sufficient energy to eject out the core shell electrons of an atom. Each core shell has some definite binding energies. If we plot the absorbance of X-rays versus the energy of it we will get a plot as given in Figure 2.21 [92].

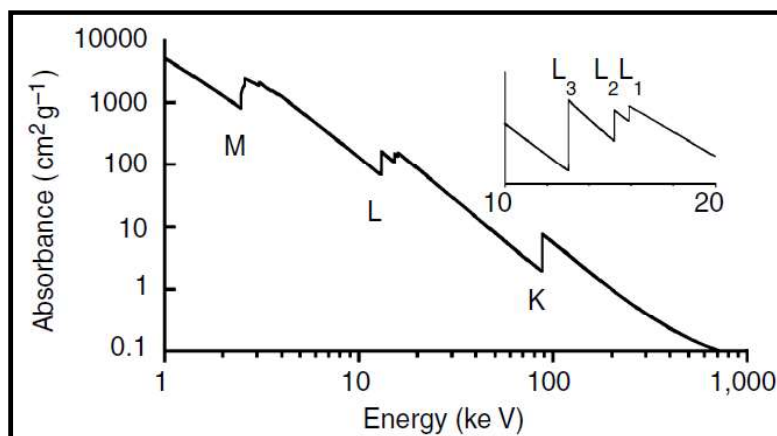


Figure 2.21: A typical X-ray absorption plot

It is observed from the plot that the absorbance is decreasing linearly with energy of X-rays, but there is an abrupt jump in the absorbance at some energy, and these energies are called absorption edges. From the figure we can see that there are several absorption edges for L and M shells. If we closely look into that figure we can further see that there are three different L viz. like L_1 , L_2 and L_3 edge. These edges can be understood by the energy level diagram as shown in Figure 2.22. The L_1 edge shown in the Figure corresponds to excitation of a 2s electron [93]. Now 2p excitation is split into two edges i.e. L_2 and L_3 . L_2 edge corresponds to higher energy excited state $2P_{1/2}$ and L_3 edge corresponds to lower energy excited state $2P_{3/2}$. Due to degeneracy L_3 edge has twice the edge jump of L_1 and L_2 .

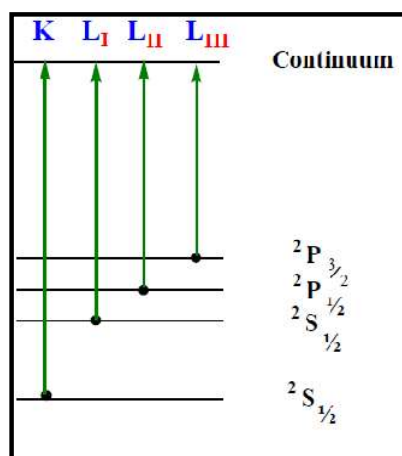


Figure 2.22: Different excitation states give different absorption edges

2.6.2 Absorption edges

Now if any one closely observe L_3 edge of the Figure 2.23; many information are hidden in it. Absorption edge is not only a simple abrupt jump of absorption, but there are many structures hidden in it. The structure in the vicinity of the edge is known as X-ray absorption near edge structure (XANES). The oscillation above the edge which can be extended up to 1000 eV is known as extended X-ray absorption fine structure (EXAFS). Generally XANES region contain below and above 100 eV energy near the absorption edges. The remaining portion above 100 eV and up to 1 keV is called EXAFS region. The whole region is called XAS (X-ray absorption spectra). From XANES region we can obtain information about the oxidation state, co-ordination state of different elements. From EXAFS oscillations we can obtain valuable information about the local structure around some element of our interest like its coordination number, bond length around it, local defect centre etc [94].

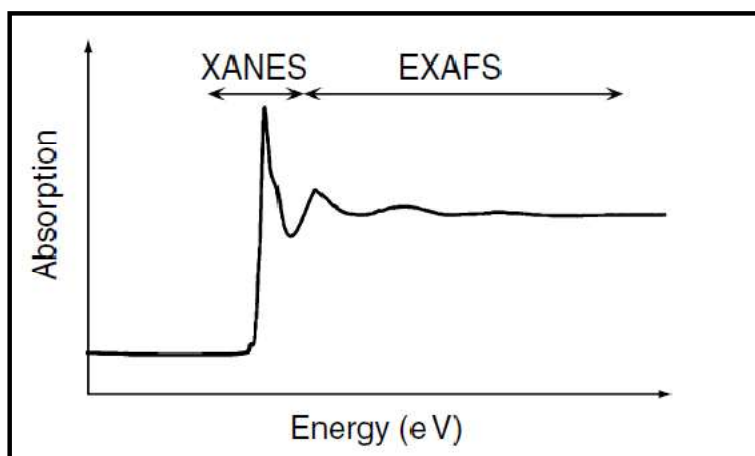


Figure 2.23: Different regions of an XAS spectrum including XANES and EXAFS

2.6.3. XAS measurements in florescence mode

XAS measurements can be done by simply measuring the incident (I_0) and transmitted X-ray flux (I). But this methodology will not work when the sample amount is less or it is very

much diluted. So in that case it is always desirable to do XAS measurements in fluorescence mode especially in TXRF geometry for better detection. For fluorescence measurement, the arrangement will remain almost same like before with some detector is placed closed to the sample to obtain the fluorescence signal (I_F) coming from the sample. The intensity of the X-ray fluorescence is proportional to the X-ray absorption cross section. The arrangement for XAS measurement in fluorescence and transmission modes are shown in Figure 2.24.

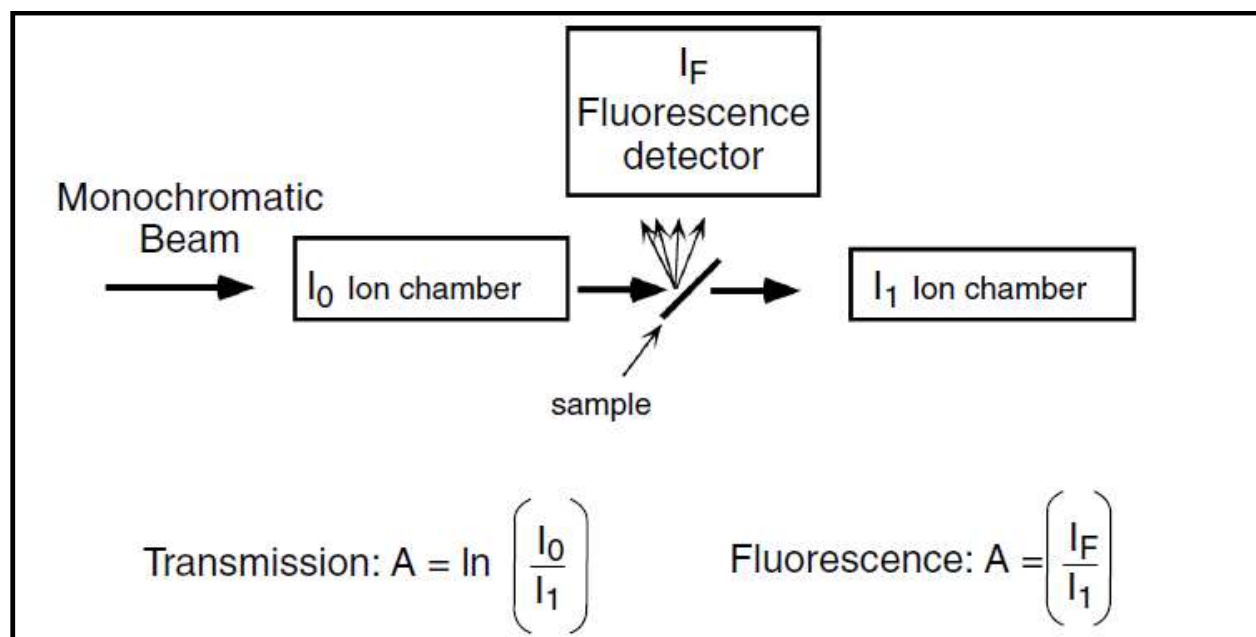


Figure 2.24.: XAS measurements using absorption and fluorescence mode

2.6.4. TXRF-XANES measurement procedure

Now during XANES measurements, we are actually doing XAS measurements for a limited range (-100 to 100 eV around the absorption edge of the element of interest) where instead of analyzing the whole XAS; we are interested around the edge portion; which will give the information about the oxidation states of the element being studied. It has been already discussed that TXRF has better detection limit compared to XRF. The same XAS experiment can

be carried out in fluorescence mode using TXRF geometry in the XANES region and the method is then known as TXRF-XANES. The main advantage of using TXRF-XANES is requirement of very small amount of sample (ng level analytes on support) during the analysis. So this technique will be highly useful for analysis of radioactive, precious, forensic and environmental samples where analyte amount available and desirable is very small. During TXRF-XANES measurements a tunable energy source is required and TXRF spectrum is recorded at each of energy (the energy scanning interval is generally chosen as 0.5 eV or 1.0 eV) for a live time of 5-10 seconds depending upon the sample amount. The ratio (I_f/I_0) is plotted against the energy, which will generate XANES spectrum.

2.7. TXRF facilities used in this work

During this study, both lab as well as synchrotron based TXRF spectrometer were used. Synchrotron based TXRF was mainly used for the analysis of low Z elements and results have been compared with that obtained using lab based X-ray source. The TXRF-XANES study has been used to determine oxidation states in mixed valent uranium oxides; which is a technologically important material.

2.7.1. Lab source based TXRF instrument

2.7.1.1. ITAL STRUCTURE TX-2000

This spectrometer can be operated both in total reflection as well as conventional XRF geometry. It has Mo target. The tube voltage and tube current applied during the TXRF measurement were 40 kV and 30 mA, respectively. This high power X-ray tube needs a chiller which serves as a constant source of chilled water to cool down the Mo anode during the TXRF measurements. A W-C multilayer with $2d=49.4 \text{ \AA}$ is used as multilayer monochromator to diffract Mo $K\alpha$. This monochromatic Mo $K\alpha$ beam is allowed to fall on TXRF support at an

angle less than critical angle. The instrument contains a multi-sample holder where 12 samples can be loaded and measured sequentially. The X-ray fluorescence emitted from the sample is detected with Si (Li) detector having resolution of 139 eV at Mn K α (5.91 keV). A liquid N₂ Dewar is attached with the detector to maintain the Si (Li) crystal at liquid N₂ temperature (77K). The picture of the ITAL-STRUCTURE TXRF instrument is shown in Figure 2.25.

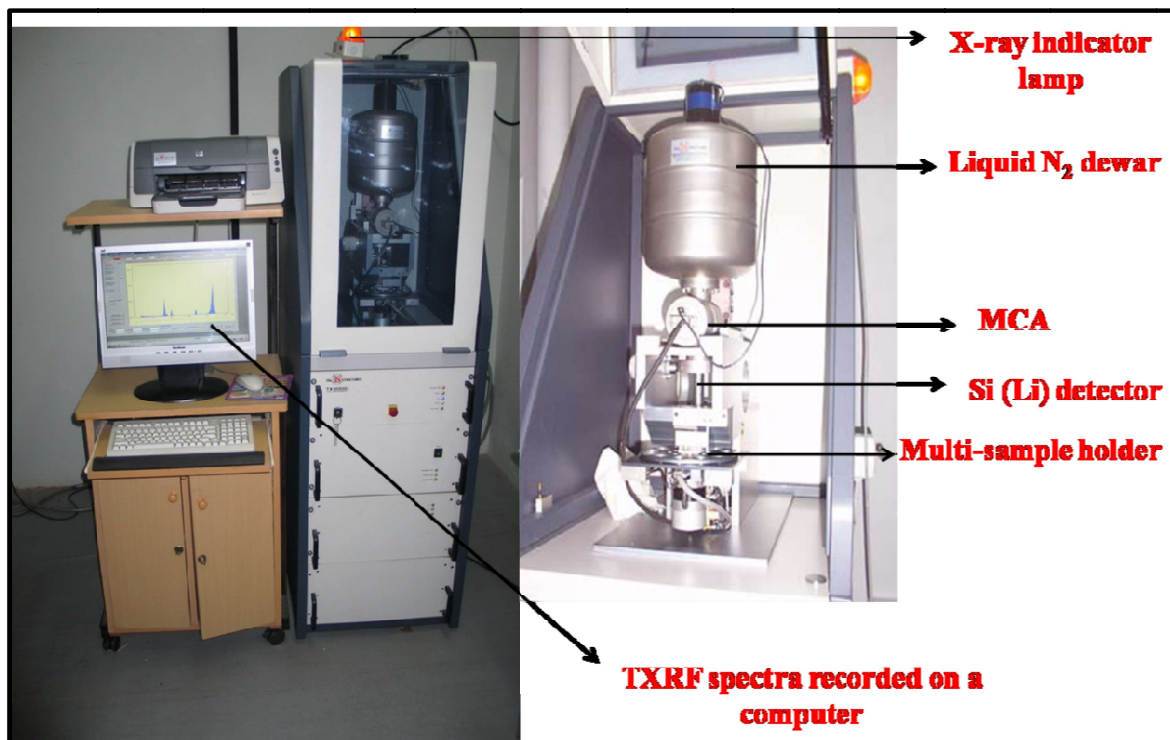


Figure 2.25: ITAL STRUCTURES TXRF SPECTROMETER TX-2000

2.7.1.2. Low Z – High Z TXRF spectrometer (WOBISTRAX)

Another TXRF instrument which has been used in this study is low Z – high Z TXRF spectrometer. The instrument was developed by the Atominstitut of the Technical University in Vienna, Austria and it is in our laboratory. The spectrometer consists of two low power X-ray tubes. One a low power X-ray tube having Cr target and other is Rh targeted tube. Both the X-ray tubes are coupled with a suitable multilayer (Ni/C, $d=4.03$ nm for Cr X-ray tube and Pd/B₄C,

d=3.24 nm for Rh X-ray tube) to diffract monochromatic Cr $K\alpha$ and Rh $K\alpha$ respectively. The tubes can be slided on rails to fit into the sample chamber.

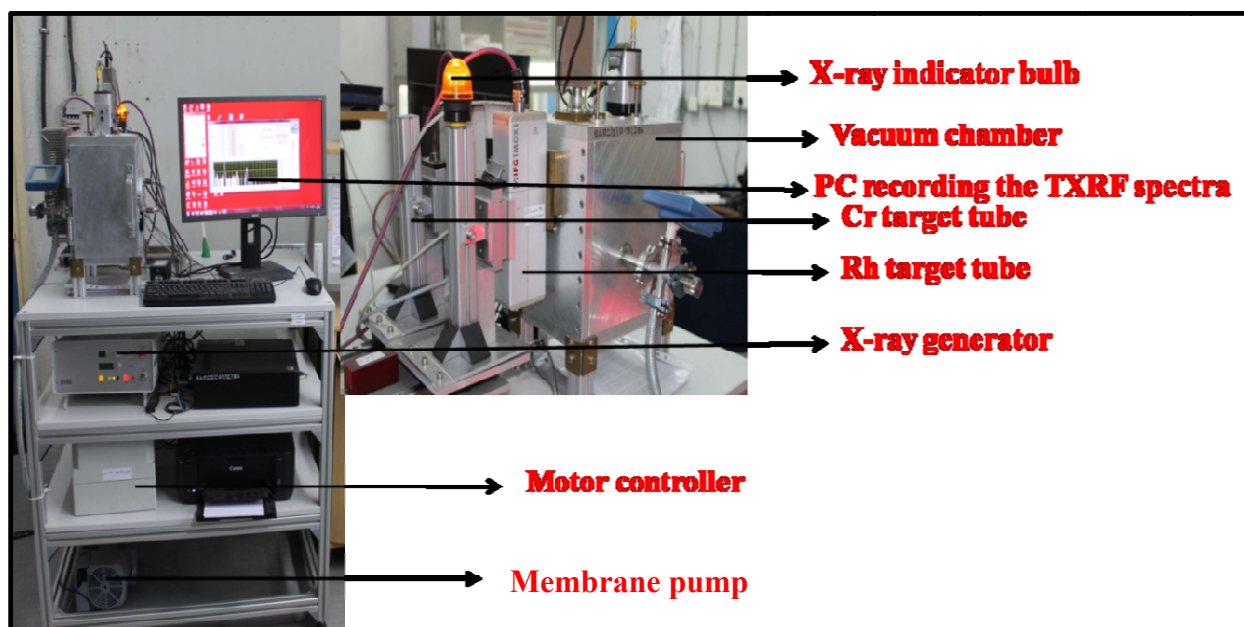


Figure 2.26.: Picture of the Low Z – High Z TXRF spectrometer having Cr and Rh target X-ray tubes

The Cr $K\alpha$ tube can be used for the determination of low Z elements ranging from C ($Z=6$) to Ti ($Z=22$) by using their K emission lines and from Mo ($Z=42$) to Ba ($Z=56$) by using the L emission lines of those elements. The Rh $K\alpha$ can be used for the analysis of medium Z elements ($Z=19-42$) using their K emission lines and high Z elements ($Z=42-94$) using their L emission lines with different detection limits. So using this TXRF spectrometer one can determine elements ranging from C ($Z=6$) to Pu ($Z=94$). The Cr and Rh tubes are operated at tube voltage and tube current of 30 kV/1300 μA and 50 kV /700 μA respectively. The X-rays emitted from the samples are detected by a KETEK silicon drift detector (SDD) having an area of 20 mm^2 . The detector window is made of an ultra thin polymer having thickness of 300 nm. This detector has a resolution of 120 eV at Na $K\alpha$ (1.04 keV) and 136 eV at Mn $K\alpha$ (5.91 keV).

An electron trap is placed around the polymer window to reduce the spectral background due to the production of Auger electrons and photo electrons. A membrane pump is attached with the vacuum chamber to maintain a vacuum level of ~ 3 mbar during the analysis of low Z elements. Figure 2.26 shows the picture of a low Z high Z TXRF spectrometer.

2.7.2. TXRF based on synchrotron based source

Two synchrotron beam lines were utilized for carrying out TXRF measurements in this work. The XRF beam line at Elettra Synchrotron light Source Trieste, Italy was used for the analysis of low Z elements. For carrying out speciation studies in mixed valent uranium oxides; microprobe X-ray fluorescence beam line (BL-16), at Indus 2, RRCAT (Raja Ramanna centre for advanced technology), Indore, India was utilized.

2.7.2.1. XRF beam line at Elettra Synchrotron Trieste, Italy

This XRF beam line at its present configuration have tunable synchrotron radiation excitation source having energy in the region of 3.6 to 14.5 keV. A Si (111) double crystal monochromator (DCM) with a resolving power of 1.4×10^4 was used to produce mono energetic beam [95, 96]. The beam size at the sample position is 260 μm (H) \times 130 μm (V) respectively. The sample holder of this beam line can hold up to 4 quartz sample supports having diameter of 30 mm and 3 mm thickness. At first the sample is introduced to a load lock chamber and after attaining certain vacuum level inside the load lock chamber; the sample is finally transferred into main experimental chamber where the vacuum level is of the order of 10^{-8} mbar. This chamber is called ultra high vacuum chamber (UHV). In the main experimental chamber; the sample holder is attached with a five-axis motorized sample manipulator; which has 'theta' goniometer having very high precession, an 'XYZ' linear translation stage and an ϕ goniometer connected with the XY stage. Figure 2.27 shows the diagram of the UHV chamber along with

load lock chamber and 7 axis sample manipulator inside the UHV chamber. Here ‘Y’ by convention represents the incident beam direction; ‘X’ is the perpendicular axis to the horizontal plane. The detector axis (Z direction) is perpendicular to the sample surface, whereas the incident beam and polarization direction is on the ‘YZ’ plane. So the measurement in this particular geometry will take the advantage of the polarization property of the synchrotron radiation and the scattered background will be further lowered. This is well illustrated by Figure 2.28 where this arrangement is shown [97].

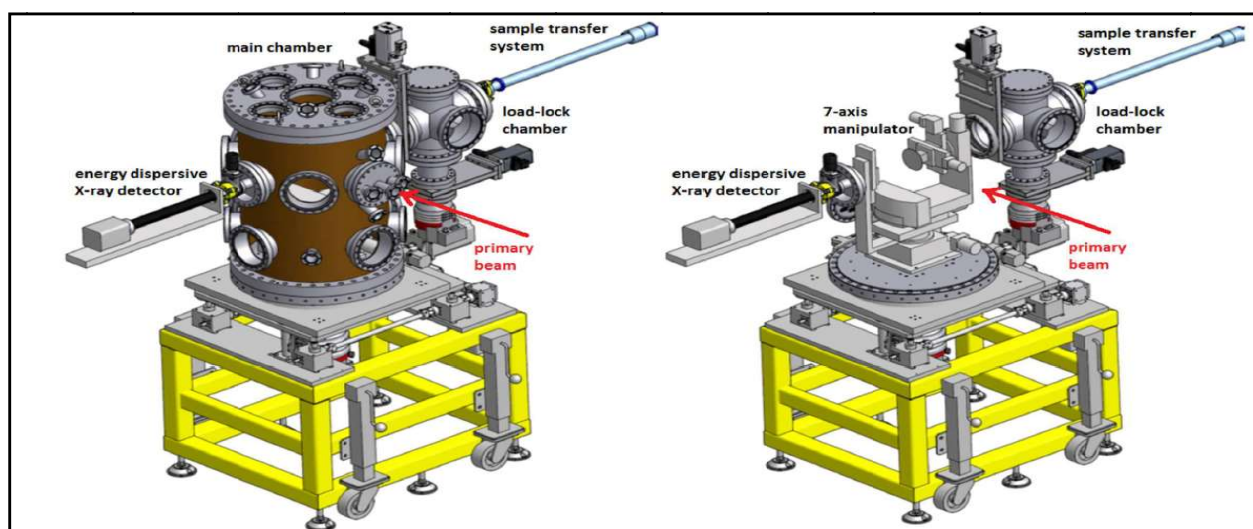


Figure 2.27: Diagram of the UHV chamber along with load lock chamber and 7 axis sample manipulator inside the UHV chamber

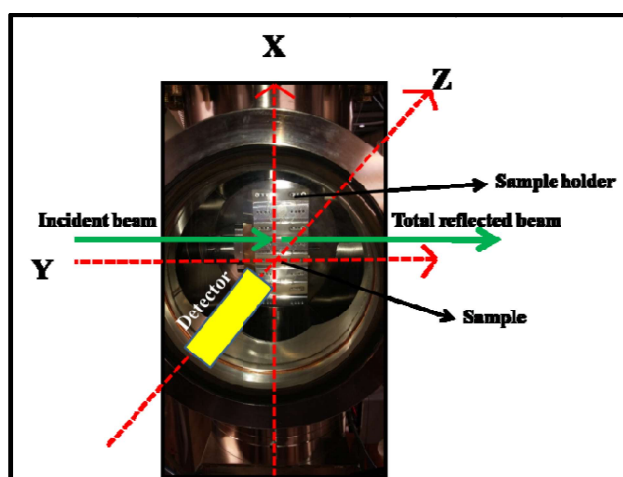


Figure 2.28: The arrangement of sample inside the main experimental chamber

The TXRF spectra were recorded by an SDD (Bruker nano GmbH, X-Flash 5030) with nominal area of 30 mm², 450 μm of crystal thickness and an energy resolution of 131 eV (FWHM) at the Mn Kα (5.9 keV) line. The SDD has super light element window. There is a magnetic electron trap situated in front of the SDD detector; which prevents the energetic electrons to reach into the detector and enhance the spectral background. Two circular discs were placed in the front and back sides of the magnetic electron trap to define a rather tightly collimated radiation that is detected by the central part of the SDD crystal area. During the present experiment, the distance of the front side of the magnetic electron trap was set at a distance of 11 mm away from the sample surface. All the SR TXRF measurements were performed at two excitation energies, i.e. 5.41 and 3.8 keV, respectively, in order to investigate the influence of different excitation energies on the precision and sensitivity of the measurements.

There are several steps involved in the alignment process to obtain total reflection condition. At first offset theta angle was determined to make the quartz sample support parallel to the incident beam. After that at each incident energies; a theta scan of the Si Kα fluorescence intensity was performed in order to find the critical angle experimentally for total reflection condition. TXRF measurements were carried out by setting the glancing angle of the incident beam 70% of the critical angle. A vertical X scan with step size of 0.1 mm is carried out subsequently to determine the finite extension (few mm) of the sample residue on the quartz sample and to find out possible in-homogeneity in the deposition of different elements during sample preparation. To account for this in-homogeneity in the deposited sample; SR TXRF scanning measurements were performed using 5.41 keV excitation energy along the X-axis (20s/step, 0.1 mm/step) for 20 μg/mL MES solution. The inhomogeneous distribution of

different elements on the TXRF sample support and in particular of the internal standard may affect significantly the quantitative results if the irradiated area seen by the detector is smaller than the sample specimen. Therefore, in the synchrotron setup, the cumulative TXRF spectra obtained by summing up the individual spectra recorded by performing the X scan measurements represent and reflect better the total mass of the specimen analytes.

2.7.2.2. Micro-focus beam line (BL-16), Indus-2, RRCAT, Indore, India:

Micro focus beam line (BL-16), Indus-2, RRCAT [98] has been utilized for the speciation studies of mixed valent uranium oxides using TXRF-XANES technique at UL_3 edge. A Si (111) DCM has been used in that beam line for selecting different X-ray energies of the exciting beam from the continuous synchrotron X-ray spectrum. Here the beam spot size is 10 mm (H) \times 0.1 mm (V). The energy resolution ($\Delta E/E$) of the monochromator was approximately 10^{-4} ; which resulted an overall energy resolution of ~ 2 eV. All the measurements were carried out in air atmosphere at room temperature conditions. TXRF-XANES measurements on each of the sample were carried out in steps of 1 eV in the energy range of 17027 to 17260 eV around UL_3 edge (17160 eV) with a spectrum acquisition time of 4s. The intensity of exciting radiation (I_0) was determined using an ionization chamber before the sample. The fluorescence X-rays emitted from the sample was detected using a vortex energy dispersive spectroscopy detector (SII Nano Technology, U.S.A.). Three spectra were measured at each step of energy for each sample. These spectra were merged in data treatment procedure. For energy calibration, a standard Zr (Zr K edge 17.99 keV) foil was used. The XANES measurements of the standard Zr foil was carried out in EDXRF mode. Figure 2.29 shows the arrangement in the experimental hutch of BL-16, Indus 2, RRCAT, Indore for carrying out TXRF-XANES measurements. From the figure it can be seen that from JJ slit monochromatic synchrotron X-rays are coming and they

will form a fine strip of dimension mentioned above after passing through the slit S2. These X-rays are falling on the sample below critical angle and totally reflected from it. An X-ray CCD detector is placed after that to detect the direct as well as totally reflected beam as shown as an inset picture in that figure. The reflected beam remains above the un-reflected part of the incident X-ray beam, and from that we can be sure that the TXRF condition has been reached (Fig. 2.29). There is an SDD detector which is situated perpendicular to the direction of the beam. The sample is situated on a 5 axis sample manipulator stage which has three translational (along X, Y, Z direction) and two angular (theta and phi) movements.

The TXRF measurements were carried out utilizing the anisotropic nature of the scattered synchrotron radiation in the horizontal direction geometry. This geometry has a significant advantage of reduced background during TXRF measurements and gives an improved signal to background ration for fluorescence peaks [99].

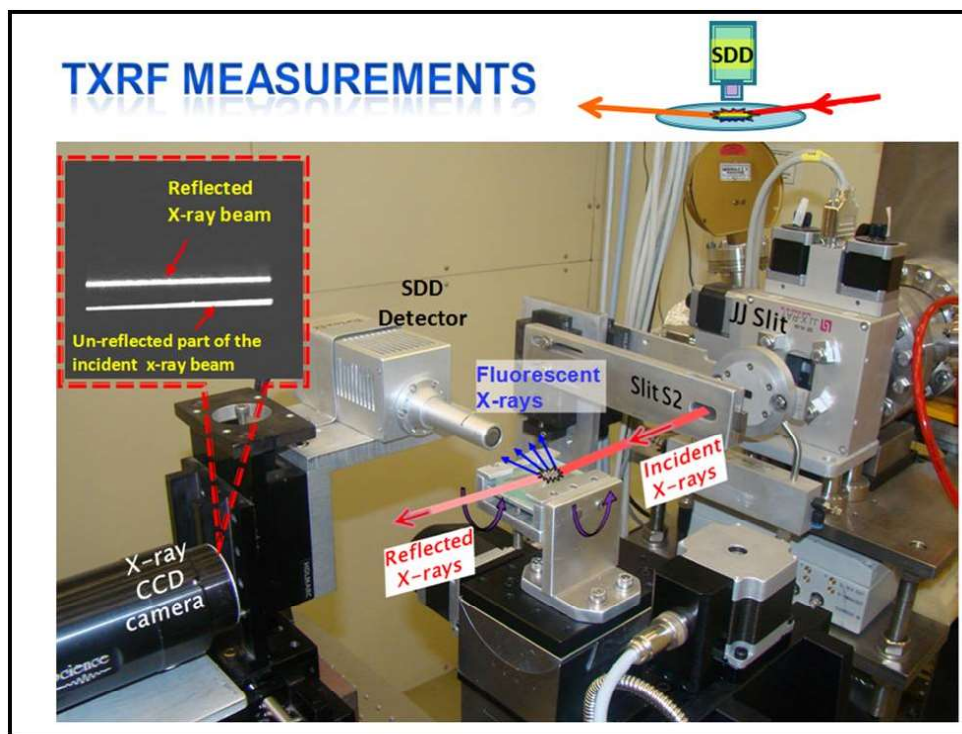


Figure 2.29.: Totally reflected beam (top) and direct beam (bottom) shown by the CCD camera indicating that TXRF conditions are satisfied during the sample measurements.

2.8. Data analysis software used

For the analysis of the TXRF spectra two software were used. The EDXRF-32, provided with ITAL-STRUCTURE TX-2000 instrument and another one is AXIL, a software package provided by IAEA. Both these software analyze the TXRF spectra by nonlinear least-squares fitting based on the Marquardt algorithm [100].

For the analysis of the TXRF-XANES spectra, a linear combination analysis of the XANES spectrum was carried out with the software ATHENA, which is included in the IFEFFIT program package. Fitting was performed over an energy range of -30 to $+30$ eV about the L_3 edge energy of uranium.

2.9. Other Instruments used

In addition to XRF based instruments some other instruments were used for synthesis and characterization purposes. For the preparation of polymer resin gel, used in solid phase extraction, UV light in a photo reactor was used. This photo reactor was procured from Heber Scientific, Chennai, India (Model no. HML-SW-MW-LW-888). It is fitted with eight 8W mercury UV lamps of wavelength 365 nm (Sankyo Denki, Japan) and highly polished anodized aluminium reflector.

The prepared polymer resin gels were characterized by different methods like PL (Photoluminescence), Fourier transform infrared (FTIR), FE-SEM (Field Emission Electron Microscope).

The PL data of the polymer resin gels were recorded on an Edinburgh CD-920 unit having M 300 monochromator. The data acquisition and analysis were done using F-900 software provided by Edinburgh Analytical Instruments, UK. A Xenon flash lamp having frequency range of 10–100 Hz was used as the excitation source. Emission spectra were recorded

with a lamp frequency of 100 Hz. Luminescence lifetime measurements were based on well established Time-Correlated Single-Photon Counting (TCSPC) technique. The FTIR spectra were recorded using the platinum-attenuated total reflection technique. All spectra were obtained at a resolution of 4 cm^{-1} (wave number) and under the same measurement conditions ($4000\text{--}500\text{ cm}^{-1}$, 36 scans). The morphology of the polymer resins were recorded by JEOL made field emission gun scanning electron microscope (FEG-SEM).

Chapter 3

Trace elemental
determinations of low Z
elements by TXRF

3.1. Introduction

The determination of low atomic number elements with $Z < 11$ is important in several technological and environmental areas [101, 102]. Certain minimum amounts of specific low Z elements are essential in drinking water and food items to maintain better human health. However, if concentrations of these elements become more than the specific value in drinking water, may cause detrimental effect to human health. The specific limits of low Z elements like F, Na, Mg in drinking water has been set by different environmental authorities like WHO (World health organization), EPA (Environmental protection agency) etc. [103]. However detection and determinations of these low Z elements has always been a challenging task using different methods [104-109]. In the field of TXRF specialized spectrometer has been developed and applied for the determination of low Z elements in different sample matrices [110, 111]. In recent times TXRF technique has emerged to be a very good analytical technique comparable with other well established trace analytical techniques e.g. ICP-AES (Inductively Coupled Atomic Emission Spectroscopy), INAA (Instrumental Neutron Activation Analysis), ICP-MS etc for many elements. However TXRF has its own limitations for the analysis of low Z elements in a similar manner as other techniques [47, 112-116]. Some main problems in the determination of low Z elements using XRF are: (1) the fluorescence yields (ω) for low Z elements are very low. (2) Their characteristic X-rays ($K\alpha$) have very low energy (down to few hundreds of eV), so they can be easily absorbed by the air molecules present in the atmosphere as well as spectrometer parts e.g. window of detector. Due to these reasons vacuum atmosphere coupled with a windowless/ thin window X-ray detector is required. (3) Strong X-ray sources which can offer relatively low excitation energies are rare, although various X-ray sources have been investigated [117]. Additional difficulties for the determination of low Z elements by XRF are obtained due

to the interferences between the $K\alpha$ analytical lines of low Z elements and L and M lines of medium and high Z elements. Moreover physical interaction of X-rays with the sample or detector usually increases the spectral background near the low-energy region of the XRF spectra; thus affecting the precision of analysis and the detection limit adversely [47, 112].

Synchrotron radiation (SR) due to its remarkable features like its energy tunability, high flux and linear polarization is well suited for trace elemental analysis by TXRF. Due to the energy tunability one can choose an energy which is just higher than that of the absorption edge of the element of interest and excite that element very efficiently. In addition polarization properties of the SR in the plane of the storage ring will minimize the scattering background in TXRF geometry [66, 97, 112, and 117].

Recently a low Z – high Z TXRF spectrometer (WOBISTRAX) has been installed in our laboratory for the dedicated R&D with low Z elements in various technologically important and environmental samples. Before utilizing this vacuum chamber TXRF for the analysis of low Z elements in different matrices, it is very important to investigate its analytical performance and compare it with some synchrotron based TXRF instrument. It is reported in the literature that the detection limits obtained for low Z elements using WOBISTRAX are higher compared to SR based TXRF technique; and it is important to compare the analytical parameters for low Z elements using these two types of excitation sources [118-120]. This comparison will provide insights for further optimization of laboratory based TXRF spectrometers for low Z elemental determination in different matrices. For such study the XRF beam line at Elettra synchrotron light source, Trieste, Italy was utilized. Two different energies of excitation e.g. 3.8 keV and 5.41 keV were chosen as excitation source for the determination of low Z elements. The

detection limits and analytical results obtained were compared with that obtained with vacuum chamber TXRF where Cr K α (5.41 keV) was used as an excitation source.

Determination of low Z elements like C, F, Na, Mg, Al, K, S, Ca etc are very important for chemical quality control and assurance of nuclear fuel which is a technologically important material in the nuclear industry. Some of these elements are metallic and some are non-metallic. Carbon, nitrogen, and oxygen are present as major elements in carbide, nitride, and oxide fuels respectively, and are required to be determined to know the chemical composition of the fuel. Fluorine is a corrosive element and its trace amounts as impurity present in fuel should not exceed the specified limits for the safe operation of the reactor. Similarly, Na, Mg, Al, K, Ca, and so forth, if present in quantities larger than the specified values, may produce uranates of much lower density during fuel fabrication (e.g., oxide conversion and sintering in case of oxide fuels) and during operation of the reactor. Formation of these uranates, during reactor operation, may lead to the fuel expansion and fissile material dilution. The specifications of the trace elements in nuclear fuel are determined on the basis of the role and chemical behavior of these elements in the fuel during reactor operation. Therefore, to satisfy the fuel specifications, before putting the fuel in the reactor, determinations of trace and major elements present in it are required [121-123]. Only a very few techniques are reported in the literature for the analysis of low Z elements [124-126]. TXRF is well suited for the characterization of radioactive materials due to its advantageous features for such materials, e.g. detection limits in pg level, requirement of very small sample amount for the analysis, multi-element analytical capability, determination of both metals and nonmetals in similar manner, simple spectra and quantification, and so forth. TXRF has been used for the determination of trace levels of different elements in actinide oxides, e.g. uranium and thorium oxides [48, 127]. It was already discussed that there are several

problems associated with analysis of low Z elements at trace level by TXRF. Some studies are reported in the literature for the determination of low Z elements in uranium matrix. In one of the studies reported earlier, the determination of trace levels of low- Z elements Na, Mg, and Al was carried out in synthetic uranium samples after separation of uranium using solvent extraction. Later, the developed methodology was extended for the determination of low- Z elements in real uranium samples. These studies were carried out under bilateral collaborative programs between our institute and L. Eötvös University, Budapest, and later with Atominstitut, Vienna, respectively [105, 110]. Tri- n -butyl phosphate (TBP) was used as liquid extractant for the separation of uranium in those studies. This organic extractant has very high affinity towards uranium, thorium, plutonium, zirconium at some specific conditions and hence it is often used for the separation and purification of these elements [128-130]. The high affinity of TBP towards uranium is due to presence of $P=O$ bond in it, which forms complex with uranyl ion (UO_2^{2+}) when it comes in contact with uranyl solution in proper acidic medium. While analyzing real uranium samples, it was observed that even if a very small amount of uranium is present in the aqueous phase (due to little solubility of TBP in aqueous phase), it resulted in interference between the escape peaks of $U\ M\alpha$ with $Al\ K\alpha$ and thereby the results obtained for low Z elements in the uranium matrix, specially for Al were erroneous [110]. In this chapter a study was carried out which shows rigorous separation of uranium is required to get better results for the determination of low Z elements in uranium matrix. Fluorine is a low Z , hazardous and corrosive element which is undesirable in many technological as well as environmental samples. Presence of fluorine above some certain concentration can have detrimental effect on the operation of a nuclear reactor over time in terms of problems in structural materials, nuclear fuel, and coolants [131-133]. Its determination in nuclear reactor components is necessary for the safe

operation of the reactor. Presence of fluorine in nuclear fuel, cladding materials or coolant can cause severe corrosion [133]. Fluorine also plays very important role for human health like bone formation and increasing bone mass [134, 135]. However excess intake of fluorine can cause skeleton fluorosis and tooth disintegration [136]. There are several fluorine containing minerals present in earth crust and their dissolution in ground water causes fluorine contamination [134]. The world health organization has specified the maximum tolerable limit of fluorine in drinking water as 1.5 mg L^{-1} [137]. Similarly a fast analytical method for the determination of fluorine is important in drinking water to protect human health, in high purity water samples to aid industrial processes, such as semiconductor production and power plant operation, and in light/heavy water cooled/moderated nuclear reactors [133]. ICP-MS and ICP-AES are often used to determine trace elements in different matrices. However it is very difficult to determine halogens because of their high excitation and ionization energies. The analytical techniques available for halogen determination are ion chromatography (IC), gas chromatography (GC), spectro-photometry, and specific ion selective electrode (ISE) [138-141]. Most of these techniques require very rigorous sample preparation; for example, a large volume of eluent is needed to separate the analyte on the IC column. Furthermore, inert gases are needed to pressurize the eluent in some IC instruments and the sample must be in the vapor phase for gas chromatography separation and determination. Such requirements make sample analysis using these techniques costly and time consuming. Another major problem of determining fluoride concentration in water samples using specific ion selective electrode (ISE) is the binding of fluoride with aluminum, which cannot be fully de-complexed using the ISE method [142, 143]. In addition to the difficulties present for the determination of low Z elements by TXRF as discussed earlier, analysis of halides like F, Cl, Br has additional problems. For the determination

of any trace element by TXRF, internal standards (IS) are used which are mostly acidic solutions of elements like Ti, Sc, Mg etc. These acidic solutions convert fluoride and other halides into volatile HF, HCl, or HBr etc. They are lost in gaseous form during TXRF specimen preparation, which involves heating a few microliters of the solutions on sample supports [38, 144]. The TXRF determination of fluorine becomes more difficult due to the interference of F K α peak (677 eV) with strong O K α (543 eV), coming from the flat polished quartz (SiO₂) sample support. Therefore when the fluorine concentration present in the sample is very small; the F K α peak is submerged under the tail of strong O K α peak. All these problems mentioned above, need to be tackled for the trace determination of low Z elements like fluorine by TXRF. Vacuum chamber TXRF; with Cr K α excitation source is ideal for analysis of low Z elements, and can be used for fluorine determination also. The strong interference of O K α can be avoided by using a suitable oxygen free sample support, such as silicon wafers. Tabuchi et al. recently reported a method for analyzing halide samples (Cl and Br) without using an internal standard. The study shows that the analyte X-ray line intensity was highly dependent on the position of the dried residue on TXRF supports. The authors controlled the position of the dried residue carefully and obtained a calibration curve with good correlation between the Cl or Br amount on the support and the respective intensity of their X-ray analytical lines [145].

Direct analysis avoids the use of acidic internal standards, and prevents the loss of halogen during preparation of the TXRF specimen for its determination. However, the authors did not attempt to determine F because the instrument available to them was not capable of low-Z element determination probably. In our laboratory we have the facility of analyzing low Z elements like F using vacuum chamber TXRF. Using this TXRF spectrometer and the calibration method adopted by Tabuchi et al., we have made some studies on the determination of F in water

samples. Interference of the O K α and F K α peaks could be reduced using Si-wafer supports. We have carefully controlled the position of the TXRF sample droplet on quartz carriers to minimize the errors associated with sample deposition. By carefully applying these experimental strategies, we developed a simple TXRF method for trace determination of F that should be useful in quality control of drinking water and other high-purity water samples of industrial importance.

In view of the above discussion, we planned the following studies on the determination of low Z elements in uranium and water samples:

- 1) Comparative study of the determination low Z elements using synchrotron and lab based TXRF spectrometry.
- 2) Improved approach for the trace determination of low Z elements in uranium samples.
- 3) Determination of trace amounts of fluorine in high purity water samples.

3.2. A comparative study on the TXRF determination of low Z elements using X-ray tube and synchrotron excitation

3.2.1. Experimental

3.2.1.1. Sample preparation

Multi-elemental standard (MES) solutions of low Z elements (F, Na, Al, S, K, Ti) with elemental concentration of 2, 10, 20, and 30 $\mu\text{g/ml}$ were prepared by mixing respective single-element standards and diluting them appropriately with 1.5% suprapure HNO_3 prepared in Milli-Q water. Sc and Mg were separately added to the solutions and used as internal standards. The final concentration of Sc and Mg in each of the solution was kept constant at 5 $\mu\text{g/ml}$. Aliquots of 10 μl of each sample were deposited on three quartz TXRF sample supports by heating the specimens on a hot plate at around 100 $^\circ\text{C}$, so that the aliquots are dried in form of a thin film on

the support. The standard deviations of the TXRF quantifications were determined by using the relative standard deviation values (1σ) of these three measurements.

3.2.1.2. Instrumentation

All the samples prepared were analyzed by using a laboratory based low Z–high Z TXRF spectrometer and at the XRF beamline of Elettra Sincrotrone Trieste, Italy. The details of the instrumentation are given in chapter 2.

3.2.2. Results and discussions

3.2.2.1. Studies on inhomogeneous distribution of elements

A comparison of three overlapped TXRF spectra of a MES solution, containing 200 ng of each element (except Mg and Sc that were 50 ng) deposited separately on three different quartz sample supports and measured by the low Z – high Z TXRF laboratory spectrometer are shown in Figure 3.1. It can be seen that the Sc and Ti $K\alpha$ X-ray line intensities do not follow the rather proportional change of the other elemental X-ray line intensities. This indicates that the spatial distribution of these two elements (Sc and Ti) is non-uniform. The inhomogeneous elemental distribution becomes critical for the TXRF trace elements' quantification when the sample size ($2\text{--}3\text{ mm}^2$) is much larger than the actual beam footprint (around 0.13 mm in X direction) of SR excitation at the Elettra XRF beamline. For this reason, SR TXRF scanning measurements were conducted by using 5.41 keV exciting SR along the X-axis (20 s/step, 0.1mm/step) for the 20 $\mu\text{g/ml}$ elemental concentration MES solution. In order to investigate, if the elements are deposited uniformly across the dried residue, the variation of the different elements characteristic of X-ray intensities obtained from the X-axis scan measurements is shown in Figure 3.2

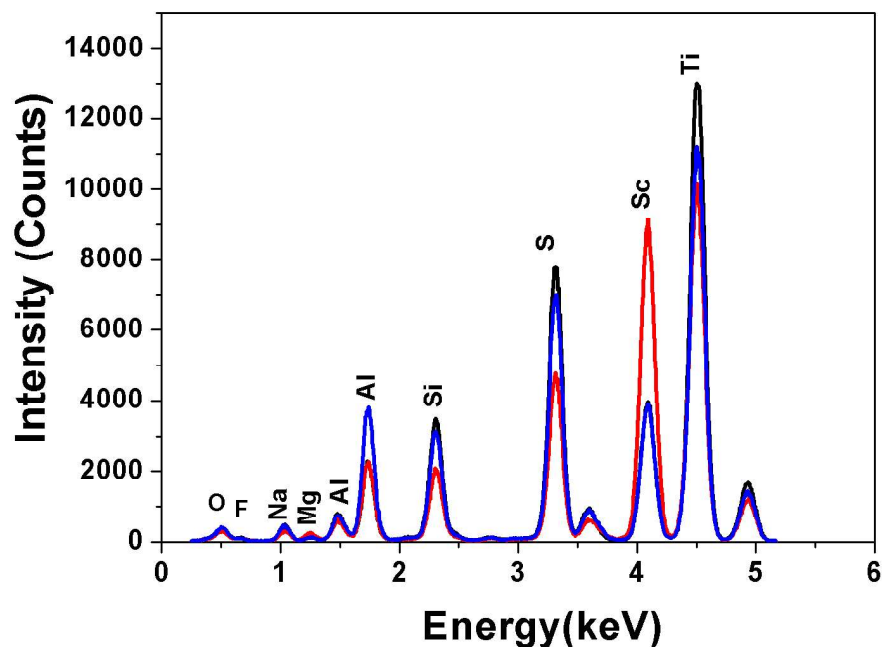


Figure 3.1: A comparison of three overlapped TXRF spectra of 20 $\mu\text{g/ml}$ MES solution deposited on different quartz sample supports and measured using the Cr $K\alpha$ as excitation, in vacuum atmosphere for a live time of 1000s

For better comparison, the elemental X-ray line intensities were normalized to that obtained in the slice #20. It can be seen from Figure 3.2 that the Sc $K\alpha$ vertical slice distribution (and to a less extent Ti $K\alpha$ too) exhibits significant inhomogeneity close to the one border of the sample residue. For this reason, it is preferable to utilize Mg as internal standards instead of Sc. The inhomogeneous distribution of different elements including internal standard on the TXRF sample support may affect the quantitative results significantly if the irradiated area seen by the detector is smaller than the total sample specimen. Therefore, the cumulative TXRF spectra obtained by summing up the individual spectra recorded by performing the X scan measurements represent and reflect the total mass of the specimen analytes in a better manner in the synchrotron set up.

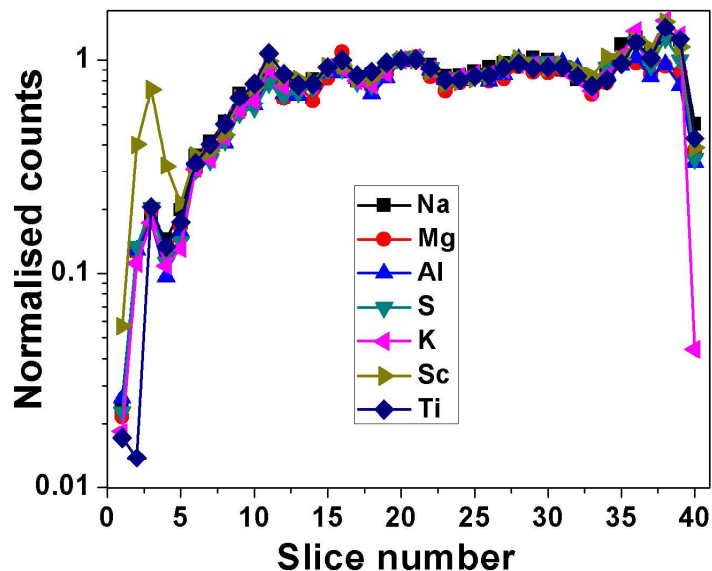


Figure 3.2: The distribution of X-ray line intensities of different elements along X-axis obtained by scanning the SR beam across the sample residue (by dividing the sample residue into different slices) with X-ray energy 5.41 keV at the XRF beamline. The counting time per slice was 20 s, and the counts recorded for different elements were normalized with respect to their respective value at the slice #20.

3.2.2.2. Detection limits

The multi-elemental standard solutions having elemental concentrations of 2 and 20 $\mu\text{g/mL}$ except Sc and Mg which were having concentration of 5 $\mu\text{g/mL}$ were used for the determination of relative sensitivity values, whereas the other remaining solutions were used for validation. The absolute detection limits (DL) expressed in picogram for each element were calculated by using the TXRF spectrum of MES having 20 ng of each element deposited (except Mg and Sc which were having 50 ng mass on the supports) on the sample support. The following equation was used to calculate the detection limit;

$$\text{DL} = \frac{3 \cdot \sqrt{I_B}}{I_A} * m_A \quad (3.1)$$

Here I_B denoted the background area below the analyte peak, I_A is the analyte peak area and m_A is the mass of the analyte deposited on the quartz sample supports.

The DLs obtained for the low-power Cr anode X-ray tube of the low Z -high Z laboratory-based TXRF spectrometer and those obtained with SR TXRF by using two excitation energies (5.41 and 3.8 keV) are reported for a measurement time of 1000 s in Table 1.1 and in Figure 3.3. It can be seen that for fluorine, in particular, the DL of 5 ng is achieved by using the Cr $K\alpha$ tube radiation, which is significantly lower compared to that reported (10–70 ng) in the literature by using high-power X-ray tubes [113]. By using a SR excitation beam with same energy of Cr $K\alpha$ radiation (5.41 keV), the respective DL for F is further improved down to 1 ng. Moreover, while using the lower energy exciting beam (3.8 keV); the DL for F can be further improved to 0.7 ng, determined by using the cumulative TXRF spectrum. So by using SR, three to five times improvement in DL can be achieved for low Z elements ($Z < 13$). The effect of shifting the exciting beam energy towards the analyte absorption edge results in a considerable increase of the photoelectric absorption and, therefore, of the analyte XRF intensity. However it should be noted that the DLs deduced from the SR tunable excitation are heavily influenced by the restricted solid angle of detection. The use of a long magnetic electron trap optimized in terms of its length and inner diameter to deflect energetic electrons with energy even more than 10 keV is not optimum in conjunction with the use of low-energy exciting beams for low Z element analysis [117]. For example, in the vacuum chamber and X-ray tube based spectrometer, the magnetic electron trap is custom made and with a minimum length of 2 mm only offers a relatively very short distance of about 3 mm between the SDD crystal and the sample carrier. A careful comparison of the solid angles of detection for the respective two experimental setups has shown that the SR has about 29 times smaller solid angle; thus, the respective DLs increase almost by a factor of about 5 times.

Table 3.1: Comparison of detection limits obtained using different excitation sources and energies

Elements	Detection limits (pg)				
	Laboratory (Cr-K α Tube excitation in vacuum) (A)	SR (Elettra) with excitation energy			
		5.41 keV [#] (B)	3.8 keV [#] (C)	A/B	B/C
F	5190	1075	698	4.8	1.5
Na	1026	317	124	3.2	2.6
Mg	753	240	103	3.1	2.3
Al	403	116	54	3.5	2.1
S	96	26	20	3.7	1.3
K	55	18	8	3.1	2.3
Sc	29	13	-	2.2	
Ti	29	13	-	2.2	

[#]: Obtained using cumulative spectrum from vertically scanned measurements

These preliminary results have demonstrated the need for a custom redesign of the magnetic electron trap used in the SR setup by correlating its geometrical features carefully in accordance with the particular excitation energy regime needed for TXRF analysis. It can be also seen that there is excellent improvement in the DL of low Z element like fluorine with 3.8 keV compared to that obtained with 5.41 keV SR excitation. This suggests that a low energy excitation shall be much beneficial for the analysis of low Z elements with lab based sources also. X-ray tube with appropriate anode materials (Rh, W), geometrical features and thin window can produce efficient low-energy exciting X-ray beams (e.g. Rh-L, W-M) that could be eventually utilized for the

sensitive analysis of low and medium Z elements by using their K and L emission lines respectively.

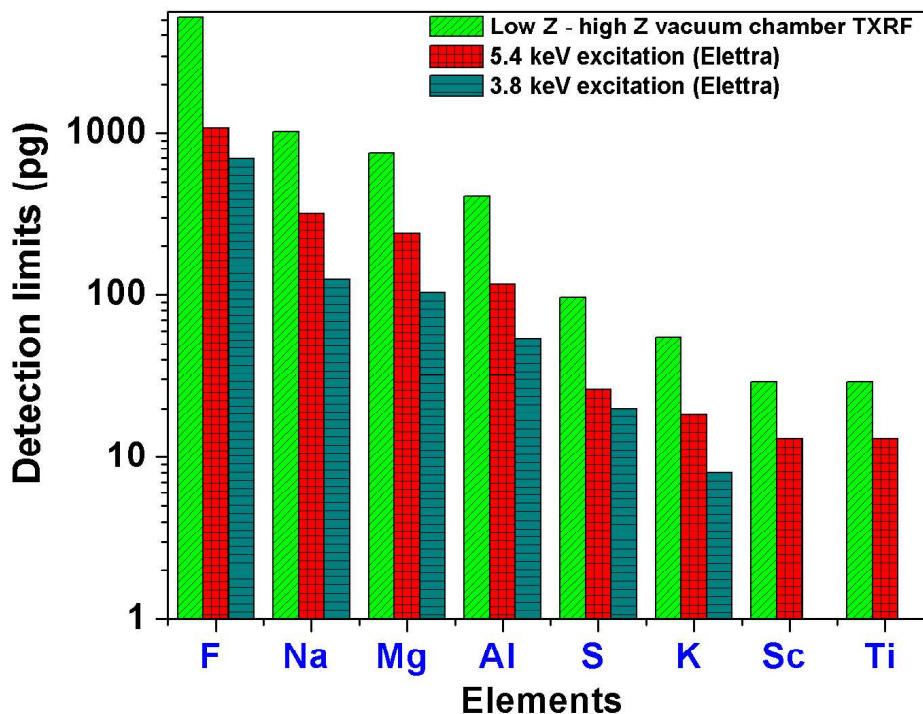


Figure 3.3 Comparison of TXRF elemental detection limits (expressed in absolute analyte mass) by using different excitation sources.

Representative TXRF spectra of a MES solution with elemental concentration of 10 $\mu\text{g/mL}$ (except the Mg and Sc with 5 $\mu\text{g/mL}$ concentration) measured by using Cr $K\alpha$ excitation in both laboratory and SR setups are shown in Figure 3.4. The improvement in the intensity of characteristic X-ray lines and the decrease in the TXRF spectral background while using SR excitation compared with that of X-ray tube-based Cr $K\alpha$ excitation are clearly visible.

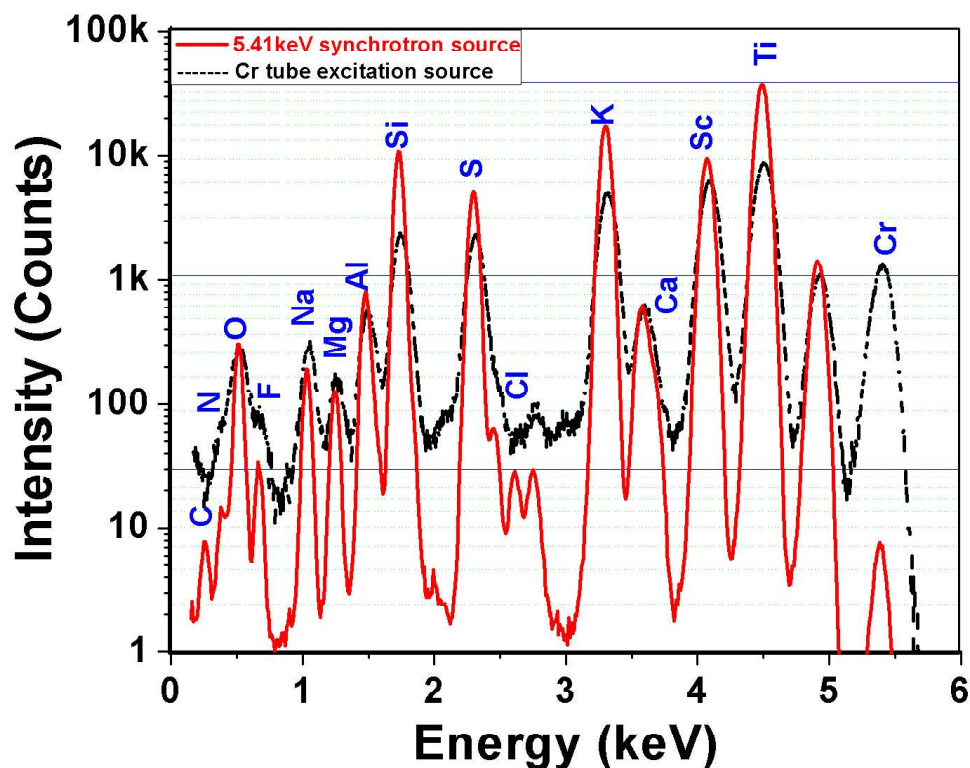


Figure 3.4 : Representative TXRF spectra (1000 s measuring time) of a MES solution containing elements with 10 $\mu\text{g/ml}$ concentration (except the Mg and Sc with 5 $\mu\text{g/ml}$ concentration) measured using 5.41 keV SR excitation (equivalent to Cr K α energy) and the tube-based Cr K α excitation

The AXIL program fitted TXRF spectra of the MES solutions having elemental concentration of 10 $\mu\text{g/mL}$ (except the Mg and Sc with 5 $\mu\text{g/mL}$ concentration) measured by using three different excitation modes, discussed before, are shown in Figure 3.5 a-c. In addition to analyte X-ray lines, the Si and O K α peaks are coming from the sample supports. Other low Z elements like C and N are also visible in the TXRF spectra. Carbon is more efficiently detected by using SR at 3.8 keV excitation energy compared to that of 5.41 keV, whereas the spectrum obtained with lab based excitation source; C K α is almost merged with O K α peak. Previous studies have demonstrated the potential of SR to carry out even quantitative XRF and grazing incidence XRF analysis of light elements contained in buried boron and carbon nano-layers on

silicon substrate excited optimally by 510 eV undulator radiations and measured by a calibrated setup with a windowless SDD [146].

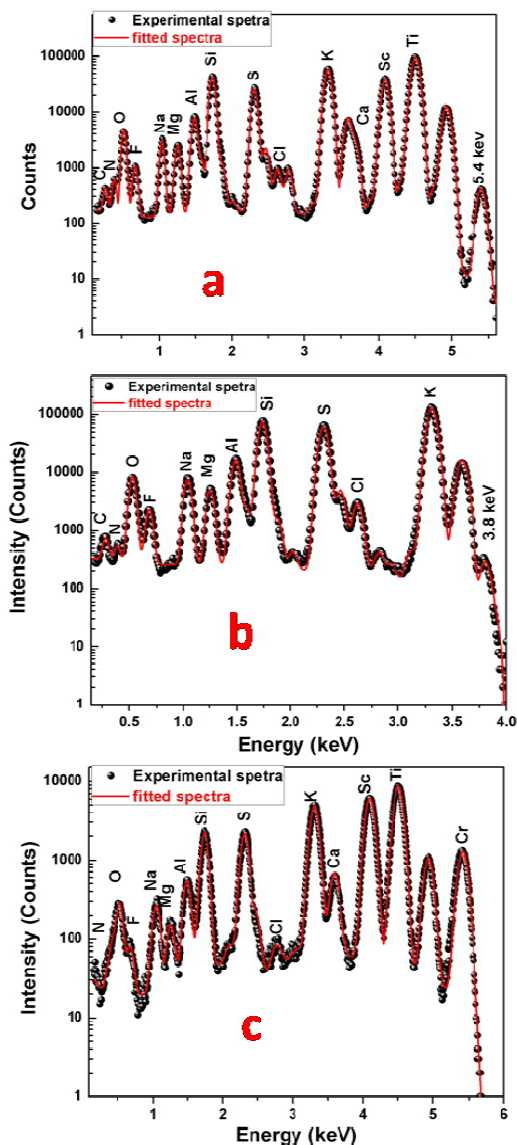


Figure 3.5: The experimental (dots) and fitted TXRF spectra (continuous line) of 10 μ g/mL, MES solution obtained using (a) 5.41 keV SR, (b) 3.8keV SR and (c) Cr K α tube based excitation

3.2.2.3. TXRF quantification

The quantitative results obtained for the 10 and 30 μ g/mL MES solutions (except the Sc with 5 μ g/mL concentration) by using low Z – high Z TXRF spectrometer with Cr K α excitation

and the SR beams of 5.41 and 3.8 keV are compared with the help of a bar diagram shown in Figure 3.6A and Figure 3.6B respectively.

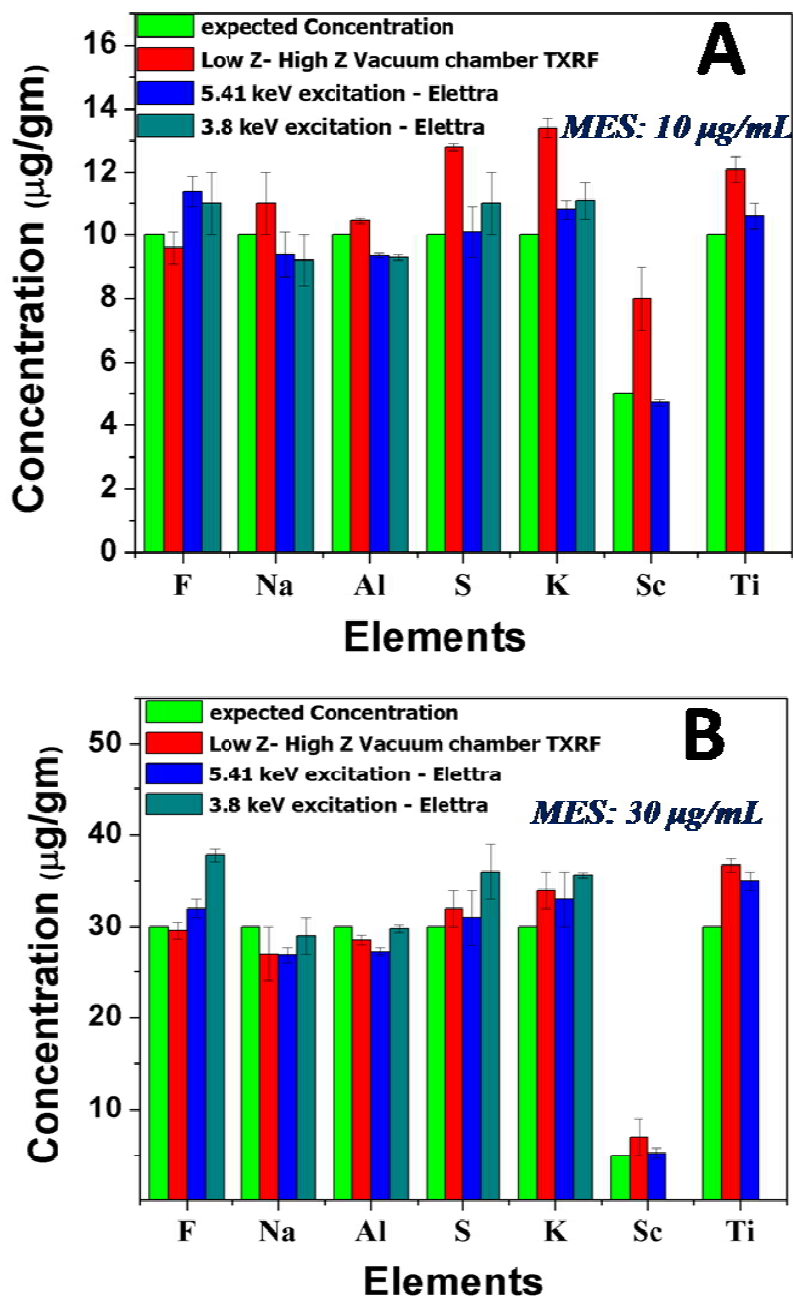


Figure 3.6: Comparison of the quantitative results obtained for the multi-elemental standard with 10 $\mu\text{g/ml}$ (A) and 30 $\mu\text{g/ml}$ (B) elemental concentrations (except Sc with 5 $\mu\text{g/ml}$ concentration) using the low Z–high Z TXRF spectrometer (Cr K α excitation) and two SR beams with 5.41 and 3.8 keV exciting energies, respectively, versus the expected concentrations

From the results included in these figures, it can be observed that the quantitative TXRF results in both setup present an average relative deviation with respect to the nominal values of less than around 10% (30 $\mu\text{g/ml}$ MES) or 16% (10 $\mu\text{g/ml}$ MES) and a precision better than 5% (excluding the results obtained for Sc by using the laboratory TXRF spectrometer that were inferior due to its inhomogeneous deposition). In the case of the Cr $K\alpha$ tube excitation, it is possible that only a part of the sample is illuminated by the incident beam or only X-rays emitted from a part of the specimen could reach the detector. Therefore, if there are elements like Sc and Ti that are inhomogeneously distributed within the specimen mass, the quantitative results for these elements are expected to be less accurate (the deviation for Sc was found in the range of 40–60% and 20% for Ti) and reproducible.

The above study suggests that detection limits and analytical parameters for TXRF determination of low Z elements improve drastically by using excitation energies just above the respective absorption edges. Also a small volume of sample specimen should be deposited on the TXRF sample supports to improve the analytical parameters.

3.3. Determination of low Z elements in uranium samples by TXRF

Using the conclusions drawn in previous study, the TXRF methodology for low Z elements determination has been utilized for the trace impurities determination in uranium samples after the separation of the major matrix uranium in a better way.

3.3.1. Experimental

3.3.1.1. Reagents

The TXRF spectrometer was calibrated for low- Z elements using MERCK single-element standard solutions of Na, F, Mg, Al, S, K, Sc, and Ti. De-ionized water having 18 $\text{M}\Omega$ -

cm of specific resistance was used for the sample preparation as well as for the dilution of the samples. Three CRMs for uranium oxide, namely, CRM-III, CRM-IV, and CRM-V, developed by Department of Atomic Energy, Government of India, were used for counterchecking of TXRF determination results in uranium oxide matrix. Concentrated supra pure nitric acid was used to prepare 4 M HNO₃ required for the uranium solution preparation. A 30% TBP solution in n-dodecane, equilibrated with 4 M HNO₃ was used for extraction of uranium from the uranium solution samples.

3.3.1.2. Instrumentation

TXRF measurements were carried out by using a low Z – high Z TXRF spectrometer (WOBISTRAX). The TXRF spectra obtained for low Z elements were processed using the IAEA QXAS package having AXIL program.

3.3.1.3. Sample preparation

For the determination of elemental X-ray line sensitivities for low-Z elements F, Na, Mg, Al, S, K, and Sc; two multi-element standard (MES) solutions having elemental concentration of 2 and 10 µg/ml were prepared by mixing the corresponding MERCK single-element standards and diluting the resultant solution mixture to the required concentrations using ~1 M nitric acid. Titanium was added as internal standard in these solutions with a constant resultant concentration e.g. 10 µg/ml.

The TXRF spectra of these standards were measured for 1000s, and the relative sensitivities of the elemental X-ray lines with respect to Ti K α were determined. For the preparation of solutions of CRMs of uranium oxide, 514, 230 and 88 mg of CRM-III, CRM-IV and CRM-V were dissolved in 2 mL concentrated suprapure HNO₃ and each of the solution obtained are evaporated to dryness and finally they were dissolved in 2 mL volume of 4M HNO₃

solution and Ti was added as an internal standard. For the major matrix uranium separation from the CRM solutions, 0.5 ml volume of these solutions was intensively equilibrated for about 5 min with equal volume of 30% TBP solution in n-dodecane equilibrated with 4M HNO₃ in a 2ml capacity tightly closed centrifuge tube using a Vortex shaker. The mixed phases were allowed to separate by leaving the centrifuge tubes on a tube stand for about 10 min. When both phases got separated with organic phase at upper part and aqueous phase at lower part of the above solution, the uranium-rich organic phase was removed carefully with the help of a micropipette and the aqueous phase was again treated in similar manner. Total eight such separation steps were performed. Finally, the aqueous phase was equilibrated with an equal volume of n-dodecane three times so that any dissolved TBP is removed from it. Such removal of TBP is necessary for getting low background in TXRF spectra. The flow chart for the sample preparation procedure is depicted in Figure 3.7. For the preparation of sample blank, all the above steps were followed except that milli-Q water was taken in place of uranium solutions in the beginning.

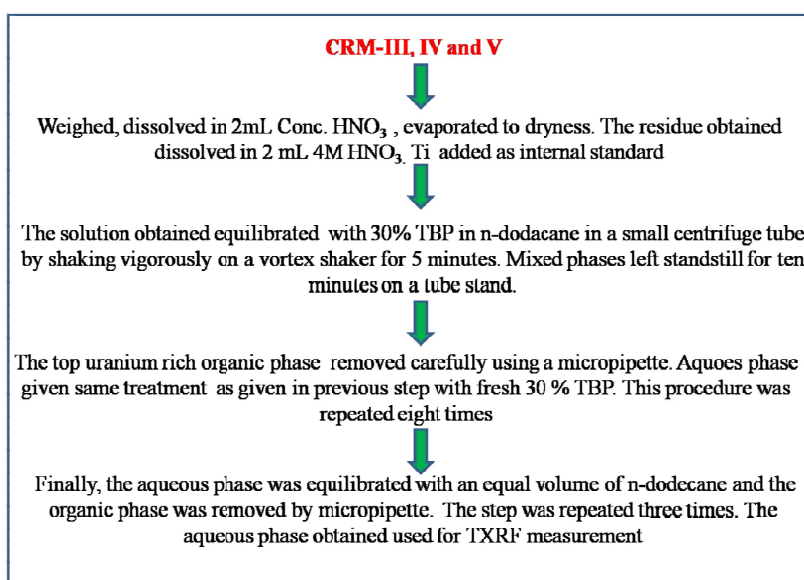


Figure 3.7: Flow chart of the sample preparation steps for the processing of uranium oxide samples for trace low-Z elements determination by TXRF

TXRF measurements were carried out with 5 μL aliquots of the aqueous phase carefully deposited on three clean quartz sample supports and vacuum dried in a desiccator so that a very small area sample specimen is formed and we can avoid the adverse effect of non-uniform migration of ions in TXRF analytical results as observed in earlier study. All the TXRF measurements were carried out for a live time of 1000s.

3.3.2. Results and discussions

Generally any element which is not present in the sample and is having its characteristic X-ray lines detectable by the instrument can be used as internal standard for TXRF measurements. However elements whose X-ray lines do not interfere with the other elemental X-ray lines observed in TXRF spectrum of the sample and having better excitation efficiency are preferred as an internal standard. Due to these reasons Ti was chosen as an internal standard as it is not present in the CRMs used, moreover Ti K absorption edge (4.96 keV) is just below Cr $K\alpha$ line energy (5.41 keV), and there is no interference of Ti $K\alpha$ with other elements present in the sample matrix except Ba $L\alpha$ which was not observed in the standards.

The relative sensitivity values of different elemental X-ray lines with respect to Ti $K\alpha$ were calculated using MES solutions having elemental concentrations of 2 and 10 $\mu\text{g/mL}$. The plot of relative sensitivity values against the atomic number is shown in Figure 3.8. During the plot of this relative sensitivity curve we have not considered the relative sensitivity value of fluorine due to the reason mentioned later. The relative sensitivity value of Sc is also not considered while making the calibration plot as we have observed before that there may be a possibility of non-uniform distribution of Sc throughout the sample residue, which can give erroneous result for relative sensitivity values.

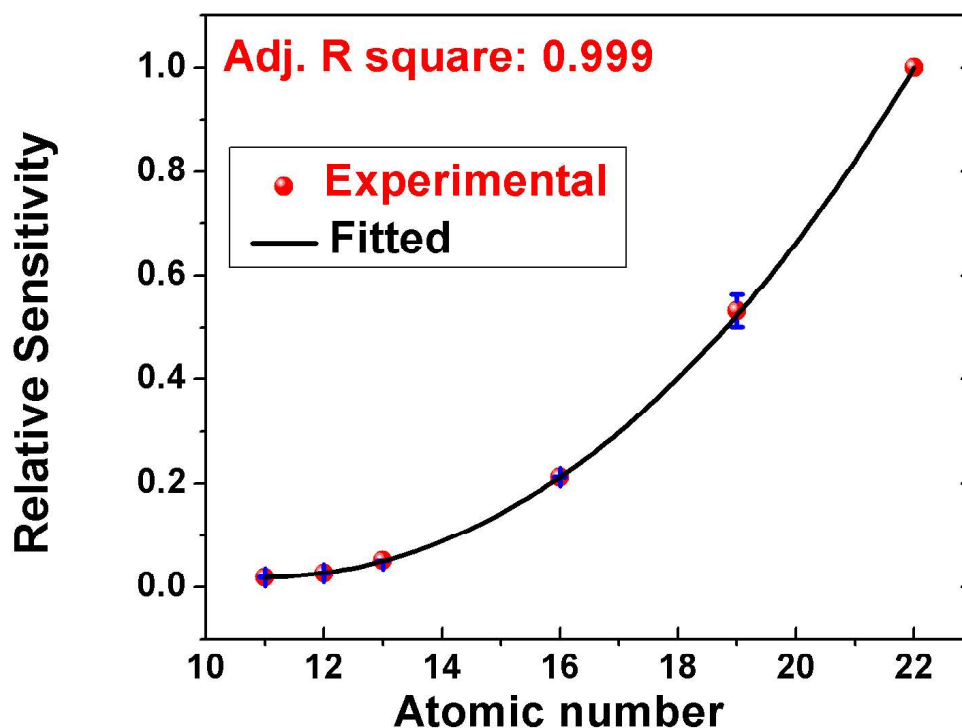


Figure 3.8: Plot of relative sensitivity values (*Cr K α* as excitation source and *Ti* as an internal standard) against atomic number. (The error bar is visible for *K* only. In other cases, the error bars are contained within the size of the dots)

The plot was fitted with a third-ordered polynomial function. The equation of the polynomial curve is

$$RS = B_0 + B_1Z + B_2Z^2 + B_3Z^3 \quad (3.2)$$

Here RS = Relative sensitivities of the elemental X-ray lines, B_0 is the intercept, B_1 , B_2 and B_3 are co-efficient of the polynomial curve and Z is atomic number. The plot shows that there is a gradual increase of relative sensitivity values with increase of atomic number, which is expected when TXRF conditions are satisfied in a good manner [47]. The relative sensitivity values of other elemental X-ray lines ($K\alpha$ lines) not present in the above MES can also be calculated by using the above equation. The low Z elements are present in ppm level in uranium oxide CRMs and hence the detection limits obtained previously for different low Z elements as

shown in Table 3.1, are sufficient to determine trace low Z elements in these uranium oxides considering the dilution of trace elements during the sample preparation in above manner.

The TXRF spectra of a processed CRM-IV solution measured after five, eight time TBP extraction and subsequent three time equilibration with n-dodecane are shown in Figure 3.9.

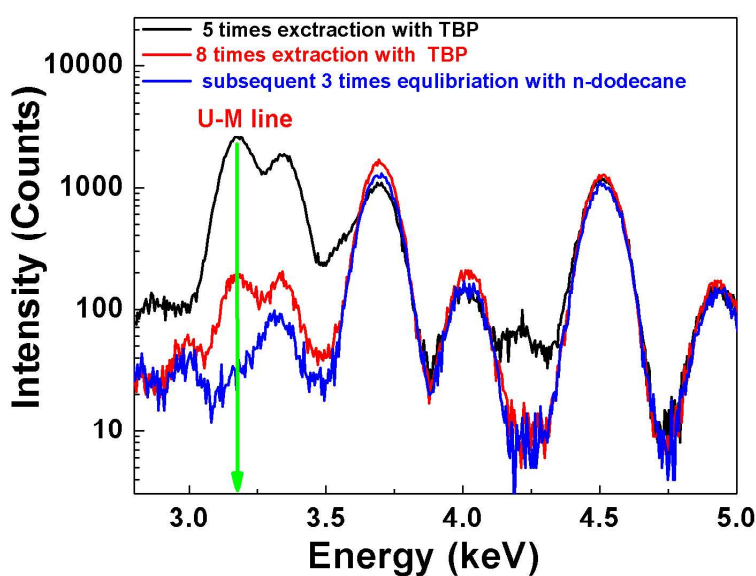


Figure 3.9: A comparison of TXRF spectra of a processed uranium oxide (CRM-IV) after five and eight time extraction with TBP and subsequent three equilibrations with n-dodecane.

It can be seen from the figure that after giving 5 contacts with TBP, although the intensity of U M lines reduced but still these are appreciably high. This may create problems in trace determination of low Z elements, especially for Al determination as the U M escape peaks ($U M\alpha = 3.171$ keV, $U M\alpha Esc = 1.421$ keV, $Al K\alpha = 1.487$ keV) will interfere strongly with $Al K\alpha$. That's why uranium should be removed completely from the solution for better analytical results. To remove the maximum percentage of uranium from the solutions; it was further equilibrated with 30% TBP for three more times. It was observed that even though the concentration of uranium decreased appreciably after eight time separations, still $U M\alpha$ (3.171 keV) peak was clearly visible in the spectrum probably due to the presence of some dissolved

TBP in aqueous phase. Such dissolved TBP contains trace amounts of uranium, which create problems in the TXRF determination of trace low-Z elements in terms of background and interference. This TBP must be removed from the solutions for better analytical results. In order to remove the dissolved TBP, the aqueous phase was given three more contacts with n-dodecane. Such processing removed the traces of TBP from the solutions. It can be seen that U M lines are almost absent in the TXRF spectrum of the aqueous phase obtained after final step processing of the sample.

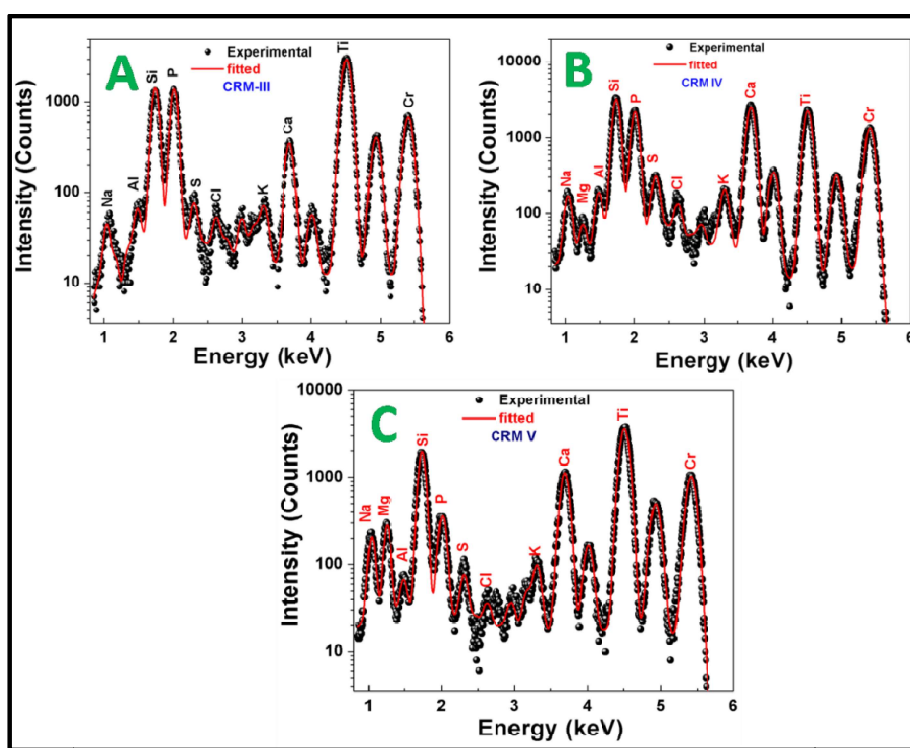


Figure 3.10: AXIL fitted TXRF spectra of the processed uranium oxide CRMs after selective removal of uranium

The AXIL software was used for the spectral fitting and analysis of the TXRF spectra. The spectra could be processed with very good fitting parameters and were used to determine the respective trace elements in the samples using the relative sensitivity values and the intensities of analytical X-ray lines. The AXIL fitted spectra of final processed CRM-III, IV and V after

complete removal of uranium as discussed earlier are shown in Figure 3.10 A, B and C respectively.

It is observed from Figure 3.10 that the fitting achieved with AXIL program is good. The Si K α line in the TXRF spectra is coming from the quartz sample supports, P K α peak is coming due to the very traces of TBP remained dissolved in the aqueous phase, whereas Ti K α peaks are due to the internal standard added in the solution. The results of TXRF determinations of trace elements present in the CRMs are shown in Table 3.2.

Table 3.2: Results of TXRF determination of low Z elements in different CRM Standards (all values in $\mu\text{g/g}$)

Elements	CRM-III			CRM-IV			CRM-V		
	Cert ^a .	TXRF ^b	A/B	Cert ^a .	TXRF ^b	A/B	Cert ^a .	TXRF ^b	A/B
	(A)	(B)		(A)	(B)		(A)	(B)	
Na	9.1	9.6 \pm 0.5	1.05	130	146 \pm 12	1.11	970	937 \pm 97	0.97
Mg	1.7	Not detected	-	56	48 \pm 6	0.86	2400	2127 \pm 108	0.88
Al	1.1	4.0 \pm 0.4	3.63	64	64 \pm 4	1.00	210	216 \pm 30	1.03
S	-	1.9 \pm 0.1	-	-	31 \pm 2	-	-	62 \pm 8	-
K	-	0.88 \pm 0.02	-	-	7.7 \pm 0.5	-	-	37 \pm 5	-
Ca	4.7	4.6 \pm 0.1	0.98	100	111 \pm 5	1.11	510	525 \pm 59	1.03
<i>Average RSD=5.0%</i>			<i>Average RSD=7.4%</i>			<i>Average RSD=11.2%</i>			

^aCertified concentration, ^bTXRF determined concentration $\pm 1 \sigma$ ($n=3$).

The certified values of S and K are not available.

From the Table 3.2 it can be seen that the concentration of Mg and Al present in CRM-III is very low and could not be detected whereas Al could be determined with poor agreement between TXRF determined and certified value. The certified concentration of Mg in CRM-III is 1.7 $\mu\text{g/g}$ of U. After considering the dissolution of the standards in HNO₃, the Mg concentration

in the solution is $\sim 0.4 \mu\text{g/mL}$ (514 mg of CRM-III is dissolved in 2 mL of 4M HNO_3). The aliquot volume of 5 μl sample solution on the quartz supports gives absolute amount of Mg deposited on the TXRF sample support $\sim 2 \text{ ng}$. The absolute detection limit of Mg determined in this study is 0.753 ng. This indicates that the amount of Mg deposited on TXRF support is very near to the limit of quantification of Mg and that is reason for not detecting Mg by TXRF in this CRM. The agreement between TXRF determined and certified values of Na and Ca is very good. In addition some elements not certified in the CRMs e.g. S and K could also be determined.

The concentrations of low-Z elements present in CRM-IV are higher compared to that in CRM-III, and that's why the intensity of respective low Z trace element X-ray lines are quite high (Figure 3.10b). Due to this reason a very good agreement between TXRF determined and certified values of trace low-Z elements including Mg and Al could be achieved for CRM-IV. The average RSD of TXRF determinations was 7.4% (1σ) and the TXRF results deviated from the certified values by 12.5% (average). Similarly, for CRM-V, the TXRF determined values were found to be in a good agreement with the certified values with an average RSD of 11.2% (1σ , $n = 3$) and the results deviated from the certified values by 5.0%. In case of CRM-III, the TXRF determined result of Al was not included while calculating these values for this CRM which were 5% (1σ) and 4% respectively.

From the above results, it is clear that improved analytical results for elements like Na, Mg and Al are obtained by using an intensive and rigorous methodology for separation of major matrix uranium from the aqueous phase and using better TXRF instrumental conditions for analysis of low Z elements. It can also be concluded that complete removal of uranium from the sample matrix is necessary to obtain the accurate concentrations of low Z elements present in it. This methodology has been applied successfully to determine trace elemental concentrations in

three certified reference materials of uranium oxide. However when the concentrations of these low Z elements are very low (below $1\mu\text{g/g}$); further pre concentration will be required to obtain better results. Analysis of non metals like F, Cl is not possible as they are lost from the sample matrix as HF and HCl respectively during the sample preparation. Separate approach is needed for the quantification of these elements [38]. Sulfur may also get lost in similar manner if it is present as sulfide. During the synthesis, the actinide oxides are heated at very elevated temperature, so any sulfur present in it as impurity shall be in the form of sulfite or sulphate. These sulfite or sulphates are stable in acidic medium, so they will not be lost during the sample preparation and we can analyze these non metals also in uranium oxides.

3.4. Direct determination of fluorine in water samples by TXRF

3.4.1. Experimental

3.4.1.1. Sample preparation

A Merck single-element standard solution of fluorine (NaF solution in water) having F concentration of $1000\mu\text{g mL}^{-1}$ was diluted to 50 mL to obtain a solution with a F concentration of $100\mu\text{g mL}^{-1}$. Aliquots of this solution were further diluted to obtain different solutions (2 mL) with F concentrations ranging from 1 to $25\mu\text{g mL}^{-1}$. Milli-Q water (resistivity, $18.2\text{ M}\Omega\text{cm}$) was used to dilute the sample. It is extremely important to obtain very clean sample supports before deposition of sample on it. Initially, the supports were rinsed with 0.05 M suprapure HNO_3 , followed by ultra-sonication for 10 min in a quartz beaker containing 0.05 M HNO_3 . Later these supports were washed several times with Milli-Q water to remove traces of nitric acid and other surface impurities. Finally, the surface of the sample supports were rubbed with by high-purity ethanol wet tissue paper and dried. The sample supports were checked by TXRF to ensure that

they were perfectly clean and fit for TXRF measurements. Aliquots (5 μL) of the above sample solutions were deposited on clean quartz and Si wafers as sample supports to prepare TXRF specimens. During sample deposition on the supports, it was ensured that the sample was deposited in the middle of the support with a very small sample spot size (1–2 mm). Similarly, stock solutions of F with different fluorine concentrations in the range 100–1000 ng mL^{-1} were also prepared. TXRF specimens were prepared from these solutions by depositing 100 μL volume on the supports by depositing 5 μL aliquots in twenty steps.

3.4.1.2. Instrumentation

A low power low Z – high Z TXRF spectrometer was used for the analysis of fluorine samples. Cr $K\alpha$ was used as an excitation source. The TXRF spectra obtained were analyzed using AXIL program.

3.4.2. Results and discussions

As discussed earlier that there are certain problems in the TXRF determination of fluorine as it can be lost from the sample as volatile HF during TXRF sample preparation using acidic internal standards. It was experimentally observed that fluorine solution prepared in HNO_3 medium having molarity higher than 0.1 M, the F $K\alpha$ line was not visible in that case, indicating complete loss of fluorine during sample preparation in acidic medium. However if fluorine solution is prepared in aqueous medium having $\text{pH} > 6.5$, appreciable intensity of F $K\alpha$ was observed in that case. This suggests that there was no loss of fluorine in that condition during TXRF specimen preparation. TXRF spectra of two fluoride solutions having fluorine concentrations of 10 $\mu\text{g/mL}$, one prepared in 0.1 M HNO_3 medium (black line) and another in Milli-Q water having $\text{pH} \sim 6.5$ are shown in Figure 3.11. Here Si-wafer has been used as sample support which does not contain oxygen on it. It can be seen from the figure that F $K\alpha$ line is not

at all visible in the TXRF spectrum of specimen prepared in 0.1 M HNO₃ medium. The oxygen peak observed in this spectrum is due to the presence of nitrate/oxide residues remaining on the Si-wafer supports, whereas for the specimen prepared in milli-Q water having pH ~ 6.5, F K α line is clearly visible. This observation confirms the loss of fluorine in acidic medium as volatile HF during TXRF sample preparation.

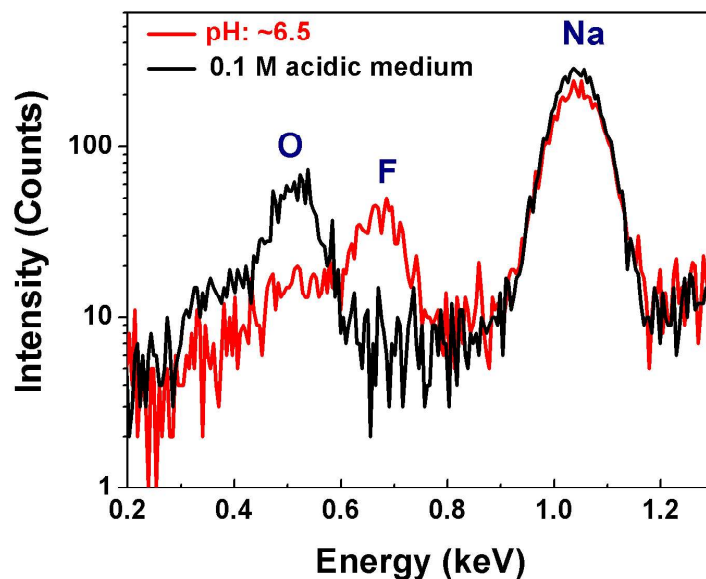


Figure 3.11.: Comparison of TXRF spectra of solutions containing 10 µg/mL of fluoride prepared in Milli-Q water at pH 6.5 and in 0.1 M HNO₃ medium.

For the trace elemental determinations by TXRF, generally a sample solution aliquot of 10 µL is deposited on the sample supports. During the sample deposition, the sample droplets can spread in-homogeneously, resulting in huge variation in analyte line intensity in the TXRF spectrum, because all X-rays emitted from the sample may not reach the detector window with the same geometry and solid angle as discussed previously in this chapter [147]. In order to avoid such problem it is always better that the size of the residue after drying should remain very small, around 1-2 mm in diameter at the centre of the TXRF sample supports. This geometry can be achieved by depositing smaller aliquots of the sample solutions precisely at the center of the

support to ensure that all the X-rays emitted from sample specimens prepared in this manner reach the detector in the same proportion for all measurements. An extensive study using this type of sample deposition was conducted by Tabuchi et al. for TXRF determinations of Cl and Br [145]. This type of sample deposition method was used on two types of support, namely quartz and Si wafer, using 5 μL aliquots of the sample solutions. While depositing the aliquots on these sample supports, it was observed that sample droplets spread over a very small area on Si-wafer supports compared to that observed on the quartz sample supports as it is shown in Figure 3.12. This is probably due to hydrophobic nature of Si-wafers, allowing sample droplets not to spread very much as compared to that on quartz surface [148].



Figure 3.12: TXRF specimen prepared with 5 μL volume of fluoride sample on Si-wafer and quartz sample supports.

TXRF spectra of a sample solution having fluorine concentration of 10 $\mu\text{g}/\text{mL}$ measured for three specimens each of Si-wafer and quartz supports are shown in Figure 3.13. The area of F $K\alpha$ was reproducible in all three measurements on both supports. Figure 3.13 also shows that the quartz sample support produces a high-intensity O $K\alpha$ peak that may cause strong interference with the F $K\alpha$ peak, especially at low F concentrations ($<5 \mu\text{g}/\text{mL}$). This interference can also affect the profile fitting results and, therefore, the quality of the analytical results. However, when the sample was deposited on Si-wafer supports, the O $K\alpha$ peak intensity in the TXRF

spectra was much lower compared with that using the quartz sample supports because the Si wafer supports did not contain oxygen. The small O K α peak intensity seen in the TXRF spectra obtained using Si wafers was attributed to oxygen adsorbed to the support and in the deposited sample. However the low intensity of the O K α peak allowed the two peaks to be clearly resolved by AXIL fitting, producing results expected to be less prone to errors in area estimation of F K α compared with those obtained using quartz supports. For these reasons, the use of quartz sample supports was not suitable for fluoride determination, especially when the fluoride concentration is < 5 $\mu\text{g/mL}$. The AXIL-fitted TXRF spectra of fluoride solution having concentration 5 $\mu\text{g/mL}$, deposited on quartz (A) and Si-wafer (B) supports are shown in Figure 3.14.

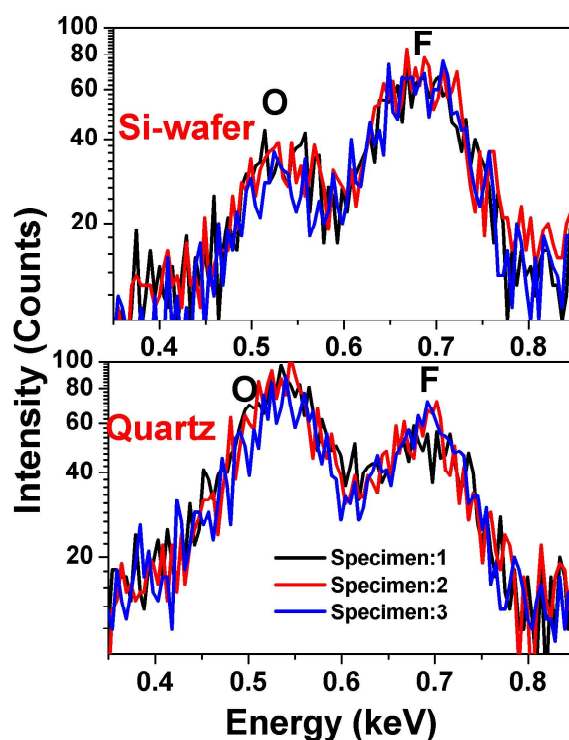


Figure 3.13: Comparison of repeatability of F K α intensity in TXRF spectra of different specimens prepared by depositing 5 μL aliquots of 10 $\mu\text{g/mL}$ fluoride solution on Si-wafer and quartz supports

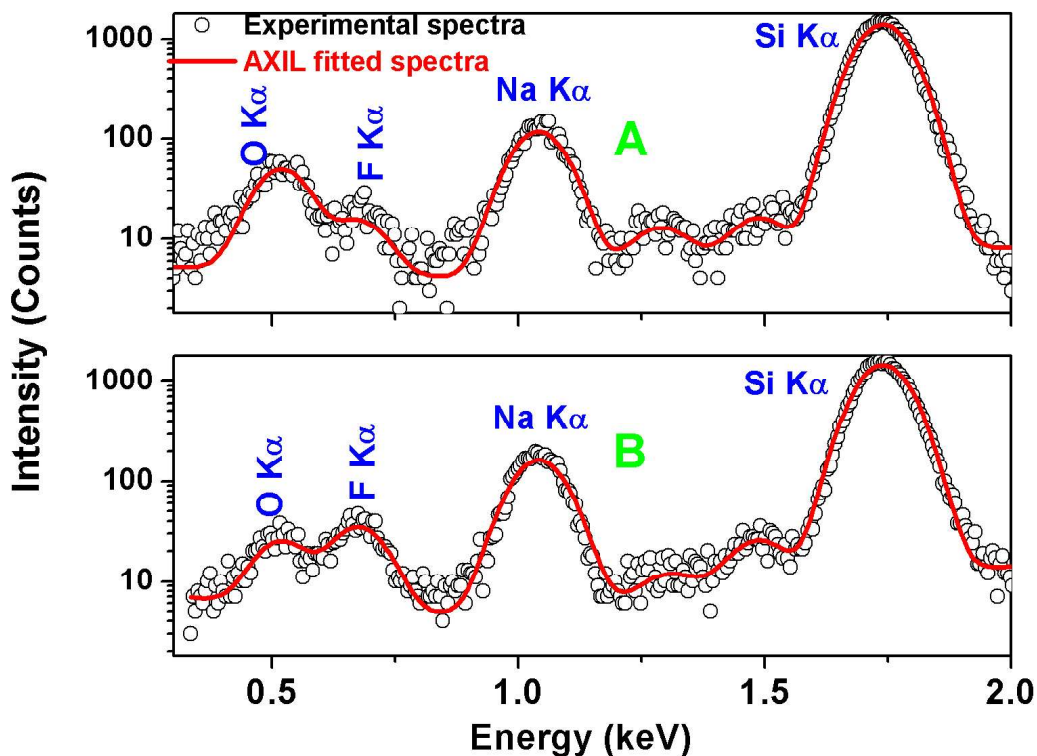


Figure 3.14: AXIL-fitted TXRF spectra of fluoride solutions (concentration 5 $\mu\text{g/mL}$) deposited on (A) quartz and (B) Si-wafer supports

The intensity of O $K\alpha$ line is much higher in the TXRF spectrum obtained using quartz sample supports as compared to that obtained using Si-wafer supports. In addition, an intense peak of Na $K\alpha$ and two small peaks at around 1.25 keV and 1.49 keV are observed. The Na $K\alpha$ peak occurs in the TXRF spectrum as NaF is used to prepare fluoride solution. The two small peaks were due to the presence of ultra trace amounts of Mg and Al, which are common impurities. Although these two peaks are situated far from the F $K\alpha$ peak, still they were considered while fitting the spectra to avoid errors in area determination of small F $K\alpha$ peak.

To determine the detection limits (DLs), 25 ng of analyte (5 μL of solution having fluoride concentration of 5 $\mu\text{g/mL}$) was deposited on both Si-wafer and quartz sample supports and TXRF measurements were made using these two sample specimens for a live time of 1000s. The DLs of fluorine obtained using these two supports are compared in Table 3.3.

Table 3.3: Detection limits for fluorine obtained using vacuum chamber TXRF (Cr K α excitation) with samples deposited on quartz and Si-wafer as sample supports.

Sample support ^a	DL ^a (picogram)	DL ^a ($\mu\text{g/mL}$)
Quartz	5100	1.02
Si-wafer	1873	0.375

^a25 ng analyte was deposited on the both the sample supports and spectral acquisition time in each case was 1000s (Live)

It is observed from Table 3.3 that there is almost three times improvement of DL for fluorine using Si-wafer sample support. This might be because of the increase of background under F K α peak due to tailing effect of the huge O K α peak on the quartz supports.

The TXRF determination of F at concentrations $<5 \mu\text{g/mL}$ was not possible using quartz supports. A comparison of TXRF spectra of fluoride solutions with different F concentrations (2.5–25 $\mu\text{g/mL}$) obtained using quartz and a Si-wafer support is shown in Figure 3.15.

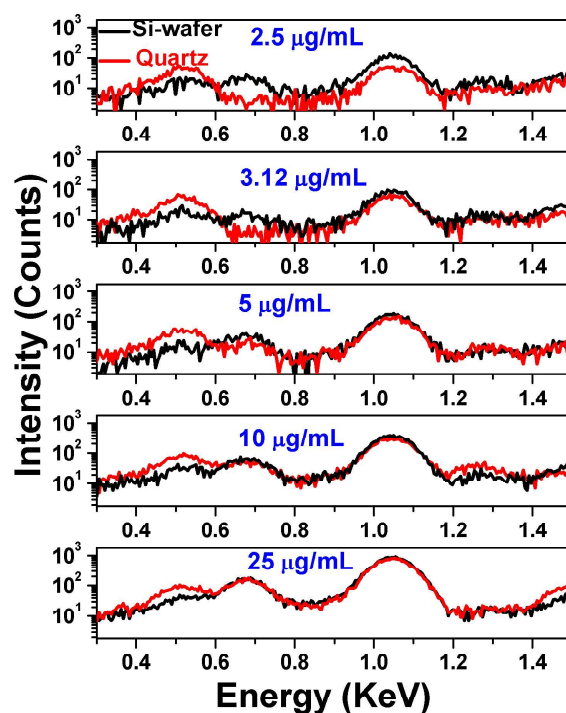


Figure 3.15: Comparison of TXRF spectra of fluoride solutions (2.5–25 $\mu\text{g/mL}$) obtained using quartz and Si-wafer supports

The F K α peak intensity was not visible in the TXRF spectra of solutions with F concentrations of 2.5 and 3.12 $\mu\text{g/mL}$ deposited on quartz supports, but was visible in those of the same solutions obtained using Si-wafer supports. The F K α intensities in the TXRF spectra obtained with quartz and Si-wafer supports for solutions with higher F concentrations were appreciable and similar.

3.4.3. Analysis without using an internal standard

After above studies, it was concluded that using Si wafer support, not using any internal standard and reducing the TXRF specimen spot size in a reproducible method, F K α intensity remain constant for a particular F concentrations limit. This methodology can be used for quantifying F with the help of a calibration curve. To prepare a calibration curve, calibration solutions having F concentrations of 1.0, 2.5, 5.0, 12.5, 15.0, and 25.0 $\mu\text{g/mL}$ were prepared. Aliquots (5 μL) of each of these solutions were deposited at the center of quartz and Si-wafer supports in triplicate and dried under ambient conditions. The TXRF spectra of these specimens were measured for a live time of 1000s. The average F K α intensities of these measurements were plotted against the respective F concentrations in the solutions to obtain calibration curves for direct determinations. For the reason discussed above, such calibration plots for F concentrations below 5 $\mu\text{g/mL}$ were not possible from TXRF spectra measured on quartz supports. For TXRF spectra measured using Si-wafer supports, the intensity of F K α was significant for all solutions, such that all six concentrations were used to obtain the calibration plot. Figure 3.16 shows the calibration plots for TXRF determination of fluorine obtained using TXRF spectra of specimens on both supports. The calibration plot obtained using Si-wafer supports was linear in the respective concentration range, whereas the corresponding calibration plot obtained using quartz supports showed limited linearity. In particular, the plot point for the

calibration solution with F concentration of 25 $\mu\text{g/mL}$ deviated from linearity on the quartz support, showing a comparatively high F $K\alpha$ intensity. This limited linearity might be due to systematic negative biased errors in obtaining the F $K\alpha$ peak area accurately in the presence of the comparatively large O $K\alpha$ neighboring peak, especially at lower F concentration solutions, resulting in a lower area of F $K\alpha$ for low-concentration F calibration solutions. Such errors may be negligible in calibration solutions with F concentrations of 25 $\mu\text{g/mL}$, resulting in the higher intensity compared with other points obtained at low F concentration solutions. Accordingly, it is not advisable to use quartz supports for F determination at lower concentrations. The origin point (0, 0) was included in both calibration plots.

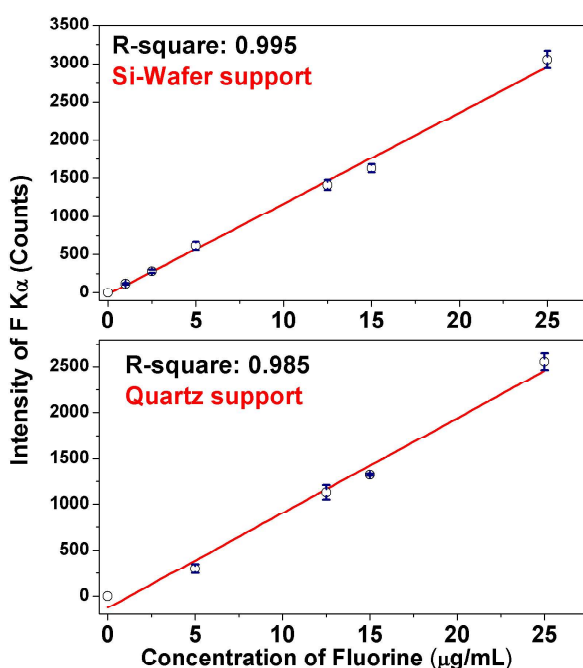


Figure 3.16: Comparison of calibration plots for direct TXRF determination of F using specimens deposited on Si-wafer and quartz supports.

Using these calibration plots, some fluoride samples prepared by diluting Merck single element fluoride standards in Milli-Q water were analyzed for F. The TXRF results obtained are

shown in Table 3.4. The results obtained with quartz supports showed negative bias for the reasons described above.

Table 3.4: Comparison of TXRF determination results of fluorine in water samples having F concentration in the range of 1.5-20 $\mu\text{g/mL}$ using quartz and Si wafer sample Supports

Samples	Expected F Conc ^a . ($\mu\text{g/mL}$)	Quartz Supports		Si Wafer Supports	
		TXRF determined Conc. $\mu\text{g/mL}$	Deviation From Expected %	TXRF determined Conc. $\mu\text{g/mL}$	Deviation From Expected %
SF-1	1.50	ND	-	1.55 \pm 0.09	3.3
SF-2	3.00	ND	-	3.1 \pm 0.1	3.3
SF-3	6.25	5.5 \pm 0.3	-12	6.1 \pm 0.3	-2.4
SF-4	10.25	9.9 \pm 0.2	-3.4	10.2 \pm 0.2	-0.5
SF-5	20.00	17.1 \pm 0.9	-14.5	19.6 \pm 0.9	-2.0
		Average RSD = 4.2% (1σ , n=3)	Average deviation = 10%	Average RSD = 3.8% (1σ , n=3)	Average deviation = 2.3%

^a Calculated on the basis of preparation of the solutions, ND: not detected

As the intensity of the F $K\alpha$ peak was not visible for sample solutions with fluoride concentrations $<5 \mu\text{g/mL}$ while using quartz supports, it was not possible to determine fluoride in such solutions using quartz supports. At higher concentrations, the average deviation of the TXRF-determined F concentrations from the expected values was 10.0%, with a RSD of 4.2% (1σ , n = 3) using the quartz supports. These corresponding values using Si wafer supports were found to be 2.3% and 3.8%, respectively. Therefore, using Si wafer clearly provided very good analytical results for the determination of fluorine compared to those obtained with quartz

supports. The reasons of the poor analytical results for fluorine determination using quartz supports can be summarized as;

- (1) Interference of strong O K α line with F K α , resulting errors in the fitting process and subsequent area deduction under the peak F K α
- (2) Non uniform spreading of the sample droplets, causing variation in the intensity of F K α during each measurement due to the hydrophilic character of the quartz surface as discussed earlier.

The above method for fluorine determination using Si wafer supports is useful when the concentration of fluorine in the sample solution remain $> 1 \mu\text{g/mL}$. However sample solution containing lower fluorine concentration could also be analyzed, but more amount of analyte has to be deposited on the TXRF supports. For such fluorine determination, 100 μL sample aliquots of the fluorine containing solution were deposited on Si-wafer supports in steps of 5 μL and then analyzed using the above approach. A calibration plot was obtained for solutions with F concentrations in the range 100–600 ng/mL using this sample preparation method. The calibration plot obtained was fitted using a linear function and is shown in Figure 3.17.

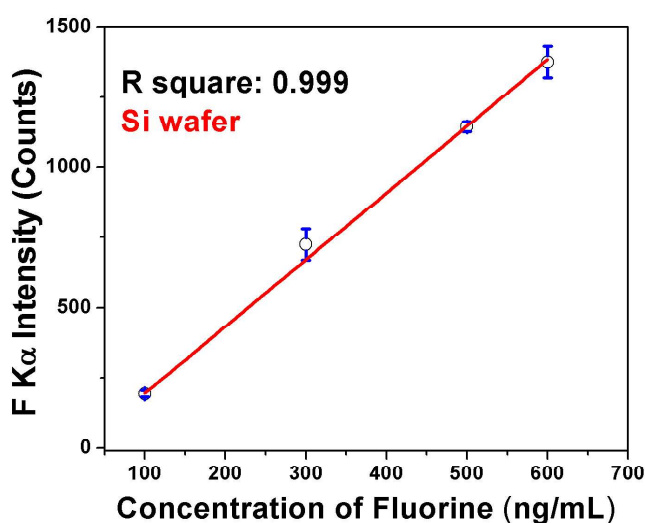


Figure 3.17: Calibration plot for TXRF determination of F in samples with F concentration in the range of 100-600 ng/mL using Si wafer sample supports

Using this approach, F concentrations in the range 200–400 ng/mL has been analyzed successfully with a RSD (1σ , $n = 3$) of 8.6%. The TXRF-determined values deviated from the expected values by 6.3%. These results are shown in Table 3.5.

Table 3.5: Results of TXRF determination of fluorine in solution samples having F concentration in the range of 100-600 ng/mL using Si wafer Supports

Samples	Expected F Conc ^a . (ng/mL)	Si Wafer Sample Supports	
		TXRF determined Conc. ng/mL	Deviation From Expected %
SF-L-1	200	194 ± 23	-3.0
SF-L-2	250	235 ± 11	-6.0
SF-L-3	400	440 ± 41	9.5
		Average RSD = 8.6% (1σ , $n=3$)	Average deviation = 6.3%

^aCalculated on the basis of preparation of the solutions

For the determination of fluorine concentration in real water samples using the above developed approach, drinking water sample obtained from a tap and a reverse osmosis (RO) water purification facility were spiked with fluorine in the concentration range of 2-16 µg/mL. These water samples were analyzed by TXRF using Si-wafer as sample supports. The TXRF analysis result is shown in Table 3.6. Using this approach, F determination in drinking water samples from the RO plant gave excellent analytical results. The TXRF values obtained were found to have an average deviation of 4.8% from the expected concentration of F in the solutions, with an average RSD of 3.6% (1σ , $n = 3$).

Table 3.6: Results of TXRF determination of fluorine in RO water samples spiked with fluorine at different concentration levels in the range of 2-16 $\mu\text{g/mL}$ using Si wafer Supports

Samples	Expected F Conc ^a . ($\mu\text{g/mL}$)	Si Wafer Sample Supports	
		TXRF determined Conc. $\mu\text{g/mL}$	Deviation From Expected %
RO-1	2	1.83 ± 0.05	-10
RO-2	4	3.8 ± 0.3	-2.5
RO-3	8	8.2 ± 0.2	-1.2
RO-4	16	15.5 ± 0.2	-0.6
		Average RSD = 3.6% (1σ)	Average deviation = 4.8%

In case of tap water samples, due to the presence of very high matrix concentration in it as compared to that of RO water, the TXRF specimens form is very much thick. Such thick specimen produces very high background. Due to this F K α line was not visible in TXRF spectra measured using such specimens. In presence of heavy matrix, the absorption of low energy X-rays is possible by the matrix. The TXRF spectra of these two water samples are compared in Figure 3.18.

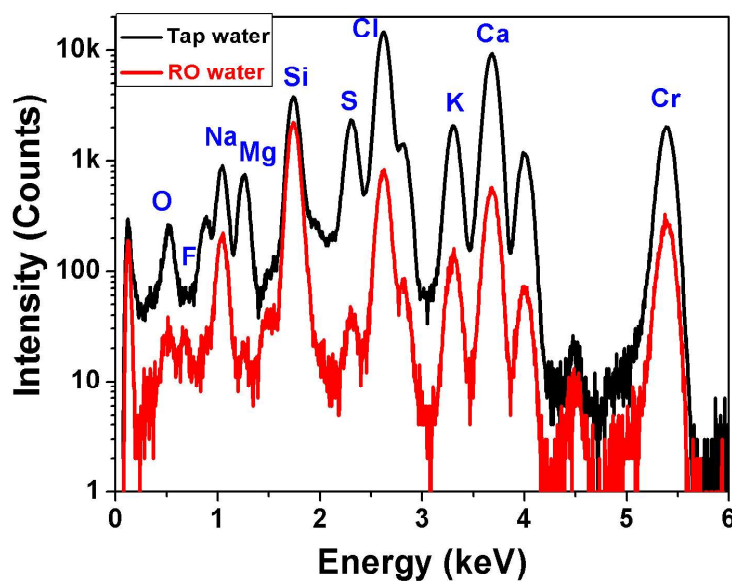


Figure 3.18: Comparison of TXRF spectra of tap water and RO water samples from same source

From this figure it can be observed that the matrix concentration in tap water is much higher as compared to that of RO water. So in case of RO water samples the F K α peak is clearly visible, but it is not at all visible in tap water sample specimen due to the presence of high matrix/background.

These studies indicate that this methodology is well suited for F determination in water samples suitable for drinking, such as RO water, commercial mineral water, and distilled water, which do not contain high amounts of matrix. Moreover, the methodology may be well suited for water samples used in industrial processes, such as semiconductor production, power plant operation, and environmental water samples from glaciers, rain, and snow water; which do not contain high matrices. The methodology could also be effective for F determination in high-purity reactor coolant and moderator heavy water.

3.5. Conclusions

In view of the above discussions we can conclude that simultaneously TXRF determinations of trace level of low Z elements in different technologically important and environmental samples is possible using a low Z – high Z TXRF spectrometer having Cr K α as excitation source with a vacuum chamber having vacuum level of ~3 mbar. The detection limits are improved due to above instrumentation of ultra thin window detector. Before analyzing low Z elements in different matrices we have done a comparative study of this lab based source instrument with synchrotron radiation (SR) based TXRF facility of newly developed multi-purpose end-station at Elettra sincrotrone Trieste, Italy. The synchrotron setup attained significantly improved DLs for low Z elements with $Z < 13$ and especially for F (down to 0.7 ng), an improvement almost by a factor of 27 with respect to the laboratory setup. In the quantitative

analysis of multi-elemental solutions, both setups have presented similar level of accuracy (<10%).

The results obtained have clearly indicated that in the case of the laboratory TXRF spectrometer, there is a possibility of further improvement of DLs by using lower energy X-ray tube-based excitation sources (instead of the Cr K α tube-based radiation) and minimizing the TXRF specimen spot size. For example, the use of W M α or Mo L α exciting beams, generated by using W or Mo as tube anode materials, can considerably increase the X-ray fluorescence intensities of low Z elements and eventually improve the respective DLs. On the other hand, the SR results, although being preliminary, are quite promising for the establishment of a highly sensitive TXRF beam line end-station facility. A careful redesign of the magnetic electron trap is required to offer deflection of only few keV energetic photoelectrons and Auger electrons, thus optimizing the solid angle of detection and further improving DLs by an estimated factor of about 5 times. Further on, the ongoing upgrade of the XRF beamline spectral range and features with the commissioning of an In-Sb (working energy range 2–4 keV) and in particular of a multi-layer monochromator with the later offering significantly higher flux of incident photons with exciting energies even below the Si K edge (best suited for ultra-trace analysis of low Z elements) will expand significantly the analytical merits of the facility towards highly sensitive TXRF analysis but also for chemical speciation studies of key low Z elements like S and Cl with importance in various disciplines. The laboratory-based TXRF system offers simpler operation of the instrumentation and sample handling, is easily accessible, whereas the synchrotron-based TXRF setup offers significantly improved DLs with the potential of chemical speciation (for high Z elements) and mapping capabilities. The studies performed at the synchrotron facility

offered data and hints for the instrumental and methodological developments that can further improve the analytical performance of the laboratory-based spectrometer.

After knowing the analytical capability of high Z – low Z TXRF spectrometer for the determination of low Z elements, it was applied for the trace elemental analysis in real uranium oxide samples. It was established that complete separation of uranium is necessary to reduce the background and avoiding the interference of U M escape peak with analytical lines of other low Z elements, especially for Al. The results obtained are very much improved compared to previously reported results especially for Al. The TXRF determined values found to have an average precision of 8.0% (1σ , $n = 3$), and the average deviation of the TXRF determined values from the certified concentrations of low Z elements was 7.3%. Samples having $<1 \mu\text{g/mL}$ trace elemental concentrations, require more pre-concentration.

The studies for the determination of low Z elements was extended for environmental samples, where fluorine was determined in water samples directly at trace level of as low as 100 ng/mL using laboratory based low Z - high Z TXRF spectrometer. The water samples were deposited on Si-wafer supports and measured directly without using any acidic internal standard. A very careful sample deposition is required where 5 μL of the sample is deposited at the centre of the Si-wafer sample supports. This simple sample preparation methodology avoided the loss of fluorine due to the addition of acidic internal standards while preparing TXRF sample specimens. Si-wafer as sample support reduced the huge interference of O $K\alpha$ with F $K\alpha$ and improves the analytical results for the quantification of fluorine in water samples. The TXRF detection limit for F was found to be 1873 pg using Si-wafer supports, which was three times better than the detection limit obtained using quartz supports. The methodology could be extended to the trace determination of F in RO water samples.

Chapter 4

Trace element determination in
plutonium samples by TXRF

4.1. Introduction

Plutonium is one of the key elements in nuclear reactor fuels for the production of energy. It is highly hazardous, radio-active and toxic element which does not exist in nature [149, 150]. Different isotopes of plutonium e.g. ^{238}Pu , ^{239}Pu , ^{240}Pu , ^{241}Pu and ^{242}Pu are produced in nuclear reactors during the irradiation of ^{238}U with neutrons. Plutonium based fuels are very important for fast breeder reactors, because of its nuclear characteristics. Many reactors have been built for the experimental purpose as well as for power generation e.g. Rapsodie, FBTR (Fast Breeder Test Reactor), EBR I & II (Experimental Breeder Reactor), PFR (Prototype Fast Reactor) etc. in different parts of the world like Europe, Japan, USA, Russia and India where plutonium is used as fuel. At present in many LWR_s (Light Water Reactors) and PFR_s; mixed uranium, plutonium oxides known as MOX (Mixed Oxide) Fuels are used [151]. Generally these fuels are used in form of pellets in different reactors. In space exploration, plutonium based fuels are very important energy source as the electrical batteries are very heavy and their lifetime is very small. The solar cells cannot be used for this purpose as they do not operate at very long distance from sun. The ^{238}Pu is well suited as compact thermoelectric power source for the power supply in satellites [152, 153]. Thus plutonium has much more peaceful applications for the advancement of human civilization in addition to its use as nuclear weapon. Due to above reasons, it is an important technologically important element.

In nuclear industry; the production or fabrication of the fuel pellets involve several steps like grinding, pelletization and other wet chemical processes. During this fuel processing, fuels can get contaminated with various trace impurities. The presence of impurities beyond some specific limits in fuel affects the neutron economy as well as the metallurgical characteristic of the fuel. A detailed description of the effects of different trace impurities on the fuel

characteristic during the operation of the reactor is given in chapter 1 of the thesis as well as in the literature [154, 155]. Due to above reasons, stringent specifications of maximum tolerable limits of different trace impurities in such fuels have been laid down. For satisfying these specifications, it is very important to determine the trace impurities before using the fuels in the reactor core.

There are many techniques available for the determinations of these trace impurities in plutonium based fuel. Spectrometric techniques are more popular for the trace determination as many elements can be determined simultaneously in a short span of time [156]. ICP-AES (Inductively Coupled Plasma – Atomic Emission Spectroscopy) and ICP-MS (ICP-Mass Spectrometry) have been used for the determination of trace impurities in different uranium, thorium and plutonium matrices after separation of the major matrix. However both the technique suffers from spectral interference. The running costs of both the instrument to maintain the plasma and Ar gas flow during the sample analysis are very high. In addition, only metallic impurities can be determined by these techniques and the separation process is also very time consuming [157, 158]. DC-arc carrier distillation technique is generally used for such purpose, but this technique is mainly applicable for volatile impurities and the sensitivity and reproducibility of this technique is also very poor [159]. The most important fact is that a large sample volume (1-10 mL) is needed in these techniques for trace elemental analysis [160]. Plutonium is highly radiotoxic element which primarily decays by alpha emission. It has high specific activity as well as high biological half life. Hence it is always better to handle minimum amount of plutonium based materials during the analysis.

TXRF has many good features like multi-elemental analytical capability, analysis of metals non metals alike, high detection power, simple, cost-effective for material characterization especially

nuclear materials etc [60, 81]. Misra et al have shown that this technique has a huge potential of the analysis of radioactive nuclear materials [127, 161-163]. The main features which make this technique an excellent candidate for the analysis of radiotoxic elements is the requirement of very small amount of sample during TXRF analysis. A few nanogram of sample is enough to give very good elemental signal. So this technique could be very much useful for the analysis of radioactive samples like plutonium as the dose to the operator and the radioactive waste generation will be very small. There are some works reported in the literature on the trace elemental analysis in uranium based samples using TXRF after separation of most of the uranium from the sample matrix [48, 105, and 110]. Although having so many advantages for the TXRF trace elemental analysis in plutonium based samples; this technique has not been explored till now for it. In this work we have developed a novel approach for the determination of trace elements in plutonium based samples using TXRF and are reporting it for the first time. Solvent extraction based technique has been used to separate almost all the plutonium from the sample matrix using TBP (Tri n-butyl phosphate); which is an ideal solvent for the separation of plutonium from the sample solution [164]. All the separation procedures were carried out inside a fume hood. Since a very small amount of sample volume (a few microlitres) shall be required for such trace determinations and the concentration of Pu in such samples shall be in the range of a few $\mu\text{g/mL}$ levels only, the radiation dose present in such specimen shall be very low. Such Pu separated TXRF specimens can be analyzed without any isolation in ambient atmosphere with proper precautions. Some time back we have made such Pu specimens for the elemental determinations of Pu in its solutions. The Pu spots in TXRF specimens of the Pu samples were covered with a thin layer of colloidian. Such samples were successfully used for Pu determinations in Pu solutions samples by TXRF. This approach made analysis of Pu based

samples very easy without putting the instrument in the glove-box. Since almost all plutonium shall be separated from the solutions by solvent extraction for trace element determinations in it by TXRF, the amount of plutonium on the sample supports shall be very small in the range of a few ng levels. Such specimens can be handled in ambient atmosphere without putting a colloidian layer on it. However, the specimen sample spot should not be touched or disturbed during analysis and care must be taken that there is no spread of material from the support to atmosphere. This approach shall avoid a lot of cumbersome operations compared to the situation when the instrument is put in the glove box or fume hood for the TXRF analysis purpose. Also, proper radiological safety kits, for example, handgloves, protective clothing, and so on, required for handling the radioactive materials must be used. The results of the studies made to develop such TXRF methodology for trace element determinations in Pu samples are being reported in this chapter.

4.2. Experimental

4.2.1. Reagents

Nuclear grade stock solution of plutonium, having initial concentration of 6 mg/mL in 4M HNO₃ medium was used as sample matrix. MERCK multi-elemental standard solution ICP-IV after dilution was used to determine the sensitivities of elemental X-ray lines as well as synthetic plutonium based sample preparation for TXRF measurements. Suprapure concentrated HNO₃ (Merck, Germany) diluted to 1.5 % level with milli-Q water having specific resistance of 18.2 MΩ.cm was used for the sample preparation and dilution. For the separation of plutonium from sample matrix; 30% TBP (Tri n-Butyl Phosphate) diluted with n-dodacane and equilibrated with 4M suprapure HNO₃ was used.

4.2.2. Instrumentation

All the TXRF measurements were carried out using a Low Z – High Z TXRF spectrometer. The instrument has two low power X-ray tubes; e.g. Cr and Rh fitted with Ni/C and Pd/B₄C to diffract Cr K α and Rh K α respectively. In this work Rh target operated at a tube voltage of 50 kV and tube current of 700 μ A was used for TXRF measurements. The X-rays coming from the Rh tube fall on the Pd/B₄C multilayer in such a particular angle that it diffracts Rh K α from it. The diffracted monochromatic Rh K α X-ray is made to fall on sample at an angle below critical angle. After the excitation of the sample; the X-ray fluorescence radiations coming out from the sample are detected by a detector which is kept very close to the sample. A SDD (Silicon Drift Detector) made by KETEK, having an active area of 20 mm² is used to detect those X-rays. The detector has ultra thin polymer window having approximate thickness of 300 nm. The resolution of the detector is 140 eV at Mn K α (FWHM at 5.89 keV). The detail of this instrument is given in elsewhere [120]. All the TXRF measurements were carried out for a live time of 1000 seconds. The TXRF spectra obtained were fitted using IAEA QXAS package software program name AXIL [100]. An alpha spectrometer was used to measure the alpha counts emitted from the sample.

4.2.3. Sample preparation

For the determination of sensitivities of elemental X-ray lines, the MERCK multi element standard (MES) solution ICP-IV was diluted to the elemental concentration level of 10 μ g/mL. The relative sensitivity values were determined with respect to Se K α , which was used as an internal standard. Before separation of plutonium, it is very important to do a similar experiment on multi-element standards TXRF determinations after equilibration with TBP to understand the extraction behavior of different elements. In additions relative sensitivity (RS) values of

elemental X-ray lines, detection limit (DL), validity and limitations of this method etc. are also required to be studied. Two multi-elemental standard solutions having elemental concentrations of 5 and 10 $\mu\text{g/mL}$ in 4M HNO_3 medium were prepared. Aliquots of 2 μL of each of these solutions were deposited on three separate clean quartz sample supports and dried on a hot plate. These specimens were presented for TXRF measurements at low Z high Z TXRF spectrometer. In order to see the extraction behavior of different elements in TBP, aliquots of 500 μL of each of these solutions were taken in small centrifuge vial having 1.5 mL volume. The MES solutions were equilibrated with 30% TBP (Tri-n-Butyl Phosphate) in n-dodecane with vigorous shaking. Later, the solutions were kept stand still for 5 minutes and then the top layer organic portion was carefully pipette out and discarded. The aqueous portions remaining in the tube were further equilibrated with TBP. This process was repeated for three times and finally the aqueous phase was given one time equilibration with n-dodecane, so that any remaining dissolved TBP in is separated. In both aqueous phases Se was added as an internal standard in such a manner that it's final concentration remain as 10 $\mu\text{g/mL}$. TXRF measurements were made from these solutions. All the TXRF measurements carried out in this experiment were for a live time of 1000s. For the TXRF determinations of trace elements in plutonium solutions aliquots having some fixed volume of the plutonium solutions in 4M HNO_3 medium and plutonium concentration of 6 mg/mL were taken in four separate centrifuge vials (1.5 mL of volume capacity) inside a fume hood. These solutions were mixed with known different volumes of diluted MERCK MES ICP - IV in 4M HNO_3 medium. A fixed volume of Se internal standard in 4M HNO_3 was added in these vials. The final elemental concentrations of the elements added in these vials were 5, 13.33 and 20 $\mu\text{g/mL}$ respectively. These samples were named as Pu-S-1, Pu-S-2 and Pu-S-3 respectively. In Pu-S-2, Se was not added. This solution was analyzed with respect to Ga (used

as internal standard) present in it. Similarly a blank solution was also prepared with the same plutonium stock solution. For blank preparation, 50 μL of 4M suprapure HNO_3 was taken in place of MES solution, added. The detail of the sample preparation is shown in Table 4.1.

Table 4.1: Details description of plutonium based sample as well as blank preparation before the separation with TBP

Sample name	Plutonium solution taken	MERCK-MES	Se (IS)	Resultant solution
Pu-S-1	Volume: 130 μL Conc.: 6 mg/mL	Volume: 50 μL Conc.: 20 $\mu\text{g}/\text{mL}$	Volume: 20 μL Conc.: 100 $\mu\text{g}/\text{mL}$	Pu conc.: 3.9 mg/mL Elemental conc.: 5 $\mu\text{g}/\text{mL}$ Se (IS) conc.: 10 $\mu\text{g}/\text{mL}$
Pu-S-2	Volume: 200 μL Conc.: 6 mg/mL	Volume: 50 μL Conc.: 60 $\mu\text{g}/\text{mL}$	Se not added	Pu conc.: 4.8 mg/mL Elemental conc.: 13.3 $\mu\text{g}/\text{mL}$
Pu-S-3	Volume: 130 μL Conc.: 6 mg/mL	Volume: 50 μL Conc.: 80 $\mu\text{g}/\text{mL}$	Volume: 20 μL Conc.: 100 $\mu\text{g}/\text{mL}$	Pu conc.: 3.9 mg/mL Elemental conc.: 20 $\mu\text{g}/\text{mL}$ Se (IS) conc.: 10 $\mu\text{g}/\text{mL}$
Blank	Volume: 130 μL Conc.: 6 mg/mL	NO MES was taken. Instead 50 μL of 4M HNO_3 was added	Volume: 20 μL Conc.: 100 $\mu\text{g}/\text{mL}$	Pu conc.: 3.9 mg/mL Se (IS) conc.: 10 $\mu\text{g}/\text{mL}$

* IS: Internal standard, Conc.: Concentration, S-Pu-1, S-Pu-2, and S-Pu-2: Sample

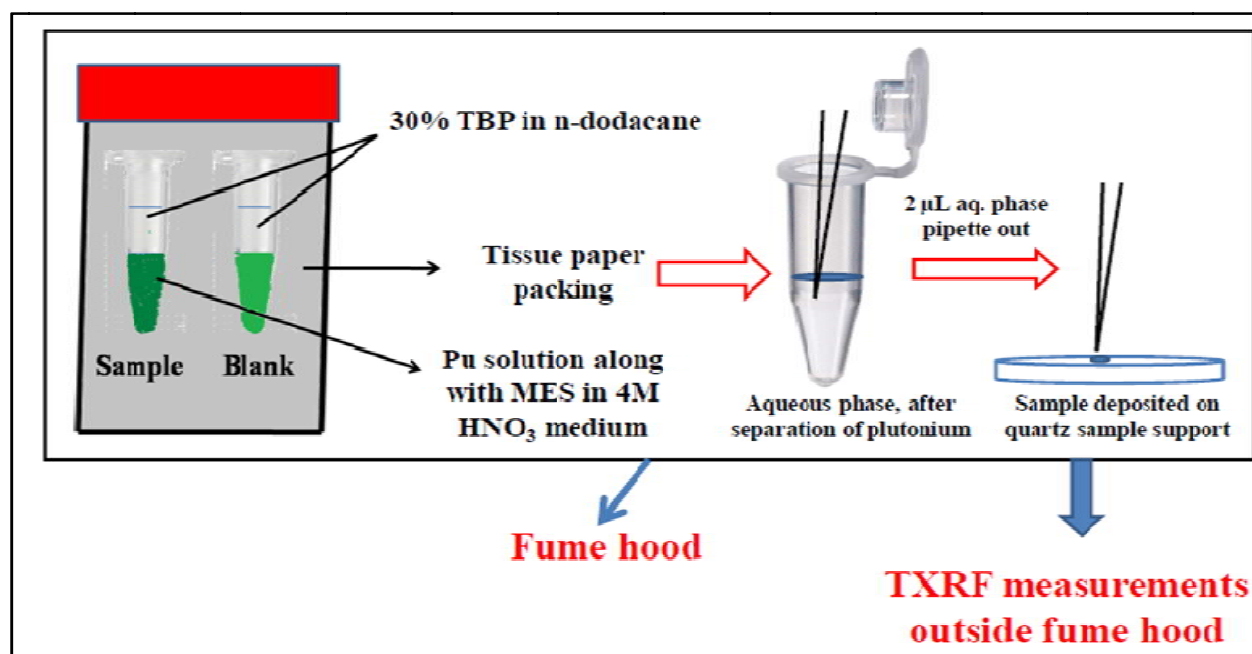


Figure 4.1: Separation of plutonium from the sample matrix for the trace elemental determinations in it using TXRF

In each of these vials containing the samples, 200 μL of 30% TBP in n-dodecane was added. In order to adopt more safety precautions during Pu separation, the vials were kept in a small polythene bag and then placed in an air tight Perspex container. The empty space of the container remaining after keeping these polythene vials was filled with tissue paper, so that the centrifuge vials inside the bottle do not fall and remain in standing conditions. Now the whole system was shaken very carefully for 10 minutes. The lid of bottle was opened and the vials were kept standstill for 10 minutes after opening their lid carefully so that no Pu comes out and any formed gases escape carefully. The top organic phase containing most of the plutonium was removed slowly from each of the vials. This whole process was repeated three times so that most of the plutonium gets separated. It was observed that after the three equilibrations with 30% TBP, the solution became colorless indicating that almost all the plutonium got separated. Finally each of these solutions was equilibrated with n-dodecane to remove any dissolved TBP in it which may contain traces of Pu. Aliquots of 2 μL from each of these solutions were pipetted out and deposited at the centre of three clean quartz sample supports. These supports containing aqueous phases on top of these were kept in a Petridishes and covered with another Petridis and left overnight for drying. After drying the sample; the uncovered surfaces of these sample supports were cleaned with wet tissue paper to ensure that there is no loose contamination around the sample. After ensuring that samples do not have any lose contamination, these were put in another clean Petridis covered from the top and taken out of the fume hood. All the operation related to plutonium samples till now was done inside a fume hood equipped for plutonium sample handling. Each of the sample specimens were checked with alpha monitor to ensure that the Pu amount fixed on the support is well within the amount of Pu allowed to be handled in ambient atmosphere. The specimen's alpha activity was very small <100 Bq and hence these can

be handled in ambient atmosphere. In order to see the absence of any loose activity around the sample spots each of the specimens were taken in counting room and gently touched by a piece of soft tissue two-three times. The alpha activity in this tissue was measured which did not show any appreciable alpha counts. These sample specimens were loaded in TXRF spectrometer for TXRF measurements. However, additional care was taken that the Pu spot was neither touched by hand nor allowed to come in contact with any part of the spectrometer during the sample transfer or measurement in the TXRF spectrometer. The TXRF spectra of each of these specimens were measured for 1000s time. Similarly, real plutonium oxide sample solutions in 4 M nitric acid were processed and analyzed for the trace impurities present in these.

4.3. Results and discussions

The elemental X-ray line sensitivities were determined with respect to Se $K\alpha$ as Se is not normally present in plutonium samples and hence was used as an internal standard. The TXRF spectra of a MES solution along with Se internal standard having elemental concentration of 10 $\mu\text{g/mL}$, before and after equilibration with 30% TBP in n-dodacane are shown in Figure 4.2.

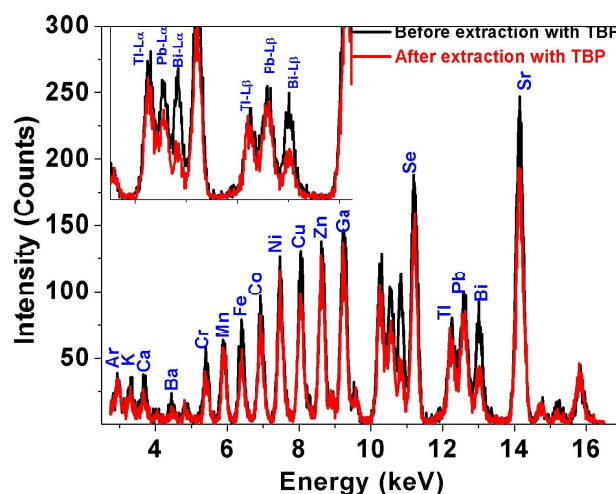


Figure 4.2: Comparison of the TXRF spectra for MES solution having elemental concentration of 10 $\mu\text{g/mL}$ before and after equilibration with 30% TBP in n-dodacane

Here both the spectra look same, having almost similar peak intensity, except for Bi L_{α} and Bi L_{β} . The intensities of both Bi L_{α} as well as Bi L_{β} have drastically reduced (the inset graph shows it more clearly). The intensities of all other elemental X-ray lines in spectra with respect to the respective peak intensity of Se K_{α} remain almost same in the two spectra. The observation becomes clearer when two MES solutions after equilibration with TBP were analyzed. The results are shown in Table 4.2. From this table it can be clearly seen that the TXRF determined elemental concentrations in the MES solution is very much in agreement with the expected concentrations except for Bi. The average deviation of TXRF determined values from the expected values and average RSD (relative standard deviation) values of the TXRF results obtained for MES solution having elemental concentrations of 5 and 10 $\mu\text{g/mL}$ were 4.8%, 3.9% and 7.8%, 5.7% respectively. These values were determined without taking the analytical results of Bi determinations. The disagreement of Bi values suggests that Bi cannot be determined using such approach.

Table 4.2: Comparison of TXRF determined and expected elemental concentrations in multi-element standard solutions after equilibrations with 30% TBP in *n*-dodecane and analyzing by TXRF

Elements	Expected conc. ($\mu\text{g/mL}$)	TXRF determined conc. ($\mu\text{g/mL}$)	Deviation %	Expected Conc. ($\mu\text{g/mL}$)	TXRF determined conc. ($\mu\text{g/mL}$)	Deviation %
K	5	4.5 \pm 0.1	-10	10	9 \pm 1	-10
Ca	5	4.8 \pm 0.3	-4	10	8.3 \pm 0.5	-17
Cr	5	4.8 \pm 0.4	-4	10	9.7 \pm 0.9	-3
Mn	5	5.1 \pm 0.2	2	10	10.6 \pm 0.6	6
Fe	5	4.9 \pm 0.2	-2	10	11 \pm 1	10
Co	5	4.9 \pm 0.1	-2	10	10.7 \pm 0.7	7
Ni	5	5.3 \pm 0.3	6	10	11.0 \pm 0.9	10
Cu	5	5.1 \pm 0.2	2	10	10.9 \pm 0.4	9
Zn	5	5.4 \pm 0.2	8	10	10.9 \pm 0.2	9
Ga	5	5.2 \pm 0.2	4	10	10.58 \pm 0.07	5.8
Sr	5	4.95 \pm 0.02	-1	10	10.5 \pm 0.4	5
Ba	5	5.6 \pm 0.5	12	10	11 \pm 1	10
Tl	5	4.87 \pm 0.02	-2.6	10	10.3 \pm 0.2	3
Pb	5	5.36 \pm 0.03	7.2	10	10.6 \pm 0.3	6
Bi	5	2.4 \pm 0.6	-52	10	5.7 \pm 0.2	-43
Average % deviation: 4.4 Average RSD in %: 3.9				Average % deviation: 10.2 Average RSD in %: 5.7		

Figure 4.3 shows the TXRF spectra of the blank solution of plutonium, after 3 contacts with 30% TBP in n-dodacane and subsequent contact with n-dodacane.

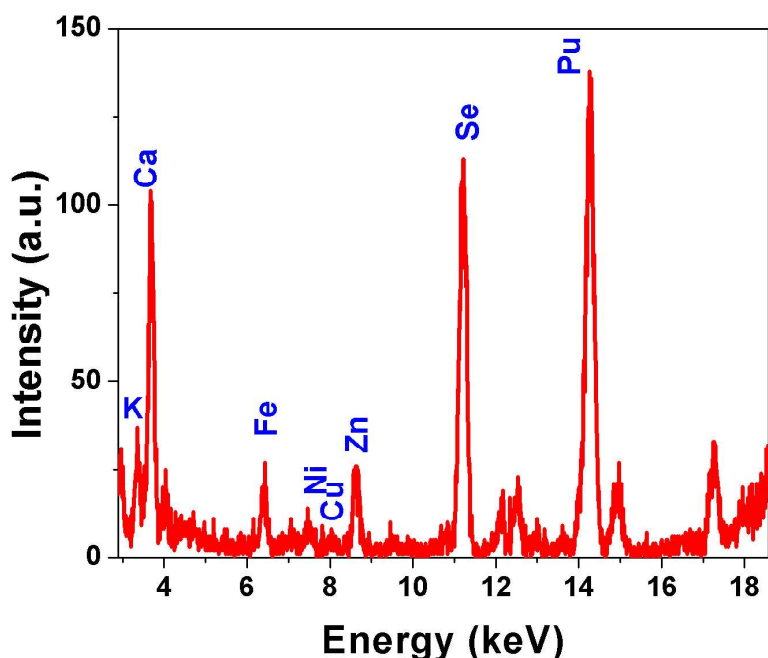


Figure 4.3: TXRF spectra of the aqueous phase of the blank solution for trace element determinations in Pu after separation of plutonium using TBP

Before the extraction of plutonium, the resultant concentration of plutonium in the blank solution was 3.9 mg/mL as shown in Table 4.1. After the extraction of plutonium from the blank solution we can still see Pu $L\alpha$ line, but its intensity is much smaller now. Trace impurities like K, Ca, Fe, Ni, Cu, and Zn are also seen in the spectra. The final Pu concentration in the solution after its extraction was found to be $23.6 \pm 0.5 \mu\text{g/mL}$; indicating almost 99.4 % of Pu extraction. Similar calculation was also done for other sample solutions to determine the final Pu concentration after the extraction and it is shown in Table 4.3. The % of Pu extracted was calculated using the following equation

$$E = \frac{c_i - c_f}{c_i} \times 100 \quad (4.1)$$

Here E is Pu extraction in percentage, C_i is initial Pu concentration, C_f is the final Pu concentration after the extraction with 30% TBP in n-dodacane. So it can be seen from Table 4.3 that Pu in the range 99.4 to 99.7 % could be removed using this extraction method. So the final solution contains very low alpha activity after extraction of plutonium. Since only 2 μ L of this solution is enough for recording the TXRF spectra; the net amounts of Pu deposited on the supports are very small in the range of 20 ng only as shown in Table 4.3, so only Pu in the range of 20 ng has to be handled. Handling of such small amount of Pu, fixed on TXRF support is safe and can be carried out without requirement of the glove box or fume hood with proper precautions. The amount of radioactive dose as well analytical waste generated during such analysis shall be very small. This study has shown that the above features are real advantages of TXRF for the analysis of highly radiotoxic elements like plutonium for trace elements.

Table 4.3: Percentage of Pu separated in all the Pu based samples using 30% TBP in n-dodacane and net amount of Pu deposited on TXRF sample supports

Sample	Initial Pu Conc. (μ g/mL)	Final Pu Conc. determined by TXRF (μ g/mL)	% of Pu separated by TBP	Absolute amount of Pu deposited on support (2 μ L solution) (ng)
Pu-S-1	3900	10.05 \pm 0.3	99.7	20.1
Pu-S-2	3900	11.7 \pm 0.6	99.8	23.4
Pu-S-3	3900	11 \pm 1	99.7	22
Blank	3900	23.6 \pm 0.5	99.4	47.2

As already mentioned three sample solutions named as Pu-S-1, Pu-S-2 and Pu-S-3 were taken for the analysis of trace elements in Pu based samples (Pu concentration 3.9 mg/mL), The concentration of trace elements in these solutions were 5, 13.3 and 20 μ g/mL respectively. Figure 4.4 shows the AXIL fitted TXRF spectra of two of these samples (Pu-S-1 and Pu-S-3) after separation of Pu. The elemental X-ray lines of the elements present in the samples are

clearly visible in the spectra. The Pu $L\alpha$ line is almost merged with the Sr $K\alpha$ line. These lines were deconvoluted using AXIL fitting and we can get the individual X-ray line area [165].

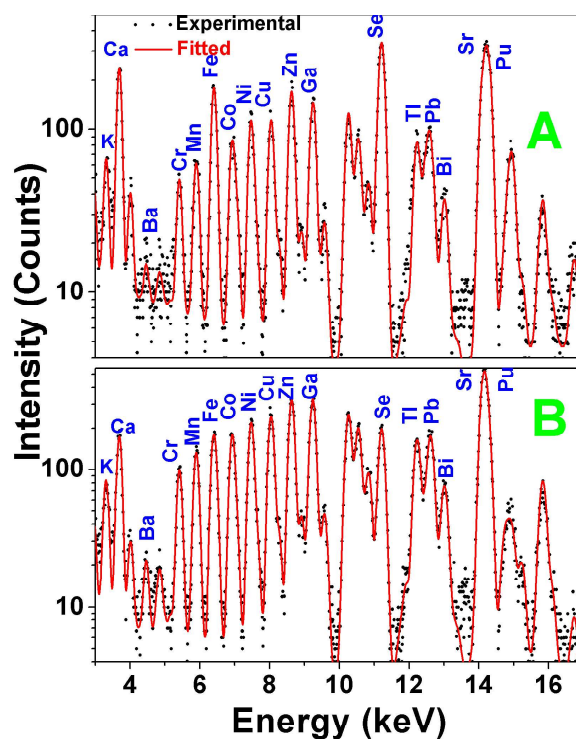


Figure 4.4: AXIL fitted TXRF spectra of the solution obtained after the separation of plutonium from the sample matrix having multi elemental standard of elemental concentrations 5 (A) and 20 (B) $\mu\text{g/mL}$ respectively with Se internal standard having concentration of 10 $\mu\text{g/mL}$ in each of these solutions

Table 4.4 shows a comparison of the TXRF determined elemental concentrations in these solutions with the expected values obtained on the basis of preparation of these solutions. It can be seen that the TXRF determined concentrations are in very good agreement with the expected one for all the three sample solutions for all elements except for Bi. We have previously seen that Bi is being partially extracted by TBP. The comparison of the TXRF determined and expected values for different elements are given in Table 4.4 which shows a very good agreement for all the elements except Bi due to reasons mentioned earlier. It can be seen from the table that, in spite of strong interference between Pu $L\alpha$ and Sr $K\alpha$ line, the TXRF determined concentration of Sr is in good agreement with the expected one for all the three Pu samples. The results further

authenticate the literature reported validity of TXRF results obtained on the basis of profile fitting [165]. The average RSD of TXRF determined values were 7.1, 3.0, 3.4% and the average deviation of TXRF results from the expected values was 8.5, 6.7, and 2.4% respectively for the samples Pu-S-1, Pu-S-2 and Pu-S-3. Such deviation for Ba determination was 24% and was not included in above calculation. This is because of the poor peak intensity of Ba L α line, resulting in error in AXIL fitting; which is also seen in Figure 4.4A.

Table 4.4: TXRF determined elemental concentrations of three Pu based samples after separation of almost all the Pu (>99.8%) from the sample matrix.

Elements	Sample name								
	S-Pu-1			S-Pu-2			S-Pu-3		
	TXRF determined conc (µg/mL)	Expected conc. (µg/mL)	Deviation %	TXRF determined conc (µg/mL)	Expected conc. (µg/mL)	Deviation %	TXRF determined conc. (µg/mL)	Expected conc. (µg/mL)	Deviation %
Cr	5.2 ± 0.4	5	4	11.9 ± 0.1	13.3	-10.5	20 ± 1	20	0
Mn	4.8 ± 0.2	5	-4	12.4 ± 0.5	13.3	-6.8	19.7 ± 0.3	20	-1.5
Fe	5.6 ± 0.5	5	12	14.5 ± 0.4	13.3	9.0	19.7 ± 0.8	20	-1.5
Co	5.1 ± 0.7	5	2	14 ± 1	13.3	5.3	19.4 ± 0.7	20	-3
Ni	5.5 ± 0.5	5	10	13.9 ± 0.2	13.3	4.5	20.3 ± 0.6	20	1.5
Cu	5.3 ± 0.8	5	6	13.2 ± 0.4	13.3	-0.8	19.8 ± 0.7	20	-1
Zn	4.7 ± 0.4	5	-6	14.0 ± 0.1	13.3	5.3	20.4 ± 0.2	20	2
Ga	5.2 ± 0.2	5	4	13.9 ± 0.3	13.3	4.5	20.2 ± 0.7	20	1
Sr	4.6 ± 0.1	5	-8	14.2 ± 0.5	13.3	6.8	19.2 ± 0.2	20	-4
Ba	3.8 ± 0.2	5	-24	14.5 ± 0.8	13.3	9.0	18 ± 2	20	-10
Tl	5.8 ± 0.3	5	16	14.6 ± 0.1	13.3	9.8	20.4 ± 0.2	20	2
Pb	4.7 ± 0.1	5	-6	14.1 ± 0.4	13.3	6.0	20.3 ± 0.4	20	1.5
Bi	1.6 ± 0.2	5	-68	6.9 ± 0.5	13.3	-48.1	7.8 ± 0.3	20	-61
	Average RSD: 7.1% Average deviation: 8.5%			Average RSD: 3.0% Average deviation: 6.7%			Average RSD: 3.4% Average deviation: 2.4%		
(1 σ , n=3) σ : standard deviation, n: number of replicates									

4.4. Analysis of a real Pu based sample:

Now this sample preparation methodology has been utilized to analyze a real Pu based sample for the trace elemental analysis. The real plutonium solution was obtained by dissolving PuO₂ in HNO₃. The PuO₂ sample was dissolved in Conc. HNO₃ and diluted to maintain the molarity of 4. The internal standard Se in 4M HNO₃ medium was added in this solution. Plutonium was separated from this solution using TBP extraction, and the TXRF spectra of the

sample were measured as described above. One representative TXRF spectrum of the aqueous phase of this sample solution obtained after Pu separation as mentioned above is shown in Figure 4.5. Similarly a blank solution was prepared in the above manner but using 4M HNO₃ instead of plutonium solution. The spectrum of the blank is also given in that figure. Different trace impurities like K, Ca, Ni, Cu, Zn were observed in that spectrum. Table 4.5 shows the TXRF determined concentrations of the trace elements after blank correction. The results of TXRF determinations of trace elements in real Pu sample also have good precision.

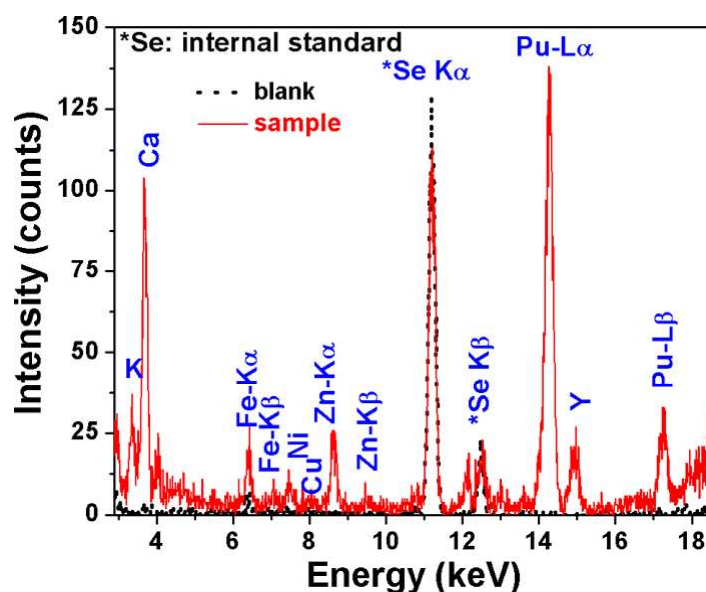


Figure 4.5: TXRF spectra of aqueous phase of the Pu solution obtained after extraction of Pu by TBP along with the TXRF spectra of a blank sample solution. Se was added as an internal standard in both

Table 4.5: Result for the TXRF trace elemental determinations in a real Pu sample

Elements	TXRF determined conc ($\mu\text{g/mL}$)
K	12.6 ± 0.9
Ca	61 ± 1
Fe	7.9 ± 0.6
Ni	0.8 ± 0.02
Cu	0.25 ± 0.03
Zn	2.1 ± 0.2

4.5. Conclusions

The applicability of TXRF for trace elemental determinations in plutonium samples has been tested in this work. The novelties of TXRF for trace determinations in a radiotoxic material like plutonium has been successfully demonstrated. The method is non-consumptive, requires very small amount of sample (2 μL on TXRF supports) and is thus very much suitable for handling of plutonium samples with equally good results. Such type of study on Pu samples is reported for the first time. Since only a few ng of plutonium is present on the sample supports, the TXRF spectra could be measured without putting the instrument inside a glove box. This simplifies the instrument handling and maintenance to a large extent compared to the condition when the instrument is required to be put inside a glove box: a practice normally followed in trace determinations of analytes by other conventional spectroscopic techniques. The methodology was tested on simulated as well as real plutonium samples. The method developed could not be used for Bi determinations. In addition to the advantageous features mentioned above, small sample requirement and small analytical waste produced, save the operator from radioactive dose as well as cumbersome radio-analytical waste disposal to a large extent.

Chapter 5

Trace elemental determination
in uranium samples by TXRF
after major matrix separation by
solid phase extraction

5.1. Introduction

Uranium is the key element of nuclear fuel used in nuclear reactors [166]. In research reactors metallic uranium is used as fuel, whereas in power reactors natural or enriched uranium oxides are used as nuclear fuel [123]. Mixed oxide and carbide i.e. (U, Pu) O₂ and (U, Pu) C are also used as nuclear fuels. The fuel may get contaminated with trace elements during fabrication as mentioned in previous chapters [15]. There are stringent limits for each of these impurities which can be tolerated for the safe operation of the reactors. The performance of nuclear fuel is very much dependent on the concentrations of these trace impurities. Total reflection X-ray fluorescence (TXRF) has also been used to analyze uranium samples for trace elemental determinations due to its advantageous features mentioned earlier [81, 167]. Before analysis of trace elements in uranium based nuclear fuels, it is very important to separate major matrix uranium to make thin specimen of the sample on the sample support to satisfy TXRF conditions and reduce the matrix effect to negligible level [168]. In earlier studies, tri-n-butyl phosphate (TBP) based solvent extraction was used for separation of uranium for the trace elemental determination in uranium matrix by TXRF [48,105,110,169]. Though TBP based extraction is well established, it is very laborious and generates many organic waste and its disposal is a troublesome process. Recently solid phase extraction (SPE) methodology is gaining popularity among the researchers due to its several advantages over liquid-liquid based extraction methodology. It is very simple, fast, produce less amount of waste, does not form emulsions and the extractant can be regenerated and reused. The basic principle of SPE is the transfer of analytes from the aqueous phase to the active sites of the adjacent solid phase. This transfer process can be enhanced by using right combinations of solvent (aqueous medium) analyte and sorbent [170-172]. Different types of solid sorbents like silica, silica gel, modified cellulose,

graphene or functionalized graphene oxide, carbon nanotubes, nano particles, polymer based membranes are used in SPE based separation or pre-concentration method [173-180]. For such extraction a small amount of solid phase extractant is equilibrated in aqueous phase. The acid molarity of the aqueous phase is a very important factor, for efficient SPE. The solid sorbent may behave differently in different molar solutions. There are many reports on the separation of uranium by using SPE based methods [178-180]. Sadananda Das et.al. has developed phosphate functionalized poly (propylene) membrane for the separation of uranium from the sea water [181]. There are some phosphate based polymer membranes reported for the separation of uranium. However these polymer membranes are not very efficient when large amount of uranium is present in the solution [182]. There is a report on the uranium U (VI) absorption by graphene oxide nano sheets [176]. This SPE technique can be very useful for trace elements determination in uranium oxide by TXRF due to the features discussed above. This methodology can be extended to Pu based samples for which this approach shall be highly beneficial as vigorous shaking of radioactive analytical waste can be avoided, sample amount is reduced drastically and radiation dose to the analyst will be minimum. In this work a systematic study to use SPE based uranium separation methodology for trace element determination in uranium oxide by TXRF is reported for the first time. We have developed a new solid phase extractant for the separation of uranium from the sample matrix and used it in this work.

5.2. Experimental

5.2.1. Reagents

Suprapure nitric acid and de-ionized water (18 M Ω cm specific resistance) purified by a model Quantum from Millipore (Mumbai, India) were used throughout the sample preparation and dilution in the present study. Monomers 2-acrylamido-2- methyl propane sulfonic acid

(AMPS) and bis [2-(methacryloyloxy) ethyl] phosphate (BIS-MEP), ethylene glycol dimethacrylate (EGDM) and 2, 2-dimethoxy-2-phenylacetophenone (DMPA) were purchased from Sigma-Aldrich (Steinheim, Switzerland). Tetrahydrofuran (THF) and N, N'-dimethyl formamide (DMF) used were obtained from Merck, Germany. Suprapure concentrated HNO₃ (Merck, Germany) was used for diluting the samples to the required molarity. For the determination of X-ray line sensitivities of different elements, MERCK ICP multi-element standard (MES) solutions and single element standards were used.

5.2.2. Preparation of polymer resin gel

Two types of polymer resin gels: Bis-MEP based polymer denoted as resin 1 and 1: 1 combination of Bis-MEP and AMPS based polymer resin gel designated as resin 2 were prepared for this work. For the preparation of resin 1; Bis-MEP and UV initiator DMPA (1 wt %) along with cross linker EGDMA (5 mol %) were dissolved in DMF solvent and exposed to 365 nm UV light in a photo reactor (Heber Scientific, Chennai, India, Model no: HML-SW-MW-LW-888) for a period of 20 min. The photo reactor is fitted with eight 8W mercury UV lamps of wavelength 365 nm (Sankyo Denki, Japan) and highly polished anodized aluminium reflector. After UV irradiation, the gels were washed with DMF and Milli-Q water for 3-4 times to remove un-polymerized components and then vacuum dried. For the preparation of resin 2; Bis-MEP and AMPS were taken in 1:1 molar ratio along with UV initiator DMPA (1 wt%) and cross linker EGDMA (5 mole%) and dissolved in DMF and then same procedure, as mentioned above, was repeated. The schematic of the synthesis of these polymer resins are shown in Figure 5.1. It can be seen that when 1:1 combinations of Bis-MEP and AMPS is used to prepare polymer resin gel there can be three types of combinations possible. One combination is just like the Bis-MEP based polymer resin, where only two P=O groups (-MEP-MEP-MEP- type) are available for

bonding with UO_2^{2+} moiety. The other two combinations have one (-AMPS-MEP-MEP- type) and two (-AMPS-MEP-AMPS- type) amide C=O groups available in addition to the two P=O groups for coordination with UO_2^{2+} moieties.

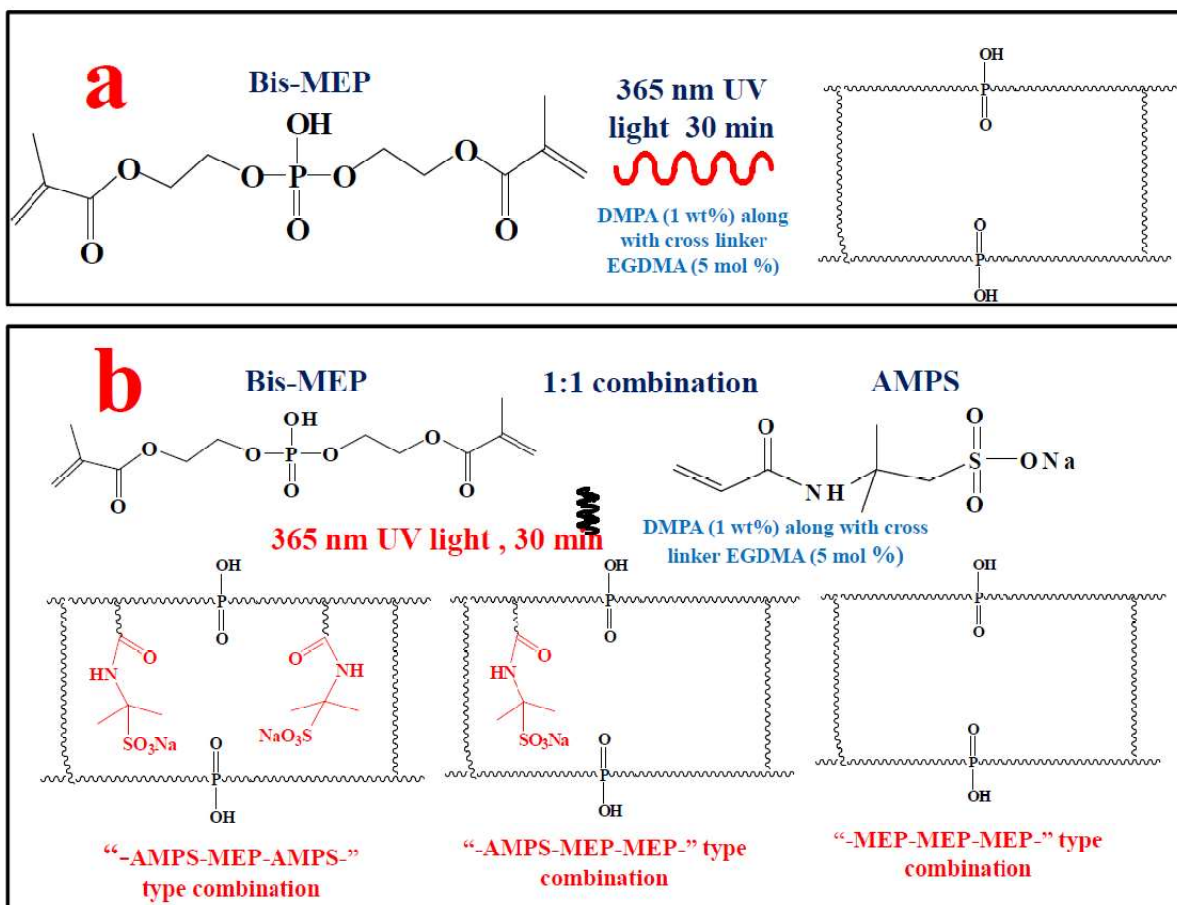


Figure 5.1: Schematic of the preparation of Bis-MEP based polymer resin gel (resin 1) (a) and three possibilities of 1:1 combination of Bis-MEP and AMPS based polymer resin gel (resin 2) (b)

5.2.3. Instrumentation

The prepared polymer resin gels (resin 1 and resin 2) were characterized by different methods like PL (Photoluminescence), Fourier transform infrared (FTIR), FE-SEM (Field Emission Electron Microscope).

The PL data of the polymer resin gels were recorded on an Edinburgh CD-920 unit having M 300 monochromator. The data acquisition and analysis were done using F-900 software provided by Edinburgh Analytical Instruments, UK. A Xenon flash lamp having frequency range of 10–100 Hz was used as the excitation source. Emission spectra were recorded with a lamp frequency of 100 Hz. Luminescence lifetime measurements were based on well established Time-Correlated Single-Photon Counting (TCSPC) technique [183]. The FTIR spectra were recorded using the platinum-attenuated total reflection technique. All spectra were obtained at a resolution of 4 cm^{-1} (wave number) and under the same measurement conditions ($4000\text{--}500\text{ cm}^{-1}$, 36 scans). The morphology of the polymer resins were recorded by JEOL made field emission gun scanning electron microscope (FEG-SEM).

For the analysis of uranium as well as trace elemental concentration, an ITAL STRUCTURES, Italy TXRF spectrometer Model TX-2000 and Atominstitut Vienna Low Z – High Z TXRF spectrometer were used [120].

5.2.4. Uranium extraction efficiency

Uranium extraction efficiencies of both the polymer resin gels were assessed. Weighted amount of uranium oxides ($\sim 15\text{ mg}$) were dissolved in 1 mL 4M supra pure HNO_3 in two separate beakers. Both the polymer resin gels (resin 1 and resin 2) having same amount (200 mg) was dipped in these two beakers separately for about one hour. Both the aqueous solutions obtained were analyzed by TXRF to determine final uranium concentrations in them. For the analysis of uranium concentration, $5\ \mu\text{L}$ aliquots of both of these solutions were put on the flat polished quartz sample supports along with $5\ \text{uL}$, $100\ \mu\text{g/mL}$ of Ga solution. The solutions on the support were thoroughly mixed by a micropipette by sucking and releasing the solutions several times at same spot. Later the solutions on the supports were dried using a hot plate and a

thin film was formed on the quartz sample support. Three sample specimens of each solution obtained after equilibration were prepared. These sample specimens were presented for TXRF measurements for live time of 300 s each. The concentration of uranium in those two solutions (equilibrated with resin 1 and resin 2) were determined using the pre determined relative sensitivity value with respect to Ga. The uranium extraction efficiency for the polymer resin gels was obtained using the following equation:

$$E = \frac{C_b - C_a}{C_b} \times 100 \quad (5.1)$$

Where E = Extraction efficiency of the resin in %, C_b is the concentration of uranium in solution before putting polymer resin in it and C_a is the concentration of uranium in solution after equilibration with the polymer resin for 1 hour.

5.2.5. Molarity studies

Uranium extraction efficiency of any solid sorbent is highly dependent on the acid molarity of the solution phase. To determine the optimum acidic molarity for the separation of uranium using the polymer resin 2, sorption study was carried at different molarities of HNO_3 ranging from 0.1 M to 6 M. Uranium solutions (2 mL volume) in 0.1, 0.5, 1, 2, 3, 4, 5, 6 M HNO_3 were prepared in different beakers and weighted amounts of 80 mg of the resin 2 was dipped in each of these beakers for overnight. Aliquots of 5 μL of the uranium solutions were pipette out from each of these beakers on quartz sample supports and analyzed by TXRF for uranium as mentioned above and the uranium recoveries were calculated by using the equation 1. In order to determine the selectivity of the polymer resin gels, another experiment was conducted. Aliquots of 2mL of diluted Merck ICP multi-elemental standard Solution IV to 10 $\mu\text{g}/\text{mL}$ elemental concentration level in 0.1, 0.5, 1, 2, 3 and 4M HNO_3 medium were taken in different beakers. About 50 mg of polymer Resin 2 was dipped in each of these solutions and left

overnight. Thereafter, the solutions were analyzed by TXRF using 5 μL of the solutions and 5 μL of Y internal standard having concentration of 20 $\mu\text{g}/\text{mL}$. Similar studies for the selective uptakes were carried out using lanthanides also. For such studies, a lanthanide solution containing different concentrations of La, Ce, Pr, Nd, Gd, Er, and Ho was prepared in 4M HNO_3 medium and taken in a beaker along with Ga internal standard. TXRF spectra of the solutions measured before and after equilibration with 200 mg of Resin 2, and were analyzed.

5.2.6. Sorption isotherm

Equilibrium isotherm studies were carried out to determine the maximum sorption capacity of resin 2 for U (VI). The concentration of uranium was varied from 0.3 mg/mL to 80 mg/mL, keeping the other parameters constant (weight of the resin 2 = 150 mg, molarity of the HNO_3 medium: 4M).

5.2.7. Kinetic study

The absorption of uranium by the polymer resin 2 was studied as a function of time. For this experiment; 12.8 mg of uranium oxide was dissolved in 2 mL 4M HNO_3 and 400 mg of the weighted polymer resin was dipped in that solution. The solution was well stirred and the concentration of uranium was determined at different time interval by TXRF.

5.2.8. Regeneration of the polymer resin

The polymer resin after sorbing uranium from the sample solution became yellow in color as it was loaded with uranium in U (VI) chemical state. In order to use this polymer resin again, it has to be stripped out from uranium. For such study, this uranium loaded polymer resin was dipped in 5 wt % Na_2CO_3 solution and sonicated for 1 h. The resin was taken out from the solution and this process was again repeated. Finally the resin was taken out from the solution and washed with milli-Q water for several times and dried. It was seen that U (VI) was

completely desorbed from the resin and the resin could be reused for the removal of U (VI) from the fresh

5.3. Results and discussions

5.3.1. Characterization of polymer resin gel samples

It is very important to understand the mechanism of uranium absorption by the two types of resins. Photoluminescence (PL) study was carried out on the uranium loaded resin 1 and resin 2. Figure 5.2 shows the emission spectrum of uranium loaded resin 1 and resin 2 at an excitation wavelength of 230 nm. From this figure it can be seen that the emission spectra have characteristic bands at 480, 500, 520, 546 and 572 nm. Such vibronic progression with constant spacing is specific signature of uranium in +6 oxidation state in the form of UO_2^{2+} [183, 184].

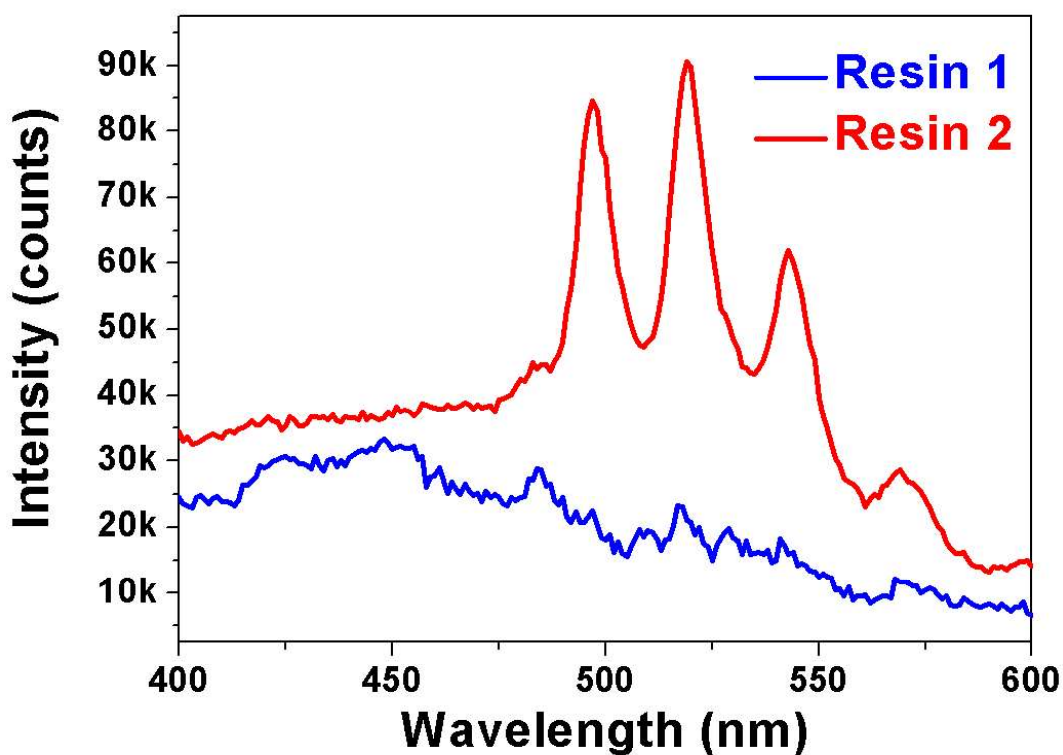


Figure 5.2: Emission spectra of uranium loaded Resins: resin 1 and 2 at an excitation wavelength of 230 nm

This vibronic progression is clearly visible in the PL spectrum of resin 2 but not clearly visible in case of resin 1. However, it is clearly visible in the Time Resolved Emission Spectra (TRES) of both resins at 100 μ s delay time as shown in Figure 5.3.

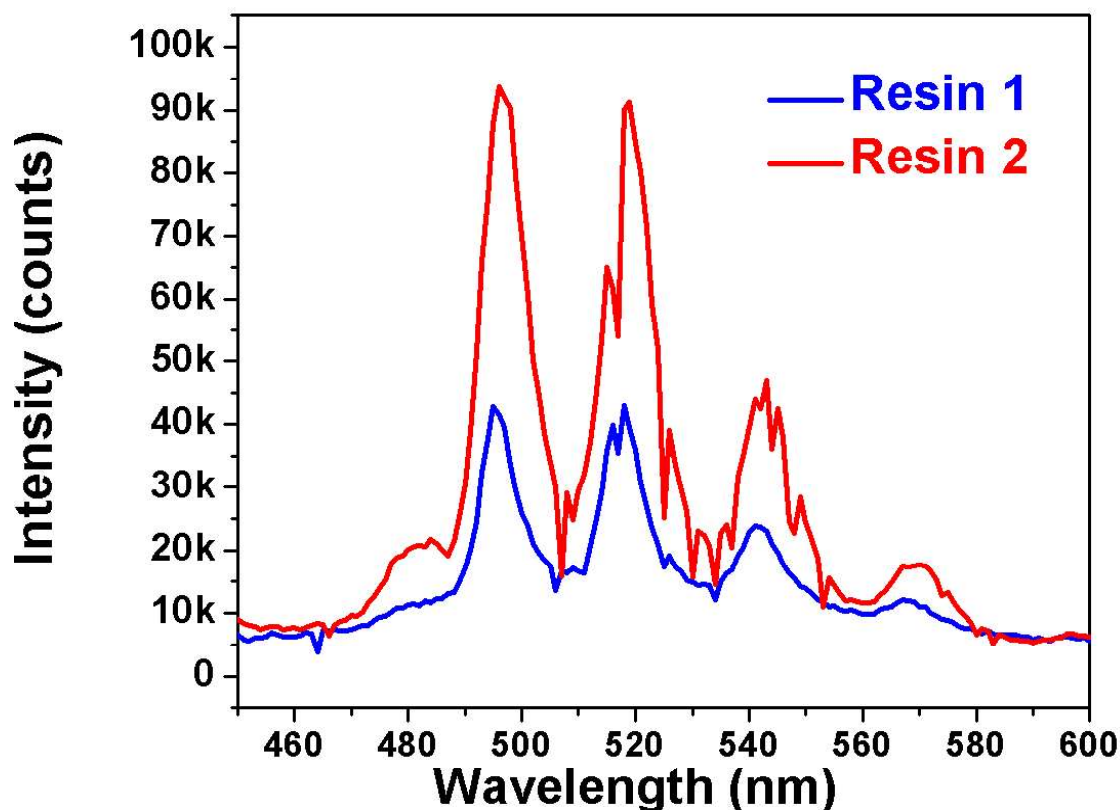


Figure 5.3: TRES spectra of uranium loaded resin 1 and 2, at an excitation wavelength of 230 nm

From the TRES spectra of both the uranium loaded resin 1 and 2, vibronic structure characteristic of UO_2^{2+} are clearly visible. Both uranium loaded resins has five line spectra. However uranium loaded resin 2 spectral lines have less intensity than that of resin 2. From these observations it can be argued that the uranium absorption efficiency of resin 2 is more than resin 1. In order to understand the coordination around the uranyl ion in more detail, it is important to analyze the life time of the decay curve obtained from TRES spectra.

Figure 5.4 represents the decay curves for uranium loaded resins at $\lambda_{ex} = 230$ nm and $\lambda_{em} = 546$ nm. For both the cases; the decay curves were fitted using the following bi exponential equation [185].

$$I(t) = A_0 + A_1 \exp(-t/\tau_1) + A_2 \exp(-t/\tau_2) \quad (5.2)$$

Where A_0 , A_1 and A_2 are scalar quantities obtained from the curve fitting, t is the time and τ_1 , and τ_2 are decay time values for exponential components, respectively. The respective decay times for both the resins are tabulated in Table 5.1.

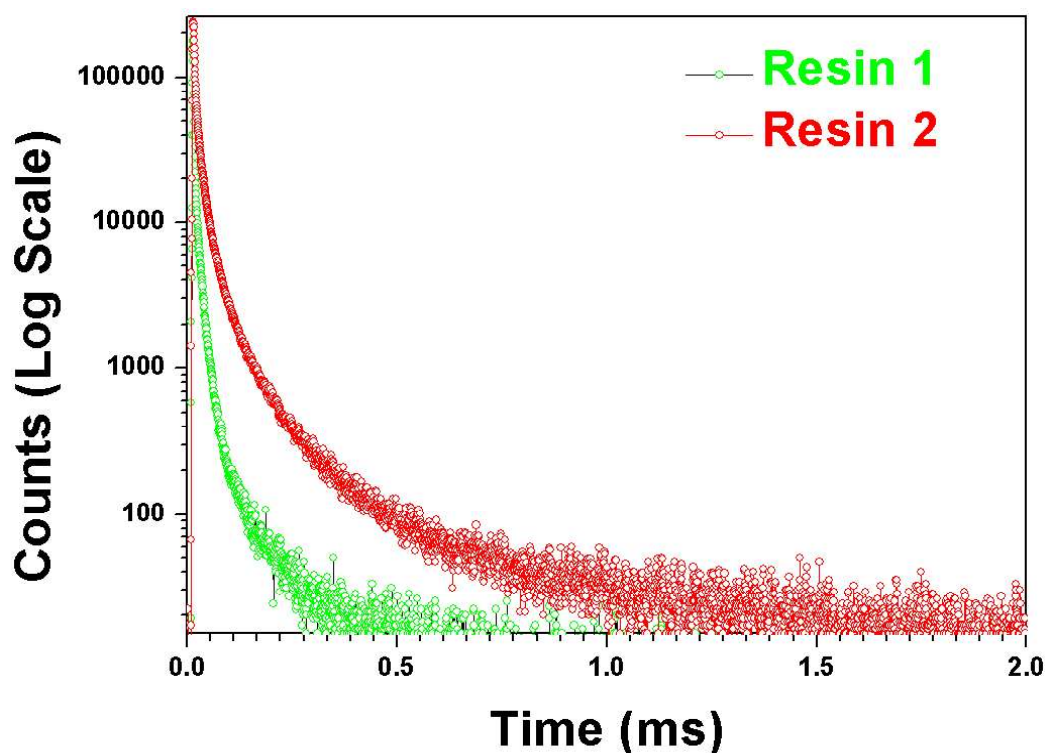


Figure 5.4: Decay curves for uranium loaded resin 1 and 2 at $\lambda_{ex} = 230$ nm and $\lambda_{em} = 546$ nm

The decay curves shown in Figure 5.4 clearly indicate that the excited state of uranium loaded resin 2 decays faster than uranium loaded resin 1. The life time of both the excited states were calculated and are shown in Table 5.1. From that table it can also be seen that life time values for uranium loaded resin 1 are shorter ($\tau_1 = 13.36$ μ s and $\tau_2 = 73.19$ μ s) than uranium loaded

resin 2 ($\tau_1=19.79 \mu\text{s}$ & $\tau_2=166.94 \mu\text{s}$). The difference in the life time values can be explained from the differences in coordination environment of uranyl species inside the polymer resin gel, and are shown in Figure 5.5.

Table 5.1: Lifetime values obtained by fitting the decay curve of uranium loaded resin 1 and resin 2

Uranium loaded polymer resin	$\tau_1 \mu\text{s}$ (%)	$\tau_2 \mu\text{s}$ (%)
Resin 1	13.36 (74 %)	73.19 (26 %)
Resin 2	19.79 (55 %)	166.94 (45 %)

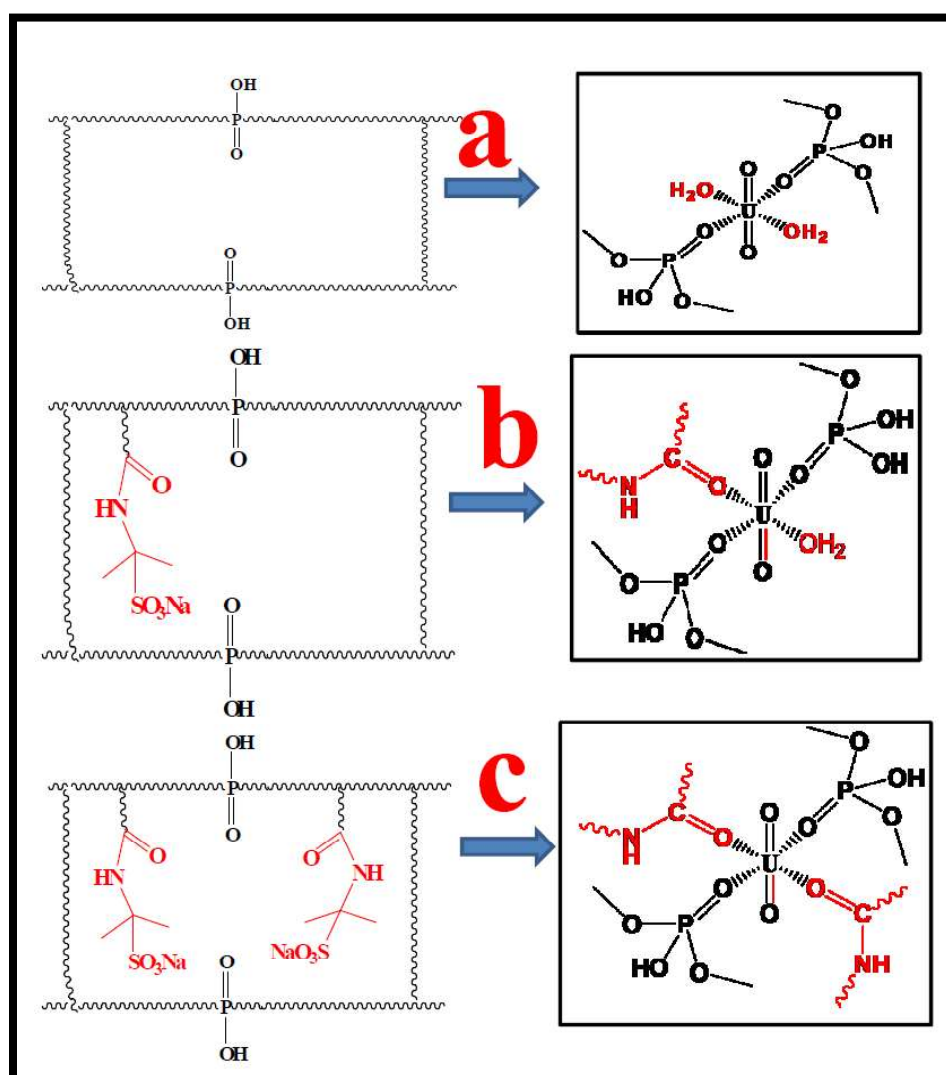


Figure 5.5: Schematic of coordination of UO_2^{2+} moieties in 4M HNO_3 medium with the two types of polymer resins

From Figure 5.5a it can be seen that for, resin 1; there are only two P=O group available in the pocket to coordinate with the UO_2^{2+} species and the rest of the co-ordinations are satisfied by the water molecules. While in case of resin 2, two more pockets with amide group (Figure 5.5 b and c) are available for coordination with the UO_2^{2+} species in addition to that available for resin-1 (Figure 5.5a). Now since water molecule is more efficient as fluorescence quencher than the amide group, any involvement of water molecule in the coordination with uranyl moiety will results in quenching of photoluminescence intensity of the vibronic spectra characteristic of uranyl group and shall also reduce the life time value as reported in literature cases [180]. This is reflected in case of resin-1, where two water molecules are coordinated to the uranyl group, resulting in quenching of uranyl luminescence and low life time values. However, for uranium loaded resin 2, where amide group can also coordinate to the uranyl group as there are many pockets available (Figure 5.5b and c), the intensity and lifetime values shall be much higher. This is reflected in Figure 5.3 and Figure 5.4. Thus the shorter lifetime values in both the cases of resin 1 ($\tau_1=13.36 \mu\text{s}$) and resin 2 ($\tau_1=19.79 \mu\text{s}$) are due to involvement of water molecules in coordination with UO_2^{2+} species. On the other hand the longer lifetime value ($\tau_2=166.94 \mu\text{s}$) in case of resin 2 is due to environment around uranyl species as shown in Figure 5.5c where no water molecule is involved and the coordination were satisfied with amide C=O group present in some of the pockets of resin 2. Further to support this argument of amide group involvement with uranyl moiety further; FTIR study of the uranium loaded resin 2 was carried out.

Figure 5.6 shows the FTIR spectra of resin 2 before and after sorption of uranium from the solution. Figure 5.6a, which is FTIR spectra of resin 2 ; shows the vibrational bands of sulfonyl group at 1040 cm^{-1} (S-O), 1380 cm^{-1} (S=O) and 1455 cm^{-1} ($-\text{SO}_2-$), amide carbonyl group at 1650 cm^{-1} (C=O), phosphate group (P=O) at 1160 cm^{-1} and carbonyl group (C=O) at

1730 cm^{-1} . Figure 5.6b is the FTIR spectra of uranium loaded resin 2. Strong absorption band around 930 cm^{-1} is observed in it which is characteristic band of uranyl stretching (U=O) frequency. These bands were assigned on the basis of the literature reports [181, 186]. Figure 5.6c and 6d focus on the changes in the P=O and C=O stretching frequencies respectively, before and after the absorption of uranium by resin 2.

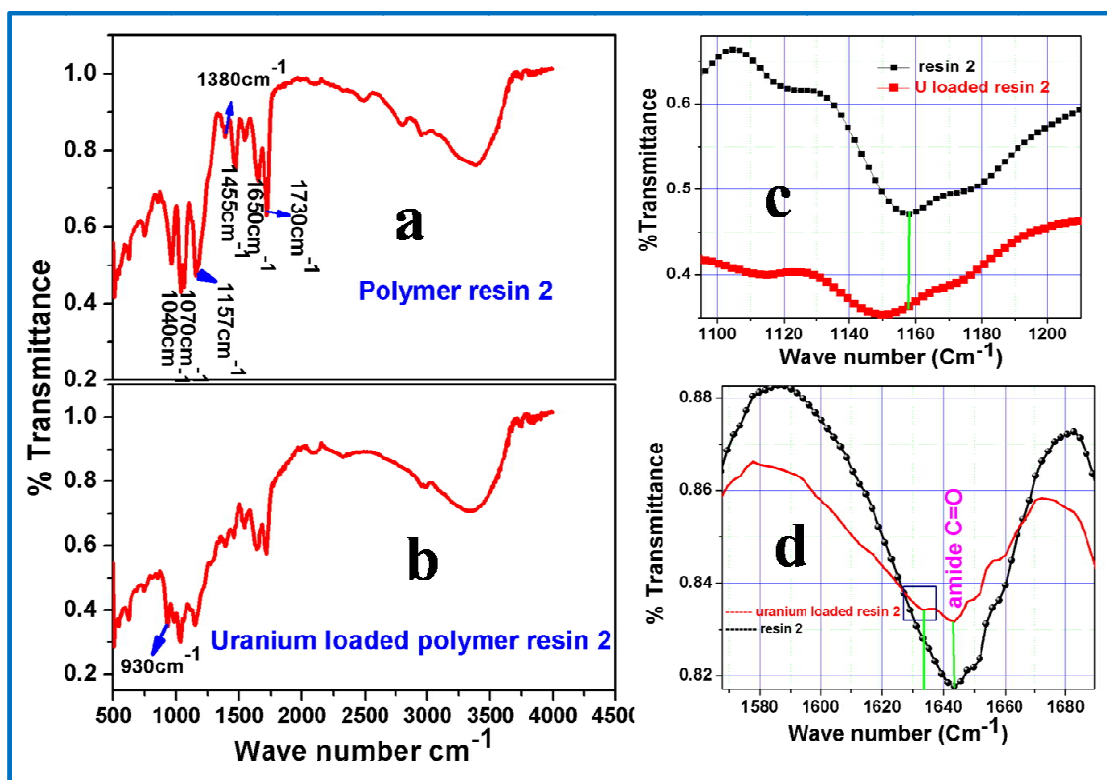


Figure 5.6: FTIR spectra of resin 2 before and after loading of uranium

It can be observed from Figure 5.6c that there is a small decrease of ($\sim 10 \text{ cm}^{-1}$) P=O stretching frequency of resin 2 after absorption of uranium. This small shift can be attributed due to the involvement of P=O group in coordination with uranyl moiety as we have discussed before. Figure 5.6d compares the amide C=O stretching frequencies between resin 2 before and after absorption of uranium. It can be seen from the figure that in case of uranium loaded resin 2,

in addition to the characteristic stretching frequency of amide C=O (1640 cm^{-1}), there is another additional band situated at lower stretching frequency ($\sim 1630\text{ cm}^{-1}$). This lower stretching frequency is due to the involvement of amide group with the uranyl moiety as predicted from the PL study. During TRES study we have observed a component having larger life time ($167\ \mu\text{s}$) in the decay curve of the uranium loaded resin 2. We have predicted that this component having larger life time is due to the non involvement of water molecules in co-ordination with uranyl moiety and instead of that amide carbonyl groups are involved in coordination. The involvement of amide carbonyl moiety is further established from the FTIR study. In the FTIR spectra of uranium loaded resin 2, the un-shifted stretching frequency of amide C=O was also observed. It shows that not all the amide carbonyl groups are involved in coordination with uranyl moiety, only few of them are involved and because of which we have seen a shifted spectra of amide C=O at lower stretching frequency. Thus PL as well as FTIR study confirm the fact that amide carbonyl group is also involved in the bonding with uranyl species in resin 2.

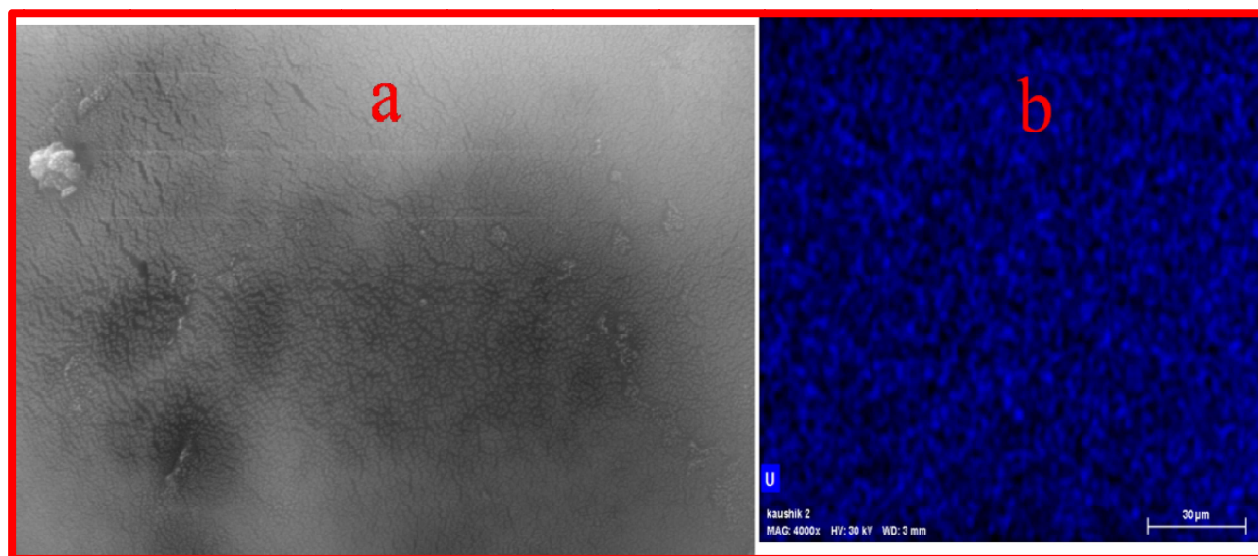


Figure 5.7: (a) FE-SEM images of resin 2 and (b) EDS image of the uranium loaded resin 2.

Figure 5.7a shows the FE-SEM image of resin 2. The presences of cross linking's in resin 2 are clearly visible in the FE-SEM image. The average pore size as found from FE-SEM is in the range of 5-25 nm. The EDS spectrum of the uranium loaded resin 2 is shown in Figure 5.7b indicating uniform uranium $L\alpha$ intensity distribution. This concludes uniform uranium uptake by the resin throughout its matrix.

5.3.2. Uranium absorption studies

Uranium sorption studies on the resins revealed that resin 2 has higher uranium sorption efficiency (94.2%) compared to that of resin 2 (67.2%) within 1 hour of contact time. So resin 2 has a higher potential of uranium absorption and can be used as an efficient solid phase extractant to separate uranium from its solution for the determinations of trace elements in it. Figure 5.8 shows photographs of resin 2 before (a) and after (b) absorption of uranium from a uranium solution. It can be seen from the photographs that initially when the resin was dipped in the solution, it was white in color and after the absorption of uranium, it turned to yellow color.

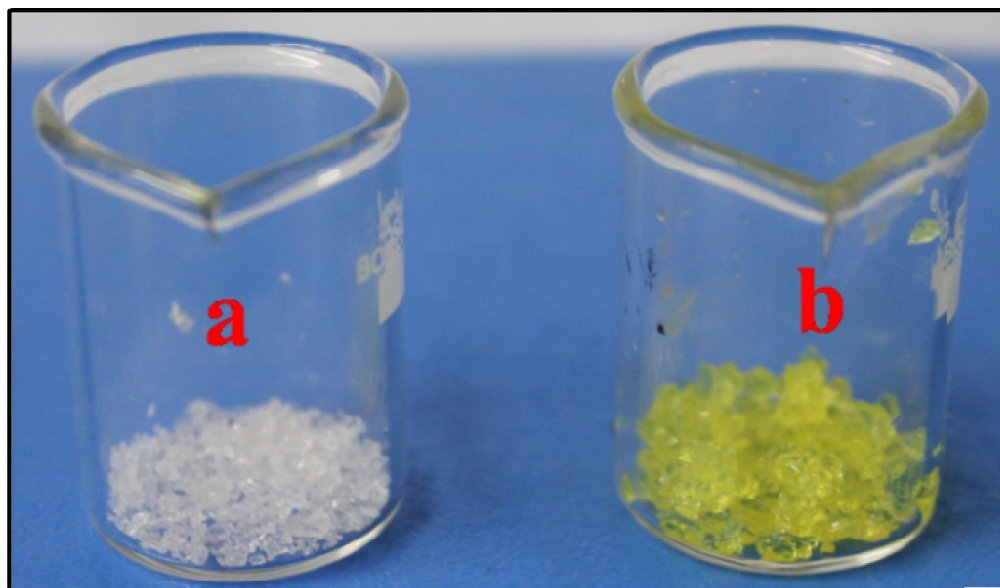


Figure 5.8: Photographs of resin 2 before (a) and after absorption of uranium (b)

From molarity studies it was observed that uranium uptake efficiency is maximum at 0.1 M HNO_3 medium and as the molarity increases, uranium uptake efficiency of resin 2 decreases as shown by a plot of HNO_3 molarity vs. recovery of uranium in Figure 5.9.

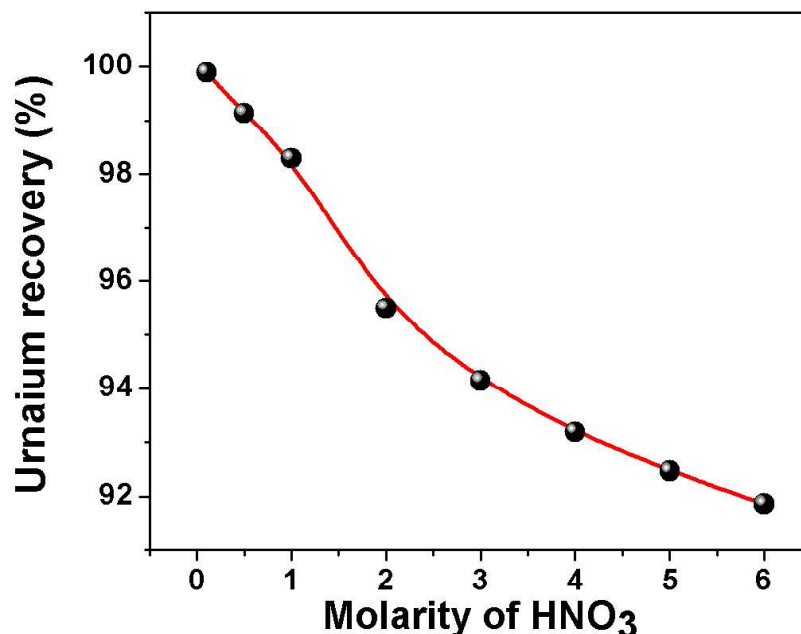


Figure 5.9: Plot of uranium extraction efficiency of resin 2 as a function of molarity of the HNO_3 medium

However another important factor that one has to remember for the application of the resin for trace elemental determinations uranium samples is that the resin should not take other elements. So it is important to determine the optimum molarity where the uranium uptake efficiency is satisfactory as well as the resin is selective to absorb uranium only. This aspect was studied by finding out the sorption of other elements by the resin with respect to molarity of HNO_3 in the solutions using multi-elemental standard solution having elemental concentration of 10 $\mu\text{g/mL}$. The concentrations of different elements were determined by TXRF after equilibration with the resin for an hour of contact. Figure 5.10 shows the change in concentrations of different elements in MES solutions having HNO_3 molarities of 0.1, 0.5, 1.0, 2.0, 3.0, and 4.0 after equilibrations with this polymer resin from different multi-elemental

standard solutions. From that figure it can be seen that at lower molarity, the TXRF determined concentrations of all the elements were less than the expected concentration, which is 10 $\mu\text{g/mL}$. This observation shows that at lower HNO_3 molarity the resin is not only absorbing uranium, but other elements also. This is because of the fact that in lower molar solutions, this resin behaves at cation exchange resin which absorbs other elements in similar manner. So the selectivity is lost. The figure also shows that at 4M HNO_3 medium the TXRF determined concentration of all the elements are very near to 10 $\mu\text{g/mL}$ except for Fe. This may be due to the fact that Fe^{3+} has similar complexation behavior with that of uranyl ion. Therefore, Fe^{3+} is absorbed by the polymer resin at 4M HNO_3 medium leaving behind other elements in solution.

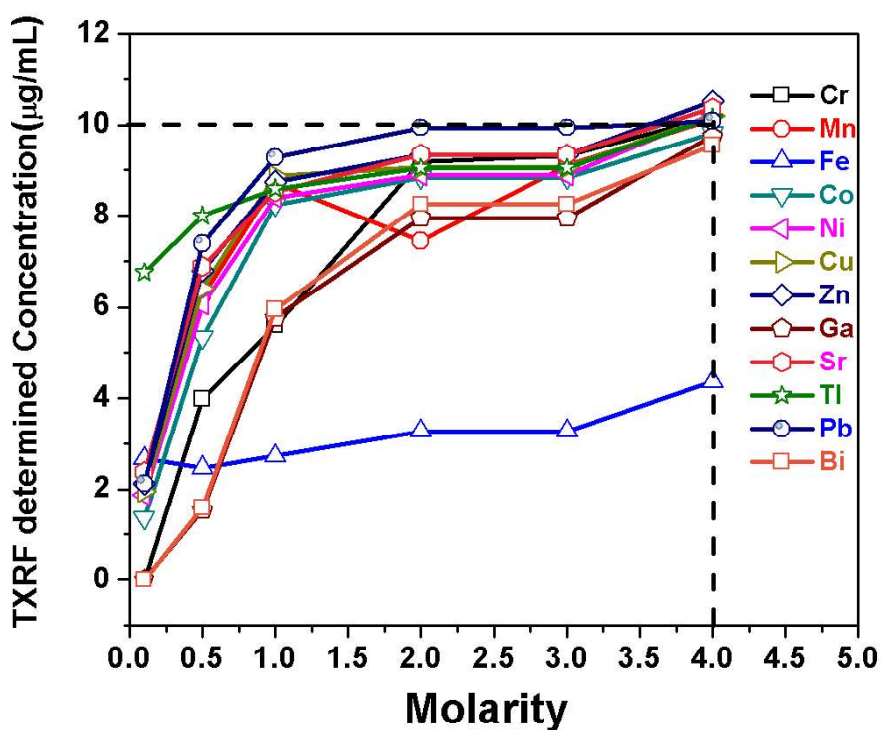


Figure 5.10: Variation of elemental concentration in MES solutions of 10 $\mu\text{g/mL}$ concentration prepared in different HNO_3 molarities, after overnight equilibration of 50 mg of polymer resin 2.

It is also very important to determine the absorption behavior of the resin for lanthanide elements. Figure 5.11 shows the TXRF spectra of a multi-element solution having La, Ce, Pr,

Nd, Gd, Ho, and Er with different elemental concentration along with Ga as internal standard before and after equilibration with resin 2 in 4M HNO₃ medium. It can be seen from the figure that the peak intensity ratio for all the lanthanides were same with respect to Ga internal standard, before and after equilibration with resin 2 in 4M HNO₃ medium. Table 5.2 shows the ratio of area under each of the lanthanide L α peak and Ga K α . It can be seen that this ratio remains almost same before and after equilibrating the aqueous phase with resin 2 in 4 M HNO₃ medium solutions of lanthanides. This observation confirms that the developed polymer resin-2 does not absorb lanthanides also in 4M HNO₃. So this resin can also be used for the analysis of lanthanides in uranium matrix.

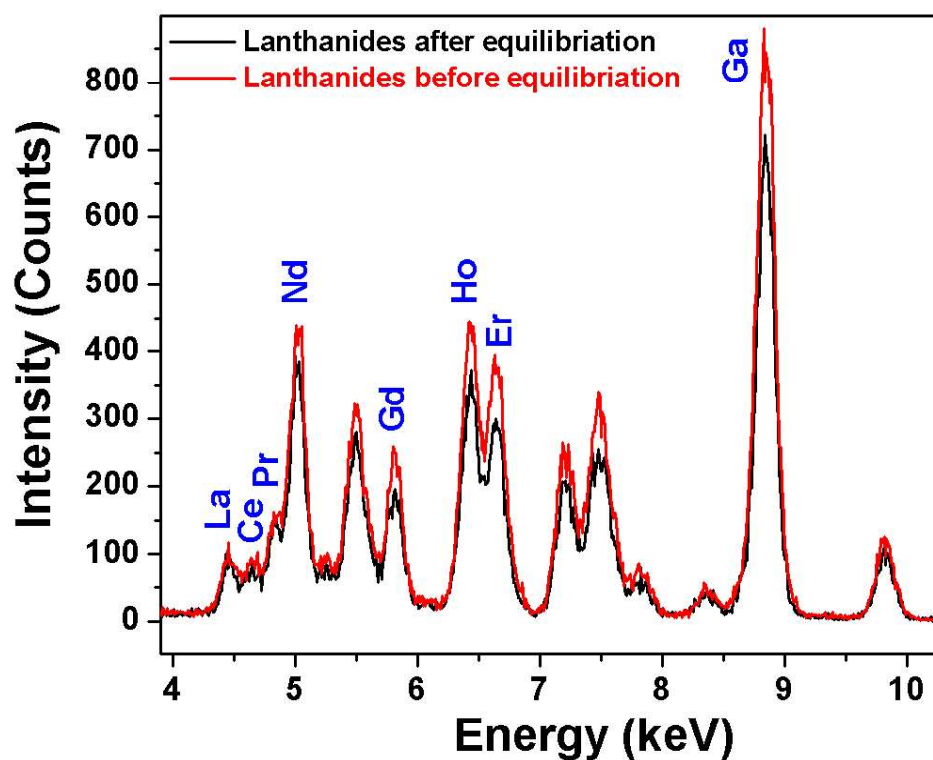


Figure 5.11: TXRF spectra of solutions in 4M HNO₃ having lanthanides before and after equilibration of resin 2 with the solution

Table 5.2: The intensity ratio of lanthanide element La lines and Ga K α before and after equilibration of the 4M HNO₃ solution of lanthanides with resin 2

Lanthanide elements (Ln)	Intensity ratio[(Ln) L α area/ Ga K α area]		
	Before equilibration with resin 2 (B)	After equilibration with resin 2 (A)	B/A
La	0.0774	0.07304	1.06
Ce	0.0757	0.07078	1.07
Pr	0.0602	0.06878	0.88
Nd	0.3038	0.33272	0.91
Gd	0.1363	0.13484	1.01
Ho	0.3474	0.37005	0.94

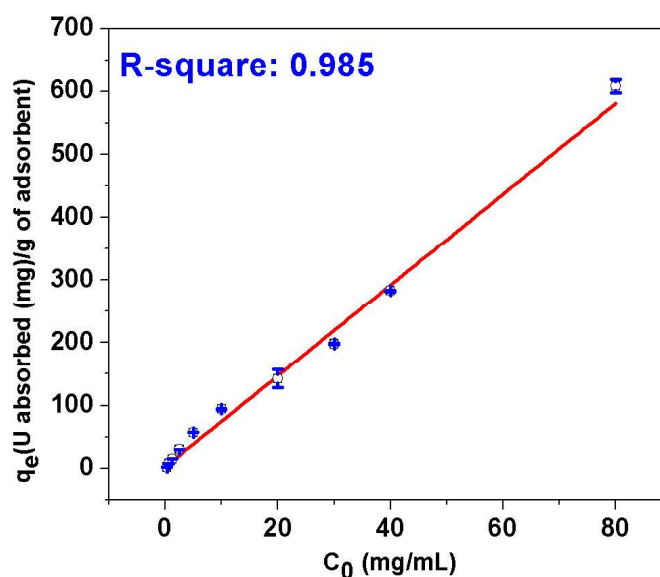


Figure 5.12: Sorption isotherm of U (VI) ions on resin 2, having weight of 150 mg in 4M HNO₃ medium for overnight contact

The sorption capacity of resin 2 versus the equilibrium concentration of U (VI) in the aqueous solution is plotted in Figure 5.12. It can be seen that the sorption isotherm do not follow Langmuir or Freundlich isotherm models, but it is following a linear equation. So the absorption capacity of the resin 2 is increasing with increasing U (VI) concentration up to 80 mg/mL, and at 80 mg/mL of U (VI) concentration the absorption capacity of the resin is 600 ± 2 μ g/mg. This

could be attributed to a possibility of change in U (VI) to ligand ratio depending upon the uranium concentration in the Resin 2.

Kinetic study for the sorption of uranium by resin 2 was carried out to determine the optimum time needed to separate almost all the uranium matrix from the sample. The sorption profile as a function of time obtained has been shown in Figure 5.13A. From this figure it can be seen that within 2 hours of contact with resin 2; 95% of the uranium was separated from the solution. After 6 hours of equilibration, 97% uranium was removed from the solution by this polymer resin. In order to further separate more uranium from the solution, a second contact with fresh resin shall be required. So the leftover solution after the first contact with resin 2 was pipette out in a separate beaker and 100 mg of the fresh resin 2 was dipped in it. The solution was kept stirring with the help of a magnetic stirrer. Uranium present in the solution was determined as a function of time by TXRF. The absorption profile after the second contact with the polymer resin is shown in Figure 5.13B. From this figure it can be seen that within 10 minutes more than 99.5% of uranium has been removed from the solution after second contact with the polymer resin.

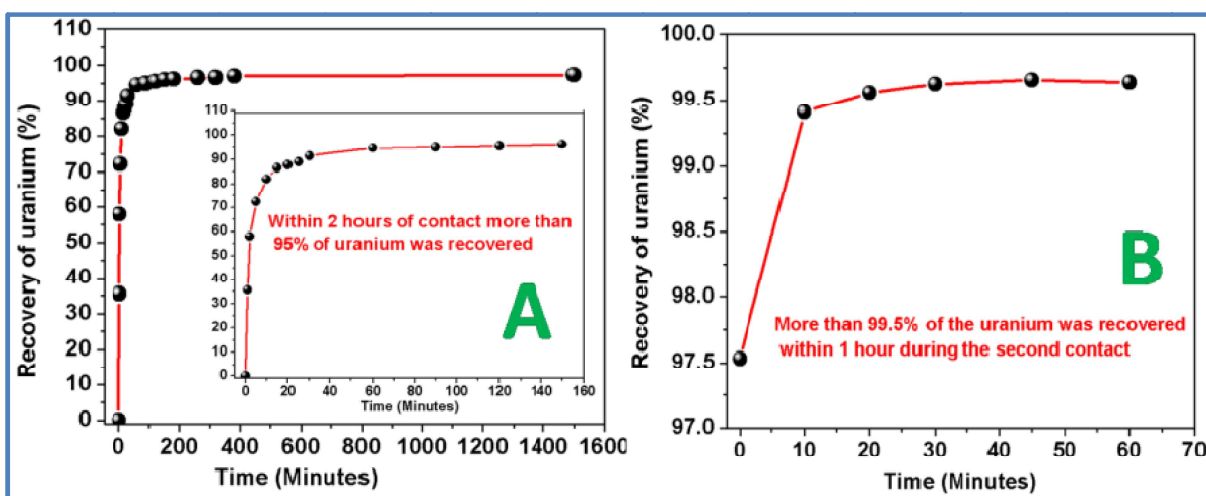


Figure 5.13: Recovery of uranium from its 4H HNO₃ solutions on first (A) and second (B) contact with resin 2 as a function of time

There are three commonly used kinetic models for the analysis of sorption profile, i.e. pseudo-first order, pseudo-second order and diffusion model. The sorption profile obtained in this work has been fitted with these three models, and it was found that it is following pseudo-second order kinetics. The pseudo-second order rate equation is expressed as

$$\frac{t}{q} = \frac{1}{K_2 q_e^2} + \frac{1}{q_e} \quad (5.3)$$

Here K_2 is the pseudo second order rate constant and q and q_e are the amounts of solute sorbed in unit weight of the polymer resin at time t and at equilibrium [181]. The fitting is shown in Figure 5.14. From this figure it can be seen that the sorption profile is following pseudo-second order kinetics very well.

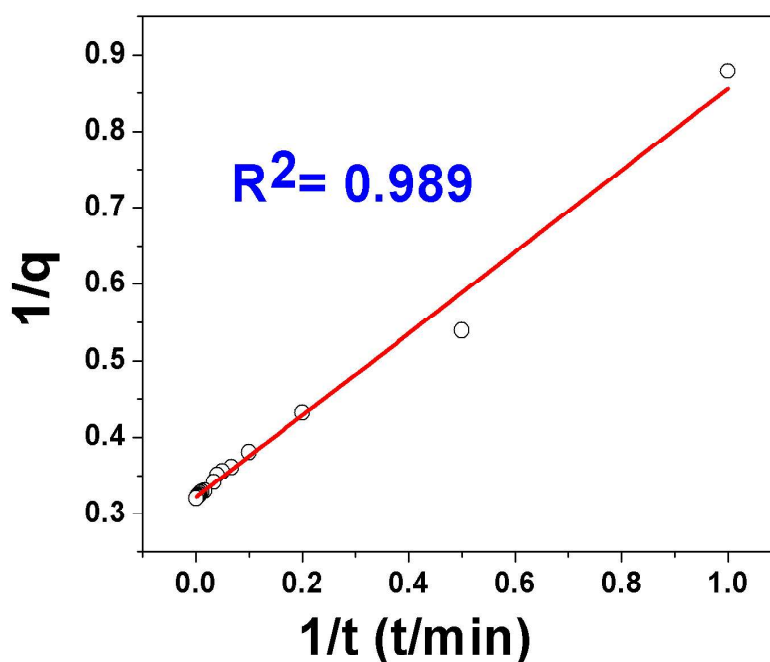


Figure 5.14: Pseudo second order kinetic model used to fit the sorption profile of the polymer resin gel for the absorption of uranium in 4M HNO₃ medium

5.4. Application of the resin for trace elemental determinations in uranium

In order to use the new polymer resin 2 for the trace elemental determination in synthetic as well as real uranium samples, two synthetic samples of uranium were prepared by adding

MERCK multi elemental standard solution ICP-IV in a uranium solution with 5 mg/mL of uranium concentration. The final trace elemental concentrations in these two solutions were maintained as 5 and 10 $\mu\text{g/mL}$ respectively. A weighted amount of (200 mg) resin 2 was added in each of these two synthetic solutions and left for 2 hrs. Figure 5.15 shows the TXRF spectra of the solution having elemental concentration of 5 $\mu\text{g/mL}$ before and after the separation of uranium from it. From the Figure 5.15 it can be seen that presence of large amount of matrix causes severe matrix effect and the elemental X-ray line peaks are almost suppressed. However after removal of most of the uranium from the solution by resin 2 using the above methodology, all the elemental X-ray lines of different trace elements are clearly visible with appreciable intensity in the TXRF spectrum.

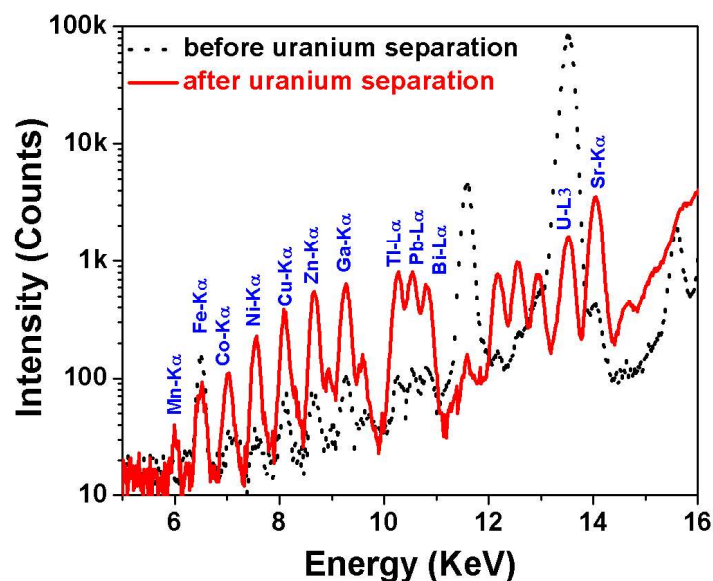


Figure 5.15: TXRF spectra of the multi elemental standard solution having concentration of 5 $\mu\text{g/mL}$ before and after separation of the uranium matrix by resin 2

In order to determine the trace elemental concentrations in these two solutions after separation of most of the uranium by resin 2, a small volume of each of these solutions were

pipetted out and Y was added as internal standard. The final concentration of Y in each of the solution was maintained to 20 µg/mL. Table 5.3 shows the TXRF determined elemental concentrations. From the table it can be seen that the TXRF determined concentrations are in good agreement with the expected concentration for all the elements present in the multi elemental standard solution except Fe. The polymer resin gels partially absorb Fe⁺³ ions in that condition, which give erroneous results for analysis of Fe. So the developed polymer resin gel can be successfully used for the trace analysis in uranium matrix. However Fe cannot be analyzed using this methodology.

Table 5.3: Comparison of expected and TXRF determined elemental concentrations in uranium solutions of trace elements

Elements	Expected Conc. (µg/mL)	TXRF determined Conc. (µg/mL)	Deviation %	Expected Conc. (µg/mL)	TXRF determined Conc. (µg/mL)	Deviation %
Cr	5	5 ± 1	0	10	10 ± 1	0
Mn	5	4.8 ± 0.6	-4	10	10.8 ± 0.7	8
Fe	5	1.7 ± 0.7	-66	10	3.6 ± 0.6	-64
Co	5	4.5 ± 0.3	-10	10	9 ± 1	-10
Ni	5	4.8 ± 0.2	-4	10	11 ± 1	10
Cu	5	5.0 ± 0.5	0	10	9.8 ± 0.9	-2
Zn	5	4.9 ± 0.1	-2	10	10 ± 1	0
Ga	5	4.6 ± 0.1	-8	10	9.4 ± 0.6	-6
Sr	5	4.5 ± 0.1	-10	10	9.7 ± 0.5	-3
Tl	5	5.0 ± 0.2	0	10	9.8 ± 0.5	-2
Pb	5	4.6 ± 0.2	-8	10	10 ± 1	0
Bi	5	5.5 ± 0.6	10	10	10 ± 1	0
Average % deviation: 5.0 Average RSD in %: 7.2				Average % deviation: 3.7 Average RSD in %: 8.5		

**The average deviation and average RSD are calculated without considering results of Fe*

This polymer resin gel has been finally utilized for the trace elemental determinations in a real uranium sample. For this, a certified reference material (CRM) developed by Department of Atomic Energy, Government of India was used. A weighed amount (200 mg) of the CRM-IV was dissolved in 1 mL of suprapure HNO₃ in a small beaker. The solution obtained was

evaporated to dryness. The residue of uranyl nitrate obtained was dissolved in 2 mL of 4M HNO_3 to get the yellow colored uranium solution. A weighted amount of (300 mg) resin 2 was dipped in this solution. After 4 hours the resin was taken out from the solution and this process was repeated three times so that almost all the uranium present in the solution is removed. A clear colorless solution of uranium was obtained. An aliquot of 500 μL of the solution was pipetted out into a small centrifuge vial and Ga was added as internal standard in it and well mixed. The solution was analyzed by TXRF using 5 μL aliquots for specimen preparation in triplicate. A blank solution was also prepared in similar way, except the addition of CRM in it. Figure 5.16 shows a schematic of the sample preparation.

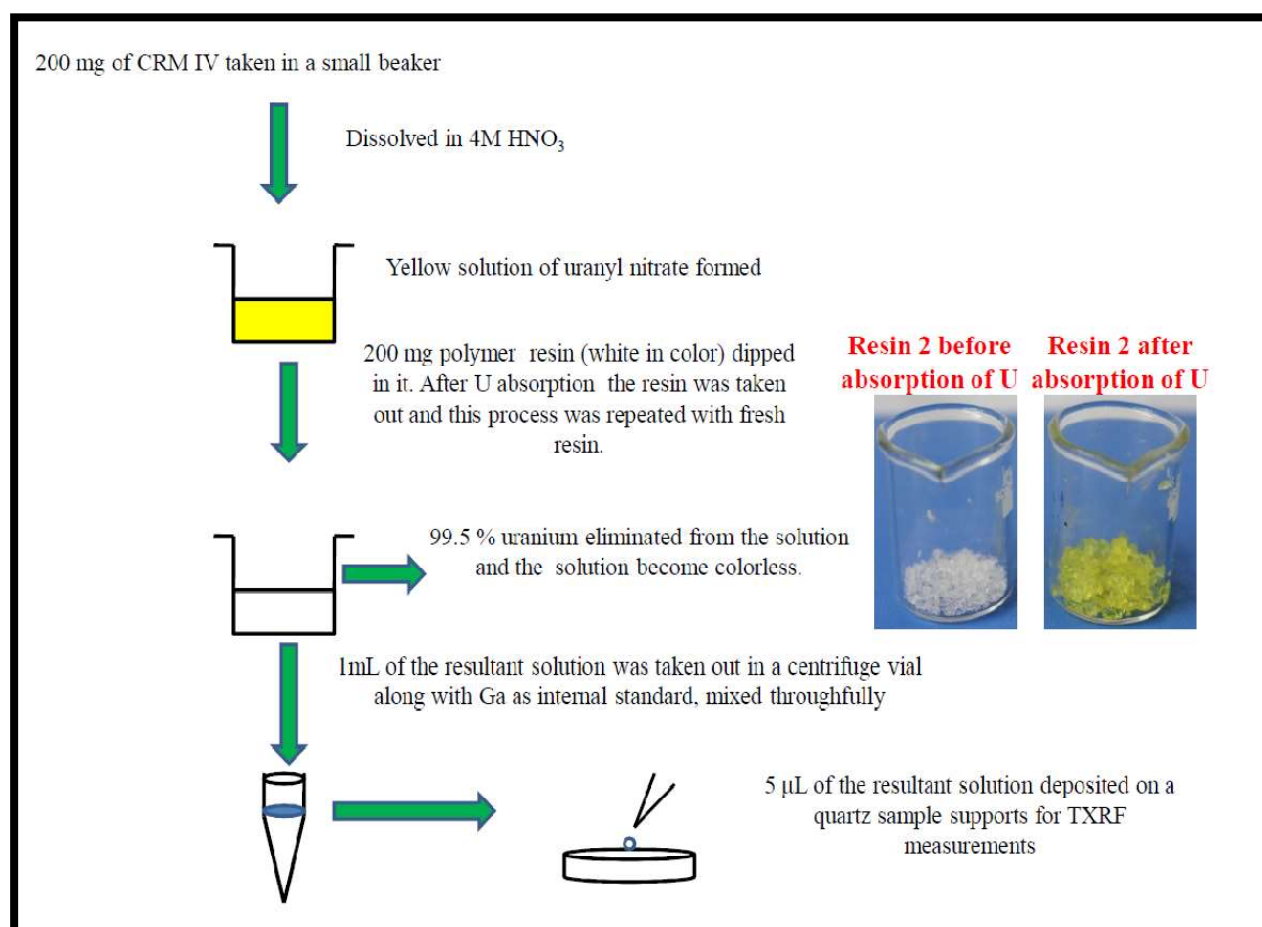


Figure 5.16: Schematic diagram of the separation of uranium from real uranium oxide (CRM-IV) sample matrix using polymer resin 2

Figure 5.17 shows the TXRF spectrum of CRM-IV solution after separation of almost all the uranium from it by SPE method using polymer resin 2. From the figure it can be seen that elemental X-ray lines of Si, P and S are present in the TXRF spectrum, which arises from the polymer resin, due to its little solubility into the aqueous phase. Si K α line is coming from the quartz sample support. Elemental X-ray lines of Ca, Cr, Mn, Fe, Co, Ni, Cu, Zn etc. are clearly visible in the TXRF spectra which arise from the trace impurities present in the CRM. Although most of the uranium was separated from the sample matrix, still some uranium is present in the aqueous phase, which gives U L α line in the TXRF spectrum. The concentration of the remaining uranium was determined and it is $25 \pm 1 \mu\text{g/mL}$ which is much smaller compared to the initial concentration of uranium i.e. 100 mg/mL indicating 99.98% of the uranium matrix separation.

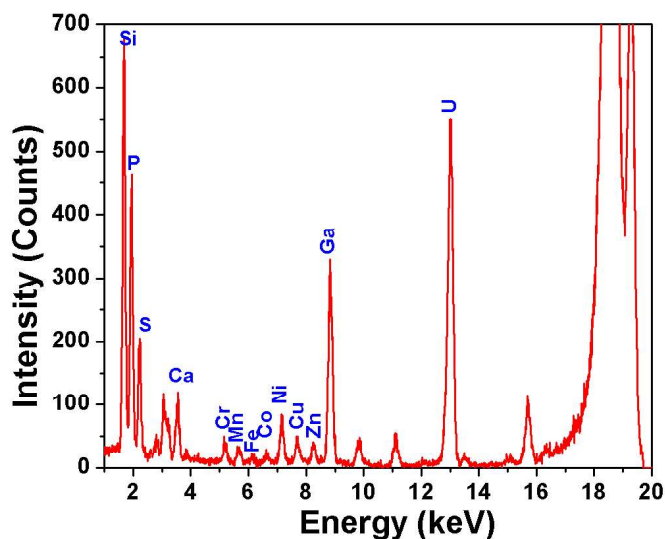


Figure 5.17: TXRF spectrum of processed CRM-IV solution after separation of uranium from the solution matrix using polymer resin 2

The concentrations of these trace elements present in uranium oxide CRM samples after the analysis is shown in Table 5.4 and it is compared with the reported one.

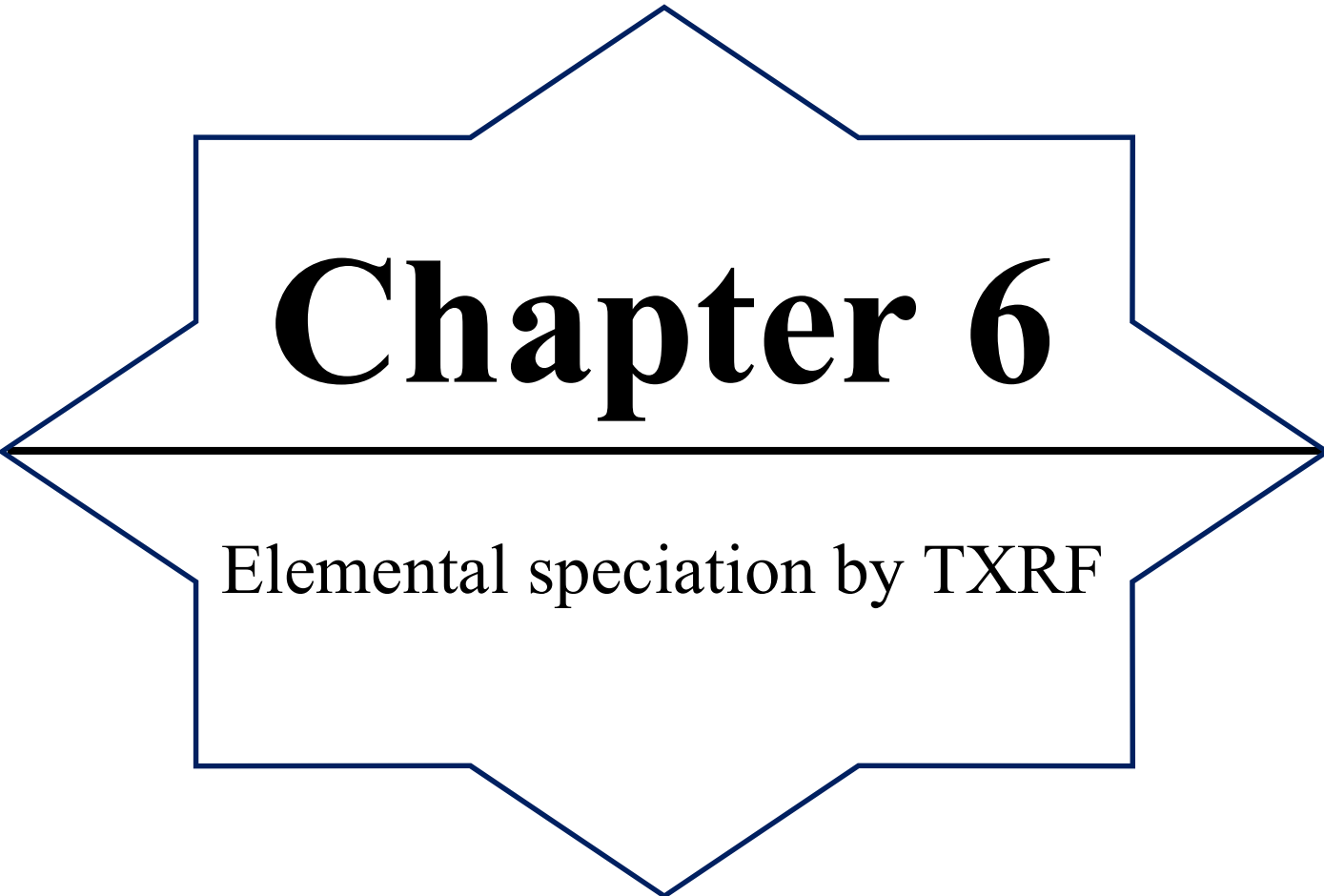
Table 5.4: Comparison of TXRF determined elemental concentrations and certified elemental concentrations for the trace elements present in CRM-IV

Elements	Expected conc. ($\mu\text{g/g of U}$) (A)	TXRF determined conc. ($\mu\text{g/g of U}$) (B)	B/A
Ca	114 ± 6	100	0.88
Cr	31 ± 2	32	1.03
Mn	15 ± 2	15	1.00
Fe	11 ± 5	170	15.45
Co	7.6 ± 0.9	8.5	1.12
Ni	18.1 ± 0.6	17	0.94
Cu	10.8 ± 0.6	9.2	0.85
Zn	7.9 ± 0.6	6.6	0.84
Average RSD: 7.6%			
Average deviation from expected concentration: 10.2%			

- The RSD and average deviation were calculated without considering Fe

5.5. Conclusions

A new polymer resin has been developed for separation of uranium in a solution and subsequent determinations of trace elemental concentrations in it by TXRF. The new polymer resin has been developed by the combination of monomers MEP and AMPS, and the polymer resin shows very good selective uranium uptake efficiency at 4M HNO₃ medium. The resin is very much selective at this condition and do not absorb other elements except Fe. The usage of SPE based methodology made the separation of uranium simple and less laborious. Moreover the polymer resin gel can be easily re-generated after absorbing uranium. So the amount of organic waste generation will be very low. The requirement of very small amount of sample in TXRF and generation of very small organic waste combined with ease of separation by just dipping the gel in solution makes this methodology very useful for the handling and analysis of plutonium based radioactive samples.



Chapter 6

Elemental speciation by TXRF

6.1. Introduction

Speciation is the determination of individual concentrations of the various forms/species of an element that together makes up the total concentration of that element [187]. Chemical speciation has both technological as well as environmental aspects. There are many technologically important materials having good catalytic, magnetic, conducting properties. These properties are very much dependent upon the oxidation states and thereby species of the elements present in those materials [188-191]. Determination of oxidation state of uranium is very much essential in nuclear technology as the specific form of uranium is required in fuel fabrication and disposal of nuclear waste. On the other hand chemical speciation in the environmental samples is also very much important. The nature of toxicity of the elements like arsenic, chromium, Cu, Sb etc is very much dependent upon their oxidation states and their species. As an example Cr (III) is a micronutrient which is very much necessary for proper functioning of living organism. However, Cr (VI) is considered to be carcinogenic and toxic [192-193]. Similarly inorganic arsenic has mainly two types of species i.e. As (III) and As (V). Both are toxic but As (III) is much more toxic compared to As (V) [194]. Certain amounts of selenium are extremely beneficial for human health but its beneficial effect is strongly dependent upon its chemical form and concentrations [195]. Thus we can see that speciation is very important step in chemical characterization of technological as well as environmental samples. So in this chapter we have done speciation studies in two types of samples. One is different mixed valent uranium oxides, which is technologically very important material used as nuclear fuel. Another is speciation of arsenic in water sample, which is environmentally very important one.

Uranium oxide (UO_2) has fluorite type structure and it is a very important technological material in nuclear industry [166, 196]. Depending upon the oxygen potentials, UO_2 can be converted into different types of mixed valent uranium oxides like U_4O_9 , U_3O_7 , and U_3O_8 etc [197]. These mixed valent uranium oxides may contain uranium having different combinations of mixed oxidation states. Now it is very important to determine the oxidation states of uranium in these types of mixed valent uranium oxides to understand the properties of these compounds. Knowledge about the properties of these compounds is necessary to use them for various applications like fuel production, spent fuel reprocessing, magnetic and electrical usage etc [44, 45 198, 199]. During course of oxidation, UO_2 finally gets converted into U_3O_8 which is a stable compound and exists mainly in three phases. At room temperature it exists as orthorhombic phase and at elevated temperature the compound exists in hexagonal and tetragonal phase [200-202]. U_3O_7 is another mixed valent oxide of uranium which has two different mixed oxidation states of uranium, similar like U_3O_8 . The oxidation states possible on the basis of charge balance in U_3O_8 and U_3O_7 can be represented as $\text{U}_2^{\text{VI}}\text{U}^{\text{IV}}\text{O}_8$ or $\text{U}^{\text{VI}}\text{U}_2^{\text{V}}\text{O}_8$ and $\text{U}_2^{\text{IV}}\text{U}^{\text{VI}}\text{O}_7$ or $\text{U}_2^{\text{V}}\text{U}^{\text{IV}}\text{O}_7$ respectively. If U (V) is present in these mixed valencies of uranium, these can have good catalytic and magnetic properties [203-205]. Although these types of mixed valent uranium oxides are well known to us, but still there are many conflicting reports about the oxidation states of uranium in them [206, 207]. Due to surface oxidation and disproportionation of U (V) into U (IV) and U (VI) in solutions, it is very difficult to determine oxidation states of uranium in these oxides. X-ray photo electron spectroscopy (XPS) technique is a well known method for the speciation studies. However for actinides, especially in case of uranium in mixed valent states this technique has limitation, because the chemical shift of the main U 4f lines are very small [208]. Ultra violet and visible photoelectron spectroscopy (UPS) is also used for the

determination of oxidation states, but this technique cannot distinguish between different oxidation states of uranium [209].

Synchrotron radiation (SR) based X-ray absorption near edge spectroscopy (XANES) is now days become very popular and reliable technique to provide the information of oxidation states of different elements. Normally during XANES measurements the sample amount required in milligram level, which is used in either pellet form (with boric acid as binder) or suspended in membrane supports. These types of sample preparation methodology is not desirable for the analysis of highly radiotoxic samples containing radioactive elements like Pu, Am etc as they will cause high radiation hazards risk and the radioactive waste generation will also be very high. Moreover due to the use of binder mixed with the sample, there will be loss of precious material. Additionally during such elaborate sample preparation; there is possibility of oxidation of those samples.

Total reflection X-ray fluorescence (TXRF) spectrometry now a day has become very potential analytical technique for the trace analysis of radioactive nuclear materials [38, 48]. Requirement of very small amount sample in the nanogram level and minimum sample preparations, multi-elemental analytical capability are main features which made this technique very much favorable for the characterization of radioactive samples [210]. Due to the very small sample amount required in this technique, the TXRF study of nuclear materials poses comparatively less radiation hazard to the operator and generates a small amount of radio-analytical waste. It is possible to carry out XANES measurements in TXRF geometry using a variable energy source and by measuring the fluorescence intensity as a function of energy below and above the absorption edge of the element of interest [97]. So this approach can drastically reduce the sample amount required for the XANES analysis, which is very advantageous for the

speciation studies of highly radioactive, toxic and precious samples. Moreover the sample preparation using TXRF-XANES can be very simple, where the sample can be studied as such after sticking few particles on TXRF sample supports without any processing like pelletization with boric acid or dispersion in hexane. If a very small amount of the sample gently rubbed on the surface of the quartz sample supports, it should be possible to directly use it for TXRF-XANES measurements for elemental speciation [161]. Due to the possibility of these superior features, we planned to use TXRF for such speciation of actinides and initiate our studies of speciation in mixed valent oxides of uranium. Recently there is a report on the determination of oxidation states of uranium in U_4O_9 and U_3O_8 , using the U-M₅ edge, where about 10 mg of the sample in pellet form was used for XANES measurement and it was concluded that uranium present as U (VI) and U (V) in U_3O_8 and in U_4O_9 , uranium present as U (V) and U (IV) forms [36]. For the speciation studies of these types of sample it is very important to avoid any chemical transformation during the sample preparation. The pellet preparation may change the oxidation state. Moreover the sample amount requirement in normal XANES is governed by the edge jump of one of the elements and cannot be reduced below this mass which is in milligram levels. This will produce lots of waste of such precious materials. Since TXRF-XANES measurements proposed by us need very minimum sample preparation, only gentle rubbing of few nanogram of the sample on TXRF support will be sufficient for speciation studies of actinides. Although there are some reports of speciation studies of arsenic in cucumber leaves, and speciation of copper and zinc in aerosol samples using TXRF-XANES technique, but till now this methodology has not been yet used to do speciation study of nuclear materials using this approach [62, 63]. So keeping this point in mind the speciation studies were carried out on two mixed valent uranium oxides e.g. U_3O_7 and U_3O_8 using UL₃ edge (17.16 keV). We choose UL₃

edge for our studies as U M edge experiments are not feasible in Indus 2 beamline, which we used for our studies.

Speciation studies using TXRF-XANES technique requires variable energy source, which only can be obtained from synchrotron radiation facility. But this facility is not always available. Moreover for the speciation studies of environmental samples it is very important to detect and analyze elements at ultra trace level, because the maximum permissible limit of different toxic elements in water and other environmental samples are at trace level only. For such samples, TXRF-XANES will not be sufficient. There are many literature reports where people have used chemical pre-concentration methodology for the speciation studies of toxic elements like arsenic, chromium in different environmental samples. This pre-concentration methodology can also be applied in combination with TXRF for the speciation studies of different elements present in the environment, to monitor and control their concentrations. This approach will be simple and can be done using simple TXRF instrumentation. So keeping these points in mind, chemical pre-concentration approach has been utilized in combination with TXRF for the speciation study of arsenic in different types of water samples.

Arsenic contamination in drinking water is a major concern for human health. Arsenic is the 20th most abundant element found on the earth crust. There are many anthropogenic activities which lead to the contamination of arsenic in water. As an example in semiconductor industry arsenic is used and it can be released in water. Moreover as arsenic is widely distributed in nature as rock samples, so there are many natural activities like erosion of rock samples containing arsenic can release arsenic in water [211, 212]. The contamination of arsenic in water sample is very severe in some parts of countries like India, Bangladesh, Hungary, China, Vietnam, Argentina, Taiwan, Japan etc. Prolonged intake of arsenic by human body can cause

many deceases of skin, nervous system, lever, lung etc. World Health Organization (WHO) and Environment Protection Agency (EPA) strictly recommended that the concentration of arsenic in drinking water should remain < 5 ng/mL [213, 214]. Arsenic can exist in the environment both organic as well as inorganic form. The extent of toxicity of arsenic in human body is very much dependent on its chemical form. The inorganic form of arsenic is much more toxic than organic form. Inorganic arsenic can remain in trivalent (As^{+3}) arsenate (H_3AsO_3) and pentavalent (As^{+5}) arsenite (H_2AsO_4^-) form. The trivalent form is more toxic than the pentavalent form [215]. So determination of arsenic at trace level and identifying its chemical form is necessary for environmental quality control. That's why speciation of arsenic in trace level is very important topic of research now days. Colorimetric method for the speciation of arsenic is reported in literature. However this method is not sensitive. Moreover this type of experiment involves the production of arsine (AsH_3) gas which is highly toxic in nature [216]. Some electrochemical methods also have been developed for the speciation of arsenic at ultra trace level. Acidic environment has to be maintained in those cases (pH: 1-2) [217, 218]. As most of the analytical techniques are not highly sensitive; so a pre-concentration step is generally required to enhance the sensitivity of the technique. Speciation study also sometime requires some types of separation methodology to separate a particular species in presence of other species. There are many types of separation and pre-concentration techniques available like liquid-liquid based extraction, precipitation, ion exchange chromatography (IEC), Gas chromatography (GC), High Performance Liquid Chromatography (HPLC) etc. There are many chromatographic techniques in combination with ICP or AES already reported in the literature for the speciation of arsenic in water samples. However chromatographic technique in combination with ICP-MS or ICP-AES requires rigorous sample preparation, for example a large column of eluent is needed to separate

the analyte in the IC column. Furthermore inert gases are needed to pressurize the eluent. Such requirements made sample analysis using these techniques very costly and complicated. Moreover the polyatomic species $^{40}\text{Ar}^{35}\text{Cl}^+$ interferes during the analysis of arsenic by this technique [219, 220]. Many solid phase extractions (SPE) based techniques have been utilized for the same purpose. X-ray fluorescence (XRF) technique can be used for the determination of arsenic. There are literature reports of the analysis of arsenic in drinking water of Bangladesh, using this technique by combining it with pre-concentration of arsenic in water samples. However the detection limit achieved using this methodology is not very low [221]. Total Reflection X-ray Fluorescence (TXRF) spectrometry; which is a variant of XRF can be used more efficiently for the speciation of arsenic in water samples due to its greater sensitivity; which is due to the following reasons:

1. X-rays falling on the sample at less than critical angle at sample supports. The penetration of the X-rays into the sample will be less and the background caused due to the scattering of the X-rays will be very low.
2. Both the incident as well as totally reflected X-rays are exciting the sample. The fluorescence intensity will also be doubled approximately.
3. Detector can be placed very close to the sample (about 2-3 mm) in 0-90 ° geometry.

Moreover this technique is very simple and fast [47, 56, 60, 91, 127]. Different researchers have used TXRF in combination with XANES (X-ray Absorption Near Edge) technique for the speciation of arsenic in cucumber xylem sap, using synchrotron excitation source. This technique can be used for speciation of arsenic down to concentration level of 30 ng/mL. It is not possible to do speciation, if arsenic is present below that concentration level even with SR source [63]. There are few reports where TXRF in combination with SPE has been used for the speciation of arsenic [222, 223, and 177]. There is a report where graphene oxide

nano sheet as solid phase adsorbent has been used for the speciation of arsenic by TXRF. The detection limit obtained by this method is the lowest one so far (0.064 ng/mL) using TXRF. However this technique requires very time consuming sample preparation steps [177]. Previously people have developed many types of membranes immobilized on the quartz; used as sample support in TXRF for the trace determination and speciation of uranium and chromium respectively [224, 225]. This membrane based methodology is very fast and simple, where quartz sample support immobilized with the membrane is simply dipped into the water sample from which the elements has to be pre-concentrate and analyzed. After some time it is taken out from the water sample; and directly used for TXRF measurement. In present study, we have utilized this membrane based pre-concentration methodology for the speciation of arsenic in water samples for the first time using TXRF. N methyl d glucamine (NMDG) which can absorb As (V) species very efficiently and it is highly selective in presence of complete ions like sulphate, phosphate etc. at some particular pH [226-228].

The most dominant species of As (V) in natural water is the H_2AsO_4^- . The As (III) has only one pK_a and existing at very high pH (9.1) value. Due to this reason As (III) in natural water mostly remains as uncharged species H_3AsO_3 [227]. NMDG contains quaternary ammonium group in normal pH and exhibits very high affinity towards monovalent species H_2AsO_4^- compared to sulphate or phosphate ions. In the literature, NMDG functionalized polymembrane application for the selective removal of As (V) from water sample is reported. We have utilized this concept for the speciation of arsenic in water samples using TXRF in the present work. Generally quartz is used as a sample support for the TXRF measurements. In the present work, TXRF sample supports has been grafted with NMDG as a thin membrane on its top surface and these quartz supports grafted with the membranes were directly dipped into the water sample that

we wanted to analyze. The As (V) species will be directly absorbed by the membrane and thus As (V) shall be pre-concentrated on the membrane surface of the quartz sample supports. This arsenic can be directly analyzed by TXRF. The total arsenic concentration was determined by oxidizing all As (III) species into As (V) species and the As (III) concentration could be obtained by simply subtracting the As (V) concentration from the total arsenic concentration. The detection limit obtained using this procedure is 0.05 ng/mL which is the lowest detection limit obtained for the speciation of arsenic using TXRF reported so far in the literature.

This type of speciation of arsenic in water samples using TXRF is also being reported for the first time. All the detailed procedure to calibrate and validate this method is discussed in this chapter. As we have used TXRF in combination with SPE based pre-concentration methodology; the analysis becomes very simple and straight forward and minimize the time for sample preparation. The developed methodology can be applied for the speciation studies of different types of water samples like drinking water, ground water, lake water, river water, tap water etc very efficiently.

In view of the advantages of TXRF for nuclear material characterization using minimum sample amount as well as to minimize radioactive waste, we have done studies on speciation studies of uranium in mixed valent uranium oxides using SR based TXRF-XANES technique. Also in view of applicability of arsenic speciation in different water samples using SPE based pre-concentration technique in combination with TXRF has been carried out.

6.2. Speciation of mixed valent uranium oxides by TXRF-XANES

6.2.1. Preparation of standards and samples

In this experiment mixed valent uranium oxide U_3O_7 and U_3O_8 were used as samples. The oxidation states of uranium were determined in these two mixed valent oxides. For the speciation studies standards of uranium oxides are also needed. Here UO_2 , $TiUO_3$ and UO_3 were used as standards having uranium in +4, +5 and +6 oxidation states respectively. Here U_3O_8 (alpha phase) was prepared by heating UO_2 in a furnace at 600°C temperature for 24 hours [229], and U_3O_7 (beta phase) was prepared by carefully heating UO_2 in air atmosphere at around 150°C for 24 hours [230]. For the preparation of UO_3 ; U_3O_8 was dissolved in HNO_3 and a solution of NH_3 was added to this solution. The precipitate $(NH_4)_2U_2O_7$ was filtered and heated in air atmosphere at about 300°C to obtain UO_3 . $TiUO_3$ was prepared by following the procedure reported in the literature [231].

6.2.2. TXRF-XANES specimen preparation and measurements

The sample preparation used for the TXRF-XANES measurement was very simple. A few tiny particles of the samples/standards were taken directly in powder form at centre of quartz sample supports using a small tip of a micropipette. A few tiny particles got stuck with the supports in this process. Finally the sample particles were gently rubbed at the supports with the help of micropipette. These support specimens were dabbed vertically to remove any loose particles on it. This type of sample preparation brings fresh surface of the sample on the supports and avoids any error due to surface oxidation for which uranium oxides are more prone to. These specimens were loaded one by one for TXRF-XANES measurements.

All the XANES measurements were carried out at UL_3 edge (17.16 keV) at the micro-focus X-ray fluorescence beamline (BL-16) of Indus-2 synchrotron facility.

6.2.3. Results and discussions

After ensuring the TXRF geometry is satisfied by using the sample specimens prepared for XANES measurements, TXRF XANES measurements of the mixed valent uranium oxides were done. Figure 6.1 shows the TXRF spectrum of one of those specimens for an acquisition time of 10 seconds. From the Figure 6.1 it can be seen that a few nanogram of the sample is giving very good fluorescence intensity in TXRF geometry for an acquisition time of 10 seconds only. The region of interest (ROI) for the U $L\alpha$ line for each spectrum was fixed and averaged to get the U $L\alpha$ ROI counts at each energy. The mass absorption co-efficient is proportional to (I_f/I_0) , where I_f is the fluorescent counts of the ROI selected and I_0 is the initial X-ray intensity. So (I_f/I_0) versus energy is plotted to generate the XANES spectrum. The raw XANES spectra thus obtained were normalized using ATHENA software programme. There is one literature report on the damping of white line of XANES spectra in TXRF mode while doing speciation of arsenic by Meirer et.al [232]. Their result shows that when arsenic amount is near or above 100 ng, these types of damping become very significant. However Tiwari et.al have reported that not only the sample amount but also particle size plays a very important role during such kind of absorption effect in TXRF geometry [233, 234]. It was observed that particle size above 1 μm , severely affects the intensity of emitted fluorescence intensity. For direct determination of U and Th in U, Th mixed oxide by TXRF, it is reported that the particles stucked on the quartz sample supports during such sample preparation were in the range between 200 – 500 nm [161]. We are using the same sample preparation methodology in this work and expect that particle size shall not create much absorption effect.

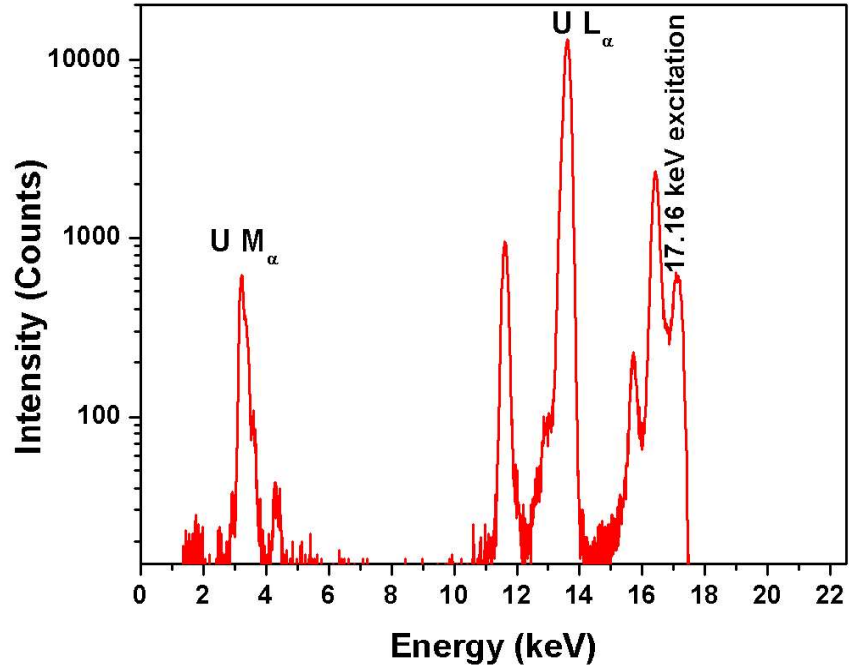


Figure 6.1: TXRF spectrum of an U_3O_8 specimen during TXRF XANES measurements

The normalized TXRF–XANES spectra of all the compounds e.g. UO_2 , $TiUO_3$, U_3O_8 and UO_3 are shown in Figure 6.2.

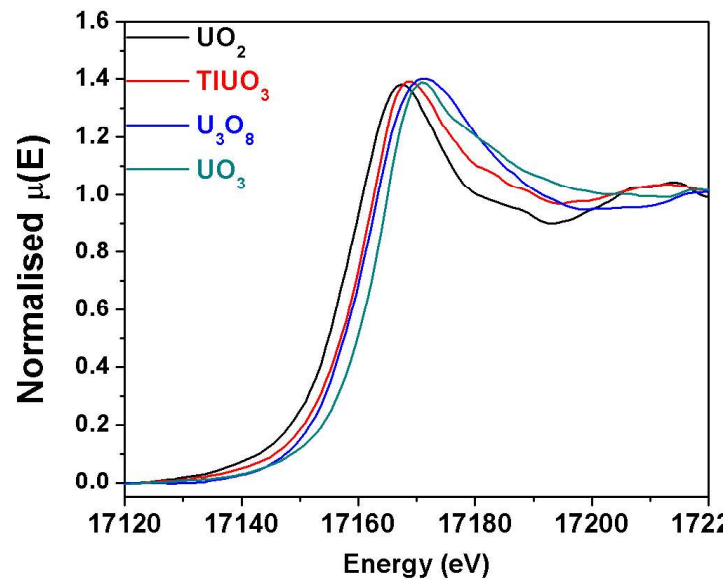


Figure 6.2: TXRF-XANES spectra of U_3O_8 along with standard compounds

From Figure 6.2 it can be seen that as the oxidation state of uranium increases from UO_2 to UO_3 , the absorption edge position of uranium is shifting towards higher energy side. The exact value of the absorption edges can be deduced from the maxima of the first derivative of the XANES spectrum, which is shown in Figure 6.3. It can be clearly seen that the edge position of U_3O_8 is situated in between the edge position of uranium in TiOU_3 [U (V)] and UO_3 [U (VI)], which gives us an initial idea that U_3O_8 is mixed oxide of U (V) and U (VI). The edge energy values of all these compounds of uranium oxides are shown in Table 6.1.

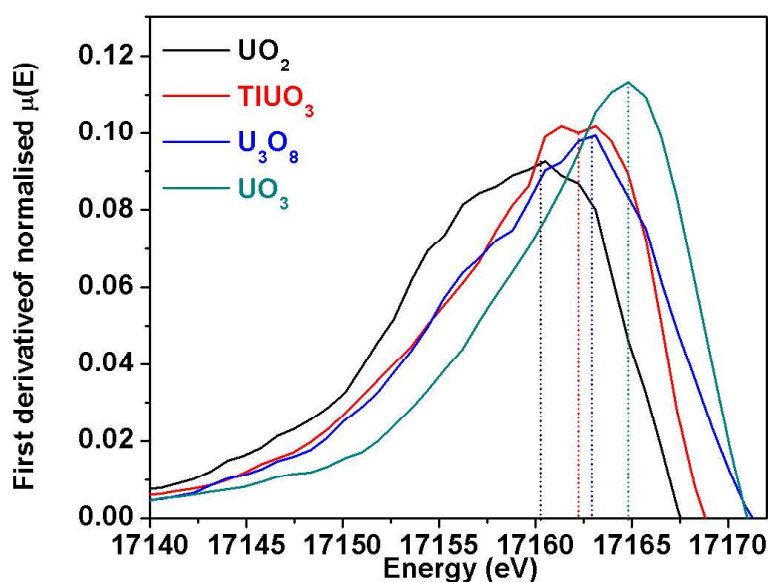


Figure 6.3: First derivative of the TXRF-XANES spectra of different uranium oxides showing shift in the edge position

Table 6.1: The edge energy values of different oxide compounds of uranium as obtained from the maxima of the second derivative of their TXRF-XANES spectra

Compound	Edge position (eV)
UO_2	17161
TiOU_3	17162
U_3O_8	17163
UO_3	17165

Now to determine the different percentages of oxidation states of U present in these types of mixed valent oxides, linear combination analysis of the XANES spectrum was done using a software ATHENA. During the fitting process of U_3O_8 , we have considered two probable combinations [either U (V) & U (VI) or U (IV) & U (VI)] of oxidation states of uranium present in it. Other combination [U (IV) & U (V)] will not satisfy the charge neutralization condition for U_3O_8 . The best linear fitting obtained using these two combinations are shown in Figure 6.4.

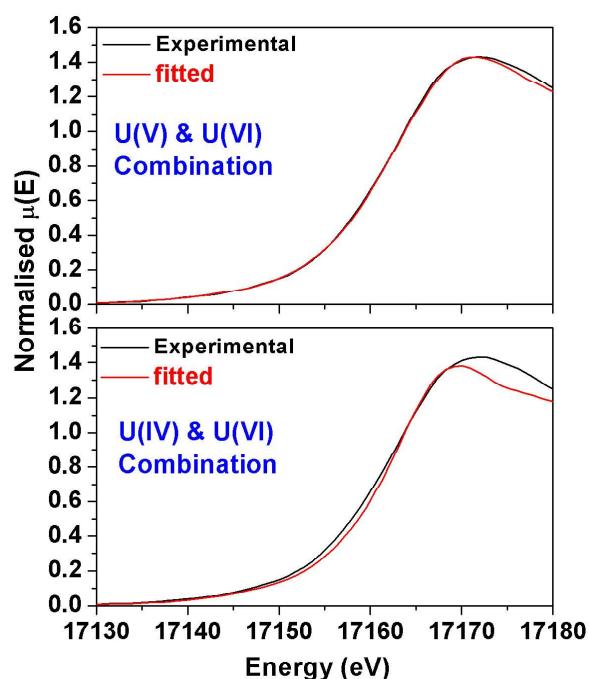


Figure 6.4: Linear combination fitting of TXRF-XANES spectra of U_3O_8 using two different oxidation state combinations: U (V) + U (VI) and U (IV) + U (VI)

From Figure 6.4 it is clear that fitting results obtained by using U (V) and U (VI) combination are much better than that of U (IV) and U (VI) combination. The percentage of U (V) and U (VI) in best fitting condition was 70% and 30% respectively. These values are very much in agreement with the theoretical value [U (V): 66% and U (VI): 34%] when we consider U_3O_8 is composed of U (V) and U (VI). These values are also in good agreement with the work reported by Kvashnina et al. who concluded the presence of U(V) and U(VI) in U_3O_8 [36]. These

authors have done XANES measurements at U M edge, as most properties of U compounds originate from the localized 5f states and can be probed using UM absorption edges directly. However it is very difficult to probe these edges due to several reasons like significant absorption of low energy U M by air molecules, the energy differences between several U M edges are very small. Moreover at present condition, the micro-focus beam line of Indus-2, RRCAT, Indore is not equipped for measuring low energy X-rays. Due to these reasons we have performed all of our XANES experiments at U-L₃ edge in TXRF geometry, and we have compared our results with literature reported experimental as well theoretical outcomes [36, 235].

Table 6.2 shows the percentage of U (V) and U (VI) species obtained in U₃O₈ after doing linear combination fit of TXRF XANES spectra using ATHENA. The quality of the fitting can be expressed by different parameters like χ^2 , reduced χ^2 and R-factors. These values are included in Table 6.2, which suggests good fitting of the TXRF-XANES spectra of U₃O₈ using the combination of U (V) and U (VI) compared to the other combination. Moreover the experimentally determined U (IV) and U (VI) percentage obtained [U (IV): 98%, U (VI): 2%] using the other combination is violating the charge neutrality restriction.

Table 6.2: The relative amounts of U (V) & U (VI) or U (IV) & U (VI) present in U₃O₈ from the linear combination fit of the TXRF-XANES spectra of U₃O₈

U ₃ O ₈					
Combinations	Percentage		R-factor	Chi-square	Reduced chi-square
U(V)-(VI)	U(V)	U(VI)	0.000245	0.0167	0.0003
	70±5	30			
U(IV)-(VI)	U(IV)	U(VI)	0.001	0.090	0.001
	98±4	2			

Similarly a linear combination fit for U_3O_7 was also carried out using two probable combinations i.e. U (IV) - U (VI), and U (IV) - U (V) using ATHENA software. The fitting results are shown in Figure 6.5. The best fitting result was obtained when the combination of U (IV) and U (VI) was considered. The weight fractions calculated from the fitting is shown in Table 6.3.

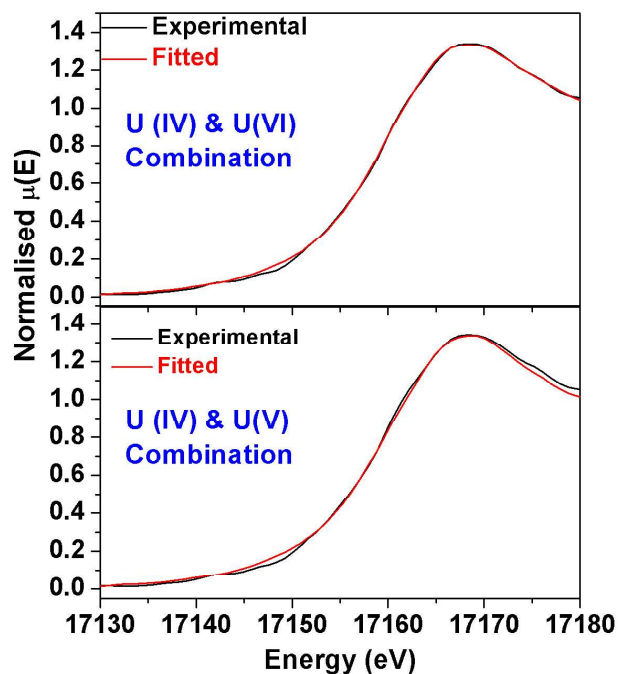


Figure 6.5: Linear combination fitting of TXRF-XANES spectra of U_3O_7 using two different oxidation state combinations: U (IV) +U (V) and U (IV) +U (VI)

Table 6.3: The relative amounts of U (IV) & U (VI) or U (IV) & U (V) present in U_3O_7 from the linear combination fit of the TXRF-XANES spectra of U_3O_8

U_3O_7					
Combinations	Percentage		R-factor	Chi-square	Reduced chi-square
U(IV)-(VI)	U(IV)	U(VI)	0.0001	0.007	0.0001
	70±2	30			
U(IV) -(V)	U(IV)	U(V)	0.0006	0.030	0.0004
	98±4	2			

From Table 6.3 it can be seen that considering the combinations of U (IV) and U (VI), the percentage obtained are 70% and 30% respectively which is very much close to the theoretically predicted value (66% and 34% respectively) using this combination. However when considering the other combination for U_3O_7 which is U (IV) and U (V), Table 6.3 shows that there is slight detritions in the fitting parameter compared to the other combination, but the most important fact that the experimental outcome of this combination [U(IV): 98% and U(V): 2%] do not satisfy the charge neutrality. In addition to that, the results are in agreement with the earlier reported literature data [229].

6.3. Speciation of arsenic at ultra traces level by TXRF using pre-concentration and separation

6.3.1. Experimental

6.3.1.1. Chemicals and instrument

N-methyl-D-glutamine (**NMDG**), (3-Glycidyloxypropyl) tri-methoxy-silane (98 % pure), N, N-dimethyl formamide (**DMF**), suprapure HNO_3 were purchased from sigma Aldrich. Milli-pore water, with a resistance of $18.2 M \Omega cm^{-1}$ was used for dilution and sample preparation purpose. Suprapure 30% H_2O_2 was purchased from Sigma Aldrich, and Lab grade (LR) concentrated H_2SO_4 were used as oxidizing agents. Lab grade ethanol was used. Chloro-auric (**HAuCl₄**) acid with gold concentration of 1mg/mL was purchased from MERCK. All the standard solution of As^{+5} and As^{+3} were prepared by dissolving sodium arsenate (**NaAsO₃**), sodium meta arsenite (**NaAsO₂**) respectively, in milli-Q water which were purchased from Sigma Aldrich. The pH of the solutions was adjusted by adding $0.1 mol L^{-1} HNO_3$ and $0.1 mol L^{-1} NH_3.H_2O$.

All the TXRF measurements were carried out using a low Z – high Z TXRF spectrometer in our laboratory. The instrument has two X-ray tubes (Rh and Cr). For the present study the Rh target X-ray tube was used. All the TXRF measurements were carried out for a live time of 1000s. Quartz sample supports having diameter of 30 mm and a thickness of 3 mm were used as a sample supports for the TXRF measurements. All the measurements were carried out for 1000s (live time). The TXRF spectra obtained were analyzed by IAEA QXAS package software programme name AXIL.

6.3.1.2. Immobilization of NMDG on quartz surface

The quartz sample support surface was first oxidized with Piranha solution, which is a 1:3 mixture of concentrated H_2SO_4 and 30% H_2O_2 . Piranha solution is a powerful oxidizer, which is prepared by slowly pouring H_2O_2 into concentrated H_2SO_4 in a 500 mL volume of quartz beaker. The addition of H_2O_2 into concentrated H_2SO_4 will generate lot of heat; so the addition should be done very slowly and carefully, shaking the beaker time to time and also giving its outer surface a contact with cold tap water. Once the mixture is stabilized it can be further heated to retain its reactivity. The quartz sample supports were dipped into the preheated piranha solution and kept for 30 minutes. The piranha solution will clean all the organic contaminants and oxidize the surface of the quartz sample supports. Piranha is a strong oxidizer and hydroxylate the quartz surface by increasing silanol group and Si-O⁻ species [237]. Later the sample supports were rinsed with milli-Q water and dipped into ethanol for half an hour so the quartz surface is fully covered with silanol group. After that the quartz sample supports were taken out from it; washed with milli-Q water and dried in ambient air atmosphere. The dried quartz sample supports were taken and 2 μL of (3-Glycidyloxypropyl) tri-methoxy-silane was pipette out and deposited on it followed by addition of 2 μL of 0.1 M HNO_3 and kept it in ambient air atmosphere for 30 minutes. In presence of the acidic condition; (3-

Glycidyloxypropyl) tri-methoxy-silane will be attached to the quartz surface. Now 4 μL of 1% NMDG dissolved in DMF is pipetted out and added to the quartz surface which is attached with (3-Glycidyloxypropyl) tri-methoxy-silane. Then the quartz sample supports were kept on a hot plate at 80° for 1 hour. The NMDG will be immobilized on the quartz surface by an in-situ ring opening reaction with (3-Glycidyloxypropyl) tri-methoxy-silane. All the procedure is described as a schematic in Figure 6.6. The picture of the quartz sample supports after immobilization of NMDG on it is shown in Figure 6.7. From this figure it can be seen that a very thin layer of membrane is formed on the centre of the quartz sample supports which act as a solid phase extractant for the speciation studies of arsenic.

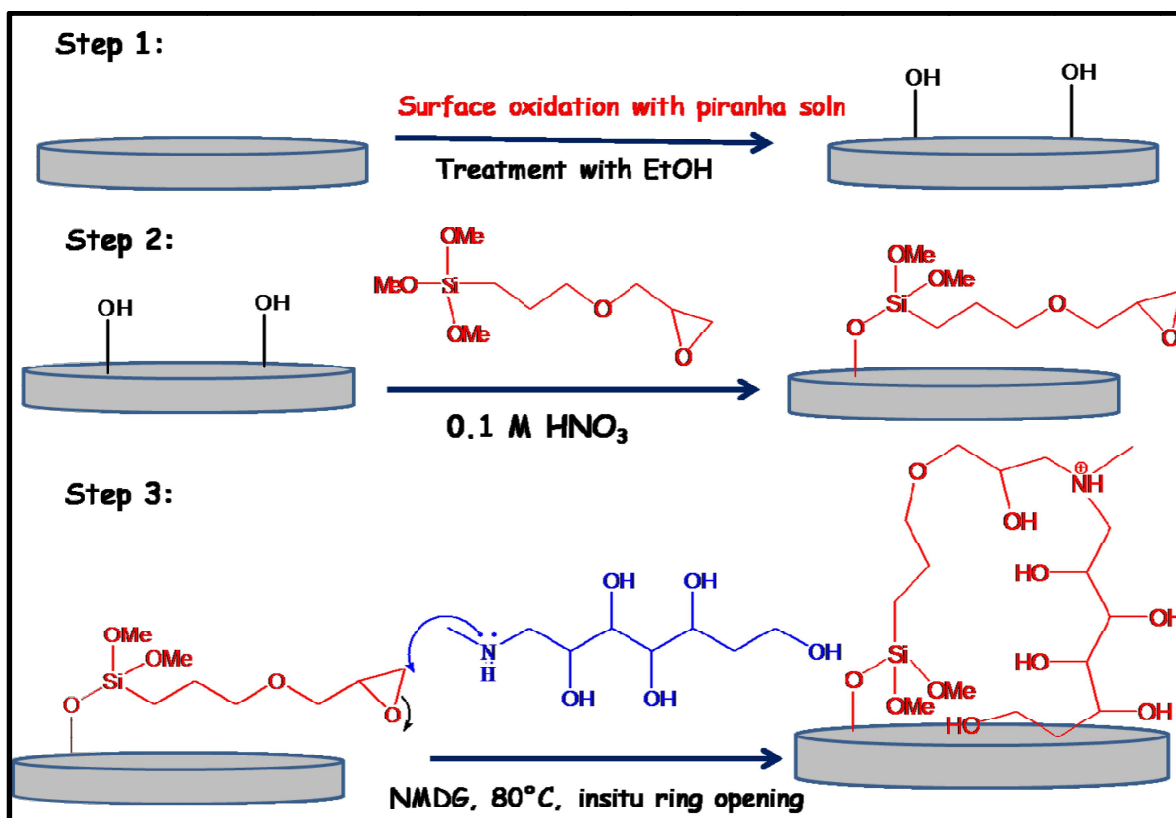


Figure 6.6: Schematic representation of immobilization of NMDG on quartz sample supports



Figure 6.7: Quartz sample supports after immobilization of NMDG

6.3.1.3. Loading Au-Np's as internal standard

During TXRF measurements an internal standard is generally used and elemental concentrations are determined with respect to it. In this study we have used gold as an internal standard. In literature it is reported NMDG is used for the reduction and stabilization of noble metal NPs like Au, Ag, Rh, and Ru [238]. We have used similar procedure to load Au NPs into the thin membrane which was formed on the quartz sample support surface. The quartz sample supports immobilized with NMDG is dipped into a beaker containing 50 mL of HAuCl_4 having Au concentration of 50 ng/mL for 2 hours. So the HAuCl_4 will be reduced by the hydroxyl group attached with NMDG and a very small fixed amount of Au will be loaded with the membrane in form of NPs, which will be used as an internal standard during analysis of arsenic. After that the Au-loaded sample supports were taken out from the solution and rinsed with milli-Q water for several times. The whole procedure of loading Au NP into the surface of the membrane is shown as a schematic in Figure 6.8.

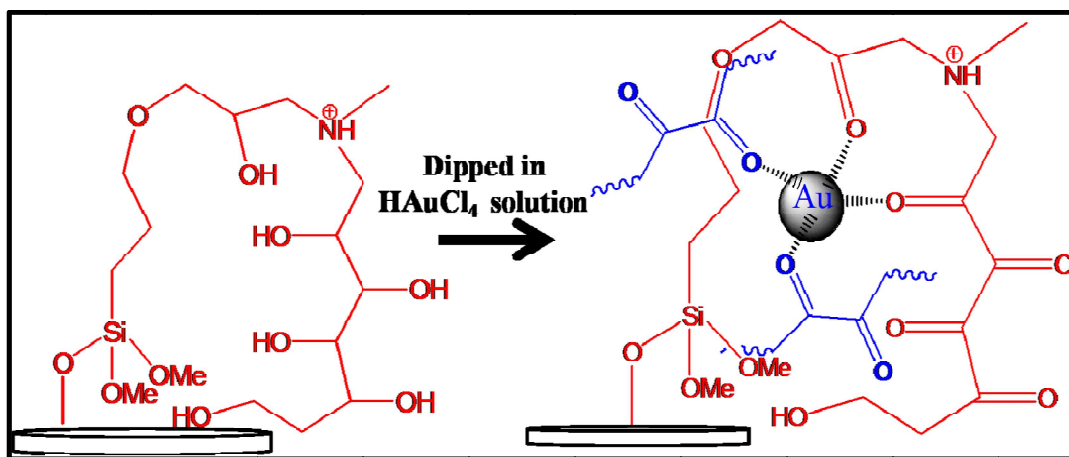


Figure 6.8: Loading of Au NPs on the surface of the membrane immobilized with quartz sample supports

The formation of Au nano-particles (Au NPs) was confirmed by taking the absorption spectra of the Au-loaded NMDG membrane grafted on quartz sample supports by using diffusive reflectance spectroscopy having light source (AvaLight-DH-S-BAL) and spectrometer (USB4000-UV-VIS-ES, Ocean optics). As shown in Figure 6.9 the surface plasmon resonance was observed at 500-600 nm which confirms that the Au loaded on the NMDG membrane is in the form of nano-particles.

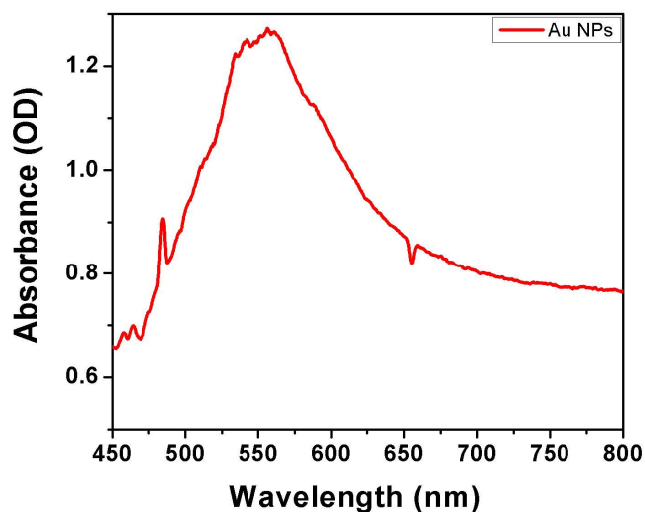


Figure 6.9: Absorption spectra of the Au-loaded NMDG membrane showing the surface Plasmon resonance around 500-600 nm due to the formation of Au-Nps

Figure 6.10 shows the TXRF spectra of the quartz sample support loaded with Au Nps after following the above procedure. It shows clear peaks of both Au L α and Au L β . The Si K α peak in the spectrum is coming mainly from the Si present in (3-Glycidyloxypropyl) trimethoxy-silane. If we fix the volume and concentration of Au solution; a fixed amount of Au will be loaded inside the membrane as NPs. So the fixed amount of loaded Au NPs can be used as an internal standard. In order to neutralize the area and geometry of the membrane deposited, in all analysis we have used the ratio of As K α / Au L α . This ratio was plotted against concentrations to obtain the calibration curve. Similarly this ratio is plotted against all the parameters with respect to which the absorption conditions should be optimized.

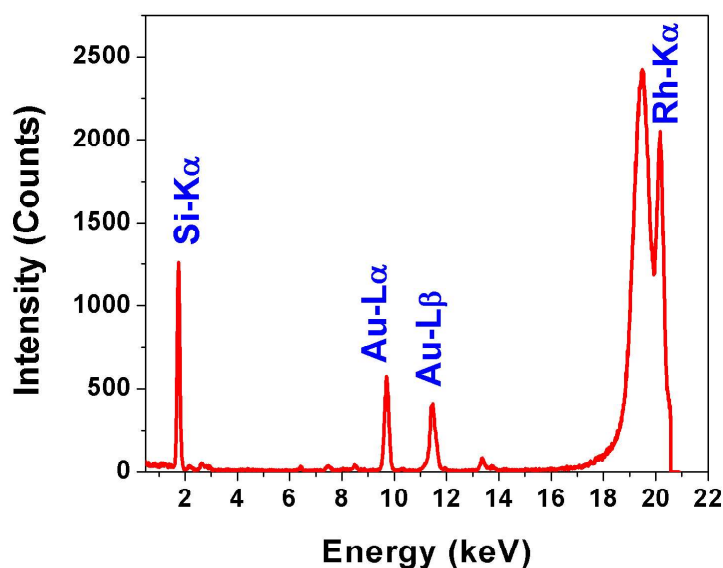


Figure 6.10: TXRF spectra of the quartz sample support loaded with Au NPs

6.3.1.4. Speciation studies

6.3.1.4.1. Determination of As (V) species concentrations

After immobilization of NMDG on the sample supports, they were simply dipped in solutions of 50 mL of volume containing known concentrations of arsenic species or in real samples for overnight in a beaker. The pH of the solution was maintained to 7 by using 0.05 mole L⁻¹ NH₃.H₂O and 0.1 M HNO₃ solution. The As (V) species in that condition will be

absorbed by the NMDG membrane due to electrostatic interaction as shown in Figure 6.11. As (III) species if present in the water sample will remain as neutral species in that pH condition and will not be absorbed by the NMDG membrane. The sample supports were taken out from the solution and rinsed with milli-Q water for several times and dried in ambient air atmosphere. These sample supports were loaded into the TXRF spectrometer and measurements were carried out for a live time of 1000s for each one. A blank sample was also prepared in similar way, where instead of standard solution; 50 mL of milli-Q water was used.

6.3.1.4.2. Determination of total arsenic concentration

The total arsenic concentration was determined in a similar procedure as described above but after oxidation of all the As (III) species into As (V) using 30 % H_2O_2 [239]. The oxidation procedure is carried out as follows: volume of 50 mL sample containing As (III) species or real sample was taken in a beaker and 200 μL of 30% H_2O_2 was added in it and kept for half an hour. After this the pre-concentration steps were carried out in the same manner as described above. The arsenic concentration in this solution determined by TXRF shall give total arsenic concentration. The As (III) concentration could be determined from the difference between total concentration and concentration of As (V) species determined above.

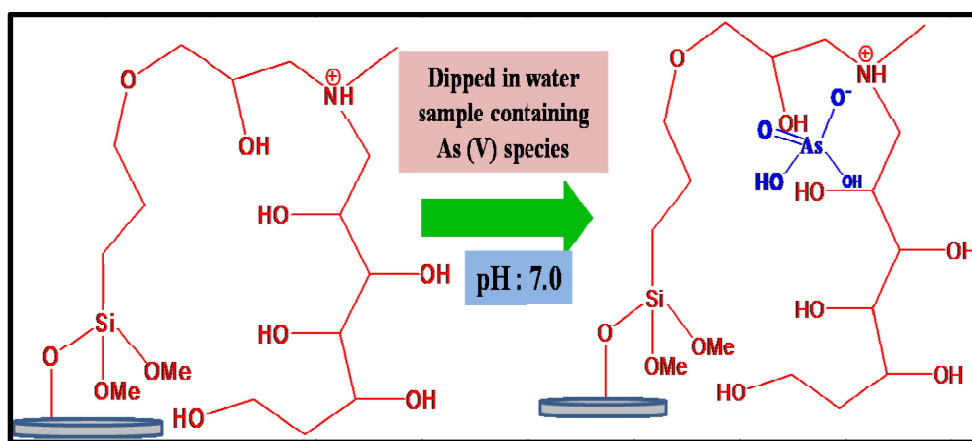


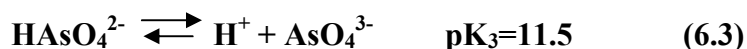
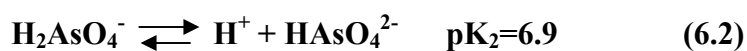
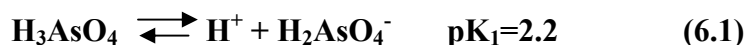
Figure 6.11: Pre-concentration procedure for As (V) species using NMDG membrane immobilized on the quartz sample support

6.3.1.4.3. Speciation of real water samples

Some real water samples like tap water, RO-water, ground water samples were taken and speciation studies were performed by using the same methodology as described above before and after spiking with certain known concentrations of arsenic of different species.

6.3.2. Results and discussions

All the pK_a values of As (V) are shown in the equation bellow.



From these equations it can be understood that in aqueous medium As^{+5} ions can remain in different charged species H_2AsO_4^- , HAsO_4^{2-} or AsO_4^{3-} . The type of species present depends upon the pH of the solution. However As (III) has only one pK_a and that is also at very high pH (9.1) value. So As (III) in natural water mostly remains as uncharged species H_3AsO_3 . As already mentioned that due to the presence of quaternary ammonium group in NMDG, it has very high affinity towards monovalent species H_2AsO_4^- compared to sulphate or phosphate ions. So pH of the medium is a very important parameter on which the absorption efficiency of the sorbent is very much dependent. There are also many other parameters like sample volume, sorption time, NMDG amount etc. that can affect the sorption efficiency.

In order to optimize separation and pre-concentration conditions for speciation of arsenic in water samples, the effect of pH, sample volume on the quantitative recoveries of the analyte ions were examined in detail. All parameters that affected the sorption process on NMDG membrane were optimized independently and in all cases three replicates were carried out. In all cases the optimization was performed using a fixed volume of (3-Glycidyloxypropyl) tri-

methoxy-silane, and NMDG which is 2 and 4 μL respectively and the sample supports immobilized with NMDG membrane were dipped in As (V) solution for overnight. In all cases recovery was determined using TXRF technique in combination with SPE method.

6.3.2.1. Effect of pH of the water samples:

The sorption efficiency of the NMDG membrane immobilized on quartz sample supports was determined at various pH conditions ranging from 1-10. After dipping the NMDG immobilized quartz sample supports in different synthetic solutions of As (V) having concentration of 50 ng/mL in each and pH ranging from 1-10 for overnight, the solutions were analyzed by TXRF.

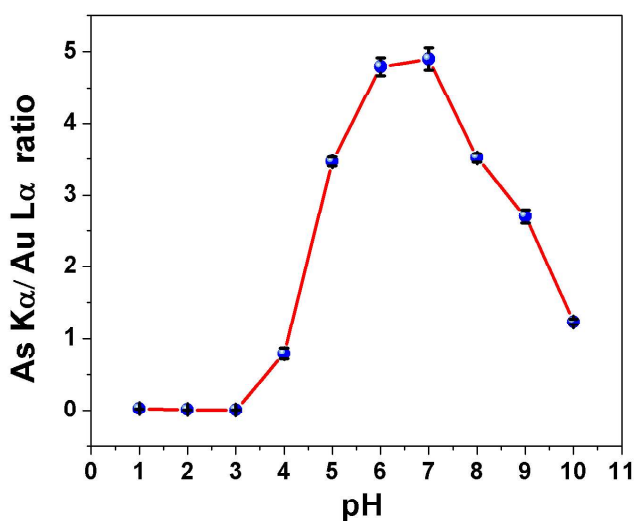


Figure 6.12: As (V) absorption efficiency of the membrane a function of pH of the aqueous medium

Figure 6.12 shows a plot of As (V) sorption efficiency of the membrane as a function of pH of the aqueous medium. It can be seen from the figure that at lower pH (1-3) values, the membrane does not absorb any As (V) as most of the As (V) species remain in un-dissociated form. After that as the pH increases the concentration of H_2AsO_4^- species increases and the membrane absorbs more As (V) species. At pH value 7, the membrane has highest As (V) uptake efficiency and after that it decreases. This observation can be explained by two reasons:

- 1) After pH 7, the singly charged As (V) species H_2AsO_4^- further dissociates into doubly charged HAsO_4^{2-} species which will not be absorbed by the NMDG membrane
- 2) Above pH 7, the ternary amine group gets de protonated and it will remain in free base form.

This observation is similar to that reported in the literature [227]. So in the range of pH 6-7 as we can see that the sorption efficiency of the membrane is maximum. The pH of most of the natural water samples generally remain in that pH range only. This condition is favorable as most of the water samples remain at that pH range, thus a lot of time can be saved.

6.3.2.2. Effect of sample volume

Taking into account for the low concentration of arsenic in water samples and to improve the detection limit, the effect of sample volume on As (V) absorption was investigated. A series of sample solutions having volume in the range of 10-400 mL with 50 ng/mL of As (V) concentration were taken in beakers and the sample supports with immobilized membrane were dipped in them for overnight and analyzed by TXRF. The result is shown in Figure 6.13.

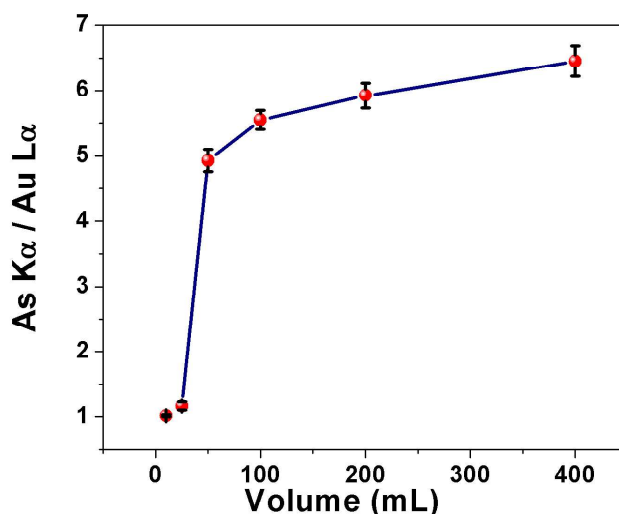


Figure 6.13: Effect of sample volume on As (V) absorption by NMDG membrane immobilized on quartz sample supports

From this figure it can be seen that as the sample volume is increasing the As $K\alpha$ /Au $L\alpha$ ratio increases. It can be also seen that increasing the sample volume from 25 mL to 50 mL results in rapid jump in As $K\alpha$ /Au $L\alpha$ ratio and after that with increasing sample volume this ratio increases very slowly. For practical purpose 50 mL of the sample volume was used for the studies.

6.3.2.3. Determination of pre-concentration factors

Figure 6.14 compares the TXRF spectra of a 20 ng/mL of arsenic solution before and after pre-concentration using SPE based methodology.

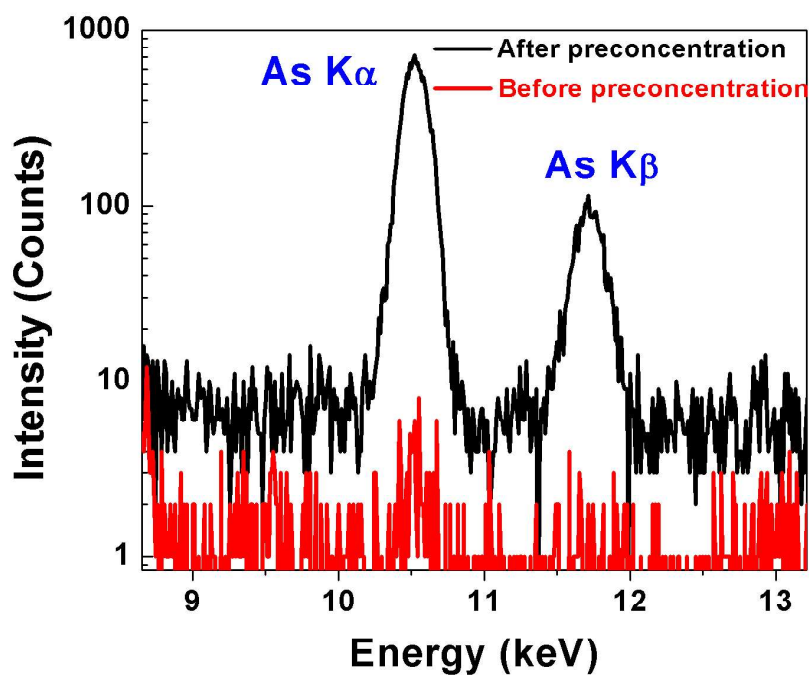


Figure 6.14: TXRF spectra of As (V) solution having concentration of 20 ng/mL before and after pre-concentration using SPE based methodology

It can be seen from the figure that before pre-concentration, it is almost impossible to detect As $K\alpha$ peak, while after pre-concentration the As $K\alpha$ as well as As $K\beta$ peaks are clearly visible with appreciable intensity. This indicates that a great degree of sensitivity can be achieved using the SPE based pre-concentration method in combination with TXRF technique

with a detection limit of 0.05 ng/mL, which is the lowest detection limit achieved for the analysis of arsenic using TXRF so far. The detection limits are also compared and shown in Table 6.4. It can be seen from the table that after pre-concentration using the above methodology, the detection limit could be improved by a huge factor of 140. It is very much clear that the SPE based pre-concentration method in combination with TXRF is very much suitable for the analysis as well as speciation of arsenic in different types of water samples. Moreover this methodology does not require any complicated sample preparation steps, making the experimental procedure easier and convenient for onsite analysis of arsenic.

Table 6.4: Comparison of detection limit of arsenic before and after pre-concentration by using the SPE methodology in combination with TXRF

DL of As before pre-concentration (ng/mL)	DL of As after pre-concentration (ng/mL)	Pre-concentration factor
7	0.05	140

6.3.2.4. Calibration and validation of the method

Under optimal pre-concentration conditions a calibration curve was obtained by preparing a series of reference samples containing different concentrations of As (V) species according to the recommended procedure. A linear calibration plot was obtained by plotting As $K\alpha$ / Au $L\alpha$ ratio with respect to the concentration of As (V) across the concentration range of 1-50 ng/mL with a correlation coefficient of 0.9981. This calibration plot is shown in Figure 6.15. The equation obtained from the calibration plot is used to analyze unknown concentrations in various water samples. In order to validate this methodology further, sample containing different amounts of As (III) and As (V) ions were prepared according to the recommended procedure. As mentioned earlier 100 μ L of 30% H_2O_2 was added as an oxidizing agent to oxidize all the As (III) ions into As (V) to determine the total arsenic concentration and As (III) concentration was obtained by subtracting determined As (V) concentration from the total arsenic concentration.

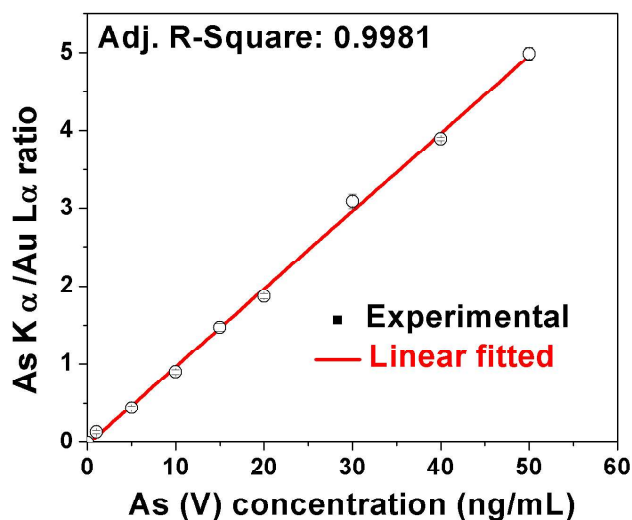


Figure 6.15: Calibration curve obtained using the SPE based pre-concentration method in combination with TXRF across the As (V) concentration range of 1- 50 ng/mL

The validation result is shown in Table 6.5. It can be seen from the table that the developed methodology can be very successfully used for the speciation of arsenic in water samples at very low concentration levels with an average RSD of 6.3% and deviation of 3.5%. Figure 6.16 shows AXIL fitted TXRF spectra of a water sample containing 20 ng/mL of arsenic along with fixed amount of Au as internal standard.

Table 6.5: Determination of the total arsenic content in a simulated samples containing As (III) and As (V) (sample volume 50 mL, n = 3)

Added arsenic Conc. (ng/mL) (A)		TXRF determined Arsenic Conc. (ng/mL) (B)		(B/A)	
As (III)	As (V)	As (III)	As (V)	As (III)	As (V)
-	25	-	26 ± 2	-	1.04
1.5	1.5	1.5 ± 0.1	1.5 ± 0.1	1	1
5	2	4.8 ± 0.5	2.1 ± 0.1	0.96	1.05
10	20	10.8 ± 0.4	19.4 ± 0.6	1.08	0.97
25	-	26 ± 2	-	1.04	-

For As (III): Average RSD = 7.1%, Average Deviation=4%
For As (V): Average RSD = 5.6%, Average Deviation=3%

Conc.: Concentration, As: Arsenic

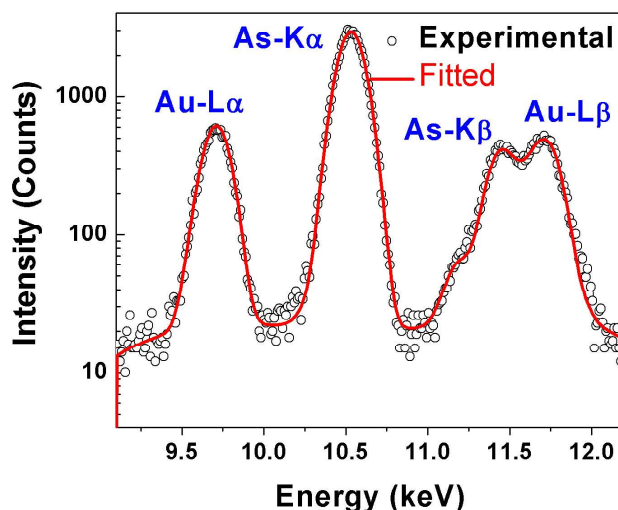


Figure 6.16: AXIL fitted TXRF spectra of a water sample containing 20 ng/mL of arsenic along with fixed amount of Au as internal standard

6.3.2.5. Speciation of real water samples

Now the developed methodology was applied for the analysis of two types of water samples e.g. tap water and ground water. Some known concentration of both As (III) and As (V) were spiked in these samples and analysis has been done by following the same methodology. The results are shown in Table 6.6.

Table 6.6: Speciation of As (III), As (V) in natural water samples (mean \pm standard deviation, $n = 3$, and sample volume 50 mL)

Sample	Added arsenic Conc. (ng/mL)		TXRF determined Arsenic Conc. (ng/mL)		(B/A)	
	(A)		(B)		As (III)	As (V)
	As (III)	As (V)	As (III)	As (V)		
Ground-water	-	-	< DL	< DL	-	-
	4	4	4.0 ± 0.3	4.0 ± 0.1	1	1
	5	10	5.6 ± 0.2	11.2 ± 0.2	1.12	1.12
	20	20	19 ± 3	19 ± 1	0.95	0.95
Tap water	-	-	< DL	< DL	-	-
	4	4	3.9 ± 0.3	3.9 ± 0.1	0.98	0.98
	5	10	4.9 ± 0.2	9.8 ± 0.5	0.98	0.98
	20	20	20 ± 3	18.6 ± 0.6	1.00	0.93
For As (III): Avg RSD = 9%, Avg Dev=3.6% For As (V): Avg RSD = 3.4%, Avg Dev= 4.8%						

Avg.: Average, Conc.: Concentration, Dev: Deviation, As: Arsenic

From the table it can be seen that the analytical result obtained is very much satisfactory with an average RSD (n=3) and deviation of 5.5% and 3.5 % respectively. This confirms the applicability of the developed methodology for the speciation of arsenic in different types of real water samples

6.4.Conclusions

The present chapter describes the applicability of TXRF for the speciation of nuclear and environmental samples. TXRF-XANES technique has been successfully applied in this work to determine the oxidation states of uranium in two mixed valent uranium oxides U_3O_7 and U_3O_8 . Here U L_3 edge has been probed for the XANES measurements. The study reveals that U_3O_8 contain uranium having two different species e.g. U (V) and U (VI) having relative amount of 70% and 30% respectively. This result is very much in agreement with the literature reported theoretical results as well as experimental results using U M edge. Similarly for U_3O_7 , uranium was found to be in mixed valent states of U (IV) and U (VI) (70% and 30 % respectively). The study reveals that TXRF-XANES is a reliable technique which can give similar results as obtained using XANES spectroscopy with an added advantage for the analysis of highly radioactive materials that it requires only nano-gram amount of samples with almost no sample preparation. These features are well suited for other materials also especially surface reactive materials as the samples can be probed fast without much sample preparation.

However recently there was a literature report saying that U_3O_7 is combination of U (IV) and U (V) [236]. Thus our results using TXRF-XANES are matching with the most of the literature reported data and theoretical prediction on the oxidation state of uranium in its mixed valent oxidation. The above studies indicate that TXRF-XANES can be successfully applied for

the speciation studies of mixed valent compounds in a simple manner without almost any consumption of sample.

A simple, sensitive and novel TXRF based methodology using SPE based pre-concentration has been developed for the speciation of arsenic at ultra trace level in different types of water samples. The method is based on the combination of solid phase extraction with TXRF. NMDG grafted on quartz TXRF support was used as a solid absorbent. Excellent detection limit along with satisfactory result of arsenic speciation was obtained in wide concentration range of 1-50 ng/mL. The detection limit of arsenic obtained using this methodology is lowest compared to any other TXRF based methodology, with an added advantage of very simple and cost-effective pre-concentration procedure. Some spiked real water samples were also analyzed using this methodology which gave excellent agreement between the expected and TXRF determined results.

So TXRF method has been successfully applied for the speciation both nuclear fuel samples, which are technologically very important materials as well as environmental samples like water samples. TXRF-XANES technique can be used successfully for the speciation studies of both nuclear as well as environmental samples with minimal sample preparation which is a very important advantage for the analysis of highly radioactive samples. However when the concentration of any species is very very low, and synchrotron based facility is not available then preconcentration method is required, which is also successfully carried out during the speciation of arsenic in water samples by using lab based TXRF.

Chapter 7

Summary and future scopes

7.1. Introduction

The present thesis describes the trace level elemental characterization of some technologically important materials and environmental samples using Total Reflection X-ray Fluorescence (TXRF) spectrometry in combination with better sample preparation as well as sample introduction approach. The thesis is divided in total seven chapters including this one. In this chapter the total summary of the work and future scopes possible by extending some of the work carried out in this thesis are being presented.

7.2. Summary of the thesis

Chapter one is basically an introductory chapter, where different technologically important materials are described in detail and their possible impacts on the progress of human civilization is also emphasized. There can be different types of technologically important materials used in different industry. The main emphasis in this thesis is on the nuclear industry, where different mixed oxides fuels of uranium, thorium and plutonium are being used as nuclear fuel which is the heart of the reactor and important technological material. This chapter describes how the presence of trace impurities in the fuel at unspecified levels is detrimental for the operation of the reactors. There is very close relationship between technological advancement and the environment. There can be different outcomes of such technological growth which can pollute the environment. There are several trace elemental analytical techniques that can be used for the characterization of nuclear fuel as well as environmental samples. TXRF technique has emerged out to be a very promising technique for such purposes due to several advantages like low detection limits, multi-elemental analytical capability, very less consumption of sample (ng level), cost-effective, fast etc. So this technique can be very efficiently used for the

characterization of both nuclear fuel and environmental samples where minimum amount of sample handling is desirable.

Second chapter is based on the theory and instrumentation of TXRF technique. The basics of this technique are described in detail in this chapter. Generally lab based X-ray sources have been used as an excitation source in TXRF technique. Synchrotron radiation (SR) as an excitation source can improve the analytical parameter drastically. The basics of the SR are briefly described in this chapter. TXRF can be used in combination with XANES (X-ray Absorption Near Edge) spectroscopy for the chemical speciation of different nuclear fuel as well as environmental samples at trace level with minimum sample preparation. The basic theory behind this technique is also described here. Moreover all the instrumental techniques used in this thesis have been described in detail.

Chapter 3 is based on the determination of low Z elements in nuclear fuel as well as water samples by TXRF. The maximum intake of different trace elements like F, Na, Mg, Al, K etc are specific and beyond this limit they can cause adverse effects on human health. Similarly presence of these low Z elements in nuclear fuel beyond some specific limit can affect the reactor safety. However determination of these low Z elements has always been a challenging task. We have used a low Z - high Z TXRF spectrometer for this purpose. Before analyzing the samples we have assess the analytical capability of this instrument and also compared the results obtained with that obtained using SR excitation source at the XRF beam line of ELETTRA, Synchrotron Light Source Trieste, Italy. It was concluded from the study that use of synchrotron radiation can improve the detection limit significantly especially for elements $Z \leq 13$. Moreover it was understood that use of low energy excitation sources like Mo-L, W-L as lab based excitation source in combination with vacuum chamber can improve the detection limit of low Z

elements. It was also observed from this study that there can be a possibility of inhomogeneous distribution of different elements on the sample supports where sample is being deposited. This can lead to erroneous results, so it is better to deposit very small droplet of the sample on the centre of the TXRF sample supports. This will ensure that all the elemental X-ray lines reach the detector equally. After assessing the analytical capability, the low Z - high Z TXRF spectrometer was utilized to determine trace impurities in uranium samples after complete separation of the uranium. It was observed that total separation of uranium from the sample matrix reduces the background counts and avoids interference of U M escape peaks with Al K α to obtain reliable results for low Z elements especially for Al. The TXRF determined results were found to have an average precision of 8 % (1σ , n=3) and the average deviation of the TXRF determined values from the certified concentrations of low Z elements was 7.3 %.

Similarly this low Z high Z TXRF spectrometer has been used to determine fluorine concentration in high purity water samples. Fluorine determination by TXRF has always been a difficult task. During TXRF sample preparation acidic internal standards are generally used and in presence of them, fluorine get lost as volatile HF from the sample during the drying step of the sample droplet on TXRF sample supports. So to avoid this problem, fluoride sample was very carefully deposited directly on the centre of Si-wafer sample support. It was concluded from the study that the use of Si-wafer as TXRF sample support is beneficial for the determination of fluorine at lower concentration level. This approach can be used for the determination of fluorine down to 100 ng/mL concentration level with RSD value of 5.1 % ($\sigma =1$, n=3) and the results deviated from the expected values by 4.1% on average . This methodology has been extended for the determination of fluorine in RO (Reverse Osmosis) water samples.

TXRF method is very useful for the analysis of highly radiotoxic elements like Pu, Am etc as very small amount of sample (nano gram level) is required for it and the involved radiation dose to the operator and the radioactive waste generation is very small. In chapter 4, TXRF has been utilized first time for the trace elemental determination in plutonium samples, after separating most of the plutonium from the sample matrix. It was concluded from the study that after separation of most of the plutonium from the sample matrix and depositing very small volume of the sample (2 μL) of the resultant solution, the TXRF sample specimen can be handled outside of the glove box with proper precaution. So this methodology avoids the complicated situation of carrying out TXRF measurements by keeping the instrument inside the glove box. The small amount of sample needed generates very small amount of radioactive waste. The TXRF determined results are in very good agreement with the expected values with an average RSD and deviation of 4.5% and 5.9% respectively.

In chapter 4, description of liquid-liquid based extraction methodology has been given for the separation of plutonium from the sample matrix. However this separation method is laborious and generates lots of organic waste. So in chapter 5 a better separation method has been proposed using a newly developed Bis-MEP—AMPS based solid polymer resin phase absorbent. This polymer resin gel was synthesized and characterized and utilized for the TXRF trace elemental determinations in uranium samples after separation of the uranium from the sample matrix using it. The average deviation of TXRF determined values with certified values and RSD obtained for the analysis of CRM (IV) are 9.2% and 7.6% (1σ) respectively (excluding Fe). As the resin gel after the experiment can be regenerated and used for fresh experiments, the organic waste generation will be minimum. Requirement of very small amount of sample in TXRF and generation of very small organic waste combined with ease of separation by just dipping the gel

in solution makes this methodology very useful for the handling and analysis of plutonium based radioactive samples.

Chapter 6 deals with the use of TXRF for the speciation studies. A TXRF method has been developed for the speciation studies of mixed valent uranium oxides as well as arsenic in water samples. TXRF combined with XANES was used for the speciation studies of different mixed valent uranium oxides e.g. U_3O_8 and U_3O_7 . This methodology avoids the complicated sample preparation for XANES measurements. A small amount of the sample (few ng) is taken on a small pipette tip and spread uniformly on the centre of quartz sample supports. Later the support is dabbed on a clean surface from its edges so that any loose particle not sticking on the support comes out. The small amount of sample stuck on the support is sufficient to carry out XANES measurement in TXRF geometry. The requirement of very small sample amount and very simple sample preparation made this technique very useful for the analysis of radioactive, precious, forensic and environmental samples where analyte amount available and desirable is very small. The study concluded that U_3O_8 contains uranium in U (V) and U (VI) states with relative amounts of 70 and 30 % respectively. These values are in agreement with the theoretical values of 66 and 34% respectively and the earlier literature reported XANES data using UM edge measurements. Similarly for U_3O_7 , uranium was found to be in mixed valent states of U (IV) and U (VI) (70% and 30 % respectively).

A simple, sensitive and novel TXRF based methodology has been developed for the speciation of arsenic at ultra trace level in different types of water samples. The method is based on the combination of solid phase extraction with TXRF. NMDG is used as a solid absorbent which is grafted on quartz supports generally used as sample carriers for TXRF measurements. This membrane grafted quartz sample support was simply dipped into the As (V) solution. This

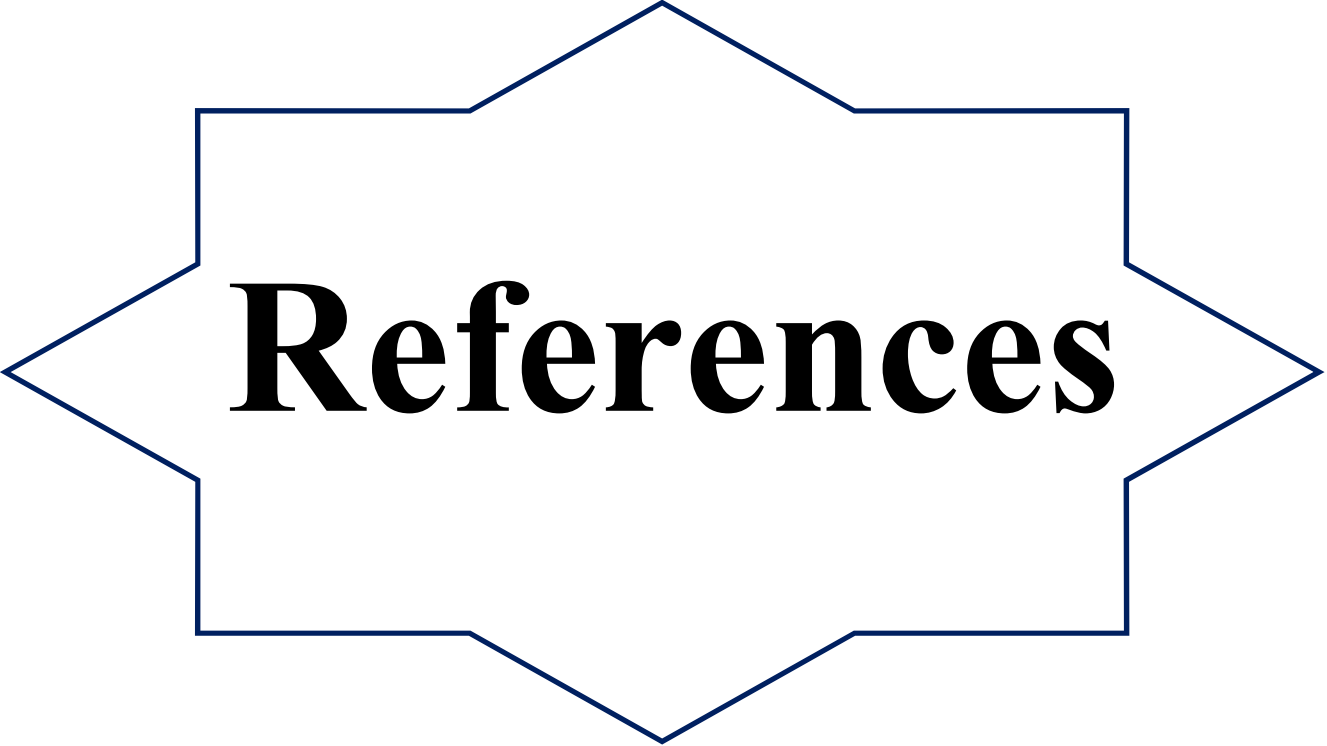
membrane is very much selective to the arsenate species [As (V)] and the interaction is mainly electrostatic. It was observed that at pH 6-7 this membrane has the highest As (V) uptake capacity. A calibration curve was constructed using this methodology and the unknown As (V) concentrations could be determined at sub ppb level using the calibration plot. The detection limit obtained using this methodology was 0.05 ng/mL which is the lowest detection limit obtained for the speciation of arsenic using TXRF technique. The total arsenic concentration has been determined by oxidizing all the As (III) species into As (V). As (III) concentration could be determined by subtracting the As (V) concentration from total arsenic concentration. This methodology has been applied for the speciation studies in some real water samples spiked with As (III) and As (V) with different concentrations. The analytical results obtained are very much satisfactory with an average RSD (1σ , $n=3$) and deviation of TXRF determined values from the expected values by 5.5% and 3.5 % respectively. This confirms the applicability of the developed methodology for the speciation of arsenic in different types of real water samples.

7.3. Future scopes

There can be a number of future possibilities for better application of the methods developed in this thesis for societal and technological applications. Some of these possibilities are as follows:

1. The determination of low Z elements can be further extended to do carbon nitrogen analysis in different technologically important samples like steel, uranium carbide as well nitride fuel etc. Carbon, nitrogen analysis is also very important for environmental samples like soil to evaluate its quality. A low energy excitation source shall be highly beneficial.

2. The determination of fluorine can be further extended in different technologically important materials like heavy water samples, nuclear fuel, zircalloy, steel etc.
3. The solid phase extraction technique can also be extended for the trace elemental determination of different plutonium samples.
4. The solid phase extraction technique can be used in combination with TXRF for the speciation of other elements like Cr, Se, and Sb etc in different environmental samples.



References

1. <http://www.world-nuclear.org/information-library/country-profiles/countries-g n/india.aspx>
2. X. Duan, C. M. Lieber, *Adv. Funct. Mater.*, 2000, **12**, 298-302.
3. A. Navrotsky, *MRS Bulletin*, 1997, **22**, 35-41.
4. G.Y. Chin, *J. Magn. Mater.*, 1978, **9**, 283-298.
5. R.K. Sinha, A. Kakodkar, *Nucl. Eng. Des.* 2006, **236**, 683–700.
6. K.L. Ramakumar, *Bull. Mater. Sci.* 2005, **28**, 331.
7. “In facets of nuclear science and technology”, S.K.Aggarwal, D.D. Sood (eds.), 1996, 137-147.
8. “Nuclear Fuel”, A. Yacout, *Energy Engineering and Systems Analysis*, 2011, 1-2.
9. “Nuclear fuels”, A. Ballagny et.al, *DEN Monographs*, 2009, 1-147.
10. A. O. Nier, *Phys. Rev.* 1939, **55**, 150.
11. “Fundamentals of radiochemistry”, D. D. Sood, A.V.R. Reddy, N. Ramamoorthy, *IANCAS*, Fourth edition.
12. M.S.Wickleder, B. Fourest, P.K. Dorhout, L.R. Morss, N.M. Edelstein, J. Fuger, “*The Chemistry of the Actinide and Transactinide Elements*” 2008, Springer, Dordrecht.
13. R.K. Sinha, A. Kakodkar, *Nucl. Eng. Des.* 2006, **236**, 683–700.
14. “Nuclear Power Reactors”, *Nuclear Reactor Technology - World Nuclear Association*, 2018,1-13,<http://www.world-nuclear.org/information-library/nuclear-fuel-cycle/nuclear-power-reactors/nuclear-power-reactors.aspx>
15. C. Ganguly, P. V. Hegde, G. C. Jain, U. Basak, R. S. Mehrotra, S. Majumdar , P. R. Roy, *Nucl Technol*, 1986, **72**, 59-69.
16. S.S. Bajaj, A.R. Gore, *Nucl. Eng. Des.* 2006, **236**, 701-722.

17. K.V. Vrinda devi, T. Soreng, D. Mukherjee, J.P. Panakkal , H.S. Kamath, *J. Nucl. Mater.* 2010, **399**, 122-127.
18. G. Wikmark, L. Hallstadius, K. Yueh, *Nucl Eng Technol.* 2009, **41**, 143.
19. M. Griffiths, R.A. Holt, *J. Nucl. Mater.*, 1995, **225**, 245-258.
20. Z.L. Pan, I.G. Ritchie, M.P. Puls, *J. Nucl. Mater.*, 1996, **228**, 227-237.
21. R. Shekhar, J. Arunachalam, H. R. Ravindra, B. Gopalan, *J. Anal. At.Spectrom.* 2003, **18**, 381-384.
22. C.R.F. Azevedo, *Eng. Fail. Anal.* 2011, **18**, 1943-1962.
23. <http://www.indymedia.ie/article/104629>
24. <https://kids.britannica.com/students/assembly/view/124590>
25. A. Chatterjee, D. Das, D.Chakraborti, *Environ. Pollut.* 1993, **80**, 57-65.
26. D. Chakraborti, et al, *Curr. Sci.* 1998, **74**, 346-355.
27. H.W. Chen, *Bull Environ Contam Toxicol*, 2007, **78**, 5-9.
28. “Arsenic in drinking water” National Academies Press, 28-Jun-1999 – Science.
29. U.K. Chowdhury et al., *Environ Health Persp*, 2000, **108**, 393-397.
30. V. Khatibikamal, A. Torabian, F. Janpoor, G. Hoshyaripour, *J Hazard Mater*, 2010, **179**, 276-280.
31. M. G. Sujana, R. S. Thakur, S. B. Rao, *J Colloid Interf Sci*, 1998, **206**, 94-101.
32. M. Dakiky, M. Khamis, A. Manassra, M. Mer’eb, *Adv Environ Res*, 2002, **6**, 533-540.
33. E. E. El-Hinnawi, *IAEA Bulletin*, 2000, **20**, 32-42.
34. “Environmental effects of nuclear power generation”, A.S. Paschoa, *Interactions: energy/environment*, 1-15. <http://www.eolss.net/ebooks/sample%20Chapters/C09/E4-23-03-03.pdf>

35. T. Nagai, N. Sato, S. Kitawaki, A. Uehara, T. Fujii, H. Yamana, M. Myochin, *J. Nucl. Mater.* 2013, **433**, 397-403.
36. K. O. Kvashnina, S. M. Butorin, P. Martin, P. Glatzel, *Phys Rev Lett.* 2013, **111**, 253002.
37. “Chemical quality control of nuclear materials”, V. Venugopal, *IANCAS Bulletin*, 2005, **3**, 205.
38. S. Dhara, N. L. Misra, U. K. Thakur, D. Shah, R. M. Sawant, K. L. Ramakumar, S. K. Aggarwal, *X-Ray Spectrom.* 2012, **41**, 316–320.
39. “Fabrication of high density ThO₂, ThO₂–UO₂ and ThO₂–PuO₂ fuel pellets for heavy water reactors”, U. Basak, M.R. Nair, R. Ramachandran, S. Majumdar, *BARC News letter, Founders day special issue, October 2001*.
40. C. Raepsaet, Ph. Bossis, D. Hamon, J.L. Be’chade, J.C. Brachet, *Nucl. Instr. and Meth. In Phys. Res. B*, 2008, **266**, 2424-2428.
41. T. Hiyama, T. Takahashi, K. Kunimura, *Anal Chim Acta*, 1997, **345**, 131-137.
42. C.F. Old, *J Nucl Mater*, 1980, **92**, 2-25.
43. “Analytical characterization of technologically important materials using TXRF and EDXRF”, S. D. Lenka, *A thesis submitted to the Board of Studies in Chemical Sciences HBNI*, 2012.
44. R.J. McEachern, P. Taylor, *J Nucl Mater*, 1998, **254**, 87-121.
45. G. Rousseaua, L. Desgrangesa, F. Charlotb, N. Millotb, J.C. Nièpceb, M. Pijolatc, F. Valdiviesoc, G. Baldinozzid, J.F. Bérare, *J. Nucl. Mater.* 2006, **355**, 10-20.
46. M. Kumar, A. Puri, *Indian J Occup Environ Med.* 2012, **16**, 40-44.
47. “Total reflection X-ray fluorescence analysis, Chemical Analysis”, R. Klockenkämper, 1996, **vol. 140**, *John Wiley and Sons*, New York.

48. N.L. Misra, K.D. Singh Mudher, V.C. Adya, B. Rajeswari, V. Venugopal, *Spectrochim Acta B*. 2005, **60**, 834-840.
49. F. Saverio Romolo, P. Margot, *Forensic Sci. Int.* 2001, **119**, 195.
50. A. Iida, K. Sakurai, A. Yoshinaga, Y. Gohshi, *Nucl. Instrum. Methods*, 1986, **246**, 736-738.
51. A. Iida, K. Sakurai, Y. Gohshi, *Adv. X-Ray Anal.* 1988, **31**, 487.
52. V. Penka, W. Hub, *Spectrochim. Acta*, 1989, **44**, 483-490.
53. G. Das, A. G. Karydas, H. Ghosh, M. Czyzycki, A. Migliori, A. K. Sinha, M. K. Tiwari, *Phys Rev B*, 2017, 96, 155444.
54. A.V. Bohlen, M. Kramer, C. Sternemann, M. Paulus, *J Anal Atom Spectrom*, 2009, **24**, 792–800.
55. W.C. Roentgen, *Ann. Phys.Chem.*, 1898, **64**, 1.
56. E.A. Bertin, “Principle and practice of X-Ray spectrometric analysis”, 2nd Edition, Plenum Press, New York, 1984.
57. B.D. Cullity, *Elements of X-ray diffraction*, Addison-Wesley publishing company, Inc. 1956.
58. “X-Ray adsorption, principles, applications, techniques of EXAFS, SEXAFS and XANES”, D.C. Koningsberger, R. Prins (ed.), **Vol. 92** John Wiley and Sons, A Wiley- Interscience publication, 1988.
59. J. B. Metson, S. J. Hay, H. J. Trodahl, B. Ruck, Y. Hu , *Curr. Appl. Phys.* 2004, **4**, 233.
60. B. Kanrar, K. Sanyal, N.L. Misra, S.K. Aggarwal, *Spectrochimica Acta B*, 2014, **101**, 130-133.
61. S. Dhara, N.L. Misra, S.D. Maind, S.A. Kumar, N. Chattopadhyay, S.K. Aggarwal, *Spectrochimica Acta Part B*, 2010, **65**, 167-170.

-
62. J. Osán, F. Meirer, V. Groma, S. Török, D. Ingerle, C. Strelí, G. Pepponi, *Spectrochim. Acta part B*. 2010, **65**, 1008-1013.
 63. F. Meirer, G. Pepponi, C. Strelí, P. Wobrauschek, V. G. Mihucz, G. Záray, V. Czech, J. A. C. Broekaert, U. E. A. Fittschen, G. Falkenberg, *X-Ray Spectrom.* 2007, **36**, 408–412.
 64. P. Brouwer, “Theory of XRF”, *Pan Analytical*, **3rd edition**, 2010, 1-62.
 65. H.Hoefler, C.Strelí, P.Wobrauschek, M.Óvári, Gy.Záray, *Spectrochim. Acta part B*, 2006, **61**, 1135-1140.
 66. H. Aiginger, P. Wobrauschek, C. Brauner, *Nucl. Instrum. Methods*, 1974, **120**, 541–542.
 67. S. Dhara, N.L. Misra, S.K. Aggarwal, V. Venugopal, *Spectrochim. Acta Part B*, 2010, **65**, 461-465.
 68. S. Dhara, S. Sanjay Kumar, N.L. Misra and S. K. Aggarwal, *X-ray Spectrometry*, 2009, **38**, 112-116.
 69. S. Majumdar, J. R.P. Videá, H.C. Michel, J. Hong, C. M. Rico, J. L.G. Torresdey, *Analytica Chimica Acta*, 2012, **755**, 1-16.
 70. D.M. Johnson, P.R. Hooper, R.M. Conrey, *Advances in X-ray Analysis*, 1999, **41**, 843-867.
 71. V. Batuman, R.P. Wedeen, J.D. Bogden, D.J. Balestra, K. Jones, G. Schidlovsky, *Environmental Research*, 1989, **48**, 70-75.
 72. J. Z. Palus, R. Borusiewicz, *Journal of Molecular Structure*, 2006, **792**, 286-292.
 73. V. Valkovic, A. Markowicz, N. Haselberger, *X-Ray spectrom.* 1993, **22**, 199.
 74. A. Iida, K. Sakurai, T. Matsushita, Y. Gohshi, *Nucl. Instrum. Methods*, 1985, **228**, 556.
 75. W. D. Coolidge, *Phys. Rev.* 1913, **2**, 409.
 76. <http://physicsmuseum.uq.edu.au/xrd-glass-x-ray-tube-dismantled>

-
77. <https://www.oxford-instruments.com/businesses/industrial-products/oxford-instruments-x-ray-technology/application-notes/typical-x-ray-spectra-by-anode-material>
 78. W. Ladisich, R. Rieder, P. Wobrauschek, H. Aiginger, *Nucl Instrum Meth A*, 1993, **330**, 501-506.
 79. Z. Szökefalvi-Nagy, I. Demeter, A. Kocsonya, I. Kovács, *Nucl. Instrum. Methods*, 2004, **226**, 53.
 80. S. Mobilio et al. (eds.), *Synchrotron Radiation*, DOI: 10.1007/978-3-642-55315-8_1, Springer-Verlag Berlin Heidelberg 2015.
 81. R. Klockenkaemper, "Total reflection X-Ray fluorescence analysis", **Vol. 140**, John Wiley & Sons, New York (1996).
 82. A.H. Compton, *Philos. Mag.* 1923, **45**, 1121.
 83. H. Yoneda, T. Horiuchi, *Rev. Sci. Instrum.* 1971, **42**, 1069.
 84. J. Knoth, A. Prange, U. Reus, H. Schwenke, *Spectrochim. Acta Part B*, 1999, **54**, 1513.
 85. F. Esaka, K. Watanabe, T. Onodera, T. Taguchi, M. Magara, S. Usuda, *Spectrochim. Acta Part B*, 2003, **58**, 2145.
 86. A. Prange, K. Kramer, U. Reus, *Spectrochim. Acta Part B*, 1993, **48**, 153.
 87. M. Theisen, R. Niessner, *Spectrochim. Acta Part B*, 1999, **54**, 1839.
 88. A. Prange, H. Schwenke, *Adv. X-ray Spectrom.* 1992, **35B**, 899.
 89. <https://www-pub.iaea.org/MTCD/Publications/PDF/TCS-51/html/pdf/Section%202.pdf>
 90. S. Kunitani, J. Kawai, *Analyst*, 2010, **135**, 1909-1911.
 91. Y. Liu, *Adv. X-Ray. Chem. Anal, Japan*, 2015, **46**, 13-26.
 92. <https://onlinelibrary.wiley.com/doi/pdf/10.1038/npg.els.0002984>
 93. <http://www.chem.ucalgary.ca/research/groups/faridehj/xas.pdf>

-
94. M. Newville, "Fundamentals of XAFS", 2004.
95. <http://www.elettra.trieste.it/lightsources/elettra/elettra-beamlines/microfluorescence/iaea-end-station.html>
96. W. Jark, D. Eichert, L. Luehl, A. Gambitta, "Optimization of a compact optical system for the beam transport at the X-ray Fluorescence beamline at Elettra for experiments with small spots, in Advances in X-Ray/EUV Optics and Components" IX (Eds: C. Morawe, A. M. Khounsary, S. Goto)Proc. of SPIE Vol. 9207, 92070G, SPIE, USA, 2014.
97. C. Strelí, P. Wobrauschek, F. Meirer, G. Pepponi. *J. Anal. At. Spectrom.*, 2008, **23**, 792–798.
98. M. K. Tiwari, P. Gupta, A. K. Sinha, S. R. Kane, A. K. Singh, S. R. Garg, C. K. Garg, G. S. Lodha, S. K. Deb, *J. Synchrotron Radiat.* 2013, **20**, 386–389.
99. G. Das, M. K. Tiwari, A. K. Singh, H. Ghosh, *J. Anal. At. Spectrom.* 2014, **29**, 2405–2413.
100. B. Vekemans, K. Janssens, L. Vincze, F. Adams, P. Van Espen. *X-Ray Spectrom.*, 1994, **23**, 278–285.
101. C. Vandecasteele, C. B. Block, "Modern Method for Trace Element Determinations, John Willey and Sons", Chichester UK, 1991.
102. I. Pais, J. B. Jones Jr, "The hand book of trace elements", St. Lucie Press, Boca Raton, Florida, 1997.
103. "Guide line for drinking water quality" **Volume 1**, WHO, 2006, http://www.who.int/water_sanitation_health/dwq/gdwq0506.pdf.
104. K. Uhlir, M. Griesser, G. Buzanich, P. Wobrauschek, C. Strelí, D. Wegrzynek, A. Markowicz, E. Chinea-Cano. *X-ray Spectrom.* 2008, **37**, 450–457.
105. N. L. Misra, S. Dhara, M. Óvári, G. Záray, S. K. Aggarwal, I. Varga, *Spectrochim. Acta Part B*, 2010, **65**, 457–460.

-
106. L. Fabry, L. Köster, S. Pahlke, L. Kotz, J. Hage. *IEEE Trans. Semicond. Manuf.* 1996, **9**, 428–436.
107. C. W. Dwiggins, *Anal. Chem.* 1961, **33**, 67–70.
108. C. Strelí, *Appl. Spectros. Rev.* 2006, **41**, 473–489.
109. R. Chul-Un, J. Osán, R. Van Grieken, *Anal. Chem.* 1999, **71**, 1521–1528.
110. S. Dhara, N. L. Misra, S. K. Aggarwal, D. Ingerle, P. Wobrauschek, C. Strelí, *X-ray Spectrom.* 2014, **43**, 108–111.
111. M. Rauwolf, C. Vanhoof, K. Tirez, E. Maes, D. Ingerle, P. Wobrauschek, C. Strelí, *Spectrochim. Acta Part B*, 2014, **101**, 118–122.
112. R. E. Van Grieken, A. A. Markowitz, “Handbook of X-ray Spectrometry”, Marcel Dekker Inc. New York, 2002.
113. G. Tarsoly, M. Óvári, Gy. Zárny. *Spectrochim. Acta Part B*, 2010, **65**, 287–290.
114. A. Pupyshev, V. T. Surikov, *Spectrochim. Acta Part B*, 2004, **59**, 1021–1031.
115. M. Doi, M. Yamagami, T. Shoji, T. Yamada, “JCPDS-international centre for diffraction data” *Adv. X-ray Anal.*, 2002, **45**, 533–537.
116. C. Strelí, P. Kregsamer, P. Wobrauschek, H. Gatterbauer, P. Pianetta, S. Pahlke, L. Fabry, L. Palmeshofer, M. Schmeling, *Spectrochim. Acta Part B*, 1999, **54**, 1433–1441.
117. J. Prost, P. Wobrauschek, C. Strelí, *Powder Diffraction*, 2015, **30**, 93–98.
118. C. Strelí, P. Wobrauschek, B. Beckhoff, G. Ulm, L. Fabry, S. Pahlke, *X-Ray Spectrom.*, 2001, **30**, 24–31.
119. C. Strelí, G. Pepponi, P. Wobrauschek, C. Jokubonis, G. Falkenberg, G. Zaray., *X-Ray Spectrom.* 2005, **34**, 451–455.

-
120. P. Wobrauschek, J. Prost, D. Ingerle, P. Kregsamer, N. L. Misra, C. Streli, *Rev. Sci. Instrum.* 2015, **86**, 083105, 1–7.
121. H. Assmann, M. Peehs, H. Roepenack, *J Nucl Matter*, 1988, **153**, 115-126.
122. M. Gopalkrishnan, K. Radhakrishnan, P. S. Dhama, V. T. Kulkarni, M. V. Joshi, A. B. Patwardhan, A. Ramanujam, J. N. Mathur, *Talanta*, 1997, **44**, 169-176.
123. K. Satyanarayana, S. Durani, *J Radioanal Nucl Chem.*, 2010, **285**, 659-665.
124. A. Zucchiatti, P. Corvisiero, *Energy Procedia*, 2013, **41**, 110-118.
125. M. S. Lai, L. W. Xiang, J. M. Lin, H. F. Li, *Sci China Chem.* 2013, **56**, 1164-1170.
126. S. Bishnoi, P. S. Sarkar, T. Patel, P. S. Adhikari, A. Sinha, *AIP Conference Proc.*, 2013, **1524**, 275-278.
127. N. L. Misra, *Pramana, J Phys.* 2011, **76**, 201-212.
128. Y. Wang, Y. Liu, T. Chu, *J Radioanal Nucl Chem.* 2016, **308**, 1071-1079.
129. P. Giridhar, K. A. Venkatesan, S. Subramaniam, T. G. Srinivasan, P. R. Vasudeva Rao, *J Alloy Compd.* 2008, **448**, 104-108.
130. M. L. Dietz, D. C. Stepinski, *Talanta*, 2008, **75**, 598-603.
131. R. M. Sawant, M. A. Mahajan, P. Verma, D. Shah, U. K. Thakur, K. L. Ramakumar, V. Venugopal, *Radiochim. Acta*, 2007, **95**, 585.
132. M. A. Mahajan, M. V. R. Prasad, H. R. Mhatre, R. M. Sawant, R. K. Rastogi, G. H. Rizvi, N. K. Chaudhuri, *J. Radioanal. Nucl. Chem.* 1991, **148**, 93.
133. M. Bojinov, V. Karastoyanov, P. Kinnunen, T. Saario, *Corros. Sci.* 2010, **52**, 54.
134. S. Suthar, V. K. Garg, S. Jangir, S. Kaur, N. Goswami, S. Singh, *Environ. Monit. Assess.* 2008, **145**, 1.
135. J. J. D. Phil, B. L. Riggs, P. J. Kelly, D. L. Hoffman, *Am. J. Med.* 1972, **53**, 43.

-
136. N. Kundu, M. K. Panigrahi, S. Tripathy, S. Munshi, M. A. Powell, B. R. Hart, *Environ. Geol.* 2001, **41**, 451.
137. C. Reimann, D. Banks, *Sci. Total Environ.* 2004, **332**, 13.
138. S. Jeyakumar, V. V. Raut, K. L. Ramakumar, *Talanta*, 2008, **76**, 1246.
139. L. E. Vanatta, *J. Chromatogr. A*, 2008, **1213**, 70.
140. S. S. Yamamura, M. A. Wade, J. H. Sikes, *Anal. Chem.* 1962, **34**, 1308.
141. E. W. Baumann, *Anal. Chim. Acta*, 1968, **42**, 127.
142. M. A. G. T. van den Hoop, R. F. M. J. Cleven, J. J. van Staden, J. Neele, *J. Chromatogr. A*, 1996, **739**, 241.
143. Y. Liu, E. Kaiser, N. Avdalovic, *Microchem. J.* 1999, **62**, 164.
144. T. V. Hoogerstraete, S. Jamar, S. Wellens, K. Binnemans, *Anal. Chem.* 2014, **86**, 1391.
145. Y. Tabuchi, K. Tsuji, *X-Ray Spectrom.* 2016, **45**, 197.
146. R. Unterumsberger, B. Pollakowski, M. Muller, B. Beckhoff, *Anal. Chem.* 2011, **83**, 8623–8628.
147. K. Sanyal, B. Kanrar, N. L. Misra, M. Czyzycki, A. Migliori, A. G. Karydas, *X-Ray Spectrom.* 2017, **46**, 164.
148. R. N. Lamb, D. N. Furlong, *J. Chem. Soc. Faraday Trans.* 1982, **78**, 61.
149. M. Taylor, David, *Appl. Radiat. Isot.* 1995, **46**, 1245-1252.
150. J. Qiao, X. Hou, M. Miró, P. Roos, *Anal. Chim. Acta.* 2009, **652**, 66-84.
151. H. S. Kamath, “Development of plutonium fuel for thermal and fast reactors”, IANCAS Bulletin on “nuclear material”, 2005, **4**, 213-225.
152. G. R. Schmidt, M. G. Houts, *AIP Conference Proceedings*, 2006, **813**, 334, doi: 10.1063/1.2169210.

-
153. D. T. Rankin, W. R. Kanne, M. R. Louthan, D. F. Bickford, J. W. Congdon, WSRC-MS-2000-00061, 179-186.
154. R.K. Malhotra, K. Satyanarayana, *Talanta*, 1999, **50**, 601-608.
155. M.V. Ramaniah, *Pure Appl. Chem.* 1982, **54**,889–908.
156. M. Gopalakrishnan, K. Radhakrishnan, P.S. Dharni, V.T. Kulkarni, M.V. Joshi, A.B. Patwardhan, A. Ramanujam, J.N. Mathur, *Talanta*, 1997, **44**, 169-176.
157. E. A. Huff, S. J. Kulpa, *Anal. Chem.* 1966, **38**, 939–940.
158. E. A. Huff, *Anal. Chem.* 1965, **37**, 533–536.
159. R. K. Dhumwad, M. V. Joshi, A.B. Patwardhan, *Anal. Chim. Acta*, 1968, **42**, 334-337.
160. C. Mahan, S. Bonchin, D. Figg, D. Gerth, C. Collier, *J. Anal. At. Spectrom.* 2000, **15**, 929-935.
161. S. Dhara, P. Prabhat, N.L. Misra, *Analytical Chemistry*, 2015, **87**, 10262-10267.
162. N.L. Misra, *J. Radioanal. Nucl. Chem.* 2014, **300**, 137-145.
163. N.L. Misra, *Spectrochim. Acta Part B*, 2014, **101**, 134-139.
164. G.F.Best, A.C.McKay, R.Woodgate, *Journal of Inorganic and Nuclear Chemistry*, 1957, **4**, 315-320.
165. S. Dhara, A. Khooha, A. K. Singh, M.K.Tiwari, N.L.Misra, *Spectrochimica Acta Part B*, 2018, **144**, 87-91.
166. P. C. Burns, R. C. Ewing, A. Navrotsky, *Science*, 2012, **335**, 1184-1188.
167. N.L. Misra, K.D. Singh Mudher, *Prog. Cryst. Growth. Ch.* 2002, **45**, 65-74.
168. J. Karjou, *Spectrochim Acta B*, 2007, **62**, 177–181.
169. K. Sanyal, S. Dhara, N.L. Misra, *X-ray Spectrom.* 2017, **46**, 442-447.

-
170. Y. Picó, M. Fernández, M. J. Ruiz, G. Font, *J. Biochem. Biophys. Methods*, 2007, **70**, 117–131.
171. T. Prasada Rao, Sobhi Daniel, J. Mary Gladis, *Trend. Anal Chem.* 2004, **23**, 28-35.
172. A. Żwir-Ferenc, M. Biziuk, *Polish J. of Environ. Stud.* 2006, **15**, 677-690.
173. B. Bennett and S. R. Larter, *Anal. Chem.* 2000, **72**, 1039-1044.
174. D. P. Curran, Z. Luo, *J. Am. Chem. Soc.* 1999, **121**, 9069-9072.
175. P. Metilda, J. Mary Gladis, T. Prasada Rao, *Radiochim. Acta*, 2003, **91**, 737–741.
176. Z. Li , F. Chen , L. Yuan, Y. Liu, Y. Zhao, Z. Chai, W. Shi, *Chem. Eng. J.* 2012, **210**, 539–546.
177. R. Sitko, P. Janik, B. Zawisza, E. Talik, E. Margui, I. Queralt, *Anal. Chem.* 2015, **87**, 3335-3542.
178. A. Schierz, H. Zanker, *Environ. Pollut.* 2009, **157**, 1088–1094.
179. A. Nilchi, T. S. Dehaghan, S. R. Garmarodi, *Desalination*, 2013, **321**, 67–71.
180. S. Chappa, S. Das, A. K. Debnath, M. Sahu, M. K. Saxena, A. K. Pandey, *Ind. Eng. Chem. Res.* 2016, **55**, 8992–9002.
181. S. Das, A. K. Pandey, T. Vasudevan, A. A. Athawale, V. K. Manchanda, *Ind. Eng. Chem. Res.* 2009, **48**, 6789–6796.
182. S. Das, A.K. Pandey, A. A. Athawale, V. K. Manchanda, *Desalin. Water Treat.* 2012, **38**, 114-120.
183. K. Sanyal, N. Pathak, A. K. Yadav, B. Kanrar, R. M. Kadam, S. N. Jha, D. Bhattacharyya, N. L. Misra, *Dalton Trans.* 2016, **45**, 7650.
184. S. K. Gupta, N. Pathak, P.S. Ghosh, R.M. Kadam, *Journal of Alloys and Compounds*, 2017, **695**, 337-343.

-
185. N. Pathak, P. S. Ghosh, S. K. Gupta, S. Mukherjee, R. M. Kadam, A. Arya, *J. Phys. Chem. C*, 2016, **120**, 4016–4031.
186. M. Alibrahim, H. Shlewit, *Per. Pol. Chem. Eng.* 2007, **51**, 57-60.
187. B.K. Mandal, “*Handbook of Arsenic Toxicology*”, 2015, 179-201.
188. S. M. Hölzl, P. J. Altmann, J. W. Kück, F. E. Kühn, *Coordin Chem Rev.* 2017, **352**, 517–536.
189. H.W.G. Heynen, H.S.van der Baan, *J. Catal.* 1974, **34**, 167-174.
190. T. Lis, *Acta Cryst.* 1980, **36**, 2042-2046.
191. A. Duba, I.A. Nicholls, *Earth Planet Sc Lett.* 1973, **18**, 59-64.
192. K. Pytlakowska, *J. Anal. At. Spectrom.* 2016, **31**, 968.
193. X. Zhu, B. Hu, Z. Jiang, M. Li, *Water Res.* 2005, **39**, 589–595.
194. X. Luo, C. Wang, L. Wang, F. Deng, S. Luo, X. Tu, C. Au, *Chem. Eng J.* 2013, **220**, 98–106.
195. Z. Pedrero, Y. Madrid, *Anal Chim Acta*, 2009, **634**, 135–152.
196. L. Van Brutzel, A. Chartie, *Phys. Rev. B: Condens. Matter Mater. Phys.* 2008, **78**, 024111.
197. F. Grønvold, *J. Inorg. Nucl. Chem.* 1955, **1**, 357–370.
198. D. Olander, *J. Nucl. Mater.* 2009, **389**, 1-22.
199. D. R. Olander, *Technical report*, 1975, DOI: 10.2172/7343826, 1-629.
200. S. Siegel, *Acta Crystallogr.* 1955, **8**, 617-619.
201. A.F. Andresen, *Acta Crystallogr.* 1958, **11**, 612-614.
202. P.G. Dickens, A.V. Powell, *J. Solid State Chem.* 1991, **92**, 159-169.
203. G. J. Hutchings, C. S. Heneghan, I. D. Hudson, S. H. Taylor, *Nature (London)*. 1996, **384**, 341-343.

-
204. D. Kumar, N. M. Gupta, *Catal. Surv. Asia*. 2005, **9**, 35-49.
205. A. Arrott, J.E. Goldman, *Phys. Rev.* 1957, **108**, 948-953.
206. S. D. Conradson et al, *J. Solid State Chem.* 2005, **178**, 521-535.
207. H. Geng, Y. Chen, Y. Kaneta, M. Iwasawa, T. Ohnuma, M. Kinoshita, *Phys. Rev. B*. 2008, **77**, 104120.
208. J. J. Pireaux, J. Riga, E. Thibaut, C. Tenret-Noe"l, R. Caudano, J. J. Verbist, *Chem. Phys.* 1977, **22**, 113-120.
209. Y. A. Teterin, A.Y. Teterin, *Russ. Chem. Rev.* **2004**, **73**, 541-580.
210. N. L. Misra, *J. Radioanal. Nucl. Chem.* 2014, **300**, 137-145.
211. "Literature Study on Speciation Analysis of Inorganic Arsenic in Aqueous Samples Using Inductively Coupled Plasma Mass Spectrometry", A. Yimer, degree project in chemistry, Umea university, 2011.
212. B. F. Urbano, B. L. Rivas, F. Martinez, S.D. Alexandratos, *Reactive & Functional Polymers*, 2012, **72**, 642-649.
213. World Health Organization, *Guidelines for Drinking-Water Quality, Health Criteria; WHO*, 1996; **2**, 940.
214. United States Environmental Protection Agency, Edition of the Drinking Water Standards and Health Advisories. EPA 882-R-04-005; U.S. EPA: Washington, DC, 2004.
215. C. K. Jain, I. Ali, *Water Res.* 2000, **34**, 4304-4312.
216. A. Hussam, M. Alauddin, A.H. Khan, S. B. Rasul, A. K.M. Munir, *Environ. Sci. Technol.* 1999, **33**, 3686-3688.
217. P. Sala"un, B. Planer-Friedrich, C. M.G. van den Berg, *Analytica Chimica Acta*, 2007, **585**, 312-322.

-
218. R. Gupta, J. S. Gamare, A. K. Pandey, D. Tyagi, J. V. Kamat, *Anal. Chem.* 2016, **88**, 2459–2465.
219. W. R. Cullen, K. J. Reimer, *Chem. Rev.* 1989, **89**, 713-764.
220. M. Moldovan, M.M.Go´mez, M.A.Palacios, C.Ca´mara, *Microchemical Journal*, 1998, **59**, 89–99.
221. M. Ali, S. A. Tarafdar, *Journal of Radioanalytical and Nuclear Chemistry*, 2003, **256**, 297-305.
222. B. Staniszewski, P. Freimann, *Spectrochimica Acta Part B*, 2008, **63**, 1333–1337.
223. H. Barros, L.M.M. Parra, L. Bennun, E. D. Greaves, *Spectrochimica Acta Part B*, 2010, **65**, 489–492.
224. V.Hatzistavros, P.Koulouridakis, N. Kallithrakas-Kontos, *Analytical Sciences*, 2005, **21**, 823-826.
225. N. Kallithrakas-Kontos, P. Koulouridakis, V. Hatzistavros, I. N. Aretaki, *X-Ray Spectrom.* 2009, **38**, 152–156.
226. L. Toledo, B. L. Rivas, B. F. Urbano, J. Sanchez, *Separation and Purification Technology*, 2013,**103**, 1–7.
227. L. Dambies, R. Salinaro, S .D. Alexandratos, *Environ. Sci. Technol.* 2004, **38**, 6139-6146.
228. R. N. Shinde, V. Chavan, R. Acharya, N.S. Rajurkar, A. K. Pandey, *Journal of Environmental Chemical Engineering*, 2014, **2**, 2221–2228.
229. S.K. Gupta, A.R. Dhobale, M. Kumar, S.V. Godbole, V. Natarajan, *J. Mol. Struct.* 2015, **1084**, 89-94.
230. P. A. Tempest, P.M. Tucker, J.W. Tyler, *J. Nucl. Mater.* 1988, **151**, 251-268.

-
231. G. Aravamudan, A.S. Giridharan, N. Ramadass, *Z. Anorg. Allg. Chem.* 1978, **444**, 246-250.
232. F. Meirer, G. Pepponi, C. Streli, P. Wobrauschek, P. Kregsamer, N. Zoeger, G. Falkenberg, *Spectrochim. Acta part B.* 2008, **63**, 1496-1502.
233. M.K. Tiwari, G.M. Bhalerao, M. Babu, A.K. Sinha, C. Mukherjee, *J Appl. Phys.* 2008, **103**, 054311.
234. M.K. Tiwari, K.J.S. Sawhney, G.S. Lodha, *Spectrochim. Acta Part B.* 2010, **65**, 434-440.
235. D. A. Andersson, G. Baldinozzi, L. Desgranges, D. R. Conradson, S. D. Conradson, *Inorg. Chem.* 2013, **52**, 2769–2778.
236. G. Leinders, R. Bes, J. Pakarinen, K. Kvashnina, M. Verwerft, *Inorg. Chem.* 2017, **56**, 6784–6787.
237. K. J. Seu, A. P. Pandey, F. Haque, E. A. Proctor, A. E. Ribbe, J. S. Hovis, *Biophysical Journal*, 2007, **92**, 2445–2450.
238. S. Chappa, R. N. Shinde, A. K. Pandey, *Green Chem.* 2015, **17**, 4157-4161.
239. M. Pettine, L. Campanella, F. J. Millero, *Geochimica et Cosmochimica Acta*, 1999, **18**, 2727–2735.